FIBRE DEGRADATION DURING THE EXTRUSION

COMPOUNDING OF GLASS FIBRE FILLED NYLON 6.6

Thesis submitted in accordance with the requirements of the

University of Liverpool for the degree of Doctor of Philosophy

by James Lunt

Department of Metallurgy and Materials Science

June, 1980

ABSTRACT

The addition of short glass fibres to thermoplastic matrices produces improvements in most mechanical properties. However, the pronounced fibre fracture encountered during the common compounding and moulding processes, results in a reduction in the potential reinforcing efficiency. The influence of design, processing and material parameters on such fibre breakage has been studied, with particular regard to the plasticating extrusion process.

Measurements of the processing stability, coupled with the fibre length analysis of extracted screw samples and extruded compounds, indicate a direct correlation with the melting process occurring in these single screw machines. The excellent agreement between the observed melting mechanism and a theoretical melting model developed for unreinforced thermoplastics is demonstrated. Such a model provides the explanation for the pattern of fibre degradation observed.

Introduction of chopped strands into the polymer melt offers useful bonuses in retained fibre lengths and composite performance. Composite properties are seen to be influenced by a matrix embrittlement effect, which accompanies chemical interaction of the fibre sizing materials and the matrix polymer. The reduced failure strains which acccompany this embrittlement, are also observed with increases in fibre length, fibre concentration and reduced polymer molecular weight.

ACKNOWLEDGEMENTS

CONTENTS

CHAPTER 5   CONCLUSIONS AND SUGGESTIONS FOR FUTURE WORK

LIST OF TABLES

CHAPTER 1 - INTRODUCTION AND LITERATURE REVIEW

1.1 Background

The technique of drawing fibres from heated rods and impressing them while hot onto the surface of fabricated articles was well known to the artisans of ancient Syria, Greece and Egypt. However, commercial exploitation of fibrous glass commenced in 1937 with the founding of Owens-Corning Fibreglass Corporation (1), which followed ten years of research between Owens-Illinois Glass Company and Corning Glass Works. The advent of viable production techniques led to products such as "white wool" insulation, coarse fibred air-filters and continuous filament material, which was used to weave a cloth subsequently impregnated with varnish for electrical laminates. The prior development of unsaturated polyester resins in 1935 gave a natural impetus to the combination leading to the use of chopped strand mat, in conjunction with the above resins, for hand lay-up operations in the 1940's. The incidence of World War II led to a rapid increase in the number of applications for these materials and the development of new moulding methods proceeded rapidly leading to many new non-metallic weight reducing components for military use. Present day consumption of these reinforced plastics is estimated at 91,000 tonne (2), major markets being in the automotive and electrical industries.

The modern thermoplastics industry dates from the 1920's when P.V.C. was in commercial production (3) followed by the introduction of polystyrene, polyethylene, and poly(methyl methacrylate) in the 1930's. The thermoplastic polyamides, given the generic name of 'nylons', were introduced commercially in the early 1940's following the development of nylon 6.6 (poly(hexamethylene adipamide)) by Du Pont's W.H. Carothers in the early 1930's.

The use of glass fibres as a reinforcement for the above materials was, however, delayed due to the lack of efficient methods of combining the glass and polymer coupled with the undeveloped state of the glass sizing and moulding techniques. By 1960 there were still only four fibre reinforced thermoplastics, although some sixteen different types of thermoplastics were commercially available. The early 1970's however, saw the rapid acceptance of glass reinforced thermoplastics as engineering materials with considerable potential, these composites finding application in markets hitherto occupied by metals.

1.1.1 <u>Glass fibre parameters</u>

The addition of glass fibres to a polymeric matrix produces increases in both stiffness and heat distortion temperature. In addition, improvements are observed in tensile, flexural and compressive strengths with increasing levels of glass fibre. Some degree of control over processing and of the resultant composite properties can be achieved by careful selection of the glass variables outlined below.

1.1.1.1 <u>Glass type</u>

The majority of fibres produced for the reinforcement of plastics are manufactured from a low alkali content alumina - borosilicate glass, designated as 'E' glass. This material was originally developed to provide enhanced electrical resistance in moulded parts, and in addition possesses a relatively high tensile modulus of 75.9 GNM^{-2} (4). Other glasses, referred to as 'S' and 'R' glass, are produced specifically for their superior tensile moduli and currently find application in high performance laminates associated with the aerospace industry.

In the forming process for glass fibres, the molten glass is drawn from a platinum bushing having up to 4000 'tips' of approximately

1.5 mm diameter - Figure 1.1. During the first one or two centi-
metres attenuation of the filaments, at speeds in excess of 1500
metres/minute, reduces the individual diameters to 3 to 25 microns.
The cooled filaments pass over a carbon roller rotating with a surface
velocity of 15 metres/min., in a trough of 'size'. Gathering of the
individual filaments to form a strand is achieved by means of a carbon
shoe, before finally passing over a traversing, rotating spiral onto a
cardboard former. This primary product is known as a 'cake' and forms
the basic package used to provide the various final products available
to the glass reinforced plastics industry.

1.1.1.2 Filament diameter

Control of filament diameter is achieved by careful adjustment of
the head of molten glass in the bushing, glass viscosity, tip diameter
and winding speed. Common filament diameters range from approximately
10 to 17 microns, although filaments as low as 3 microns in diameter
can be produced.

1.1.1.3 Size coatings

The type and level of binder or size coating applied to the glass
filaments controls the processing performance of the glass fibres and
consequently may strongly influence the properties of the resultant
composite. The basic ingredients are:-

(a) A coupling agent, to promote adhesion between the glass surface
and resin matrix, and additionally to provide resistance to
hydrolytic attack in aqueous environments. Usual coupling
agents employed are silanes although organo chromium and titanium
complexes are known. All silanes presently used can be represented
by the general formula $X-(CH_2)_n Si(OR)_3$ where R = an alkyl
group.

During size preparation the alkoxy groups are hydrolysed to silanols, which by reaction with similar groupings on the glass surface form siloxane linkages $\left(-Si-O-Si-\right)$ which are resistant to further hydrolytic attack.

The group -X- is selected so as to be reactive with the particular organic matrix considered for reinforcement. Table 1.1 indicates typical silane-matrix polymer combinations.

(b) A polymeric film former to promote adhesion between the individual filaments and also with the organic matrix. In addition, the polymer coating serves to protect the filaments from abrasion damage during the secondary conversion and processing operations. Typical film forming materials supplied commercially are polyvinyl acetate emulsions, which when deposited onto the glass surface form a highly irregular film of approximately 0.07 microns in thickness, by coalescence of the polymer particles - Figure 1.2. However, to obtain maximum protection for the glass filaments, it is reasonable to assume that the coating should be of uniform thickness and strongly bonded to the glass surface. Water soluble cationic coatings of this type have been developed (5). The uniform nature of the coating is seen in Figure 1.3.

(c) In addition to the above components, small amounts of lubricants and anti-static agents are often added to the size as processing aids.

1.1.1.4 Split and bundle tex

The splitting of the fibres, achieved after the filaments have passed over the size applicator, can be redeveloped in the final product. Typically, for thermoplastics reinforcement, strands are supplied as 4 split, 2 split and singles. These differences are characterised in terms of linear density or tex, expressed as the weight in grammes of one kilometre of fibre. Obviously bundle tex

will vary with filament diameter, degree of split and number of filaments. A useful formula which expresses the interelation between these variables is given by:-

$$N = 5 \times 10^2 . \frac{Tex}{d_f^2}$$

where N = number of filaments

d_f = filament diameter (microns)

Tex = grams per kilometre

1.1.1.5 Chopped strand length

Defines the as made length of the chopped strand. Typical lengths of fibres for thermoplastics are 3 mm to 6 mm. The actual length will often be dictated as much by strand integrity as by processing requirements. Obviously, the more integral the strand the shorter the attainable length.

1.1.1.6 Products

The 'cake' forms the primary package from which the various final products, available to the glass reinforced plastics industry, originate.

(a) Chopped strand mat

Produced from cakes by cutting into 50 mm strands which fall randomly onto a moving conveyor. The resultant glass fibre mattress is sprayed with a polyvinyl acetate emulsion or dry polyester powder binder to bond the strands together. After passing through gas fired ovens the resultant mat is collected into a roll. This product finds application in the reinforcement of thermosetting matrices.

(b) Rovings

Up to sixty cakes are unwound from the inside, the parallel strands passing through a series of guide eyes and tension gates before being wound into a precision package. Such a process obviously places severe requirements on the glass fibre size in that significant

bushing

tips

water spray

graphite
sizing roller

size

splitter

spiral

collet

cake
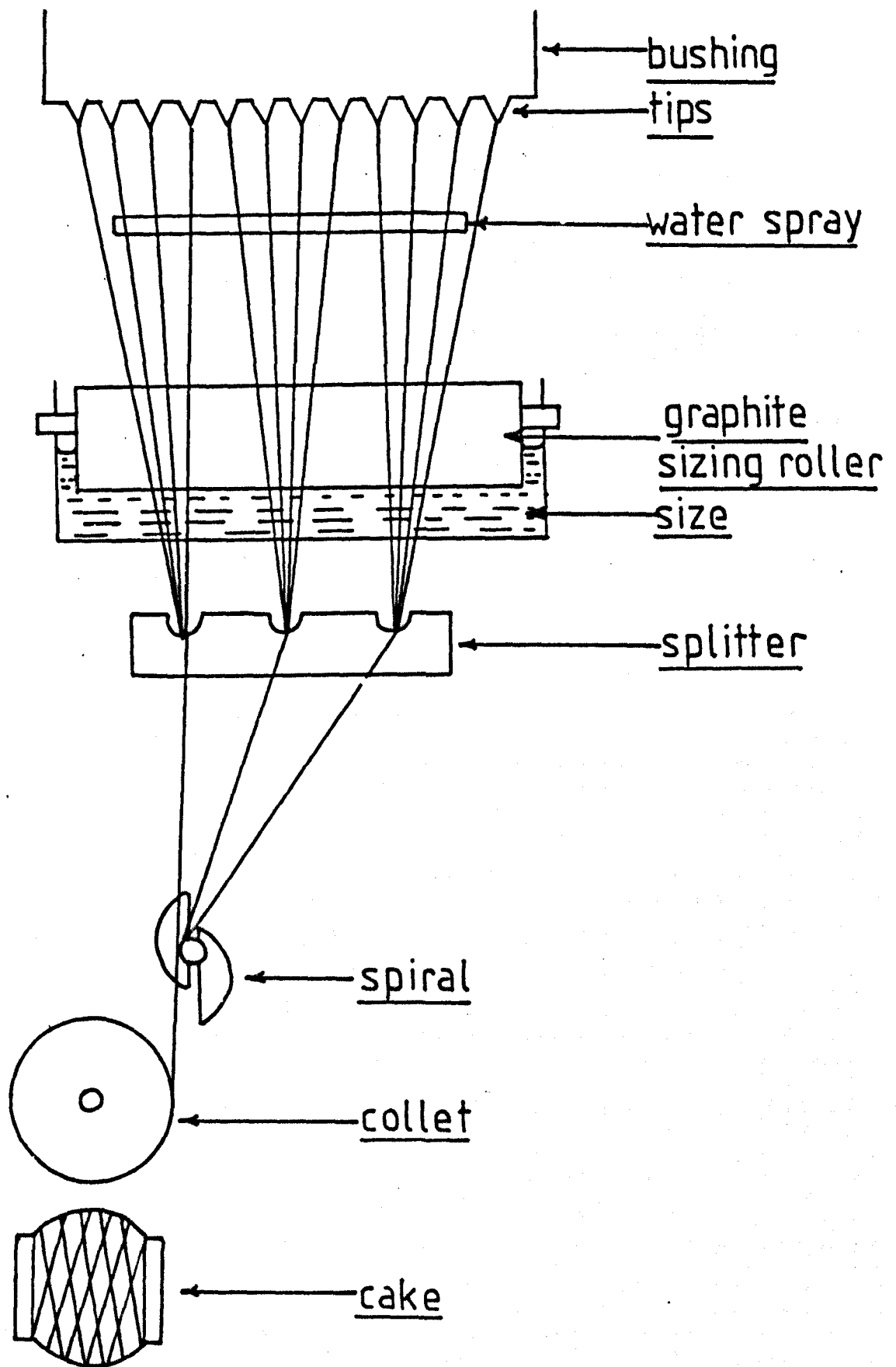
Figure 1.1 glass fiberising unit
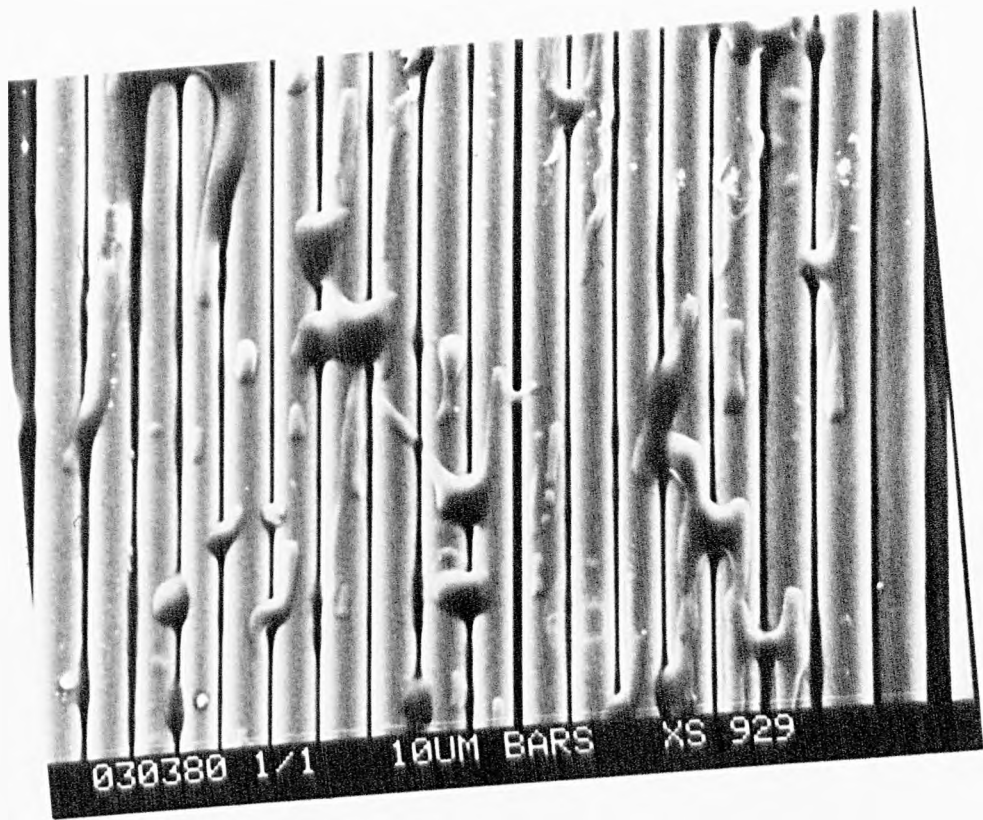
Figure 1.2 polyvinyl acetate sized fibres
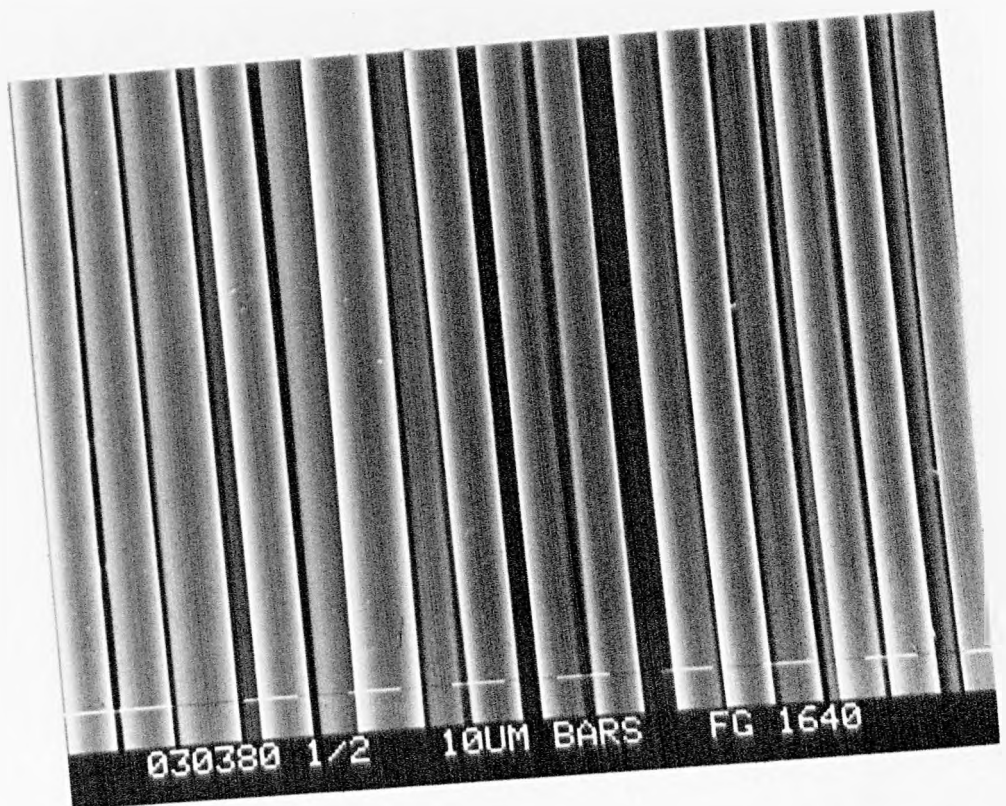
Figure 1.3 cationic polymer sized fibres

SILANE	FORMULA	APPLICATION
vinyltriethoxysilane	$CH_2=CHSi(OCH_2CH_3)$	unsaturated polymers
vinyl-tris(β-methoxy-ethoxy)silane	$CH_2=CHSi(OCH_2CH_2OCH_3)_3$	unsaturated polymers
vinyltriacetoxy silane	$CH_2=CHSi(OOCCH_3)_3$	unsaturated polymers
γ-methacryloxypropyl trimethoxysilane	$CH_2=C(CH_3)COO(CH_2)_3Si(OCH_3)_3$	unsaturated polymers
γ-(β-aminoethyl)amino-propyltrimethoxysilane	$H_2NCH_2CH_2NH(CH_2)_3Si(OCH_3)_3$	epoxides, phenolics, nylon
γ-aminopropyl-triethoxysilane	$H_2NCH_2CH_2CH_2Si(OCH_2CH_3)_3$	epoxides, phenolics, nylon
γ-glycidoxypropyl-trimethoxysilane	$\overset{O}{CH_2CHCH_2O(CH_2)_3Si(OCH_3)_3}$	almost all resins
γ-mercaptopropyl-trimethoxysilane	$HSCH_2CH_2CH_2Si(OCH_3)_3$	almost all resins
γ-chloropropyl-trimethoxysilane	$ClCH_2CH_2CH_2Si(OCH_3)_3$	epoxides

Table 1.1   typical silane – matrix combinations

abrasion damage can result if glass to glass, or glass to metal contact occurs due to breakdown of the size film. Careful selection of polymer coating and lubricants is required if an acceptable roving is to be produced. This product is used in the reinforcement of thermosets, either in the roving form for filament wound pipes, or as chopped roving for sheet moulding compounds. In addition, rovings are finding application in the twin screw extrusion compounding of glass filled thermoplastics (6). However, the major product used in the reinforcement of thermoplastics is chopped strand.

(c) Chopped strands

These are produced directly from cakes and range from 1.5 mm to 12 mm in length. Typical lengths for thermoplastics reinforcement are 3 mm and 6 mm, being supplied as either singles or 2 split strands. Common filament diameters are 10 and 11 microns, designated as 150 tex and 190 tex, respectively. This product is the major form in which glass is supplied for thermoplastics reinforcement, being particularly suited to the various compounding processes presently used to produce an intimate blend of thermoplastic matrix and fibre reinforcement.

Throughout this study a cationic sized glass, coded F.G.C.S. 1640 was used, which is specifically supplied by Fibreglass Limited for the reinforcement of Nylon 6.6. This material is supplied as 3 mm, 190 tex, 2 split strands although for the purpose of this investigation 1.5 mm and 5 mm 190 tex strands were also prepared. In addition, filament diameters of 10 micron (150 tex) and 14 micron (306 tex) were made and chopped to 3 mm lengths.

1.1.2 Thermoplastics conversion processes

Two distinct but often complimentary processes are used for the conversion of thermoplastics into finished products:-

1.1.2.1 The Extrusion process

Extrusion as a manufacturing process is considered to have

originated at the end of the eighteenth centry, the first extrusion
machine being attributed to Joseph Bramah (7). Early machines were of
the ram type in which the polymer charge was melted by means of a
heated cylinder and then moved forward by a plunger. This type of
extruder gave minimal mixing and in addition cycle times were long due
to the necessity to retract the plunger to introduce a fresh charge.
A number of attempts were made to overcome these limitations, resulting
in the development of an extrusion machine employing an Archimedean
screw in 1879 (8). A schematic diagram of such a machine is illustrated
in Figure 1.4.

Basically, solid material in granular or powder form, is
supplied to the rotating screw through a feed hopper which is located,
radially or tangentially, at the opposite end to the die. The solid
polymer is transported from the feed opening, through the heated
barrel zones, and finally consolidated by forcing the molten material
through the die. Melting of the solid thermoplastic is achieved both
by conducted heat, supplied by the barrel heaters, and by viscous
heat dissipation induced by the shearing action of the screw upon
the melt film between the solid material and the barrel inner wall.

The machine described above is referred to as a plasticating
extruder in that it performs both melting and processing functions.
Similar machines are used by polymer manufacturers to process molten
material direct from the reactor. These single screw melt pump extruders
are used solely to mix and pressurise the polymer, prior to extrusion
into a form suitable for use in the various manufacturing processes.
This type of machine is not considered in this work.

In addition to single screw extruders, twin and multiscrew
machines are commercially available (9). These machines are supplied
for the low shear mixing and compounding of dry blends of polymeric
materials containing various additives. At the present time, however,

single screw machines are still the most widely used for compounding processes.

1.1.2.2 Injection moulding

This process is the most common and versatile method for converting thermoplastics into useful articles, being particularly suited to the mass production of many components presently finding application in the automobile and domestic markets, respectively. As with extrusion, an Archimedian screw rotating in a heated barrel is used to process the thermoplastic polymer. The polymer passes down the screw channel to the front of the screw, and as the material accumulates, the screw is forced back against a pressure pad. When sufficient material has gathered in front of the screw (adjusted with limit switches) the screw stops rotating. The screw then acts as a plunger and pressure is applied to the material to inject it into the mould. Flow back of polymer is prevented by a back flow stop valve at the tip of the screw.

1.1.3 Production of glass fibre-filled thermoplastics

The dispersion of glass fibres in a thermoplastic matrix is more difficult than with liquid thermosetting systems, due to the relatively high melting points (100°C to 400°C) of these plastics coupled with their extremely high viscosities. Direct injection moulding of glass fibre - thermoplastic 'dry' blends normally leads to problems of high differential shrinkage and poor surface finish, associated with undispersed glass bundles in the finished article (10). It is thus customary to precompound the glass fibres and polymer to provide the initial "wetting" of the fibres.

The first recorded incorporation of glass fibres into thermo-plastic matrices was by Du-Pont De-Nemours and Co. in 1945 (11). Hammer milled fibres, produced by pulverising glass fibre strands until they passed through a 250 micron screen, were dry blended with

cellulose acetate, methyl methacrylate or synthetic polyamides and
passed through a single screw plasticating extruder. The resultant
compounds were diced to produce material suitable for injection
moulding. Problems of poor feeding in these early products, produced
by bridging in the feed hopper and segregation of fibres and polymer,
led to the introduction of the Fiberfil process in 1952 (12).
Glass fibre roving was passed through the polymer melt or polymer
emulsion to produce a coated strand which was subsequently chopped
into pellets. These pellets contained fibres ranging in length from
8 mm to 12 mm with the fibres parallel to the long axis. Variations of
this basic process are still utilised in the production of long glass
fibre reinforced products. However, problems associated with dispersion
of the fibres in the resultant injection moulded article, led to a
re-appraisal of the use of 'short fibres' as a means of producing
compounds suitable for injection moulding.

1.1.3.1 Extrusion of short glass fibre - polymer blends

As in the previously outlined process used for the base polymer
(Section 1.1.2.1) a single screw plasticating extruder is used to
process the glass fibre - thermoplastic blend. Generally the fibres
are tumble blended with the polymer pellets and introduced through the
feed hopper. Feeding problems encountered previously are minimised by
careful selection of initial fibre length and by improvements in
glass fibre sizing technology. Variations in which the glass is added
downstream into the molten polymer are used, but careful control of
the glass and polymer feeds is required to maintain a consistent glass
content in the final extrudate.

The presence of glass fibres imposes little constraint on the
mode of processing adopted, extrusion conditions generally being
similar to those of the base polymer. The abrasive nature of the
glass fibres, however, is reported to lead to increased wear and thus

it is common practice to nitride both barrel and screw to minimise this problem. (13)

1.1.4 Extruder screw design

Thermoplastic materials differ widely in their thermal properties. An extrusion screw is normally designed with characteristics for one particular material, however, general design features fall into three specific classes (14). Figure 1.5 illustrates three basic designs of screw in common use. The general purpose screw is characterised by a gradual reduction in channel depth in the long compression section and generally finds application for those materials which are essentially amorphous in nature, i.e. polypropylene, low density polyethylene. The gradual increase in the core diameter is designed to allow for the gradual melting of the thermoplastic as it passes through the extruder. In contrast, the rapid transition screw is used specifically for the highly crystalline thermoplastics, which exhibit sharp melting points and in addition possess low melt viscosities. Typical materials in this class are the synthetic polyamides and linear thermoplastic polyesters. An additional refinement of the latter screw is the two stage screw, which can be considered as two screws driven in series on the same shaft. Such screws are of necessity longer than single stage screws, length to diameter ratios of 32 being common, compared with 20-25 for single stage machines. Two stage screws are used in combination with vented barrels, and thus improve the quality of the extrudate by allowing moisture vapour and other volatiles to escape from the melt in the decompression region. Nylon 6 and 6.6, both unreinforced and fibre-reinforced, are processed almost exclusively on the latter type of extruders.

Since glass fibre reinforced nylon 6.6 has been used for the purpose of this study, extrusion processing investigations have been confined to two stage screws.

1.1.5 Extruder screw geometry

Figure 1.6 indicates a cross section of a typical single screw extruder. Although the screw shown has only a single flight multiple start screws are known. All the results obtained in this investigation are for single start screws and thus discussion will be limited to these.

In order to simplify the derived geometrical relationships the following assumptions are generally made (15):-

(a) The sides of the flight are radial to the screw axis.

(b) Channel depth, H, is constant across the channel width.

(c) Chamfers or fillets on the flights are neglected.

Such assumptions are generally valid for most screws.

Further simplifications involve two important assumptions:-

(i) The barrel is considered to rotate about a stationary screw. This assumption is allowable due to the viscous nature of the polymeric materials used. Since flow is laminar and the Reynolds number low then the effect of centrifugal forces on the radial pressure distribution is insignificant.

(ii) The stationary screw channel is considered to be "unwound" from the root of the screw and laid on a flat plate. Thus a Cartesian co-ordinate system is used in place of the true helical co-ordinate one. Figure 1.7 shows the screw of Figure 1.6 unrolled onto a plane through the flight tips formed by cutting along a line parallel to the screw axis.

A fuller treatment of these assumptions is given in reference (16).

1 1.6 Basic design calculations and terminology

1.1.6.1 Screw pitch (P)

Defined as the distance in an axial direction from the centre of a flight at its periphery to the centre of the next flight.

Most screws are "square pitched" in that the pitch is the same as the internal barrel diameter.

1.1.6.2 Helix angle (θ)

Defined as the angle of the flight at its periphery relative to a plane transverse to the screw axis.

Consideration of Figure 1.7 gives:-

$$\theta = \tan^{-1}\left(\frac{P}{\pi(D-2c)}\right)$$

for a square pitched screw P = D

$$\therefore \quad \theta = \tan^{-1}\frac{1}{\pi}\left(1 - \frac{2c}{D}\right) = 17.7^{\circ}$$

1.1.6.3 Radial screw clearance (C)

Defined as the radial distance from the outside diameter of the screw to the inside diameter of the barrel. The nominal radial clearance is generally $2D \times 10^{-3}$ (17).

1.1.6.4 Screw channel width (W)

The direction across the screw channel in a direction perpendicular to the flight, measured at the periphery of the flight.

The channel width is given by:-

$$W = \pi(D-2c)\sin\theta - e$$

1.1.6.5 Helical length (Z)

The length along each helical channel is given by:-

$$Z = \frac{L}{\sin\theta} \qquad \text{where L = axial length}$$

It is often useful to define the position along the screw in terms of a number of "turns" or pitch lengths from the feed hopper, i.e.

$$L = nP = nD$$

where n = number of turns.

1.1.6.6 Velocity components of flow

The Cartesian coordinate axes (x, y, z) are defined as illustrated in Figures 1.7 and 1.8. Also illustrated in Figure 1.7 is the portion of the barrel surface moving with velocity V relative to the screw, such that $V = \pi DN$. This velocity may be resolved into components parallel and perpendicular to the channel, i.e.

$$V_z = V \cos \theta$$

$$V_x = V \sin \theta$$

1.1.6.7 Compression ratio

The factor obtained by dividing the developed volume of the screw channel in the feed section, by the developed volume of the screw channel in the metering section is referred to as the compression ratio - Figure 1.9. Obviously for a two stage screw there will be two such compression ratios, referred to as the primary and secondary compression ratios, respectively. In general the secondary compression ratio will alway be lower than the primary for the reason given in the following section.

1.1.6.8 Channel depth ratio

As expected this relates the various channel depths. For a two stage screw, the ratio of the channel depth found in the final metering section to that found in the primary metering zone is often referred to as the pump ratio. Typical screws used for nylon extrusion have pump ratios of 1.3 - 1.7 : 1. This deepening of the channel in the final section is necessary to ensure a greater volumetric capacity for the final metering zone than the primary metering section. Such a system ensures that the decompression section will normally run well below its maximum carrying capacity, thereby facilitating the removal of volatiles through the barrel vent. Obviously, increased pressures at the die, caused by reducing the die diameter, will ultimately reduce the output of the second stage to below that of the

primary screw, which normally discharges at atmospheric pressure

or below if a vacuum vent is used. Such a situation will result

in polymer exuding from the vent in the barrel, unless some means

of "throttling" the output of the primary screw is provided.

Since, during the course of this study, it was often necessary

to employ high die pressures the vent was left sealed, the polymer

being used directly from previously unopened bags to prevent any

moisture contamination. No problems were encountered in operating

any of the extruders in this manner.

1.1.6.9 Shear rate

The mean shear rate, $\overline{\gamma}$, is generally calculated as the

velocity of the melt in the downstream direction divided by channel

depth, i.e. $$\overline{\gamma} = \frac{V_z}{H} = \frac{\pi D N \cos.\theta}{H} \ sec^{-1}$$

Whilst a knowledge of the shear rates is important from

a processing-design viewpoint, it is to be expected that in terms

of glass fibre degradation, a knowledge of the shear stress would

be more relevant. Such shear stresses will obviously be dependent

upon the shear rate, melt viscosity and temperatures encountered in

the extrusion process. Variations in the above parameters are likely

to influence the degree of fibre fracture occurring in the various

zones of the extruder.

1.1.6.10 Dimensionless parameters

Combining the physical variables to form dimensionless

parameters allows comparisons to be made without specific reference

to actual screw dimensions or material properties (18). Typical

dependent variables which can be expressed in dimensionless form are

pressure gradients, melt temperatures and flow rates.

The most widely used parameter is the dimensionless flow rate, π_Q,

which expresses the ratio between the actual volumetric flow rate,

Q, and the rate which would be achieved if all the melt moved down

the screw channel with the same relative velocity, Vz, as the barrel in the direction parallel to the flight i.e. $\Pi_Q = Q/WHVz$

1.2 Processes occurring in single screw plasticating extruders

Consideration of Figure 1.4 indicates the three geometrical sections of a typical single stage screw extruder. These sections are normally associated with the functions of solid conveying, melting, and mixing and metering of the resultant melt. In reality there is often considerable overlap, melting for example often commencing in the feed section and continuing well into the metering section (19).

(a) Solids conveying

This region is often limited to the first few turns of the extruder screw and is characterised by the complete absence of molten material. Transport of the solid material occurs by virtue of the differential friction existing between the solid material and the screw and barrel surfaces. The degree to which solids are conveyed will depend upon the geometry of this zone, material bulk density, screw speed and frictional coefficients (20). Efficient solids conveying requires a high coefficient of friction at the barrel surface and minimal friction between the solid material and screw. Increasing the bulk density of the solid will improve the solid conveying capacity, such an increase often being achieved by forced feeding. However, this type of operation can have undesirable side effects in that entrapped air is prevented from escaping, resulting in the poor appearance of the finished product. Such a situation will obviously not apply when using a vented machine. When processing glass fibre polymer blends, variations in feed stock bulk density occur due to changes in the glass fibre parameters i.e. fibre length, bundle tex and strand integrity (-see Section 3.1.3). Maximum packing conditions for fibres of various lengths and for various fibre-sphere

combinations have been extensively studied by Milewski (1). His results indicate that a reduction in bulk density will occur with increasing fibre length and fibre concentration. Such changes in bulk density will obviously affect the power requirement, although the overall importance of the power consumed in this region, in relation to the total power consumption, will largely depend on operating conditions for a particular machine. It is to be noted, therefore, that comparisons of total power consumptions are only strictly relevant if feed stock densities are unchanged.

(b) Transition or melting zone

Melting apparently commences with the appearance of a thin melt film between the hot barrel surface and the compacted solid in the screw channel. However, molten material has been observed to flow into the gaps in the solid prior to the formation of the melt film (21). The thickness of the melt film increases as the solid moves down the screw channel until ultimately it reaches a thickness several times the flight clearance. This region is referred to as the delay zone (22) and transport is considered to be due to viscous drag at the barrel surface, whilst Coulomb friction at the screw surface is the dominant mechanism.

Development of the steady state melting mechanism commences with the removal of a portion of the melt film by the advancing flight. The motion of the barrel, relative to the solid bed, sweeps the collected melt into the melt pool region between the solid and the leading edge of the flight. As melting progresses the melt pool increases in width in the down channel direction, exerting a pressure on the solid bed and thus forcing it to continuously deform and supply solids to contact the melt film. The solid bed is continuously "flowing" into the melt film, in addition to its movement in the down channel direction, and thus whilst maintaining an approximately constant

height its width is continuously decreasing.

The above description is based on the most commonly observed melting mechanism (23) (24). Figure 1.10 indicates a typical section through the contents of a screw channel in the melting region, viewed from the screw in the downstream direction towards the die. In reality the corners of the solid bed are rounded due to the slightly curved nature of the channel. Four distinct regions can be observed, comprising the upper and lower melt films and solid bed and melt pool regions, respectively. The lower melt film, which also comprises the film at the trailing edge of the flight, will only be formed when the screw temperature exceeds the melting point of the polymer. Since the motion of the solid, relative to the screw, is in the downstream direction, the lower film grows in thickness in this direction. This growth can be considerable due to the retention of all melted material.

Completion of melting, which is often only achieved well into the metering section, can occur in various ways. If the process is stable and the solid bed remains continuous in the downstream direction, the corners of the bed become rounded and its width or depth diminish to negligible proportions. The final disappearance of the bed can be quite rapid once the temperature of the bulk of the solid has risen close to the melting point. In many cases, however, the melting process becomes unstable in the sense that the solid bed fractures along planes normal to the downstream direction. The resulting pieces of compacted solid then continue to melt either by conduction or under the influence of the shearing action of the surrounding melt films. Such solid bed break-up was observed by Martin (25) and Tadmor et. al. (16). The fracture of the solid bed observed by the above workers differed in that the former experiments indicated that wedging of the solid between the barrel and

screw root, due to the short compression section, was the prime

cause of break-up. In the latter case, however, breakage of the

solid bed did not appear to be caused directly by screw taper,

which in this case extended gradually over about ten "turns"

of the screw. Further work by Donovan (26) confirmed the observations

of Tadmor et. al. Although computer programmes were already in

existence to model the melting process, they did not provide a

realistic description of solid bed motion particularly in the later

stages of melting. Donovan, working from experimental observations,

questioned the previously held assumption of constant solid bed

velocity and thus modified the previously used Tadmor model (16)

to allow for a solid bed acceleration parameter. More recent work

by Edmondson (27) and Fenner et. al. (28) demonstrated a close

correlation between the observed start of solid bed break-up and

the predicted onset of rapid bed acceleration. Once a break

has occurred, the gap is filled with melt, and the newly formed end of

the continuous part of the bed moves downstream until another break

occurs under the influence of the applied accelerating forces.

Bed break-up is thus a periodic instability occurring at frequencies

of the order of five to ten times lower than that of screw rotation.

Edmondson and Fenner also observed that bed break-up only occurred

when a melt film was present at the screw surface. Work using

cooled screws (16) confirms these observations, since such cooling

delays the formation of this lower melt film, thereby maintaining

a more stable balance between the shear forces acting on the bed.

Although most published experimental work serves to confirm

the melting pattern described above, there are some significant

exceptions. Street (29) observed that conduction melting occurred

at the interface of the melt pool and solid bed, leading to fusion of

the polymer granules in this region. However, such behaviour has

been attributed to the lack of compaction of the solid due to the constant channel depth screw used (27). Menges and Klenk (30), working with rigid P.V.C. powder, noted that melting appeared to occur mainly in the clearance between the flight land and the barrel, with a form of melt pool developing against the trailing edge of the flight. The overall melting rate was slow with solid material always remaining at the end of the screw. This difference in melting mechanism was attributed by the above workers to the non wetting nature of P.V.C. However, further work by Gale (31) indicates that for P.V.C. powder the melting mechanism is highly dependent on the type and concentration of lubricant used. Finally Lindt (32), using a 90 mm diameter extruder, observed that melt remained in relatively thick films surrounding the solid bed, when processing various polypropylenes, and proposed a suitable melting model.

The literature reveals only a single reference to the melting of a glass fibre filled polymer (33). In this instance a 20% by weight blend of short glass fibres and polyethylene was extruded in a variety of machines and correlations drawn between the length of the melting zone and the degree of fibre degradation occurring. However, no observations of the actual melting process were made. Also, with the exception of Martin (25), published melting studies for unfilled polymers are for screws having gradually reducing channel depths in their compression sections. As mentioned previously, glass fibre filled nylon 6.6 is processed almost exclusively on two stage screws having a rapid transition (normally one half turn) in the primary screw. It is felt that an in depth study of the melting process for this material, and its effect on fibre degradation, will provide a valuable insight into the mechanism of fibre attrition which occurs during the plasticating extrusion of glass fibre - nylon 6.6 blends.

(c) <u>Metering zone</u>

This section follows the melting zone and is characterised
by the absence of unmelted polymer, its length is thus dependent
on the previous processes. The degree of homogeneity of the extrudate
will obviously depend upon the efficiency of the metering zone in
providing adequate mixing of the molten material (34). An exact
definition of mixing, however, is difficult and of necessity must be
statistical owing to the random nature of the mixing process.

Dankwerts (35) divided mixing into two independent categories,
namely the scale of segregation and intensity of segregation. The
scale of segregation is a measure of the mean size of regions of
the same component in the mixture and is affected by both dispersive
and distributive mixing. Dispersive mixing reduces the agglomerate
size of the minor constituent of the mixture and thus depends upon
the stresses in the major component (36). Distributive mixing,
however, produces an increase in the randomness of the spatial
distribution of the minor component with no change in the ultimate
particle size. In a single screw extruder distributive mixing is
generally the more important. However, numerous special mixing
devices are now available which can be added to conventional screws to
improve the overall mixing performance. Such devices are blisters,
smear heads, torpedoes and barrier type mixing sections (37) (38).
These devices function by increasing the level of dispersive mixing
and also disturb the established flow and temperature profiles.

The intensity of segregation represents the concentration
difference between the components and as such is constant in the
extrusion process. According to McKelvey (36) an extrudate is
considered to be well mixed when the scale of segregation is less
than the scale of examination.

feed hopper

heated barrel surface

feed zone | compression zone | metering zone | die zone
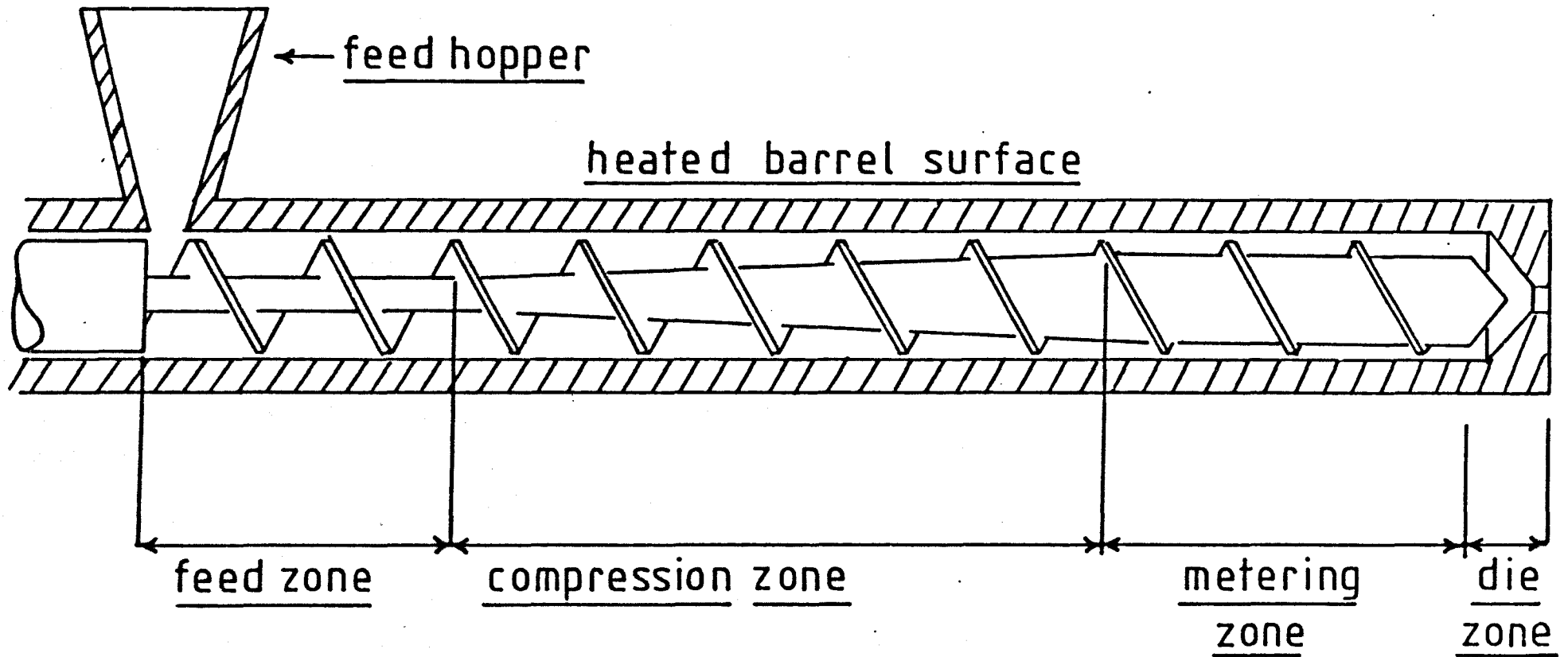
Fig.1.4 diagrammatic cross section of a single screw plasticating extruder

(a) gradual transition screw

metering compression feed

(b) rapid transition screw

metering compression feed

(c) two stage screw

secondary metering compression decompression primary metering compression feed
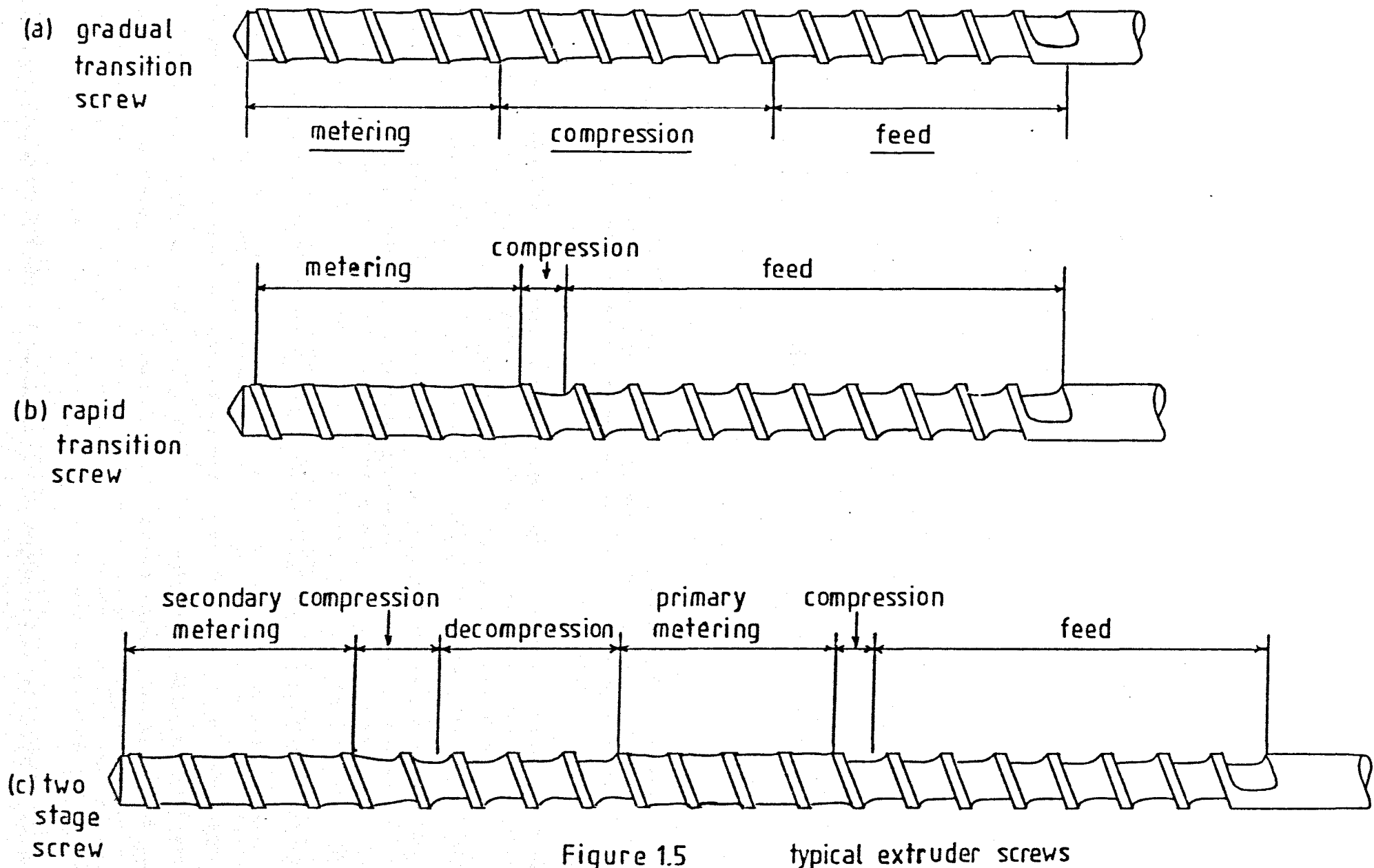
Figure 1.5   typical extruder screws
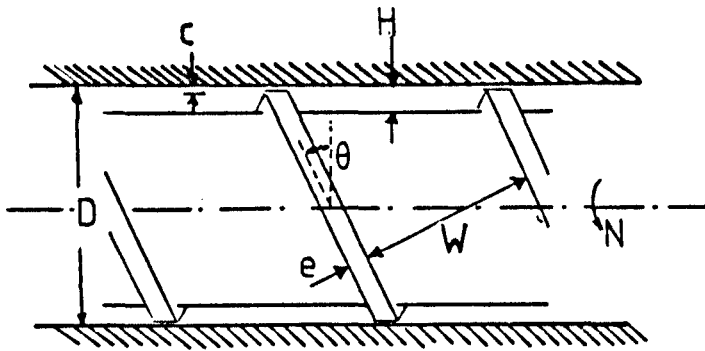
figure 1.6 geometry of an extruder screw

(single flighted)
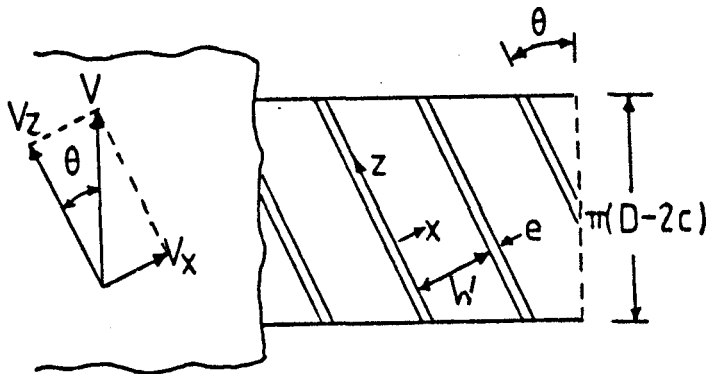
figure 1.7 cartesian coordinate system
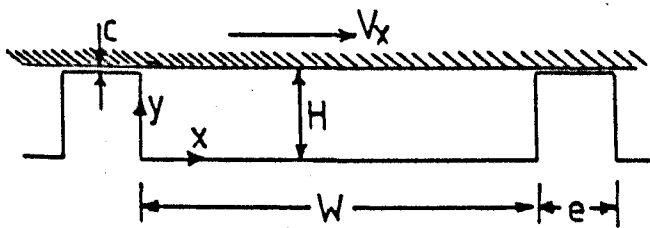
figure 1.8 view in downstream direction

assume $W_s \doteq W_b$
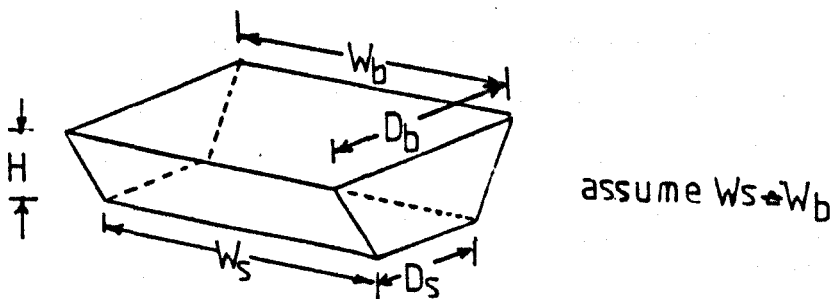
compression ratio:- $\dfrac{H_f(D_b - H_f)}{H_m(D_b - H_m)}$ figure 1.9
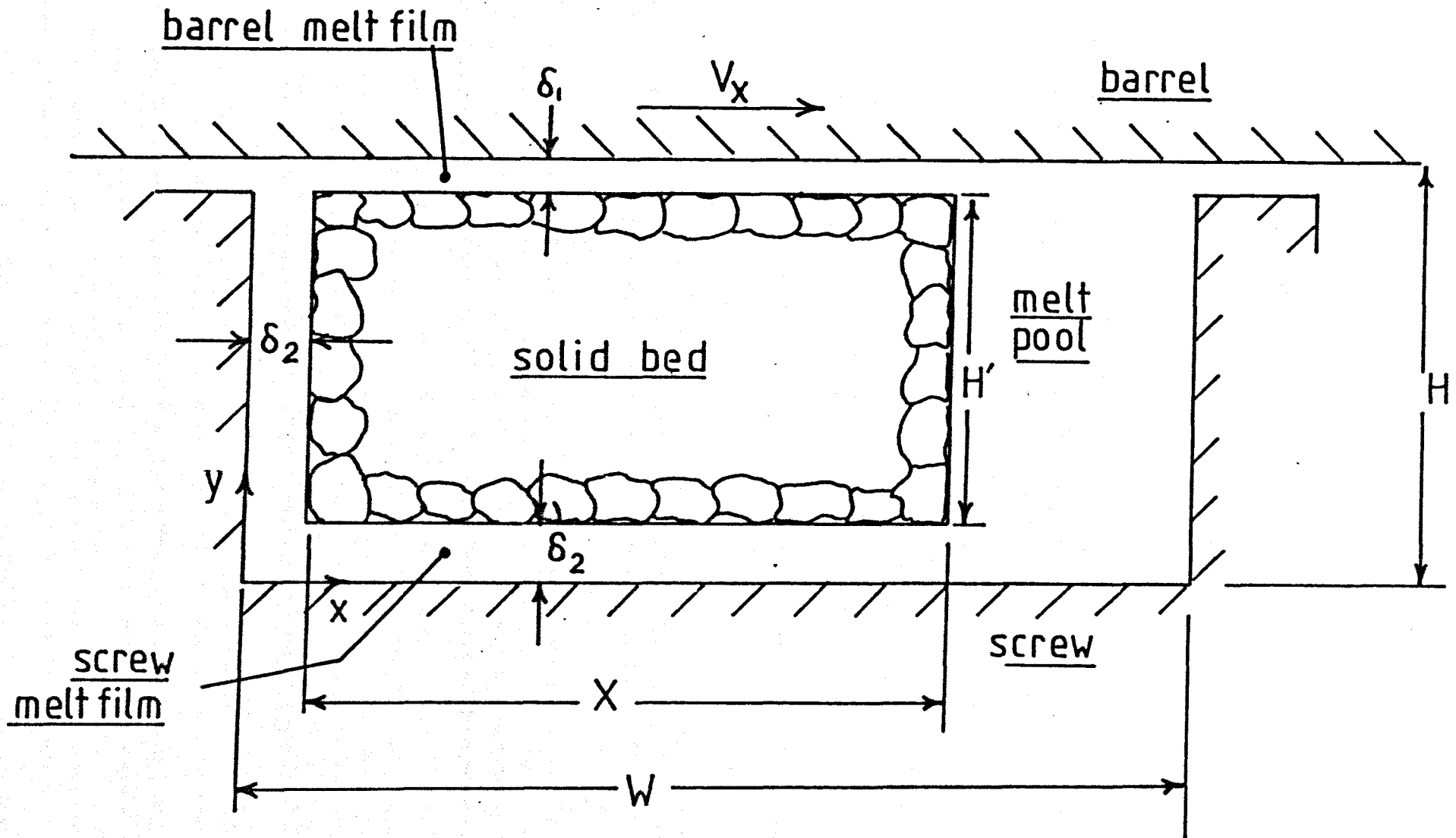
Figure 1.10 cross section of melting region

$$a = \frac{y}{H} = \frac{\text{particle depth}}{\text{channel depth}}$$

$t = \quad$ residence time

$t_o = \quad$ minimum residence time $(a = \frac{2}{3})$
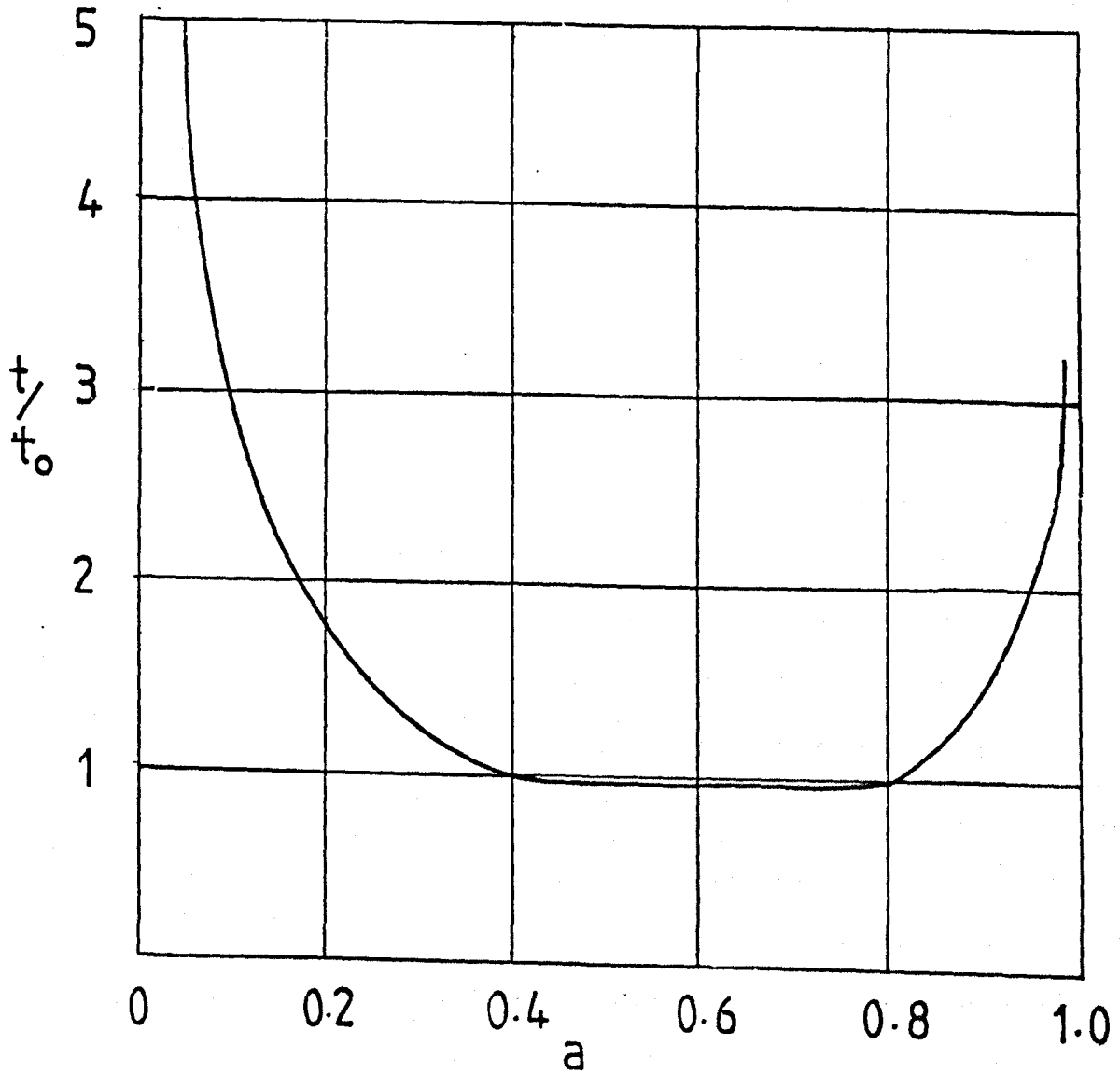
figure 1.11 relative residence time distribution

In a screw extruder particles experience different strain histories according to their initial geometrical location between screw and barrel. Mohr et. al (39) and McKelvey (36) derived expressions for the resulting strain distribution. Their derivations, which were based on the isothermal, Newtonian parallel plates flow model in screw extruders, indicate that the extrudate will not be uniformly mixed. Thus, for example, particles which are close to the screw root or barrel surface will attain a higher level of strain and hence achieve better mixing than those which enter in the neighbourhood of the centre of the channel. Obviously, particles near the centre of the channel will have the shortest residence in the extruder. Particles at the screw root and barrel surface will theoretically have an infinite residence time. However, due to interchange with particles in other fluid layers, all particles will eventually pass through the extruder, although those at the screw root may take a considerable time to do so. Such a "residence time distribution" as a function of initial position is indicated in Figure 1.11. This distribution indicates the variation in residence times for particles passing through the metering zone. Therefore, the total strain experienced by any particle will be the product of the shear rate and residence time. Fenner and Cox (28) advocate the use of a single parameter for describing the overall performance of an extruder known as the "Bulk Mean Mixing Parameter" ($\bar{M}$). Such a parameter is described by the product of the mean shear rate and average residence time in the molten state. The degree of fibre degradation occurring in the metering section of the extruder would be expected to be influenced by the residence time spectrum for the glass fibres.

1.3 Market trends - glass reinforced thermoplastics

The growth of the glass reinforced thermoplastics industry has been extremely rapid, expanding from an annual consumption in Europe

of 2,500 tonne in 1966 to 73,000 tonne in 1978 (40). Captive areas

include the automotive industry, communications, electrical and

domestic markets. Equivalent mechanical and thermal properties,

coupled with ease of processing has led to the replacement of many

components previously manufactured from aluminium and zinc. In both

Europe and the U.S.A. the transportation market provides the largest

outlet for glass reinforced thermoplastics. The actual amounts

consumed are highest in the U.S.A., probably reflecting the more

energy conscious attitude. Glass reinforced polyamides remain at an

impressive 58% of all thermoplastics reinforced in Europe the picture,

however, being quite different in the U.S.A. with polyolefins occupying

a prominent position in the market place.

Perhaps the most outstanding reinforced thermoplastic is glass

reinforced nylon 6.6. The 40% by weight glass reinforced material

possesses a tensile strength of 220 MNm^{-2} and a 0.5% tangent

modulus of up to 12.6 GNm^{-2} (see Section 3.3.2). In addition, a

heat deflection temperature of 500°F places it amongst the die cast

metals in terms of performance and superior to the common high

temperature thermoplastics such as polysulfone and poly(phenylene oxide).

As for the future, price increases in petrochemical products will

inevitably lead to cost increases for glass fibre reinforced thermo-

plastic resins. However, according to Schumann (40) the cost-performance

ratio for these materials is still highly favourable. Predictions of

an annual growth rate of 10-12% into the late 1980's are given, major

expansions occurring in the electrical and automotive industries.

1.4 Objectives

The incorporation of glass fibres into a thermoplastic matrix

leads to engineering products which compete successfully in markets

traditionally occupied by metals. However, full realisation of

properties can only be achieved by an understanding and subsequent

control of the various factors which determine composite strength. The major variables which are considered to have a dominant influence on composite performance for a particular matrix are:-

    (a) Specific fibre orientation distribution

    (b) Interfacial shear strength

    (c) Fibre aspect ratio distribution

Of these factors, control of fibre length has received the greatest attention (41), (42), (43).

It is generally accepted that to achieve optimum reinforcement the fibre length in the final moulding must be maintained at the highest possible level consistent with processability. However, the presence of undispersed strands is undesirable since such fibre 'bundles' can cause a reduction in composite strength due to inadequate 'wetting' of the individual filaments (10). Discussions have centred on the relative merits of the various compounding methods in producing adequate dispersion of the fibres whilst preventing significant fibre attrition (41). These considerations are not helped by the absence of accurate techniques for determining this fibre degradation. Assessment of such fibre diminution is therefore often arbitrary, reliance generally being placed on final composite properties.

In addition, precompounding of the glass fibre polymer 'dry' blend in single screw plasticating extruders is still the major method of producing moulding compounds, particularly from the prominent engineering thermoplastics such as nylon 6 and 6.6. However, no investigations regarding the processes by which fibres are degraded whilst passing through the various functional zones of the extruder, are recorded. Such information is obviously vital to the understanding and subsequent control of fibre degradation occurring during the manufacture of glass fibre - thermoplastic composites. Therefore, the objectives of this study are:-

(i)   To develop techniques to enable the quantitative measurement of the effect of the various extrusion, polymer and glass fibre parameters upon the extent of fibre degradation occurring during the processing of glass fibre - nylon 6.6 blends.

(ii) To apply such techniques to the resultant injection moulded composites and thereby establish the influence of the resultant fibre length distribution on composite performance. ·

(iii) To examine the processes occurring during the passage of the glass fibre - nylon 6.6 blend from the feed hopper to the extrusion die and hence correlate the pattern of fibre degradation with the observed melting and mixing processes.

1.5 Fibre reinforced composites

The importance of fibre length in controlling the degree of reinforcement achieved when fibrous materials are incorporated into a polymer matrix, may be illustrated by reference to composite theory. The simplest model is based on the law of mixtures.

1.5.1 Law of mixtures

Consider an idealised composite as illustrated in Figure 1.12. The fibres are considered to be uniformly dispersed and the load carried by the composite is shared between the fibres and matrix, respectively. In addition, it is assumed that the fibres are uniform, continuous, unidirectional and perfectly bonded to the matrix such that no slippage can occur at the interface. Thus the total load carried by the composite is given by:-

$$L_c = L_f + L_m$$

where the subscripts C, f, m, represent the composite, fibre and matrix respectively.

The above relationship can also be expressed in terms of the stress carried by the components, i.e.

$$\sigma_c = \sigma_f A_f + \sigma_m A_m \dots \dots 1.1$$

where σ = stress and A represents area.

Since the area fractions are constant in the direction of the applied load, then equation 1.1 can be written as:-

$$\sigma_c = \sigma_f V_f + \sigma_m V_m \qquad \text{and since } V_m = (1-V_f)$$

then $\qquad \sigma_c = \sigma_f V_f + \sigma_m (1-V_f) \text{\_ \_ \_ \_ \_} 1.2.1$

where V_f is the fibre volume fraction

If no slippage is allowed at the interface, then the strain experienced by the composite, matrix and fibres will be equal and thus from equation 1.2,1 $\qquad \sigma_c = E_f \varepsilon_c V_f + E_m \varepsilon_c (1-V_f) \text{\_ \_} 1.2.2.$

where ε = strain and E = Youngs' modulus

thus:- $\qquad E_c = E_f V_f + E_m (1-V_f) \text{\_ \_ \_ \_} 1.2.3.$

Equations 1.2.1 and 1.2.3 indicate the law of mixtures formula for composite stress and modulus respectively. Finally from equation 1.2.2 it is evident that the ratio of the load carried by fibres to that carried by the matrix is given by:-

$$L_f / L_m = \frac{E_f V_f}{E_m (1-V_f)}$$

Therefore, for optimum reinforcement it is necessary for the fibre modulus to be much greater than the matrix modulus. The excellent strengths achieved by glass reinforced plastics is due to this ratio being approximately 20.

The above idealised composite model suffers from several deficiencies:-

(i) In reality the fibres and matrix possess different failure strains. Two cases are possible:- (a) $\varepsilon_{fu} < \varepsilon_{mu}$ (b) $\varepsilon_{fu} > \varepsilon_{mu}$.

(a) Figure 1.13 (a) When a weak ductile matrix is reinforced by strong, stiff fibres whose failure strain is less than that of the matrix, two possibilities arise. If the matrix is unable to sustain the additional load imposed upon it when the fibres fail, then composite failure will occur. Alternatively, the fibres will undergo multiple

fracture until the matrix failure strain is achieved.

(b) Figure 1.13 (b) If the matrix possesses a lower failure strain than the fibres, as found in weak brittle matrices, then again two limiting cases are possible. If the fibres can withstand the additional loading when the matrix fails then multiple fracture of the matrix occurs. The matrix is split into a series of thin discs, the thickness of which is determined by the interfacial adhesion between the fibre and matrix. Such behaviour is found in reinforced cement (44) and in glass fibre reinforced polyester moulding compounds (45). In the second case failure of the matrix results in composite failure.

In both brittle and ductile matrices the ultimate mode of failure will be determined by the interfacial bond strength and fibre volume fraction (46).

(ii) As illustrated by Figure 1.14, the composite strength predicted by the law of mixtures formula ultimately reaches that of the reinforcing elements at 100% loading. In reality, whilst almost 91% by volume of cylindrical fibres can be packed into a composite (47), above 80% by volume the ultimate composite properties are usually not achieved. This situation arises due to the inability of the matrix to 'wet' and infiltrate the fibre bundles. The wetting of the strands by the matrix material is necessary to prevent interfilament abrasion and to allow stress transfer of the applied load between the individual fibres. In the absence of such transfer, failure of the weaker fibres will cause an increase in the load carried by the remaining strands, the broken fibres no longer providing any reinforcement. In practice, however, the broken fibres continue to contribute by virtue of load transfer through the elastic or plastic deformation of the matrix at the broken ends. Since this transfer occurs over a finite distance, a portion of the end of each finite length fibre is stressed at less than the maximum fibre stress of a continuous filament. This is

illustrated diagrammatically in Figure 1.15. Thus the average

stress within the broken fibre will be less than in the continuous

case. With successive fibre fractures a length will ultimately

be reached where the maximum stress transferred is below the fibre

breaking stress. This limiting length is referred to as "the critical

fibre length".

1.5.2 Critical fibre length, lc

Defined as the minimum length of fibre necessary for the ultimate

fibre tensile stress to be realised. Thus fibres above this critical

length will be stressed to their ultimate strength and hence fracture.

However, fibres below this minimum length, are incapable of being

stressed to this limit and therefore will slip in the matrix as the

load is increased beyond that permissible by the transfer mechanism.

This "slipping" of the fibre in the matrix acts to relieve the stress

on the fibre, thereby causing transfer of the load to surrounding

fibres or composite failure by shear at the interface.

The variation in stress distribution with length of fibres

is illustrated in Figure 1.16. Whilst numerous theories have been

proposed for describing this stress distribution, two distinct

approaches have emerged:-

(i) Fibre and matrix in the elastic state

Cox (48), Dow (49), Rosen (50) and Fujiwara (51) derived expressions

for the longitudinal stress distribution in discontinuous fibres.

Although different assumptions were made, all the equations may be

reduced to one basic form, namely:-

$$\sigma_f = K_1 \left[\frac{1 - \cosh K_2 \left(\frac{l}{2} - x \right)}{\cosh K_2 \frac{l}{2}} \right]$$

the constants K_1 and K_2 are listed in Table 1.2.

Table 1.2

Author	K_1	K_2
Cox	$\dfrac{(E_f - E_m)\sigma_c}{E_m}$	β
Dow	$\dfrac{P_{eff.}}{A_f + A_m \, ^{E_m}/E_f}$	λ/d_f
Rosen	$\dfrac{\sigma_c \, r_a^2 \, E_f}{E_a(r_a^2 - r_b^2) + E_f \, r_f^2}$	η
Fujiwara (McGary)	$\sigma_c \left(\dfrac{1 + (1 - E_m/E_f)}{E_m/E_f + A_f/A_m} \right)$	λ/d_f

The somewhat lengthy expressions for η and λ may be obtained from the literature references concerned and from Hollister and Thomas's review (126) from which the above table is abstracted. Outwater (52) presented a theory specifically for reinforced plastics. He assumed that the load was completely carried by the fibres and that there was a constant value of stress at the interface, the actual level of stress being dependent on the coefficient of friction between the fibre and matrix. He postulated that these frictional forces were generated by shrinkage of the matrix resin during polymerisation (thermosettting polymers) and that differences in performance, due to fibre surface treatments, were achieved by changes in the frictional coefficient, μ . His equation has the following form:-

$$\sigma_f \, r_f^2 \, \pi = 2\pi r_f \, P \mu x$$

where P = radial resin pressure acting on fibre

   μ = coefficient of friction

   r_f = filament radius

(ii)   Elastic fibre - plastic matrix

In 1965 Kelly and Tyson (53), working with tungsten wires in a ductile copper matrix, presented an analysis for elastic fibres in a plastic matrix. Initially, upon applying a tensile load, both fibres and matrix are considered to deform elastically. However, above a certain load plastic flow is produced in the matrix whilst the fibres continue to deform elastically. Such plastic flow originates at the fibre ends and its effect is to limit the maximum value of the interfacial shear stress, τ , to the shear yield stress of the matrix, τ_y . Since the fibre is still elastic, then at any strain ε , the maximum fibre stress is $\sigma_f = \varepsilon E_f$ (since $\sigma_f / \varepsilon_f = E_f$). For fibre failure to occur the stress transferred must equal the tensile strength of the fibre, therefore:-

$$\pi r_f^2 \varepsilon E_f = 2\pi r_f \tau x$$

and since, as illustrated in Figure 1.16, $x = {}^{L_c}\!/_2$

then $\pi r_f^2 \varepsilon E_f = 2\pi r_f \tau {}^{L_c}\!/_2$

hence $L_c = 2\pi r_f^2 \varepsilon E_f / 2\pi r_f \tau = \varepsilon E_f r_f / \tau$

then $L_c = \dfrac{\varepsilon E_f r_f}{\tau} = \dfrac{\sigma_f D_f}{2\tau} \left(\text{Since } D_f = 2r_f \right) \text{----} 1.3$

Thus, from equation 1.3, the critical length will be reduced by improving the fibre-matrix bond. For polymer matrices the stress-strain curve of the polymer alone is often non-linear and thus there is no sharp division into elastic and plastic behaviour as found in metallic matrices. In many polymer-fibre composites, therefore, both plastic and elastic deformations, in the vicinity of the fibre, occur simultaneously. Piggot (54) combined the models proposed by Cox and Kelly and Tyson to include such a situation. Improvements over the simpler treatment of Kelly and Tyson are, however, minimal and Lees (55) therefore recommends the use of the previous model although it is an approximation of the stress transfer mechanism.

1.5.3 Ultimate tensile strength of discontinuous fibre composites

In considering the ultimate tensile strength of a composite containing uniaxially aligned discontinuous fibres, two conditions are possible.

(i) Fibre length, $L \gg L_c$

In this case the ultimate strength of the fibres will be utilised. The average fibre stress can be determined by consideration of figure 1.16.

$$\text{Area } AEFD \equiv ABCD$$

thus,
$$\sigma_{fult.}\left(L - \frac{L_c}{2}\right) = \bar{\sigma_f}\, L$$

$$\therefore\ \bar{\sigma_f} = \sigma_{fult.}\left(1 - \frac{L_c}{2L}\right) \text{\_\_\_\_1.4}$$

composite tensile strength, σ_c, is given by:-

$$\sigma_c = \bar{\sigma_f}\, V_f + \sigma_m'\,(1 - V_f) \text{\_\_\_1.5}$$

hence
$$\sigma_c = \sigma_{fult}\left(1 - \frac{L_c}{2L}\right)V_f + \sigma_m'(1 - V_f)\ 1.6$$

where $\sigma_m' = $ stress in matrix at fibre breaking strain

Comparisons of equations 1.6 and 1.21 indicate that discontinuous fibres will always be less efficient reinforcing agents than continuous ones. This can be simply illustrated by putting $V_f = 1$ and plotting the theoretical ratio of $\dfrac{\sigma_c\,(disc)}{\sigma_c\,(cont.)}$ against L/L_c for various values of L, Figure 1.17. As can be seen when $L/L_c = 10$, the strength ratio is 0.95. Little loss in reinforcing efficiency is incurred until $L/L_c < 5$, below this value, however, a dramatic reduction in reinforcing efficiency is observed.

(ii) Fibre length, $L < L_c$

The ultimate strength of the fibres is not achieved and composite failure occurs when the matrix is loaded to its ultimate stress. At failure of the composite the stress in the fibre is given by:-

$$\pi r_f^2 \bar{\sigma}_f = \pi r_f \tau \frac{L}{2} \quad \therefore \quad \bar{\sigma}_f = \frac{\tau L}{D}$$

hence substitution into equation 1.5 gives:-

$$\sigma_c = \tau \frac{L}{D} V_f + \sigma_m (1 - V_f) _____ 1.7$$

since $L_c = \sigma_f D / 2\tau$ then $\tau = \sigma_f D / 2 L_c$

therefore $\sigma_c = \sigma_f \frac{L}{2 L_c} V_f + (1 - V_f) \sigma_m \_\_\_\_\_ 1.8$

As discussed in section 1.1.3 the major processes for producing

glass reinforced thermoplastics are extrusion compounding followed

by injection moulding. In consequence the glass fibre length is

often severely reduced. In practical nylon 6.6 composites reinforced

with short glass fibres the final fibre length distribution covers

a broad spectrum, typically ranging from 30 microns to 1500 microns,

the mode value being approximately 300 microns (see Section 3.3).

The fibre critical length for such a composite is calculated to

be 164 microns for 10 micron (150 tex) diameter fibres having an

ultimate tensile strength of 2.2 GNm^{-2}. The value for τ, the

interfacial bond strength, is assumed to equal the interlaminar shear

strength of 67 MNm^{-2} which was determined by a punch shear technique

(Appendix 1). Therefore, the fibre lengths are distributed about the

critical length and do not contribute equally to the composite strength.

The theoretical composite strength, for tensile loading, can be expressed

by a summation of equations 1.6 and 1.8. Such an approach was advocated

by Neilson (56) resulting in an equation of the form given below:-

$$\sigma_c = \sigma_f \left[\sum_{L_j = L_c}^{L_j = \infty} V_{fj} \left(1 - \frac{L_c}{2 L_j}\right) + \sum_{L_i = 0}^{L_i = L_c} \frac{L_i}{2 L_c} V_{fi} \right] + (1 - V_f) \sigma_m' \quad 1.9$$

1.5.4 Orientation efficiency factor

In the preceding discussion only uniaxially aligned, discontinuous

composites have been considered. However, short glass fibre reinforced

thermoplastics are anisotropic materials whose properties depend

upon the distribution of length of the fibres and also the specific

fibre orientation distribution (57). Kelly and Davies (58) observed the effect on composite strength of varying degrees of fibre misalignment to the applied force. Only those fibres aligned in the direction of the stress, or at very small angles, realise their ultimate strength. At larger angles failure was controlled by the matrix. Krenchel (59) introduced an orientation efficiency factor, η, to allow for the reduced degree of reinforcement provided by fibres at an angle θ to the applied load. He derived values of η for various cases of specific orientation, ranging from a composite in which the major fibre axis is parallel to the stress to a random 3 dimensional array.

During the injection moulding of composites the fibres may become orientated in a complex manner, often forming layers of different orientation leading to marked anisostropy in measured properties (60), (61). It has been shown by several workers (62), (63), that fibre orientation is affected by flow geometry and also that melt viscosity and shear rate can significantly alter the degree of specific orientation occurring. In injection moulded tensile bars it is observed that a high degree of fibre alignment occurs in the injection direction at the surface of the moulding. The core region, however, often exhibits a high degree of fibre misalignment (62). The ratios of the dimensions of the skin to core will obviously depend on the speed of injection, mould temperature and section thickness, being least for thick sections in which injection speeds and mould temperatures are high.

This lack of symmetry in the fibre orientation distribution has been the subject of intense studies by several workers. Darlington (64), using a contact micro-radiography technique, claims to achieve an accurate measure of the orientation distribution within a moulding. However, analysis times are approximately eight hours due to the large number of sections required. Alternative methods are described by

Thomas and Meyer (65), Metcalfe and Hull (66), and Johnson (67).
However, the techniques required are of necessity tedious and time
consuming and thus the determination of specific orientation in
fibre reinforced composites must still remain impractical for routine
studies.

1.5.5 Application of fibre orientation to composite theory

It is obvious from the foregoing discussion that equation 1.9
cannot adequately describe practical composites unless some allowance
is made for the varying degrees of fibre misalignment encountered.
Bader and Bowyer (68) proposed the incorporation of a fibre alignment
factor 'C' into the above equation. Whilst such a simplistic approach
will obviously lead to errors, correlation with experimental results
is claimed to be satisfactory for injected moulded tensile bars.
Thus the equation proposed by Bader and Bowyer takes the form:-

$$\sigma_c = C\sigma_f \left[\sum_{l_j=l_c}^{l_j=\infty} V_{fj}\left(1 - \frac{l_c}{2l_j}\right) + \sum_{l_i=0}^{l_i=l_c} \frac{l_i}{2l_c} V_{fi} \right] + \left(1 - V_f\right)\sigma_m' \cdots 1.10$$

1.6 Fibre length measurement

The literature contains many references to proposed techniques
for the length determination of short fibres. A review of such
techniques is given by Pennington (45). The methods discussed are
derived from the wood pulp industry but suffer from disadvantages
which preclude their use for the analysis of glass fibre samples.
In composite studies, Williams et. al. (69) and Filbert (42) describe
a simple technique for the analysis of fibre length distributions.
Approximately 0.5 grams of an extracted fibre sample was dispersed
in methanol and sieved through a series of screens of decreasing
mesh size. The recovered fibres were then dried and weighed and
a weight average length calculated, based on the weight of fibres and
the mean aperture size of the sieve. However, whilst the technique
claimed good reproducibility, initial studies in the course of the

present work indicated that the fibre population retained on each

sieve was highly dependent on the range of fibre lengths encountered.

Such variations in retained fibre populations are considered to be due

to 'bridging' of the sieve apertures, thereby causing a change in the

mean mesh size. The traditional method of determining fibre lengths

by photomicrographic techniques was used by several workers (70).

Fibre lengths were counted manually, between 200 and 1,000 measurements

being performed on enlarged photographs. Burns et. al (71) describe

an improved microscopy technique whereby photographs of extracted

fibre samples are counted using a Zeiss T.G.Z. 3 Particle Size

Analyser.

1.6.1 Zeiss Particle Size Analyser - Model TGZ 3

This instrument was designed by Endter and Gebauer (72) for

the determination of the size of photographic emulsion crystals.

A schematic diagram illustrating the principle of operation is

shown in Figure 1.18. The instrument is semi automatic, requiring the

operator to position the sample and perform the necessary adjustments

before the machine automatically measures and records the data. The

illuminated iris diaphragm is imaged by a lens onto a plexiglas plate.

By adjusting the iris diaphragm, the diameter of the sharply defined

circular light spot appearing on the photomicrograph can be varied so

that its diameter equals the fibre length. The different diameters

of the iris diaphragm are correlated via a collector with 48 solenoid

counters, each counter corresponding to a certain aperture interval

of the iris diaphragm. The automatic measuring and recording mechanism

is activated by depressing a footswitch and simultaneously a puncher

marks the measured fibre on the photograph. The 48 counters give a

continuous measuring range from 1 mm to 27.7 mm and thus the photographic

magnification should be chosen such that all fibres lie within this

range. If the spread of fibre lengths encountered lies outside this

range then the original photographic magnification must be selected

to encompass the largest fibres at 27.7 mm. Enlargements should

then be prepared to enable accurate measurement of the fibres which

are less than 1 mm in length on the initial photograph. Failure

to carry out such a procedure can lead to the truncated distributions

observed by earlier workers (71).

1.6.2 Automatic fibre length determination

Sawyer (73) describes the use of an image analysing computer

of the type manufactured by Cambridge Instruments under the trade

name of Quantimet. Problems associated with touching or crossed

fibres are overcome by surface treatment of the fibres with a non-

ionic surfactant. In addition an arbitrary cut off at 0.105 mm

is used to eliminate non-fibrous material which would otherwise

contribute to the count. However, since for the distributions

encountered in this study approximately 2 to 5% by weight of the

material lies below this value, such a cut off would obviously lead

to a significant error in the determination of fibre length.

Pennington (45) describes the use of the Quantimet system to determine

number average fibre length. Possible errors due to non fibrous

material and crossed fibres are eliminated by manually counting the

fibres as observed on the viewing screen of the computer. An

obvious compromise in the determination of fibre length distributions

is provided by the Modular Pen system supplied by American Optical

(74). Such a system combines the advantages of a manual method with a

direct measure of fibre length and will obviously find increasing

application in composite studies. A photograph or projected image of

the sample is placed so as to cover a region of a flat tablet which

contains magnetised steel wires running below the surface in the x and

y directions. The pulses, induced in the magnetic wires by the current

impulses emitted from the tablet sides, propagate along the wires with

a speed of 5000 mm/sec. A receiver coil incorporated in a fibre
tipped drawing pen picks up this impulse and the running time, which
is proportional to the displacement, will be electronically measured.
Thus the co-ordinates of the image point touched will be obtained in
absolute values. This equipment can be used with an integrated
microprocessor to process the data or alternatively interfaced with a
computer to provide a direct print out of length or co-ordinates.

$$L_c = L_f + L_m$$
$$L_f = \sigma_f A_f$$
$$L_m = \sigma_m A_m$$

$A_f = \Sigma a_f$
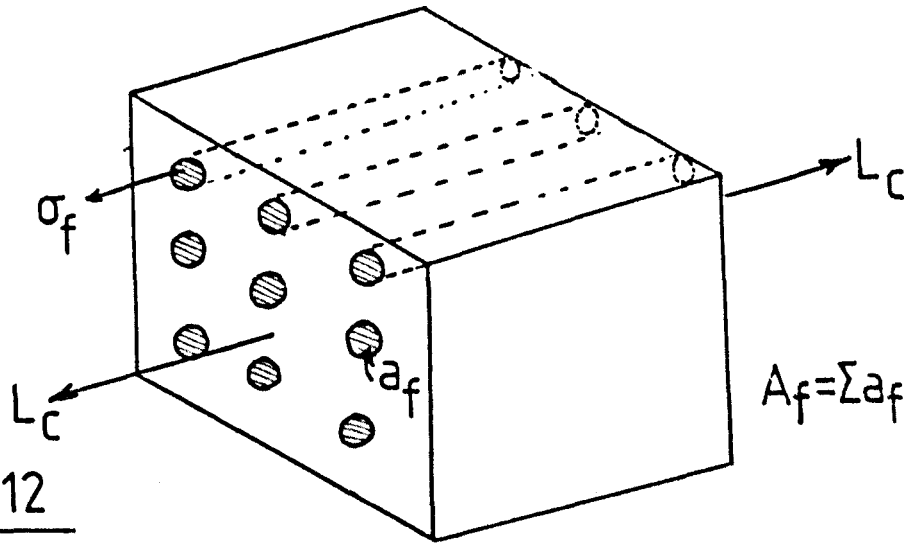
figure 1.12
Idealised composite

(a) $\xi_{fu} < \xi_{mu}$

(b) $\xi_{fu} > \xi_{mu}$
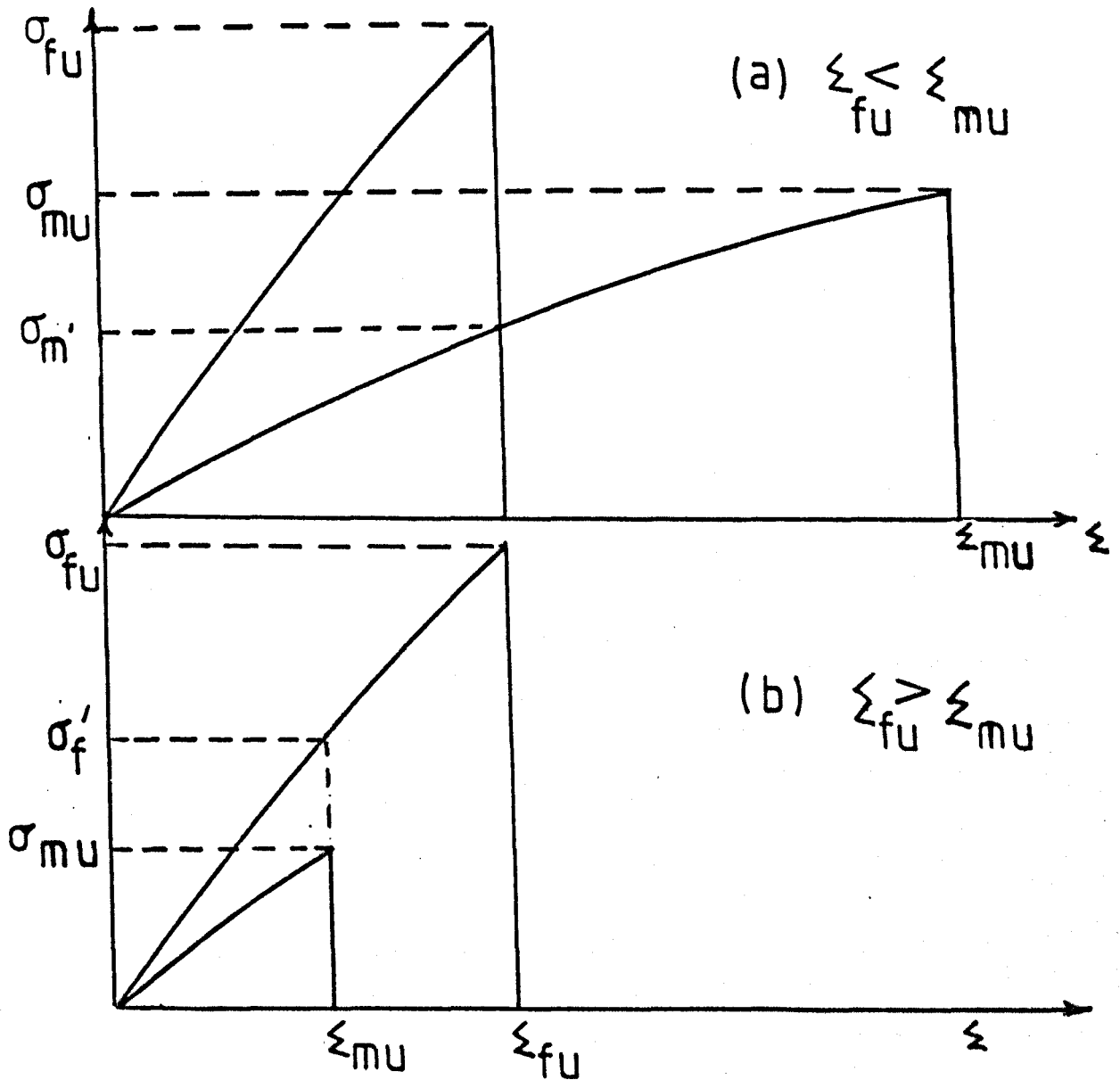
Fig. 1.13 (a) weak, ductile, matrix.
(b) weak, brittle, matrix.

- 45 -
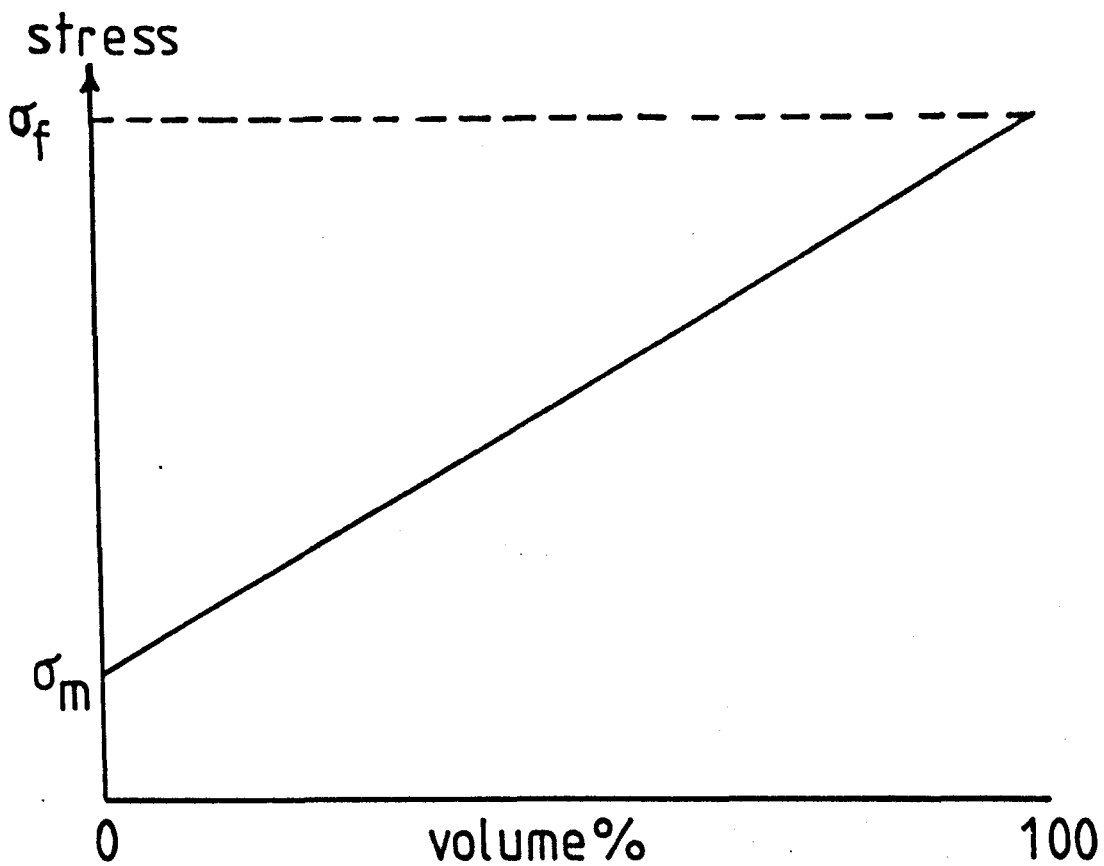
Figure 1.14 Law of mixtures composite strength
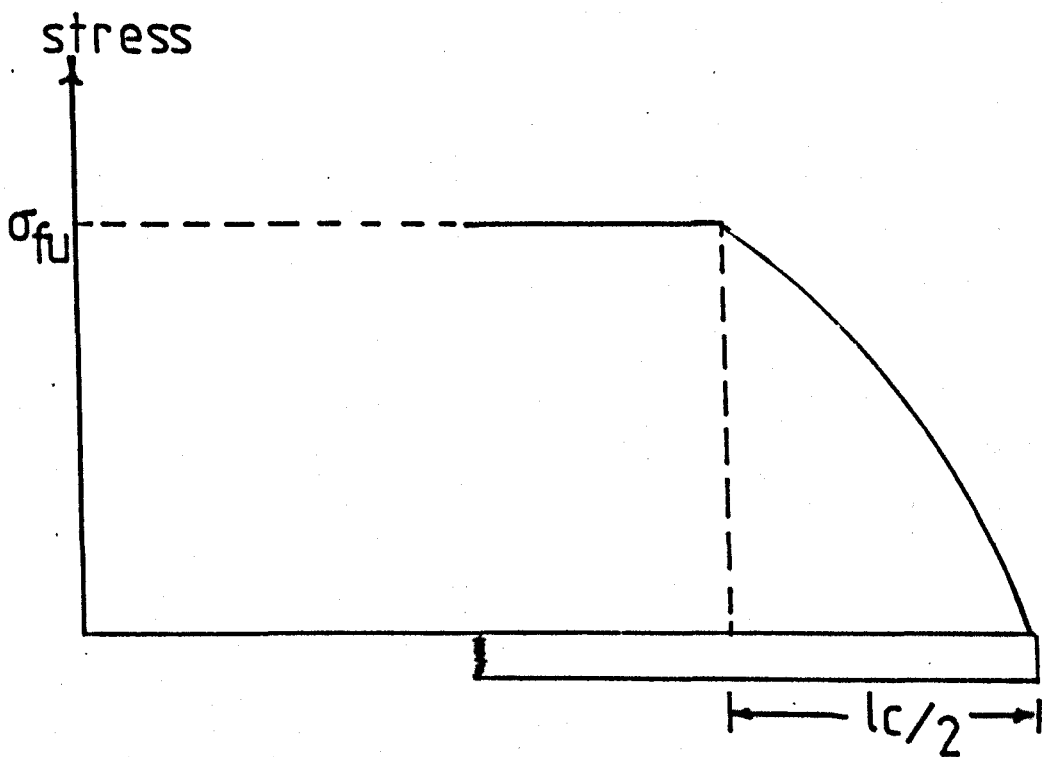
Fig.1.15 stress build up from a fibre end
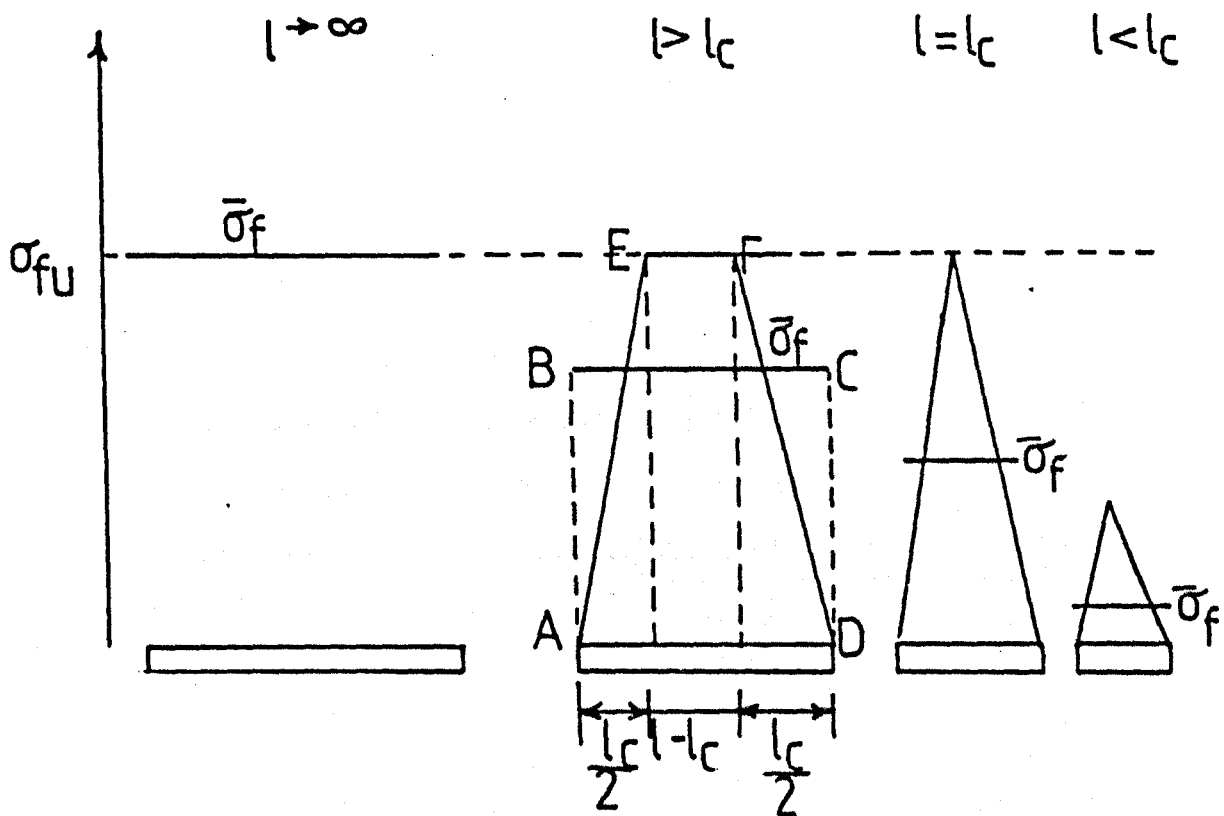
Fig. 1.16 average fibre stress according to Kelly and Tyson.
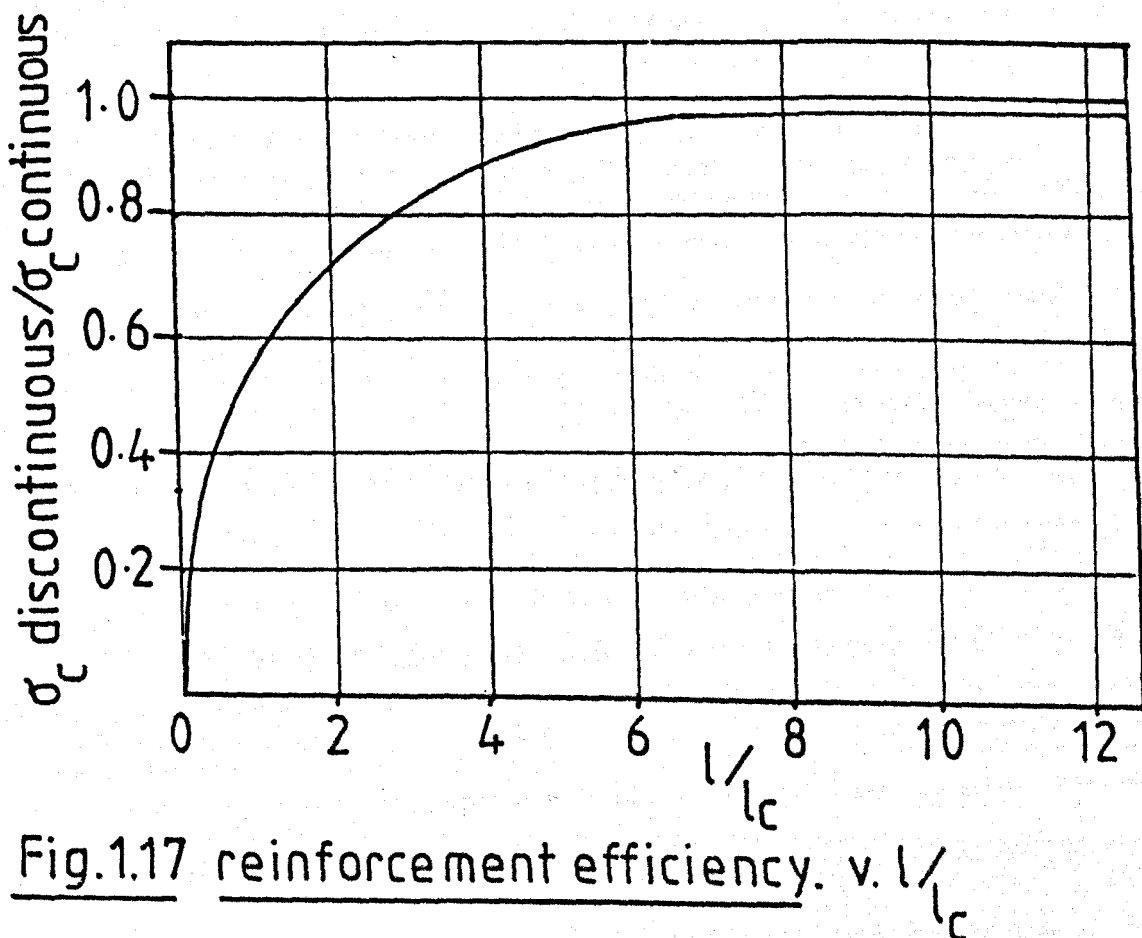
Fig. 1.17 reinforcement efficiency. v. l/l_c

photograph   iris diaphragm   light source

counters

1
2
3
4
5
6
7
8

spot diameter
control

footswitch

collector

contact pin
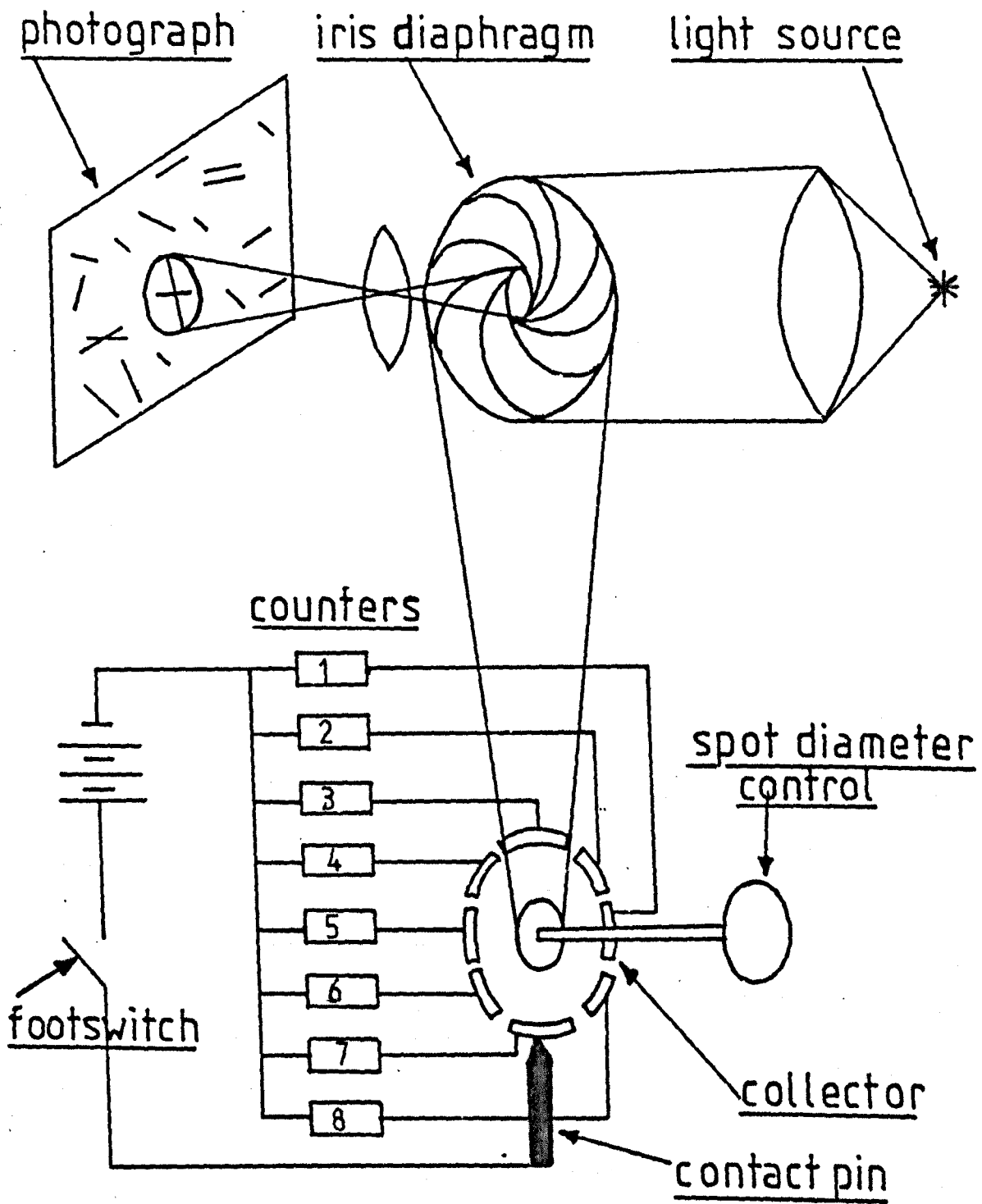
Figure 1.18
schematic diagram of the Zeiss Particle Size
Analyser model T.G.Z.3

CHAPTER 2   EXPERIMENTAL

2.1 Materials

(i) Glass fibre.

    (a) Product code:- FGCS 1640

        Size type:- MSS 1640, cationic poly electrolyte

        Chopped strand lengths:- 1.5 mm, 3 mm and 5 mm

        Nominal filament diameters:- 10 micron (150 tex),

        11 micron (190 tex), 14 micron (306 tex)

        Split:- Singles, 2 split, 4 split

        Supplier:- Fibreglass Limited, Reinforcements

        Division, Wrexham.

    (b) Product code:- XS 929

        Size type:- non ionic, polyvinyl acetate

        Chopped strand length:- 3 mm

        Nominal filament diameter:- 11 micron

        Supplier:- Specially made at Pilkington Brothers Ltd.,

        Research and Development Laboratories, Lathom, Ormskirk.

    (c) Product code:- 'Cemfil' glass, Cl.

        Size type:- MSS 1640

        Chopped strand length:- 3 mm

        Nominal filament diameter 11 micron

        Split:- 2 split

        Supplier:- Specially made at Pilkington Brothers Ltd.,

        Research and Development Laboratories, Lathom, Ormskirk.

(ii) Matrix Polymers

        Product codes:- 'Maranyl' A100, A144, A146, A148

        and A150.

        Polymer type:- Nylon 6.6

        Supplier:- Imperial Chemical Industries Limited,

        Plastics Division, Welwyn Garden City.

(iii)   Carbon fibre

  Product code:- Grafil A/S.

  Chopped strand length:- 3 mm

  Split:- Singles

  Supplier:- Courtaulds Limited, Coventry, England.

(iv)   Carbon black pigment

  Product code:- Monarch 880

  Nominal particle size:- 16 millimicrons

  Supplier:- Cabot Carbon Limited, Ellesmere Port, Cheshire.

(v)   Polyester resin

  Product code:- B.P. 4128

  Supplier:- B.I.P. Limited, Tatbank House, Tatbank Road,

  Oldbury, Warley, Worcestershire.

(vi)   Irradiated 'Cemfil' glass, Cl

  Emitter:- Na 24

  Percentage sodium:- 15%

  Dosage:- 7 micro Curies/gram

  $t_{1/2}$:- 15 hrs

  Irradiation of a 15 gram sample was carried out in the

  Universities of Manchester and Liverpool Research Reactor,

  Risley, Warrington.

(vii) Polaroid film type 107C.

(viii) Epoxide resin, used for mounting sections prior to cutting.

  Araldite AY 103 + Araldite HY 951 hardener.

  Supplier:- Ciba Geigy Limited, Plastics Division, Duxford,

  Cambridge.

2.2 Equipment

(i)   25 mm and 45 mm 'Betol' extruders

  Supplier:- Betol Machinery Limited, Craddock Road, Luton,

  Beds.

(ii)   50 mm 'Bone' extruder, I.C.I. Engineering Research Dept.,

          Plastics Division, Welwyn Garden City.

(iii) Sieves, 38 mm diameter constructed to B.S. 410. Apertures

          used:- 4.0 mm, 2.80, 1.40, 0.710, 0.300, 0.150, 0.075,

          0.045 mm.

          Supplier:- Endecottes Limited, Lombard Road, London S.W.19.

(iv)   Glass slides, 76 x 51 mm used for fibre length samples

          Supplier:- Chance Propper Limited, Spon Lane, Smethwick,

          Warley.

(v)   Stubbe SKM 76 Injection Moulding Machine.

          Supplier:- Stubbe Maschinenfabrik, 4925 Kalletal - Kalldorf

          bei Vlotho, Postfach, West Germany.

(vi)   Ankewerke Injection Moulding Machine

          Supplier:- Demag Hamilton, Gerrards Cross, Buckinghamshire.

(vii) Pressure Transducers, model TPT 432 and 422.

          Range:- 0 to 34.5 MN.m^{-2}

          Supplier:- Dynisco

          Agents:- Englemann and Buckham Ancillaries Limited,

          William Curtis House, Alton, Hampshire.

(viii) Zeiss Particle Size Analyser T.G.Z.3

          Supplier:- Carl Zeiss, OberKochen/Wuertt, West Germany.

(ix)   Quantimet 720 Image Analysing Computer.

          Supplier:- Cambridge Scientific Instruments Co. Limited,

          Chesterton Road, Cambridge, CB4 3AN.

(x)   Diamond Tooled Cutting Machine

          Supplier:- Tycet Limited, 16 Mark Road, Hemel Hempstead,

          Herts.

(xi)   American Optical Cycloptic Model 56M - 1. Microscope and

          photo-micrographic camera 682G.

          Supplier:- Reichert - Jung U.K., 820 Yeovil Road, Slough,

          SL1 4JB.

(xii) Cambridge Stereoscanning Microscope Mark 2A.

   Supplier:- Cambridge Scientific Instruments Co. Limited,

   Chesterton Road, Cambridge, CB4 3AN

(xiii) Ultrasonic bath

   Supplier:- Kerry Ultrasonics Limited,

   Hunting Gate, Hitchin, Herts. SG4 OTQ.

(xiv) MOP/AMO3, Modular Image Analysis System.

   Supplier:- Reichert - Jung U.K., 820 Yeovil Road, Slough,

   SL1 4JB.

(xv)   Radiation Counter and Spectrometer.

   Supplier:- Research Electronics, Mirfield, Yorkshire.

(xvi) Instron Capillary Rheometer

   Location:- Chemical Engineering Department, Bradford

   University, Bradford.

2.3 Extrusion processing investigation

The extent of fibre degradation occurring during the plasticating
extrusion of glass fibre - nylon 6.6 blends would be expected to be
influenced by:-

   (i) Dimensions and geometry of the extruder and screw

   (ii) Processing variables

   (iii) Glass fibre and polymer parameters

2.3.1 Extruder size and geometry

Three machines were utilised during the period of this study
the relevant screw design details being indicated in Table 2.1. With
the exception of the 25 mm Betol extruder, screw geometries were typical
of two stage screws supplied for the extrusion of crystalline thermo-
plastics. For the 45 mm Betol machine, the availability of two screws
having similar feed sections but different taper coefficient and primary
compression ratios enabled the effect of screw geometry on fibre fracture
to be observed.

2.3.2 Processing variables

For a particular screw profile and material, the output and quality
of the extrudate will be controlled by the following parameters.

2.3.2.1 Screw 'back pressure'

A variety of back pressures can be generated in an extruder simply
by varying the die dimensions or by the use of breaker plates and screen
packs (7). Generally such restrictions tend to depress the output of
single stage screws thereby reducing the length of the melting region.
In addition the developed pressure gradient serves to improve the mixing
characteristics and stability of the system. Two stage screws, however,
would be expected to be relatively insensitive to back pressure since in
general the second metering section has a greater pumping capacity than
the first stage. The initial effect of increasing die pressure would be
to increase the filled length of the secondary metering zone. Ultimately,
however, material will exude from the barrel vent unless a corresponding
restriction is placed on the output of the first stage. If, as in this
study, the vent is left sealed then it is possible for the imposed
pressure to be transmitted back to the feed section leading to a reduction
in output. At the commencement of this investigation no facilities were
available for pressure control. Since one objective was to examine the
interaction of pressure and the resultant extrudate fibre length,
modification of the die heads of the Betol extruders was required. The
simplest method of producing a controlled restriction to flow without
creating 'dead' areas, was to drill and tap the extruder head to accept
a range of dies of different internal diameters. Such an arrangement
is illustrated diagrammatically in Figure 2.1. Dies ranging in diameter
from 1.5 mm to 6 mm were manufactured from high tensile bolts, the
entrance to the die land being machined smooth to avoid any hold up of
molten material.

The pressures generated by the above arrangement were monitored by means of a Dynisco pressure transducer. This was sited in the die head of the 25 mm machine due to the absence of barrel pressure tappings. However, for the larger machines a transducer could be located in the barrel coincident with the final screw channel of the second metering section. Variations in melt pressure were transmitted, via a flexible metal diaphragm in the end of the transducer, to a fine column of mercury. This in turn produced a strain in a strain gauge arranged as one of four resistances in a Wheatstone bridge network. The resultant e.m.f. produced was essentially proportional to the applied pressure and could be amplified to give an output range of 0 to 1 volt, corresponding to an exerted pressure of 0 to 34.5 $MN.m^{-2}$ for the particular model used.

To fully utilise the ability of the transducer to follow the pressure changes occurring within each revolution of the screw a transient recorder connected to a conventional chart recorder was used. The transducer placement and recording assembly are illustrated in Figure 2.2. The use of a totally electronic transient recorder removed any problems of recorder response time and in addition provided a large degree of freedom in the presentation of the recorded profiles. By utilising the adjustable triggering circuitry of the transient recorder, the recorder could be triggered at any chosen pre-set point on the voltage waveform pulse and the profile viewed instantaneously on the display oscilloscope. When a permanent hard copy of any pressure profile was required, a single trigger pulse could be initiated in the transient recorder and a single sweep of variable duration recorded onto the chart recorder. Pressure calibration was achieved by replacing the transducer by a stable D.C. voltage source. The deflection on the transient recorder corresponding to this voltage, accurately determined with a digital voltmeter, could then be plotted onto the chart recorder. The advantages of the above system are obvious in that

the recorder sweep time was variable from well below a second to in excess of 200 seconds, allowing single cycles to be expanded for inspection or enabling a larger number of cycles to be examined for pressure cycling or pressure irregularities, respectively. Typical pressure profiles obtained are indicated in Figure 2.3. The finite area of the sensing diaphragm of the transducer had the effect of rounding any sharp pressure peaks or troughs. An approximately uniform pressure gradient was developed in the melt channel reaching a maximum pressure at the leading edge of the flight. In the much narrower flight clearance a dramatic drop in pressure occurred.

2.3.2.2 Melt temperature

The 45 mm Betol extruder was equipped with a thermocouple arranged so as to be flush with the inside surface of the barrel and diametrically opposite the transducer placement. Obviously this arrangement will not provide an accurate measure of melt temperature due to the mass of metal surrounding the thermocouple. However, changes in barrel temperature at this point caused by heat being conducted to or from the melt, will be detected if the time span is sufficient for equilibrium to be achieved. Barrel and die temperatures were set at a flat profile of 280°C for the 25 mm and 45 mm machines, a set temperature of 290°C being more suitable for the larger 50 mm machine. These settings were used for 'normal' running throughout the course of this study. However, actual temperatures indicated by the controllers often deviated significantly from the set position, the extent of deviation depending on the location of the heater/thermocouple combination and the operating conditions.

Having established the conditions for optimum operation, the influence of varying the set temperature on shaft power consumption,

output, melt pressure and resultant fibre degradation was observed for each machine. Energy input through the screw shaft was determined by monitoring the armature current and voltage of the D.C. motor for each experiment. Both current and voltage were measured for the screw rotating in an empty barrel and the power consumed subtracted from the measured power under particular operating conditions. The voltage versus screw speed relationships for the 25 mm and 45 mm machines are given in Figure 2.4. The 50 mm extruder was hydraulically driven and thus mechanical power consumed was calculated from the hydraulic pressures, the torque values being obtained from the calibration curve given in Figure 2.5. The values obtained for mechanical power consumption are expressed in terms of specific power, that is the power consumed per kilogramme of output, the units being KWh/Kg. No allowance has been made for losses in gearing, pulleys or thrust bearings and thus the measured power consumptions will slightly over estimate the true values.

2.3.2.3 Screw speed

Control of screw speed for the Betol extruders was achieved by thyristor control thereby providing continuously variable speeds between 4 and 100 r.p.m. The actual screw speed under 'no load' conditions was monitored and found to deviate from the set speed for the 25 mm machine. The extent of this deviation, however, was constant for a particular speed under a variety of loads. The calibration curve for this machine is given in Figure 2.6. For the other extruders the set speeds corresponded exactly with the actual speeds measured by the transient recorder. Screw speeds of 30, 60 and 90 r.p.m. were used in this study.

2.3.2.4 Extruder cooling

All three machines described employed neutral screws, that is they were neither equipped with cooling nor heating. Barrel cooling was not used during normal running, although the 45 mm machine was equipped with

SCREW	1	2	3	4
diameter (D)	45mm	45mm	25mm	50mm
length/diameter	31	31	25	32
feed length	11.5D	11.5D	8.75D	10.75D
feed depth	8.0mm	8.0mm	10.7mm	9.4mm
1st.compression length	0.5D	1.0D	0.5D	0.5D
1st.metering length	6.5D	6.0D	3.0D	6.75D
1st.metering depth	1.36mm	1.88mm	5.59mm	1.93mm
decompression length	1.0D	1.0D	0.5D	-
devolatilisation length	5.0D	5.0D	5.0D	6.0D
devolatilisation depth	8.13mm	8.13mm	11.0mm	9.53mm
2nd.compression length	2.0D	2.0D	0.5D	2.0D
2nd.metering length	4.5D	4.5D	6.75D	6.0D
2nd.metering depth	2.04mm	2.84mm	6.10mm	2.74mm
1st.compression ratio	5.0:1	3.6:1	1.4:1	4.1:1
2nd.compression ratio	3.4:1	2.5:1	1.3:1	3.0:1
pump ratio	1.5:1	1.5:1	1.09:1	1.4:1
pitch	45mm	45mm	29mm	50mm
flight width	4.8mm	4.8mm	3.1mm	6.4mm

Table 2.1 screw design details

thermocouple

high
tensile bolt
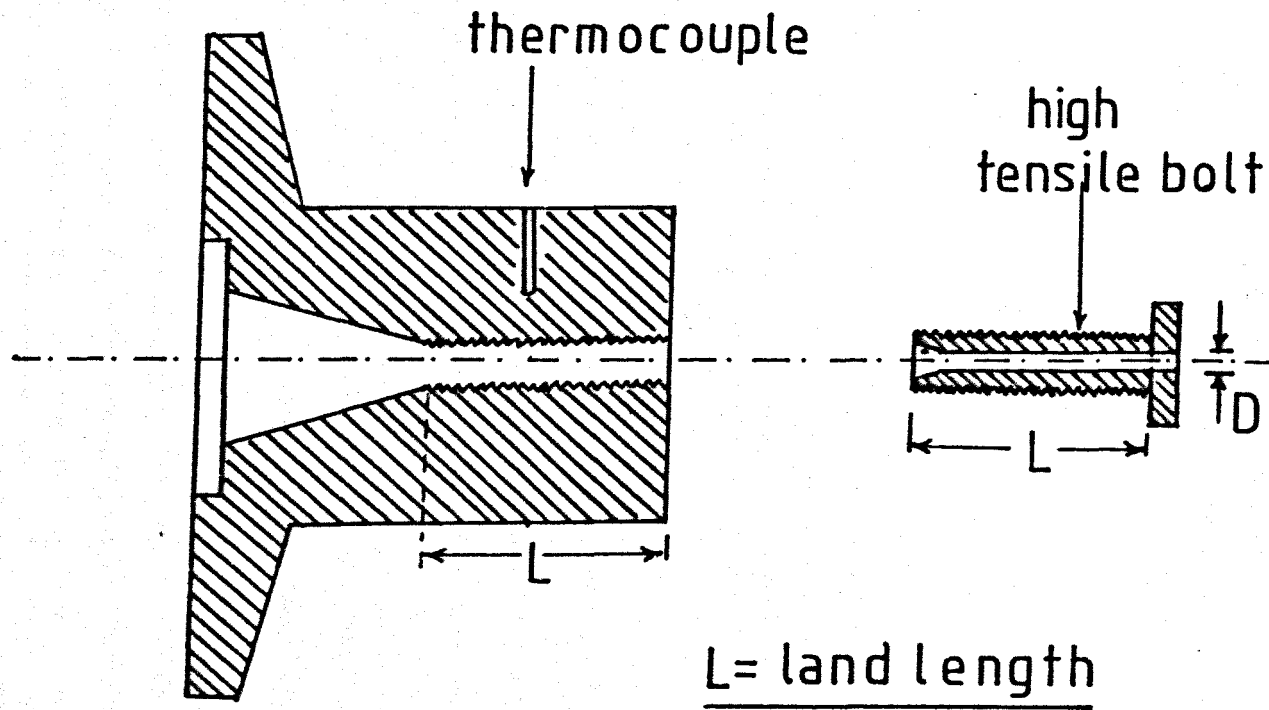
die diameter (D)

1·5mm

2·0mm

3·0mm

4·0mm

6·0mm

L

L

D

L= land length

Figure 2.1   modification of extruder die head (schematic)

Transducer placement

transducer

die head
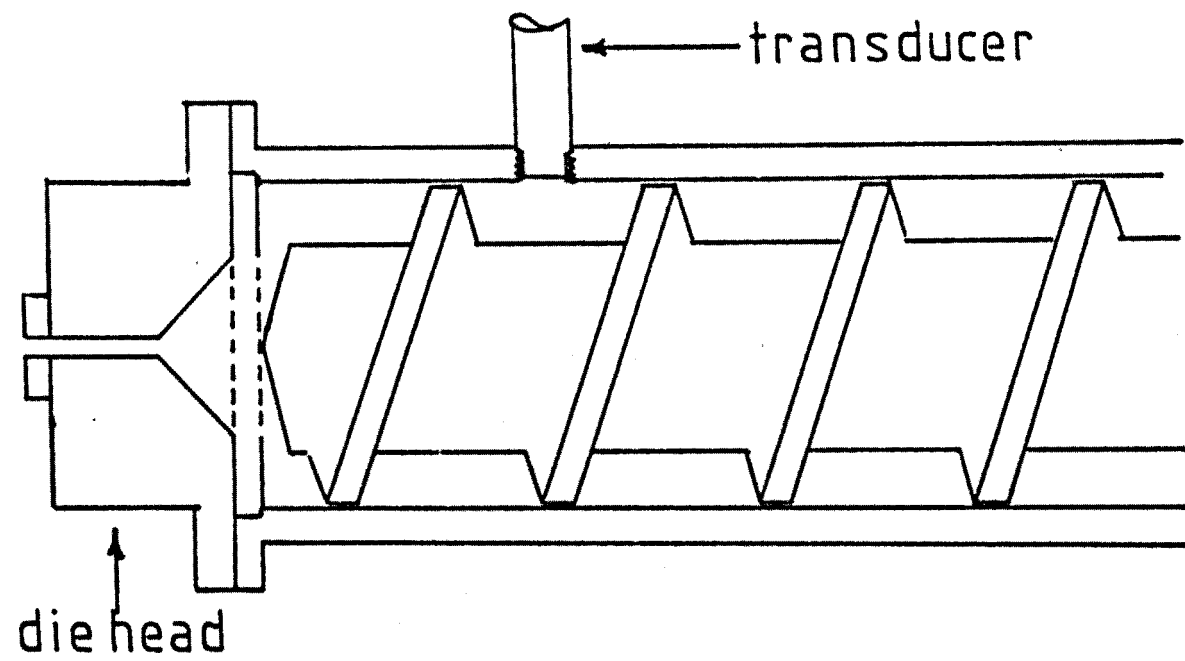
Pressure recording equipment
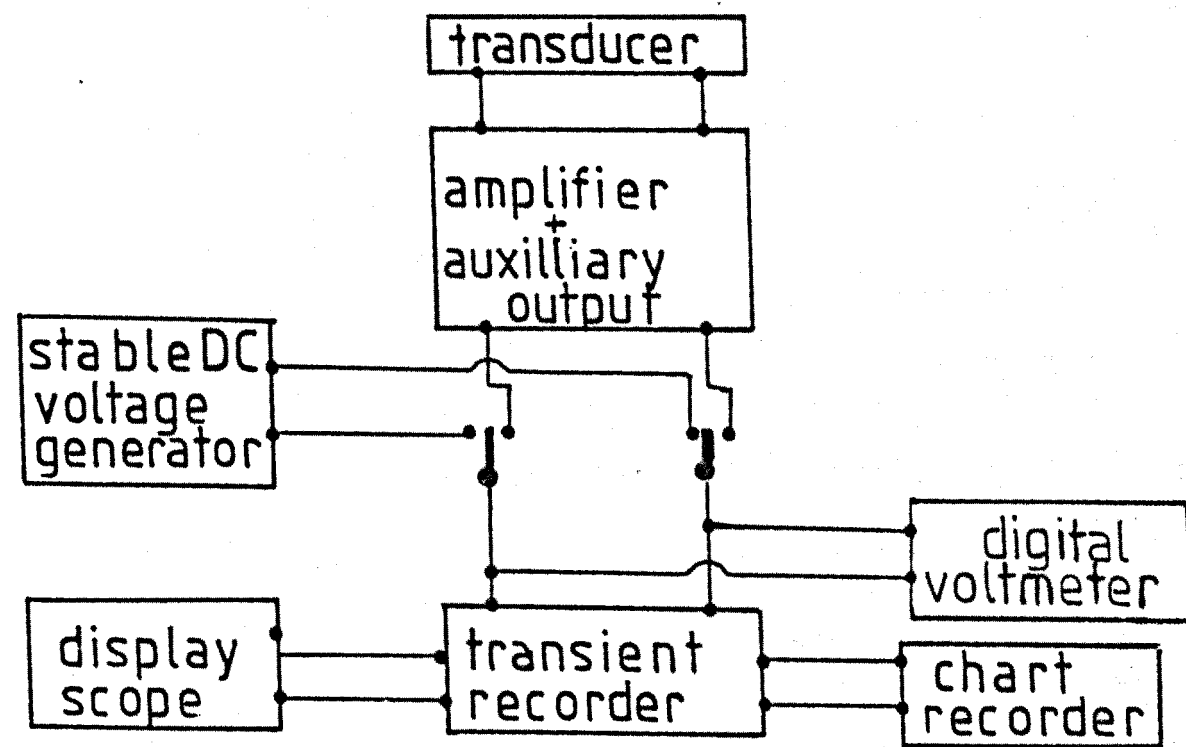
transducer

amplifier + auxilliary output

stableDC voltage generator

digital voltmeter

display scope

transient recorder

chart recorder
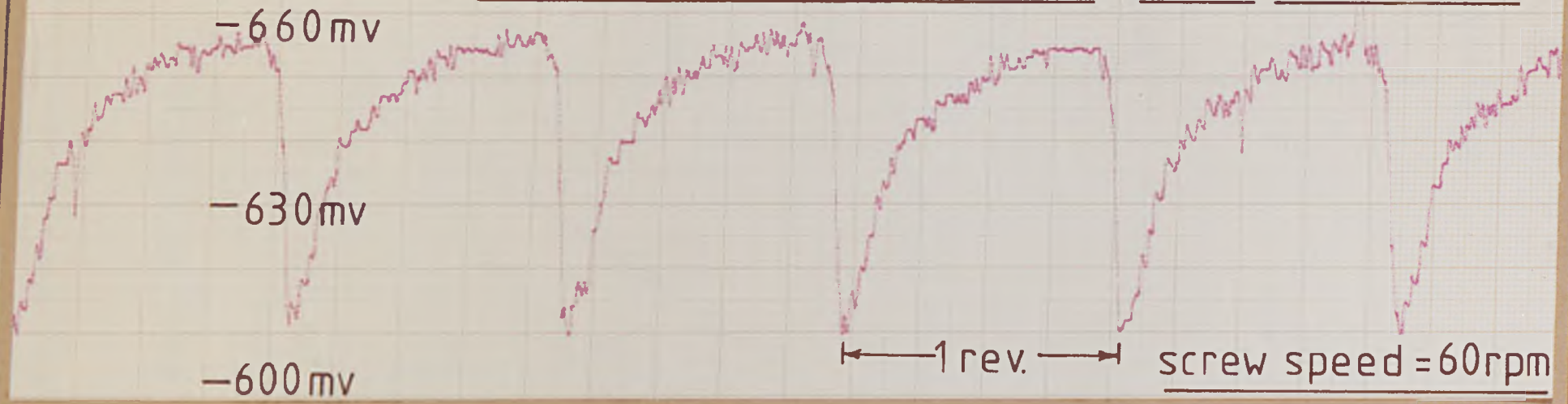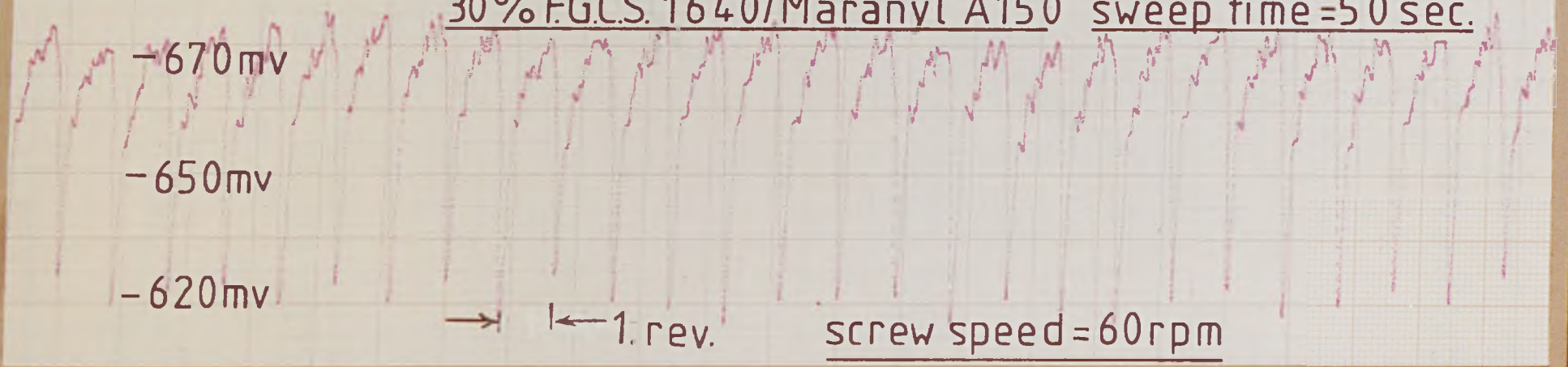
Figure 2.2

figure 2.3 typical pressure profiles
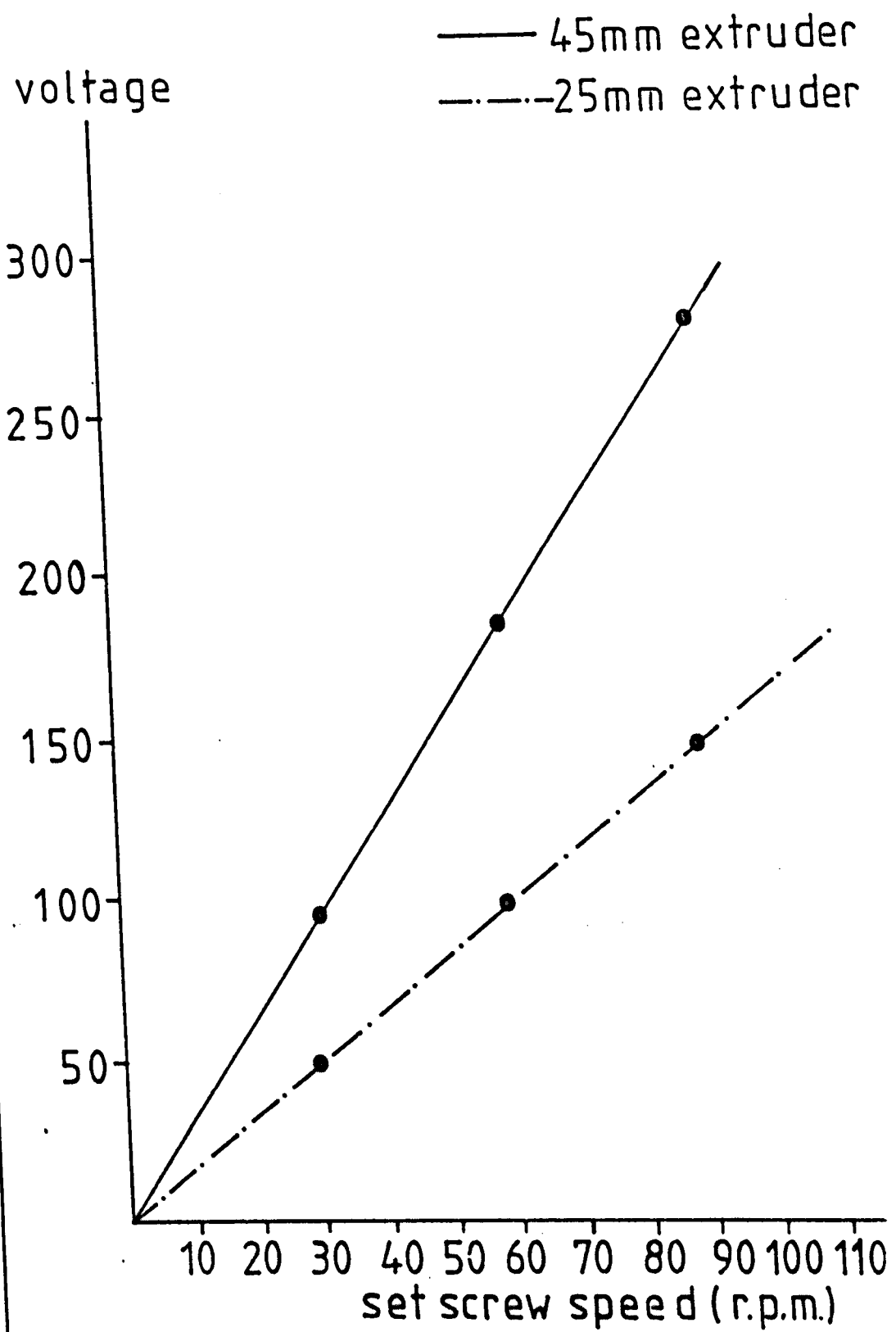
Figure 2.4 voltage-screw speed relationships

hydraulic pressure
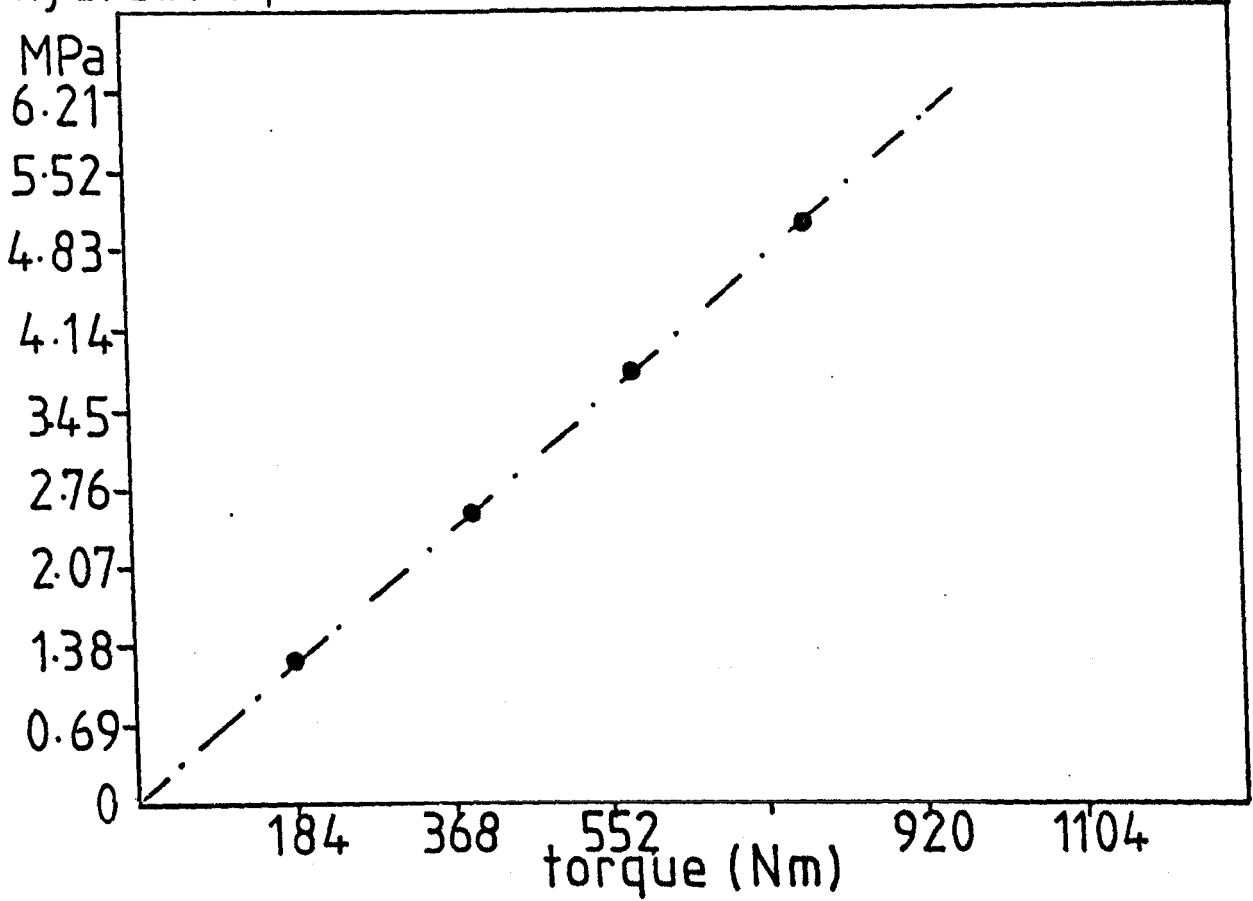
Figure 2.5 hydraulic pressure v. torque

actual speed
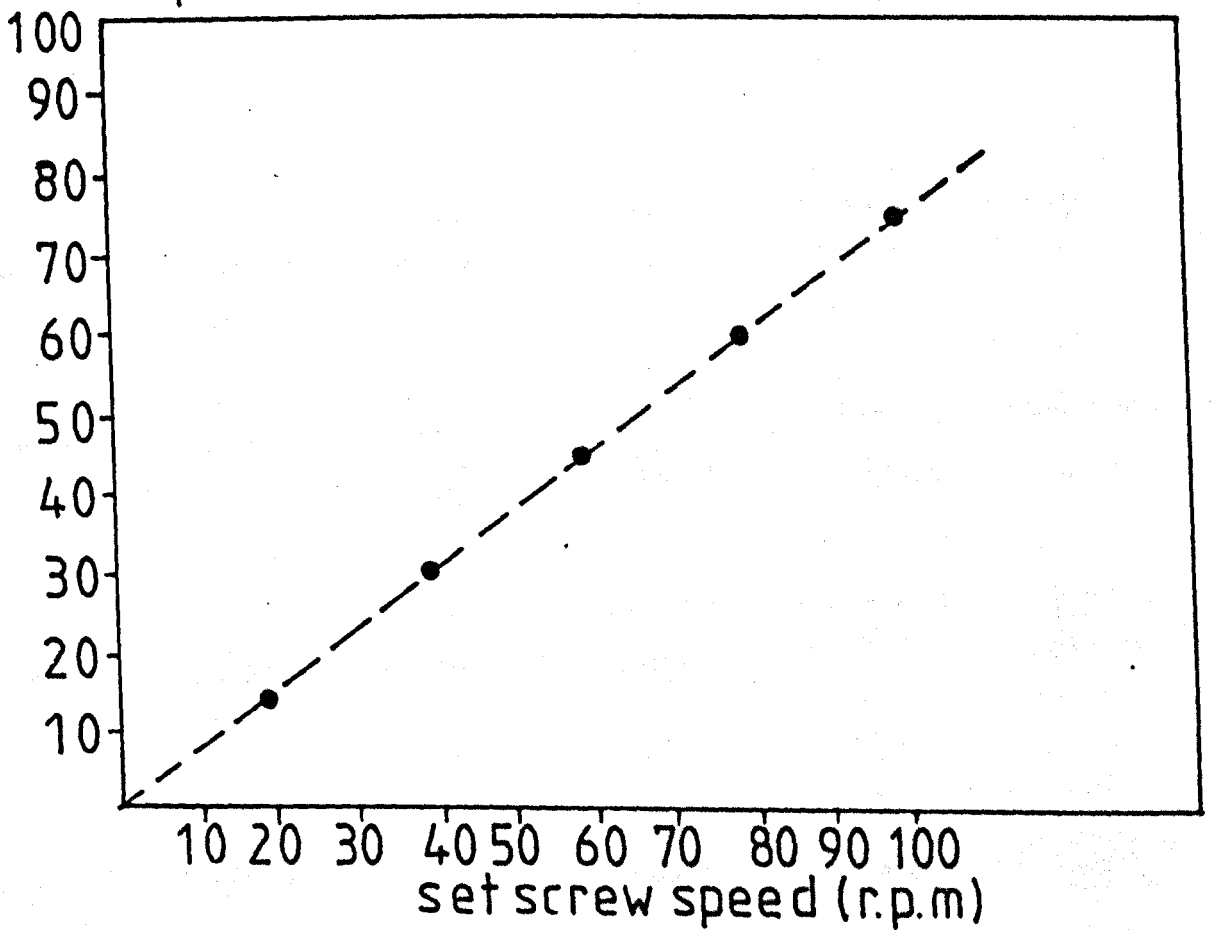
Figure 2.6 set screw speed v. actual speed

air cooling achieved by fans placed below the barrel heaters. Water

cooling of the barrel in the region of the feed port was provided

and consequently the barrel temperature in this region was well below

the melting point of the polymer. At the commencement of each days

operation the machine was allowed to reach the set barrel temperatures

and then run continuously for approximately 30 minutes before commence-

ment of the experimental series. Such a procedure was necessary to

allow the screw and barrel temperature profiles to reach equilibrium.

2.3.3 Materials selection

2.3.3.1 Glass fibre parameters

It is to be expected that the characteristics of the glass fibres

will influence both the processing performance and the resultant fibre

length distribution. Options available to the extrusion compounder are:-

(i) Strand tex/bundle tex

(ii) Initial strand length

(iii) Size type

During this study changes in initial strand length and size type

were observed to have a significant influence on feeding ability, power

consumption, output and pressure generated at the die. Such differences

originate primarily in the solids conveying region of the extruder. As

observed by Tadmor (16) increasing the bulk density of the solid

material will improve the solids conveying capacity of the machine, as

will increasing the frictional coefficients between the material and

the barrel. The addition of glass fibres to polymer pellets invariably

produces a lower bulk density blend, the extent of this reduction

being determined by the degree of filamentisation of the fibres and by

variations in fibre length and concentration.

2.3.3.1.1 Determination of Apparent Bulk Density

The literature contains several references to procedures suitable for

ranking materials in terms of their Specific Volume Index (S.V.I.) or

Apparent Bulk Density (A.B.D.) (75), (76). One such technique was utilised

by Milewski (1) to estimate the mean aspect ratio of hammer milled
fibres. A similar method has been used to assess the effect of strand
length and degree of filamentisation on Apparent Bulk Density.
Specimen results obtained in this study are given in Table 2.2.
Obviously, the Apparent Bulk Density of glass fibre-polymer blends
can be monitored in a similar manner. The technique employed is
described in Appendix 2. Such a procedure does not provide an accurate
measure of the solid density obtained in the 'dynamic' situation of
extrusion. It does, however, provide an indication of the variations in
feed stock densities which are likely to be encountered during processing
of the above materials.

An obvious additional variable open to a compounder is in the
amount of glass fibre to be blended with the polymer granules, the
practical range of interest being from 5% to 60% by weight. The higher
glass content materials are commonly supplied to moulders as 'concentrates'
designed to be blended with virgin polymer prior to moulding. During
extrusion compounding variations in glass content were found to
seriously affect the feeding ability of the glass fibre - polymer blend,
due to the reduction in bulk density and frictional changes which
accompanied increasing glass content. In addition, the inevitable
increase in the viscosity of the melt produced significant differences
in the processing performance and resultant fibre length distribution.

2.3.3.2 <u>Matrix polymer - viscosity effects</u>

The total power consumed in the extrusion process comprises both
the mechanical power supplied through the screw drive and the thermal
power supplied by the barrel heaters. The mechanical energy input includes
contributions from the solids conveying, melting and melt conveying regions
of the extruder, plus any power which may be dissipated in the clearance
between the flight land and barrel if leakage flow occurs.

For a specified operating condition, variation in feed-stock

densities would be reflected in changes in the mechanical power

utilisation of the solids conveying zone. In many cases this

variable power requirement may overshadow any differences occurring

in the melting and melt conveying processes. The energy supplied

by the drive in the above regions will, in part, be dictated by the

viscosity of the molten material. In addition to increasing the

glass fibre loading significant increases in melt viscosity can

be achieved by varying the matrix polymer. Several grades of Nylon

6.6, which differ only in their molecular weights and melt viscosities,

are commercially available. The relevant details of these materials

are given in Table 2.3. Processing-fibre degradation studies were

carried out on the 45 mm 'Betol' extruder, for a 30% by weight

blend of F.G.C.S. 1640 chopped strands and the above polymers.

Feed stock densities and thermal properties of these blends were

identical, in contrast to the blends produced from Maranyl A100 contain-

ing different levels of glass fibre.

2.4 Extrusion processing - experimental techniques and sampling

For each experimental series the following procedure was

adopted:-

Barrel and die heaters were set as required and the machine

allowed to reach "working" temperature, a period of two hours

normally being sufficient. The appropriate die was inserted in the

head and the screw speed set at the apposite level. Nylon 6.6 is

highly hygroscopic, the equilibrium moisture content being

approximately 3.5% at 65% R.H. and 20°C (77). The presence of

small levels of moisture are highly detrimental to the extrusion

process and thus rigorous precautions are necessary to exclude

water from the polymer - glass fibre blend. The polymer was used

directly from freshly opened bags, or vacuum dried at 90°C overnight

if it had been in contact with the atmosphere for any appreciable time span. The glass fibres and polymer were tumble blended for 3 minutes and then added to the feed hopper. When steady conditions were achieved, normally 30 mins. from initial start up, the experimental readings were commenced. Outputs were monitored by sampling at the die at one minute intervals, at least ten consecutive measurements being taken. In addition, measurements of the recorded melt temperature, pressure and motor power consumed were made. Approximately 3 Kg. of extrudate were prepared for each experiment, to be used for subsequent composite and fibre length studies.

2.4.1 Residence time distributions

As indicated in Figure 1.11 the residence time distribution indicates the relative strain histories of particles passing through the metering section of an extruder. Residence time is primarily a function of machine design, screw speed and throughput and, as in all continuous machines, extruders do not possess an exactly defined residence time but rather a residence time spectrum. Since such a distribution indicates the relative degrees of shear strain experienced by a particle it is likely that the extent of fibre degradation occurring in this region of the extruder will largely be related to the overall degree of mixing which occurs. Obviously the extent of mixing will be governed by the shear rate and residence time.

In order to establish the time any particle spends in the extruder, it is obvious that some means of 'labelling' the particle is required. Standard techniques of using dyes or pigments to act as tracers were considered to be unsuitable for the fibre filled nylon since the residence time for fibres may differ from that of the molten polymer. A convenient method of following the passage of fibres

through the machine was considered to be a radioactivation technique.
A similar system has been used by Barker (78) to determine throughput
rates and degree of mixing occurring in glass melting tanks and more
recently by Wolf and White (79) to determine the Residence Time
distribution in a plasticating extruder. The use of radioactive tracers
offers several advantages over conventional techniques:-

(i)   The limits of detection of such materials are extremely
       low, 10^{-15} gms of a radioactive element being readily
       detected. Thus extremely small quantities can be used which
       reduces the likelihood of any interference in the normal
       processes occurring.

(ii)   The passage of the material through the various zones can
       be detected by means of externally mounted radioactive
       counters which provide an indication of when sampling should
       commence.

The glass fibres used in this study are eminently suitable as
potential radioactive tracers, the use of such fibres avoiding the
necessity of adding any other tracer materials. Atoms of an element
already present in the glass can be 'labelled' so as to distinguish them
from other atoms of the same element. The chemical properties of these
labelled species are identical with those of unlabelled atoms and thus
their behaviour will be the same. Consequently, any problems of
segregation of the tracer from the other components are avoided.

Upon irradiation in a nuclear reactor the atomic nuclei of isotopes
of most elements capture neutrons to form compound nuclei. These
nuclei are often unstable and emit nuclear radiation which can be
measured by means of a suitable detector. The intensity of emitted
radiation depends on the following factors:-

(a)   Neutron flux (neutrons/cm^2/sec) during irradiation.

(b)   Abundance of the isotope undergoing irradiation.

(c) The probability of neutron capture, which is determined by the probability of a collision occurring. This probability is described by an effective cross-sectional area of target.

(d) Length of irradiation time and also the time elapsed prior to measurement.

(e) Efficiency of the counting assembly.

The equation relating the above factors is:-

$$S = KA = \frac{0.6}{3.7 \times 10^{10}} \frac{\phi}{M} \left[1 - \exp\left(-\frac{0.69t}{T_{1/2}}\right) \right] W \exp\left(-\frac{0.69td}{T_{1/2}}\right).$$

where S = specific activity produced/gm of substance

A = measured activity

K = constant determined by the efficiency of detection

M = atomic weight of bombarded element

ϕ = neutron flux

t = irradiation time

$T_{1/2}$ = half life of radioactive isotope

td = time interval between irradiation and subsequent measurement

Thus, for any material, knowledge of the weight of the particular element to be activated enables the calculation of the time required to produce a known specific activity.

It is essential that the tracer used should possess a high neutron excitation cross-section and also yield a $-\gamma-$ active isotope on irradiation. In addition, the half life should be sufficient to permit accurate measurement of the induced radioactivity over a time span longer than the duration of the experiment, whilst decaying rapidly enough to facilitate safe disposal. Typical elements and corresponding radio nuclides found in E-glass fibres are given in Table 2.4. As can be seen

sodium, which is present in trace quantities, is suitable for radio-activation due to its high cross-section and reasonable half-life. However, as indicated in Table 2.5 (a), E-glass also contains a significant quantity of Boron. This element is a high neutron absorber and can therefore lead to a distortion of the neutron flux in the reactor. Such a distortion creates a degree of uncertainty in the calculation of the specific activity produced, particularly for other samples which may be present in the reactor. These problems, however, are readily overcome by the use of a fiberised glass having the chemical composition shown in Table 2.5 (b), this material normally being used in cement reinforcement. 3 mm, 190 tex, 2 split strands sized with MSS 1640 had previously indicated similar retained fibre lengths after extrusion processing, as achieved with equivalent E-glass fibres (80) and thus this material was used in the residence time studies.

2.4.1.1 Radioactive tracer studies:- experimental technique

Approximately 15 grams of glass fibres were irradiated in the Universities Reactor at Risley, an exposure time of 10 seconds being calculated to produce a specific activity of 7 micro Curies/gram. 5 grams of this material were mixed with 11.7 grams of Maranyl A100 to produce a 30% by weight blend. The extruder was flood fed with the standard 30% blend of F.G.C.S. 1640/A100 until steady conditions were achieved. The level of feed in the hopper was allowed to fall and the activated material introduced directly into the screw channel, being immediately followed by the standard blend. The passage of active material through the extruder was followed by means of a portable Geiger-Counter and sampling was commenced when readings indicated that material had reached the second metering zone. Samples were collected in beakers at 15 second intervals until no further activity could be detected. To facilitate accurate measurement, the samples were weighed

MATERIAL	APPARENT BULK DENSITY
F.G.C.S. 1640 1·5 mm. 190 tex. 2split.	585 kg/m^3
F.G.C.S. 1640 3·0 mm 190 tex. 2 split.	423 kg/m^3
F.G.C.S. 1640 5·0 mm 190 tex. 2split	337 kg/m^3
X.S. 929 3·0 mm 190 tex. 2split	339 kg/m^3

Table 2.2 <u>influence of fibre length and filamentisation on app. bulk density</u>

MATERIAL	MELT VISCOSITY (285°C) shear rate 1000 sec^{-1}	Mpt. °C
maranyl A100	60 Nsm^{-2}	258
maranyl A144	120 Nsm^{-2}	258
maranyl A146	300 Nsm^{-2}	258
maranyl A148	500 Nsm^{-2}	258
maranyl A150	700 Nsm^{-2}	258

Table 2.3 <u>properties of maranyl 'A' polymers</u>

ELEMENT	EXCITATION CROSS-SECTION (BARNES)	RADIONUCLIDE PRODUCED	HALF LIFE	DECAY MODE
silicon	0.00034	^{31}Si	2.65 hours	β and γ
sodium	0.53	^{24}Na	15.0 hours	β and γ
calcium	0.013	^{45}Ca	164 days	β
aluminium	0.21	^{28}Al	2.27 min.	β and γ
iron	0.0028	^{59}Fe	45.1 days	β and γ
magnesium	0.06	^{27}Mg ^{28}Mg	9.5 min. 21.3 hours	β and γ β and γ

Table 2.4 elements and corresponding radionuclides for E glass fibres

MATERIAL	PERCENTAGE
SiO_2	54.8
CaO	21.7
SrO	0.3
Fe_2O_3	0.35
Al_2O_3	14.9
ZrO_2	0.1
TiO_2	0.04
MgO	0.4
K_2O	0.9
Na_2O	0.2
B_2O_3	6.2
F_2	0.7

Table 2.5(a) composition of 'E' glass fibres

MATERIAL	PERCENTAGE
SiO	61.6
CaO	5.4
SrO	—
Fe_2O_3	0.07
Al_2O_3	0.9
ZrO_2 HfO_2	16.6
MgO	—
K_2O	0.4
Na_2O	14.9
B_2O_3	—
F_2	0.23

Table 2.5 (b) composition of 'C$_1$' glass fibres.

Figure 2.7 typical residence time distributions - 25mm extruder

- - - - 90 r.p.m. set speed
- · - · - · 60 r.p.m. set speed
———— 30 r.p.m. set speed

%

residence time (seconds)
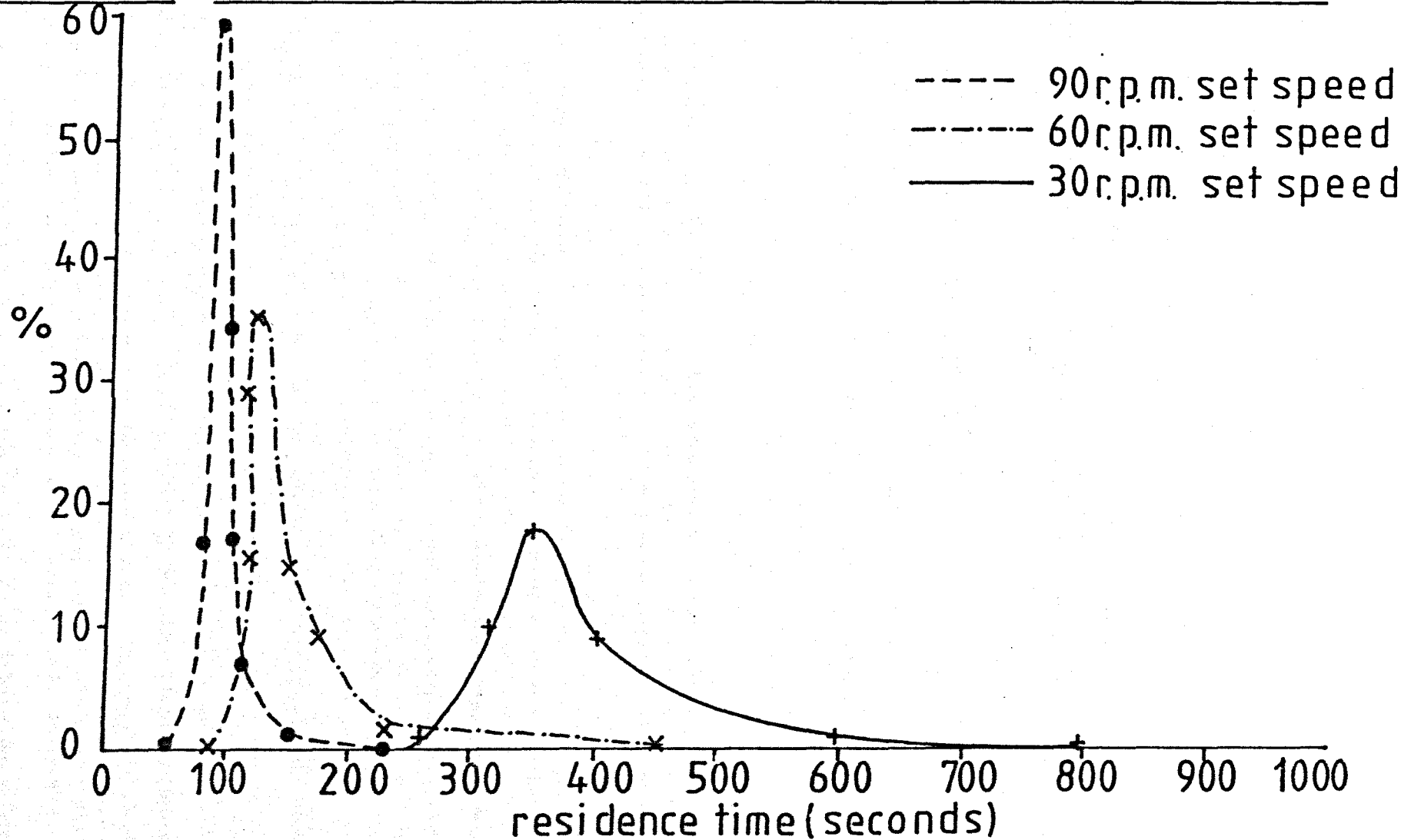
and then placed in a shielded container and counted using a Radiation

Counter - γ - Spectrometer. The residence time distribution was obtained

from a plot of percentage activity against time. Typical results

using the 25 mm extruder are shown in Figure 2.7.

2.4.1.2 Safety precautions when using radioactive tracers

Nuclear radiation constitutes a health hazard and therefore radio-

active materials should be handled with care. The code of practice

governing the handling of such materials, and the levels of radiation

allowed is given in "The Ionising Radiations" (sealed sources) Regulations

1961.

2.5 Screw extraction experiments

2.5.1 25 mm and 45 mm 'Betol' extruders

Examination of residual fibre lengths for the extrudates obtained

in Section 2.3 indicated that whilst the extrusion process was a necessary

requisite for providing uniformly dispersed monofilaments, it was the

prime factor in the loss of composite performance expected from the

incorporation of glass fibres. A major objective of this study was to

investigate the mechanism by which fibres were degraded in length. Such

information, however, could only be obtained by examination of the degree of

fibre attrition occurring as the glass-polymer mixture passed through the

various functional zones of the extruder. For both the 25 mm and 45 mm

Betol extruders no facilities were available for screw extraction. For

the 25 mm machine, therefore, a 1 tonne side jack was mounted at the rear

of the machine to push the screw out of the barrel - Figure 2.8. For the

45 mm machine a hand cranked arrangement was used to extract the screw.

In both instances withdrawal of the screw containing the fibre-polymer

blend was accomplished by removal of the die, breaker plate and transducer,

the screw then being extracted hot and the material removed from the

screw and labelled. Selected samples were analysed to determine the cross

channel fibre length distributions, the respective sampling positions being

indicated in Figure 2.9.

2.5.2 50 mm 'Bone' extruder

Samples obtained from the above machines, whilst being adequate
for fibre length analyses, provided no information as to the processes
of solids conveying, melting and mixing, occurring within the extruder.
Further studies were carried out on the 50 mm machine. This machine
was fitted with a crash cooling facility on the barrel and thus provided
samples suitable for both fibre length measurements and visualisation of
the processes occurring. The extruder was flood fed with a 30% by weight
blend of 3 mm chopped strands and Maranyl A100 using a screw speed of
60 rpm and a 'flat' temperature profile of $290^{\circ}C$. Fibres used in
these experiments comprised the standard F.G.C.S. 1640 sized material and
similar fibres sized with a non-ionic polyvinyl acetate emulsion. When
steady conditions were established the heaters were switched off and the
screw stopped using the emergency stop button. Water cooling was
introduced into the barrel, the die head and breaker plate arrangement
being removed before the polymer solidified. After approximately 1 hour,
the cooling water was stopped and the barrel reheated to $258^{\circ}C$ to aid
removal of the screw. Screw extraction was accomplished from the front
of the machine. The polymer-glass samples were removed at one-half turn
intervals and retained for subsequent analysis. In addition to the above
experiments, suitable samples were obtained for a similar blend in which
1% by volume of the glass fibres was replaced by carbon fibres. These
fibres gave excellent results in marking the solid and melt boundaries
and in addition acted as tracers highlighting any specific flow patterns
in the melt filled regions of the extruder channel.

2.6 Melt feeding studies

The principal requirement of a plasticating extruder is to convert
solid polymer into melt and to deliver this molten material at a steady
rate to the die for subsequent extrusion. It shall be shown that the
melting process largely controls the resultant fibre length distribution,

since it is in this region that the fibres are subjected to the highest stresses encountered during their passage through the extruder. An obvious alternative is to introduce the fibres downstream into the molten polymer. However, in such a system it is to be expected that the inadequacies in mixing as discussed in Section 1.2 (c) would lead to undispersed fibres being present in the resultant extrudate. Such problems can be readily eliminated by the use of mixing devices of the types indicated in Figure 2.10. A three stage screw was assembled as illustrated in Figure 2.11. Two Egan (38) mixing sections were incorporated in the screw profile. The first mixing section, located at the end of the primary screw, ensured that no unmelted polymer entered the secondary screw. The glass fibres were introduced into the feed section of the secondary screw via a screw feeder which was bolted onto the side of the extruder barrel. Devolatilisation was achieved by means of a vacuum vent situated in the feed section downstream of the glass feed. The glass fibres and molten polymer were passed through a second Egan section sited in the feed zone of the tertiary screw to ensure adequate dispersion of the fibre bundles. The resultant extrudate lace was cooled in a water bath and then diced to provide material suitable for injection moulding.

Since, in the above studies, the glass fibres were introduced into the molten polymer, control of glass content could only be achieved by synchronisation of the polymer and glass throughputs. Figure 2.12 indicates the throughput rates of nylon A100 and 3 mm F.G.C.S. 1640 chopped strands through the extruder and side screw feeder, respectively. In both instances the materials were flood fed and outputs determined at 1 minute intervals for a period of three minutes. Extrudates were produced from the above materials for a range of glass contents and screw speeds.

2.7 Measurement of fibre degradation

Two techniques were developed to assess the varying degrees of fibre fracture occurring during extrusion and subsequent injection moulding studies.

2.7.1 Wet sieving technique

Recovered fibre lengths encountered in this investigation ranged from the starting length of 3 mm to 0.030 mm for extracted screw samples, extrudates and some injection moulded coupons. In many instances undispersed bundles and monofilaments of various lengths were present in the same sample as indicated in Figures 2.13 to 2.15. Examination of the literature indicated several methods proposed for the determination of fibre length (69), (71), (73). However, of these, the technique used by Burns et al (71) provides the greatest discrimination. The above method utilised a Zeiss Particle Size Analyser to count photographs of extracted fibres. The actual size range of this instrument is 1.0 mm to 27.7 mm and thus all fibre images must lie within these limits if truncated distributions are to be avoided. Obviously, for the distributions encountered in this study, more than one enlargement would be required to encompass the whole fibre length range. In addition the spread of fibre lengths was such that approximately 2000 counts would be required to accurately characterise the fibre length distribution. It was to reduce the total number of counts that a wet sieving technique was adopted. Such a process is described below and in Appendix 3.

Approximately 0.2 grams of fibres, recovered from the matrix polymer by ignition in an electric muffle at $600^{\circ}C$, were dispersed in water in a 250 ml. measuring cylinder. Any undispersed fibre bundles were allowed to settle out before decanting the dispersed material through a sieve stack in which the level of water was maintained at a constant

height above the top sieve - Figure 2.16. The remaining fibre bundles were then dispersed by placing the measuring cylinder, containing 100 ml. of water, in an ultrasonic bath for approximately 30 seconds. This material was then decanted through the sieve stack as before. The 'fines' passing through the sieve stack were collected by filtration, dried in an air oven and then weighed. The sieves were then separated, dried and weighed. The various fractions were dispersed in isopropyl alcohol, cast onto glass slides, and photographed at suitable magnifications such that each photograph contained approximately 100-200 fibres. The fibre images could then be counted in the normal manner on the Zeiss Analyser or by means of the modular pen system described in Section 1.6.2. Such a system was used for classifying fibre lengths in the latter phase of this study.

It is evident from the sieve distributions obtained - Figure 2.16 that whilst appreciable overlap occurred for each sieve, the individual distributions were considerably narrower than the original population from which they were derived, almost all the 'long' fibres being deposited on the 2.80 mm sieve.

The sieve fractions could be accurately characterised in a relatively small number of counts, the use of a computer programme enabling the total fibre length distribution to be obtained in about 1000 counts. For those samples comprising very narrow fibre length distributions, as typified by the high glass content tensile bars and recycled materials, it was often sufficient to pass the sample through one or two sieves to remove the very fine material before counting and combining the populations as before. Average analysis time in these instances was approximately two hours. Duplicate analyses indicated excellent agreement and thus this technique was used throughout this study.

2.7.1.1 <u>Generation of original distributions from measured sieve populations</u>

Let original sample weight = Wgrams where $0.18 \leqslant W \leqslant 0.22$ gms. After sieving, this sample is divided among the various sieves and fines

such that:-
$$W = \sum_{n=1}^{n=8} ws$$

where ws = weight of sample retained on sieve or filter paper.

Also $8 \geqslant n \geqslant 1$, where n = number of sieves + 1. For each fraction

collected a sample is taken and the length distribution by number

determined in the manner described above. Since this sample

distribution is assumed to represent the population distribution of

the sieved fraction, then the length distribution by weight for

fibres in any length interval, li, is given by:-
$$ws \times n_i l_i / \sum_{i=1}^{i=48} n_i l_i$$

where n_i = number of fibres classed in a particular length interval

and i = 1,2.......48.

Thus the total weight of fibres in any fraction is given by:-
$$ws = \sum_{i=1}^{i=48} \left(ws \times \frac{n_i l_i}{\sum_{i=1}^{i=48} n_i l_i} \right)$$

Hence, the total sample weight will be:-
$$W = \sum_{n=1}^{n=8} \left(\sum_{i=1}^{i=48} ws \times \frac{n_i l_i}{\sum_{i=1}^{i=48} n_i l_i} \right)$$

dividing the above equation by W and expressing as a percentage

enables the original fibre distribution to be expressed as a weight

or volume percentage against length interval. A computer programme

was established to carry out the various summations required. The

actual length intervals for each fraction will be dependent upon

the magnifications used in producing the fibre photographs. There-

fore, a statistical apportioning technique was included in the

programme to prevent any bias occurring in the combining of the

various populations. The print out of the actual programme is given

in Appendix 4.

2.7.1.2 Number average and weight average lengths

It is common practice to quote values of average fibre lengths.

However, the expression of average length can be made in two specific

feed hopper

vent

1 tonne hydraulic jack

- 83 -
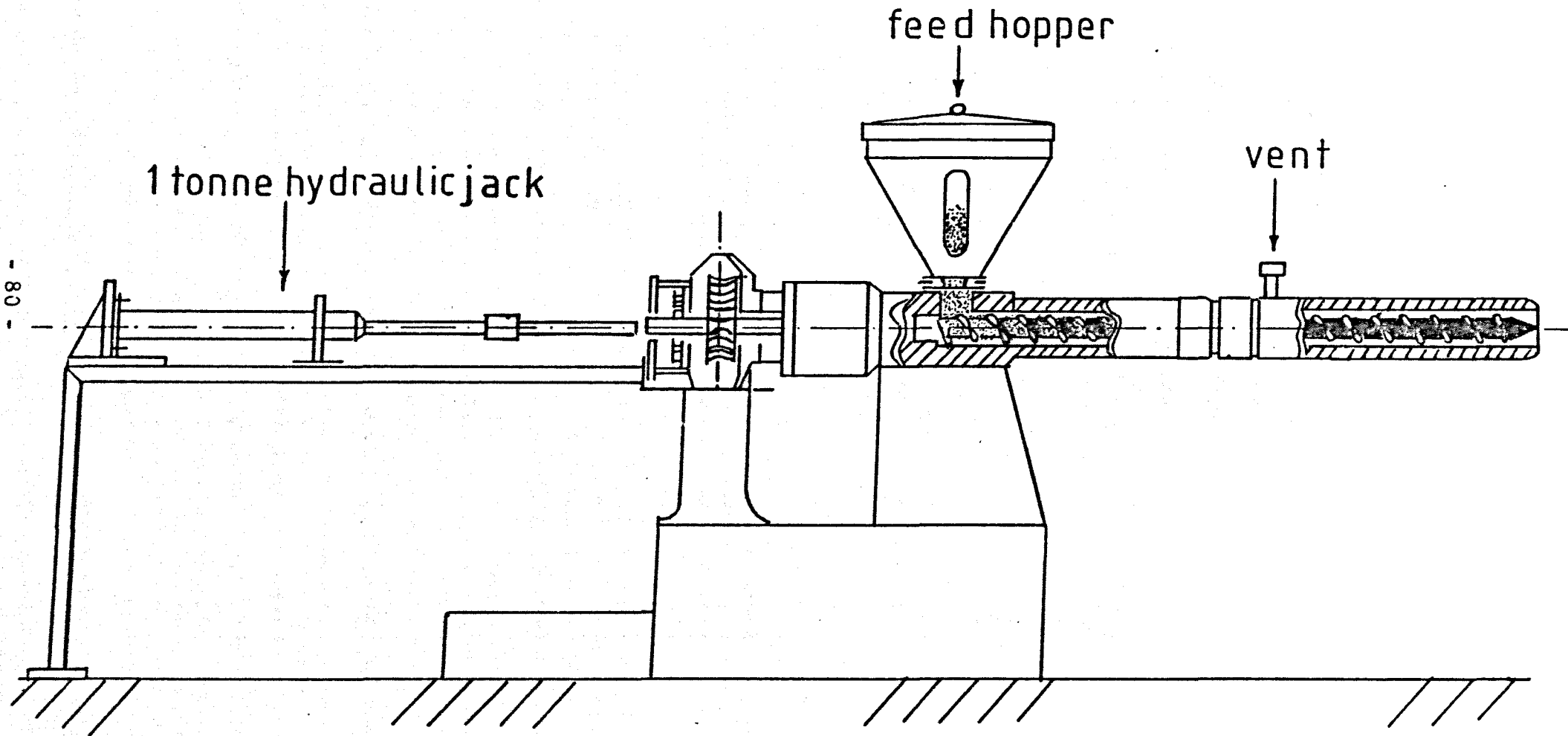
Figure 2.8 screw extraction 25mm Betol extruder

channel
number 22 →
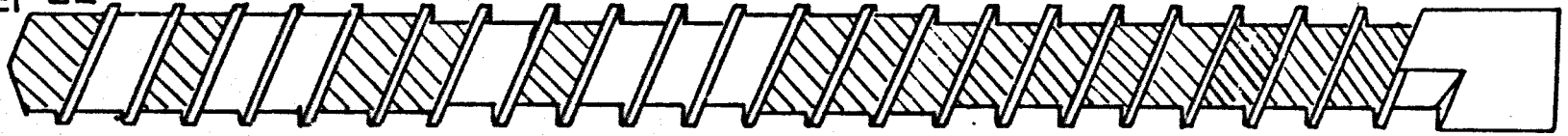
25mm Betol extruder

.31 →

45mm Betol extruder

\\\\\ sample location

Figure 2.9 sampling positions for fibre length analyses

Figure 2.10 typical mixing devices for single screw extruders (37)
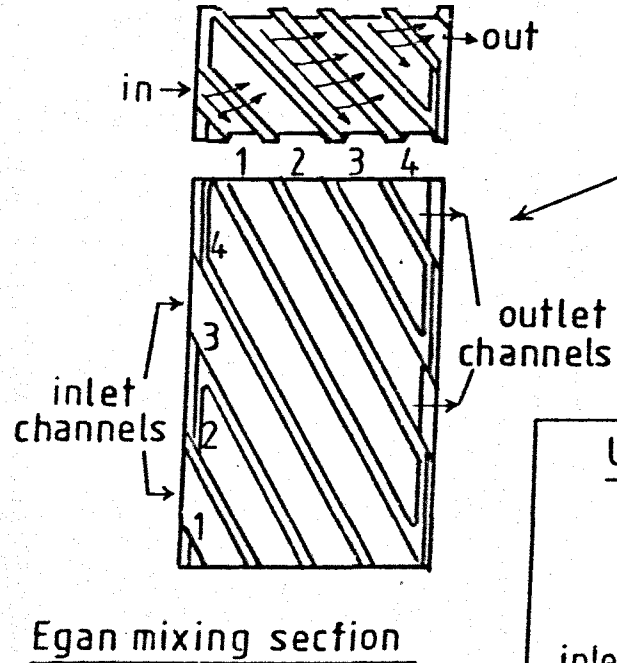
DISTRIBUTIVE MIXERS
DISPERSIVE MIXERS

Egan mixing section

Union Carbide mixing element

ABOVE :- slotted disc mixing section

BELOW :- 'DIS' mixing section
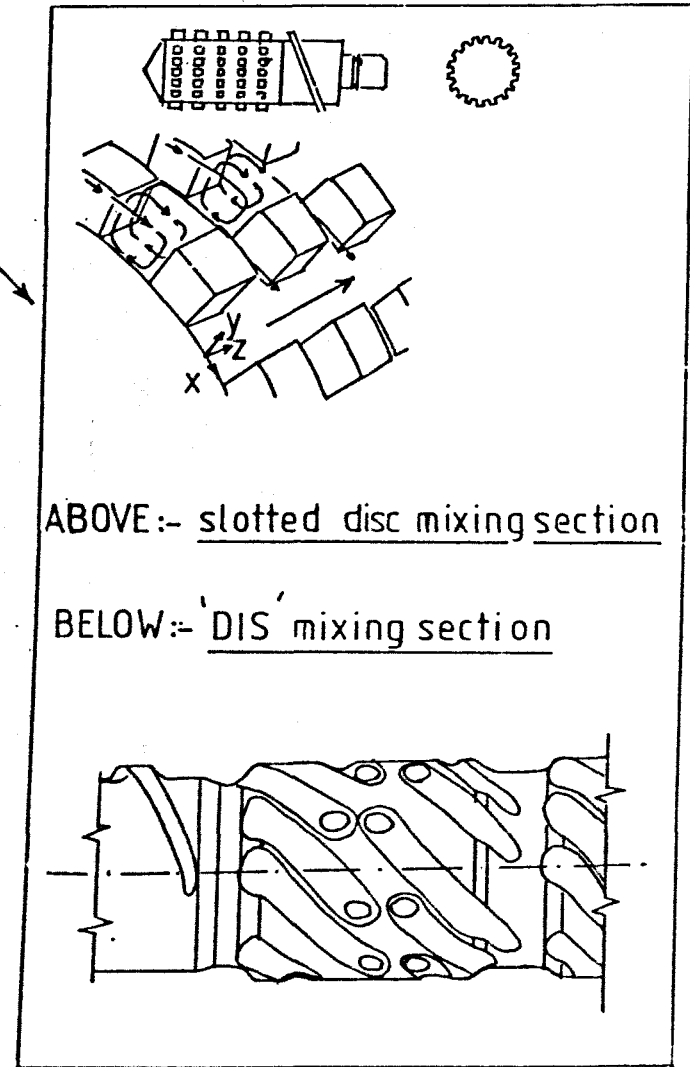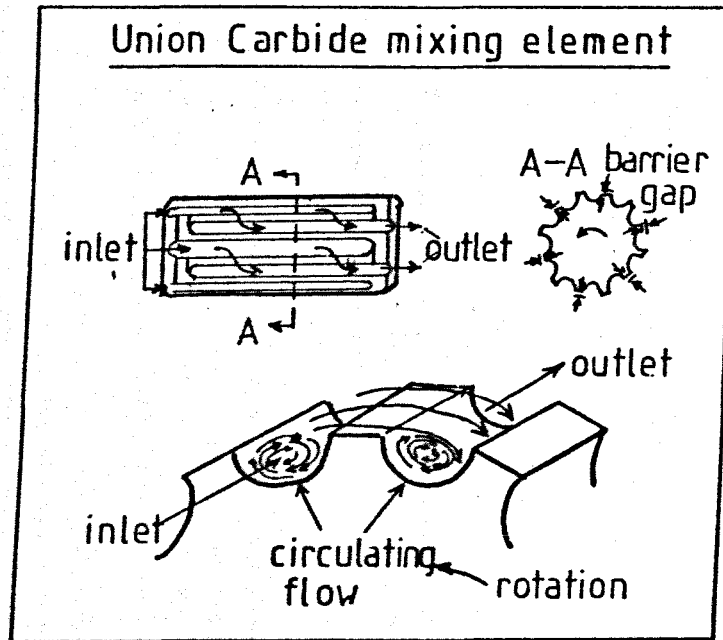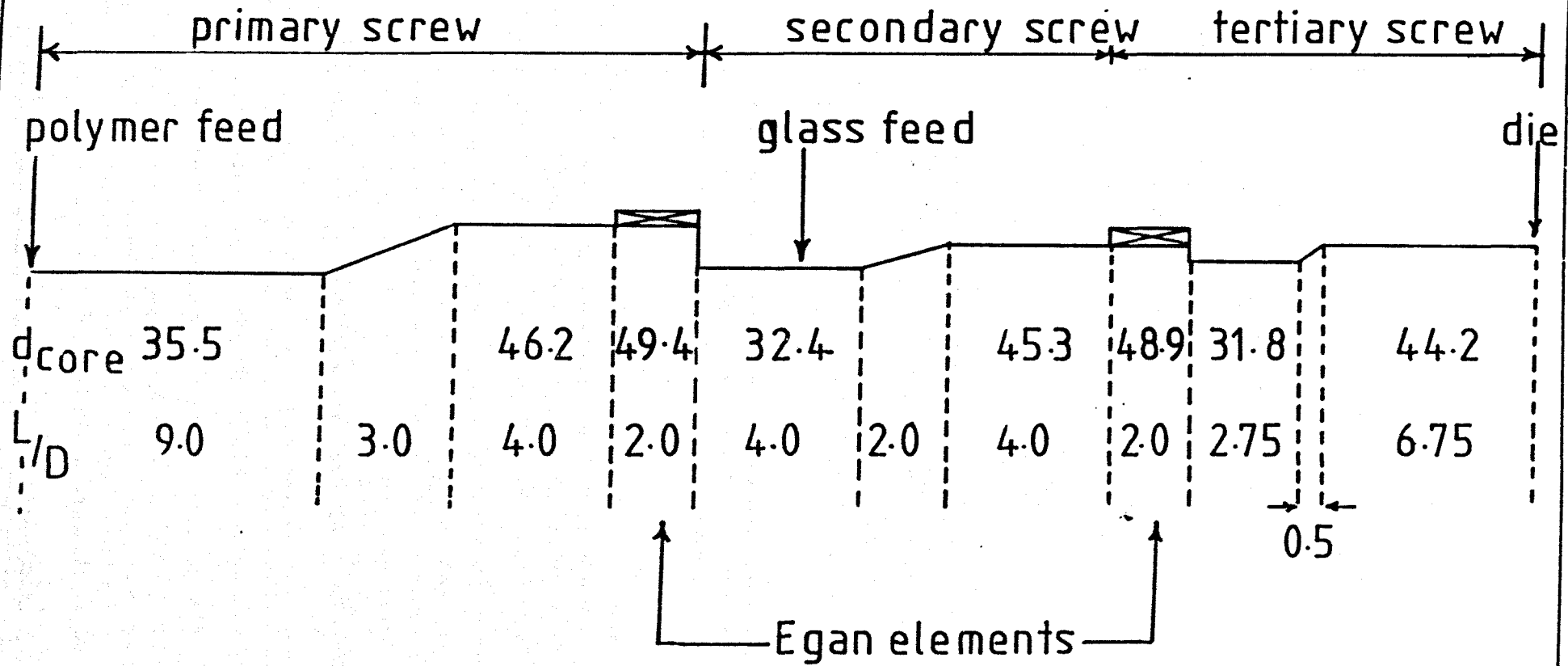
Figure 2.11 screw profile used in glass to melt experiments
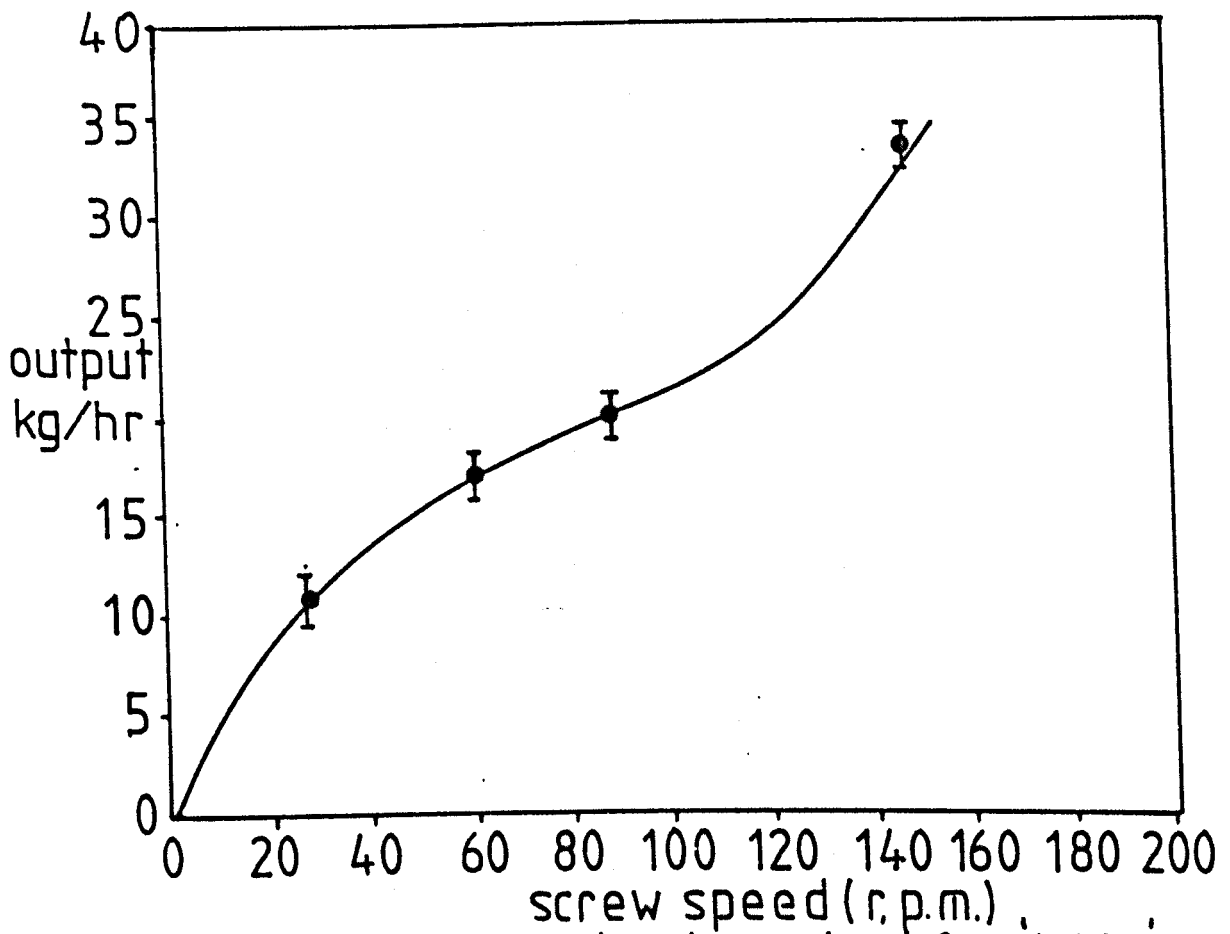
Figure 2.12(a) extruder output for A 100
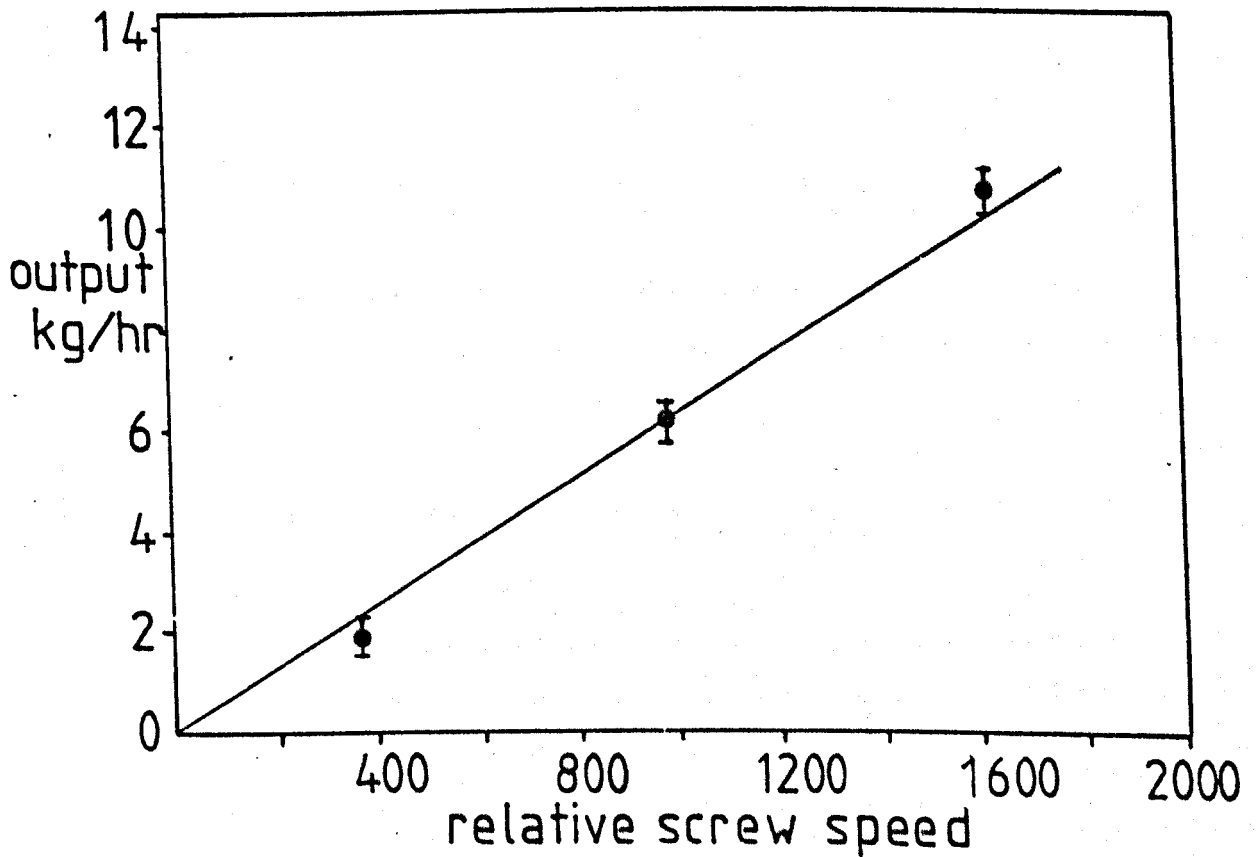
Figure 2.12(b) output of side feeder
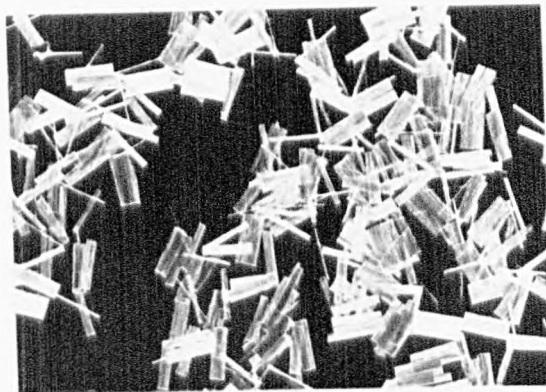
Figure 2.13 (a)

extruder
feed zone 1
screw 1

Figure 2.13 (b)
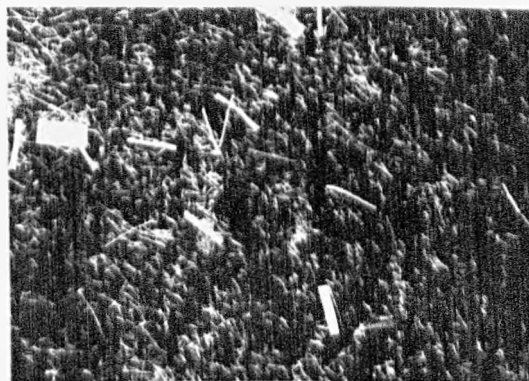
extruder
feed zone 10
screw 1
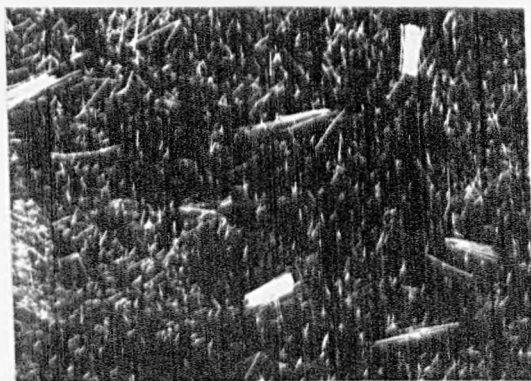
Figure 2.14

extrudate
screw 3

Figure 2.15

injection
moulding
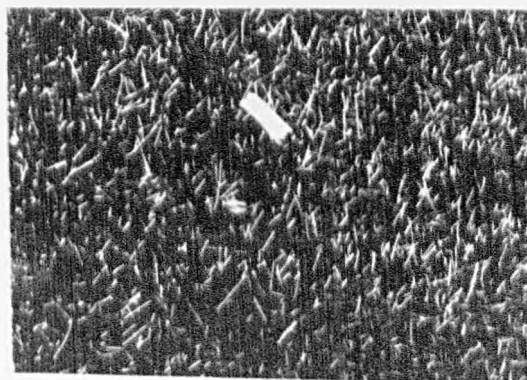
magnification = 2×

Figure 2.16
wet sieving analysis

ways:-

(i) <u>Number average length</u>

defined as:-

$$\bar{L}n = \frac{n_i L_i}{\sum n_i}$$

(ii) <u>Weight average length</u>

defined as:-

$$\bar{L}\omega = \frac{\omega_i L_i}{\sum \omega_i} = \frac{n_i L_i^2}{\sum n_i L_i}$$

Obviously the weight average length will be the more sensitive to changes in the higher fibre length region of the distribution and is therefore considered to be better suited to monitoring likely changes in composite tensile strength produced by successive fibre fracture in the manufacturing processes.

2.7.2 <u>X-ray radiographic analysis</u>

Extruded compounds produced in this study often contained undispersed fibre bundles many of which survived the subsequent injection moulding process. Such integral strands could be detected by X-ray radiography - Figure 2.17. These X-ray radiographs were used in combination with the Quantimet Image Analysing Computer to obtain a relative measure of the number of fibre bundles present in the various samples. The Experimental procedure is described in Appendix 5.

2.8 <u>Surface profile measurements - injection moulded discs</u>

Injection moulded glass-reinforced thermoplastic articles generally exhibit high differential shrinkage due to the presence of a specific fibre orientation distribution (81). Thus, whilst in general the overall contraction is less than for the unreinforced material, it will be greater in the direction transverse to the direction of flow. Problems of 'warpage' caused by the above effect are generally significantly reduced by the correct choice of gating, processing and design factors. In addition to the above problem, examples of poor surface finish caused by the presence of undispersed fibre bundles are often cited in the literature (10) (41). However, no actual measurements of this surface roughness

appear to have been carried out, the assessment of this parameter being extremely subjective. During this study the varying degrees of surface roughness, attributed to undispersed fibre bundles, were assessed using the Rank-Taylor-Hobson, Talysurf 4 (82). This equipment finds wide use in the evaluation of surface texture of steel components, the schematic arrangement being illustrated in Figure 2.18. The operation of the instrument is straightforward, complete instructions being provided in the manual. The sampling length for surface roughness measurement can be varied from 0.25 mm to a maximum of 11 mm. To obtain an adequate representation of the disturbances in surface profile occurring, the maximum sampling length was used. Typical profiles obtained for injection moulded glass fibre-reinforced nylon discs are indicated in Figure 2.19. To avoid bias in the selection of a region for measurement the Mean 'Centre Line Average' (CLA) was also determined.

2.8.1 Determination of Centre Line Average

The CLA of the roughness irregularities on a surface is defined as the average value of the departures both above and below its centre line, throughout a prescribed sampling length, see Figures 2.20 (a) and 2.20 (b). Surface texture values were assessed as mean results of at least ten CLA values determined along the surface.

2.9 The interaction of fibre sizing materials and Nylon 6.6

In common with most commercial chopped strands, fibres used in this study were coated with between 1% and 2% of a sizing material. In a typical fibre reinforced composite containing 30% by weight of reinforcement this size will constitute approximately 0.5% of the total, rising to 1.2% in the 60% by weight fibre filled materials. F.G.C.S. 1640 strands are coated with a cationic film former which softens at approximately 90°C. During extrusion compounding this material is likely to be dispersed in the molten polyamide polymer. Additionally, the polyvinyl acetate film former also used in this study is known to degrade at 250°C to generate

acetic acid (83). The presence of such an acid, at the elevated
temperatures existing in the extruder, produces chain scission of
the polyamide leading to a reduction in the molecular weight of
the matrix polymer (84). Changes in molecular weight will be reflected
in the melt viscosity and mechanical properties of the polymer (77).

2.9.1 Measurement of viscosity

Nylon pellets, coated with 3%, 1% and 0.5% by weight of the
above materials, were passed through the 25 mm Betol extruder. The
resulting compounds were cooled and diced before being vacuum dried
overnight at $90^{\circ}C$. Two techniques were used to monitor changes in
melt viscosity:-

2.9.1.1 Melt Flow Index

This value represents only a single point measurement which is
obtained at an extremely low shear rate; hence it is of little value
in assessing viscosity changes over the range of shear rates encountered
during the common processing techniques used for thermoplastics. None-
theless flow rate or melt flow indices, obtained for a particular
material, did provide an indication of changes in molecular weight
occurring. Melt flow index values were obtained for the above extrudates
by the method described in B.S. 2782, Procedure B. Initial residence
times of 5, 15 and 30 minutes were used, samples being taken between
the piston marks at 30 second intervals.

2.9.1.2 Instron Capillary Rheometer (85)

This is a constant rate apparatus which continuously measures the
force required to drive the molten polymer through a capillary at a
specified rate. Variations in shear rate are achieved by changes in
the cross-head speed. Typical shear rates are $10^{-1}sec^{-1}$ to
$10^{6}sec^{-1}$ which encompass all shear rates likely to be encountered
in practical processes. Since all commercial thermoplastics are to
some degree pseudoplastic (i.e. shear thinning) it is obviously

important to determine the melt viscosity over a range of shear rates which spans the required operating conditions. Such measurements were made for the base polymer and for extrudates containing 1% by weight of the respective size coatings at temperatures of $280^{\circ}C$, $290^{\circ}C$ and $300^{\circ}C$ for initial residences of 5 minutes. Results were corrected for entrance pressure losses after the method of Bagley (86). Shear rates and viscosities were left as apparent values in that the usual Rabinowitsch corrrection (87) has not been applied. Results for the various glass filled grades used in this study were also obtained using the above apparatus, for use in the melting programme described in Section 3.1.9.4.

2.10 Injection moulding

The various extrudates prepared during the course of this study were injection moulded to produce samples for subsequent mechanical testing and fibre length studies. The machine used was an Ankewerke Al765 Series which possessed a plasticising capacity of 4 oz. Two tensile and impact bars conforming to ASTM D638-68 and ASTM D256 respectively, were made for each moulding cycle, at least 30 impressions being made for each experiment. In addition, disc mouldings were prepared for talysurf measurements and X-ray radiographic analysis. Operating conditions are described below. These settings were used for all samples irrespective of the level of glass reinforcement or base polymer.

Injection moulder settings

Screw speed = 71 rev/min.

Temperatures, $^{\circ}C$

Nozzle   =   280

Cylinder:

Front   =   280

Middle   =   280

Rear   =   280

Mould:

Fixed   =   80

Moving   =   80

Time cycle, sec.

Injection   =   1.5-2.0

Follow up   =   10

Screw return   =   6

Cooling   =   25

Pause   =   2

Pressures MN/m^2

Injection   =   6.1

Follow up   =   5.5

Screw return   =   0

2.11   Mechanical property determination

Specimens were conditioned prior to testing by either vacuum

drying for 16 hours at 90°C or by immersion in boiling water for 72

hours. In each case the results quoted represent the mean of at least

ten determinations for tensile and impact bars. Extensions to

failure and 0.5% tangent moduli were also measured using cross head

speeds of 2 cm/min. and 0.2 cm/min.,respectively. All testing was

conducted in accordance with B.S. 2782:1970 (88). In addition to the

glass reinforced materials, tensile and impact tests were carried

out for the various unreinforced nylon 6.6 grades used in this study.

Punch shear tests (Appendix 1) were also carried out on these materials

to determine the interlaminar shear strength.

2.12   Glass content and fibre length samples

Glass contents were determined on fractured, vacuum dried tensile

bars by cutting sections approximately one cm. on either side of the

fracture zone. This material was placed in an electric muffle at

600°C for 20 minutes to remove the organic matrix. The fibre length

distribution of these extracted fibres was subsequently determined using

the procedure described in Section 2.7.1. Similar glass content
- fibre length analyses were carried out on extruded materials and
extracted screw samples. Fibre degradation occurring during direct
injection moulding of glass fibre - polymer dry blends and in the
sprue and runners of extruded/moulded materials was also monitored.

2.13 Structural studies

2.13.1 X-ray radiography

In addition to its use in monitoring fibre dispersion in injection
moulded articles, as described in Section 2.7.2, this technique was
extended to the extruder channel sections obtained from the 45 and 50 mm
extruders. After screw extraction the fibre-polymer blend was
chipped off the screw using brass chisels. The samples were taken at
one half turn intervals across the channel width at right angles to
the flight face - Figure 2.21. The fragile nature of most of the
sections required that they be encapsulated in epoxide resin prior to
final sectioning and mounting. Sections 3 mm in thickness were cut on
a diamond saw and then mounted on a card prior to irradiation. The
resulting positive prints, obtained by projection of the x-ray radio-
graphs onto photographic paper, gave good discrimination between the
regions of dispersed and undispersed fibre bundles. Comparison of
such prints with sections in which the melt and solid boundaries were
marked by incorporating carbon fibres in the glass-polymer blend are
shown in Figure 2.22. The suitability of the former technique in
monitoring the degree of melting occurring in glass fibre-polymer
blends is evident. The relative areas of solid and melt in sections
removed from the melting region of the extruder were obtained by
projection of the X-ray radiographs onto paper which was then cut into
the relevant sections and weighed.

Application of the above technique to glass fibre filled polymers
removes the requirement of a tracer material, as used by Fenner et al (23),

to discriminate between the solid and melt filled regions existing in the melting zone. The use of finely divided carbon black as used by the above workers was found to be unsuitable in this study. The success of the extrusion process in compounding glass fibre - polymer tumble blends is partly due to the static attraction of the fibres for the polymer pellets. Coating of the polymer with carbon black destroys this static attraction producing segregation of fibres and polymer and hence poor feeding and unsteady processing conditions.

2.13.2 Optical microscopy

2.13.2.1 Cross sectional studies of melting sections

Samples containing carbon fibres were sectioned to facilitate observations of fibre fracture and alignment in particular regions of the extruder channel. The various sections are illustrated in Figures 2.23 - 2.27.

2.13.3 Stereo-scanning microscopy

Fracture surfaces of broken tensile bars were examined using a Cambridge Stereo Scanning Microscope. As indicated in Figure 3.45 those composites containing undispersed fibre bundles invariably featured such bundles in the fracture surface. In addition, in many instances, these materials failed at a lower stress than similar specimens in which the reinforcing units were present as uniformly dispersed monofilaments.

2.13.3.1 Matrix cracking in strained tensile bars

During testing of tensile specimens which had previously been conditioned by boiling for 72 hours in water, pronounced matrix cracking was observed immediately prior to fracture. The region of most intense cracking was normally close to the resulting fracture zone. The Stereo-scanning microscope was used to examine the surface cracks in these specimens, see Figure 3.56.

2.14 Fibre property measurements

The total reinforcing efficiency of a glass fibre will be
determined not only by its length, but also by its diameter and
strength.

2.14.1 Filament diameter

Strands possessing nominal filament diameters of 10, 11 and
14 microns have been used in this study. However, during manufacture,
variations in viscosity and drawing speeds produce fluctuations
in filament diameter. Histograms of typical recorded values are
given in Figures 2.28 - 2.30. These variations in filament diameter
will obviously influence the value of the critical fibre length
calculated by equation 1.3.

2.14.2 Strand strength

The virgin strength of E-glass filaments is reported as 3.8
GNm^{-2} (89), although factors inherent in the production process lead
to strand strengths of 1.1 GNm^{-2} (90) for unimpregnated strands
removed from production cakes or roving. Lindsay and Hood, (91)
however, report glass strengths of 2.7 GNm^{-2} for epoxy resin filament
wound pipes. Resin impregnation prevents surface damage due to
contact abrasion and enables efficient stress transfer between the
individual filaments. It is essential, however, for the fibres to be
equitensioned and also aligned in the direction of the applied load.
Strand strengths of 2.1 to 2.2 GNm^{-2} were obtained for filaments used in
this study, see Table 2.6. Single strands were removed from the cake
and after vacuum impregnation with a polyester resin were drawn into a
0.6 mm diameter capillary tube. After curing at 105°C for 16 hrs
the rod was carefully removed from the tubing and broken on an Instron
using air grips to clamp the specimen ends. The tensile strength of a
glass fibre is also reported to be a function of its length, diameter
and the strain rate to which it is subjected (92). Strength apparently
increases with increasing strain rate and reduction in length and
filament diameter.

1·5 mm die
extruded
compound
screw 3

2 mm die
extruded
compound
screw 3

FIG. 2.17 X-RAY POSITIVE PRINTS OF INJECTION MOULDED DISCS
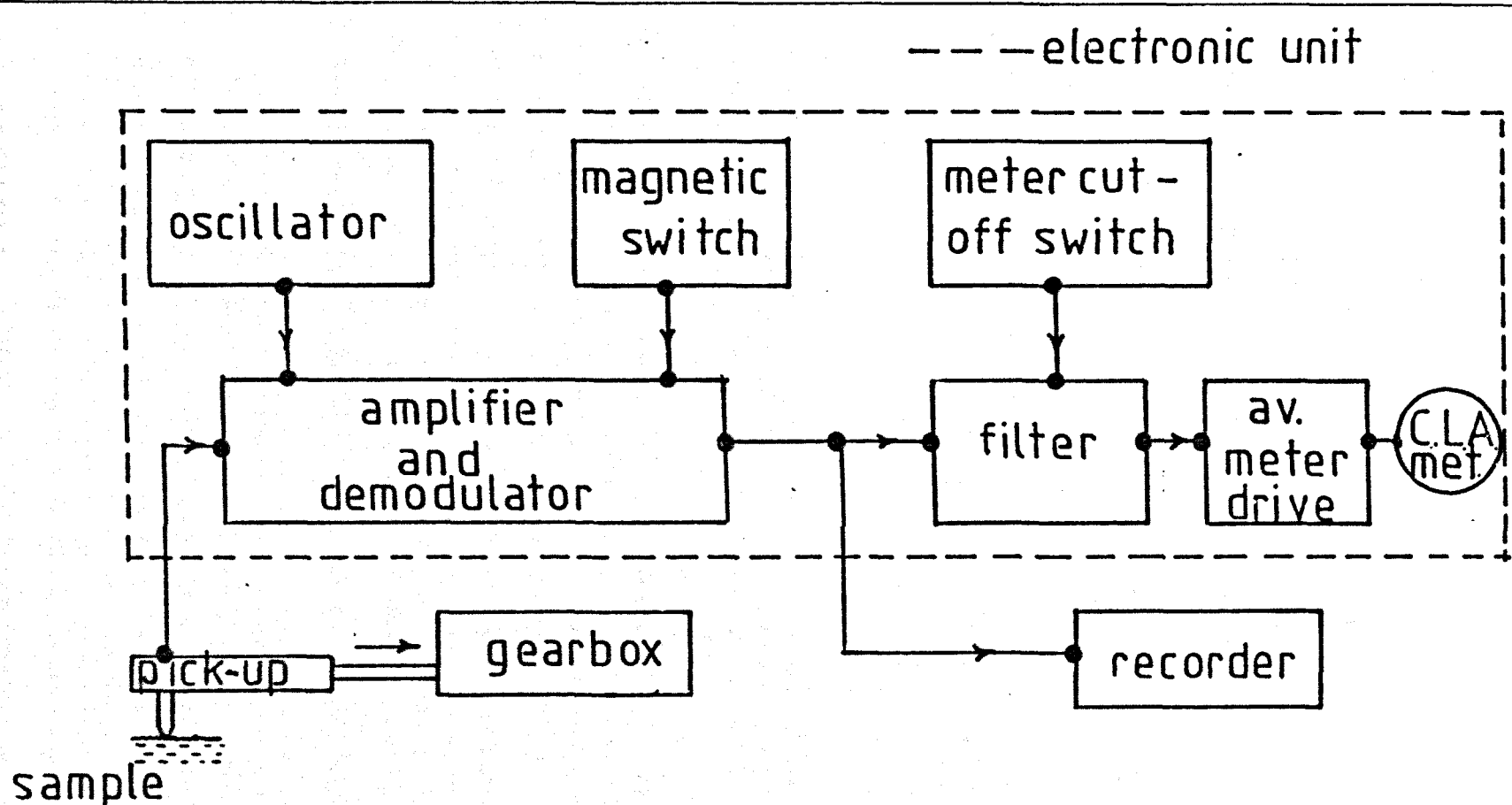
Figure 2.18 schematic arrangement of the Talysurf

mean C.L.A.= 51·1
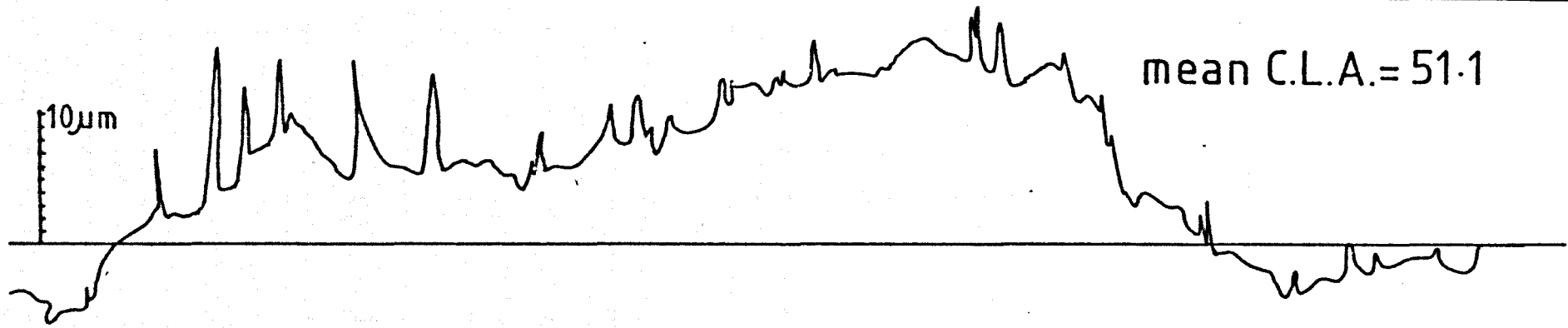
directly injection moulded glass fibre reinforced disc.
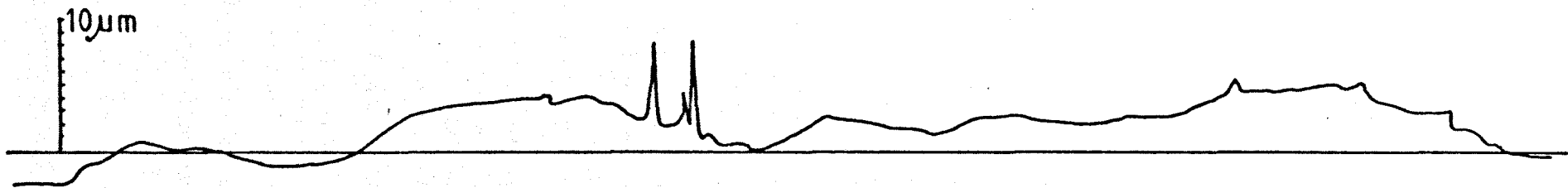
pre-extruded glass fibre reinforced disc.

mean C.L.A.= 30·0

Figure 2.19. Talysurf surface profile measurements
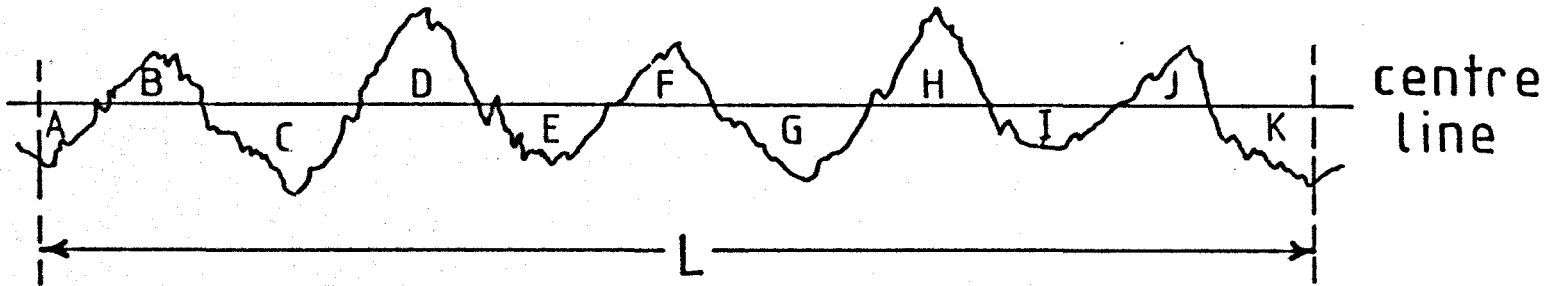
areas $B+D+F+H+J = A+C+E+G+I+K$

Figure 2.20(a)   definition of the centre line
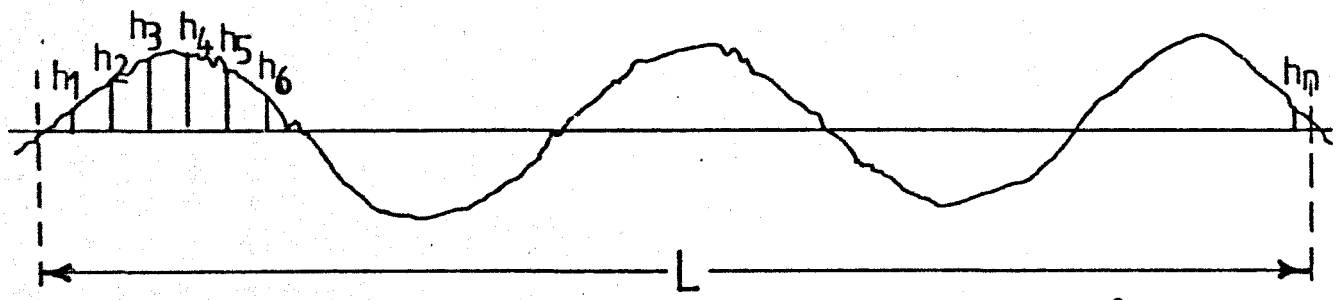
centre line average $= h_1 + h_2 + h_3 + \text{-----} h_n = \dfrac{1}{L} \displaystyle\int_L^0 h_n \, dL$

Figure 2.20(b) derivation of C.L.A.

melt flow

3 2 1

sample section

sample number indicates
number of full turns from flight
start

identification
of
pushing flight
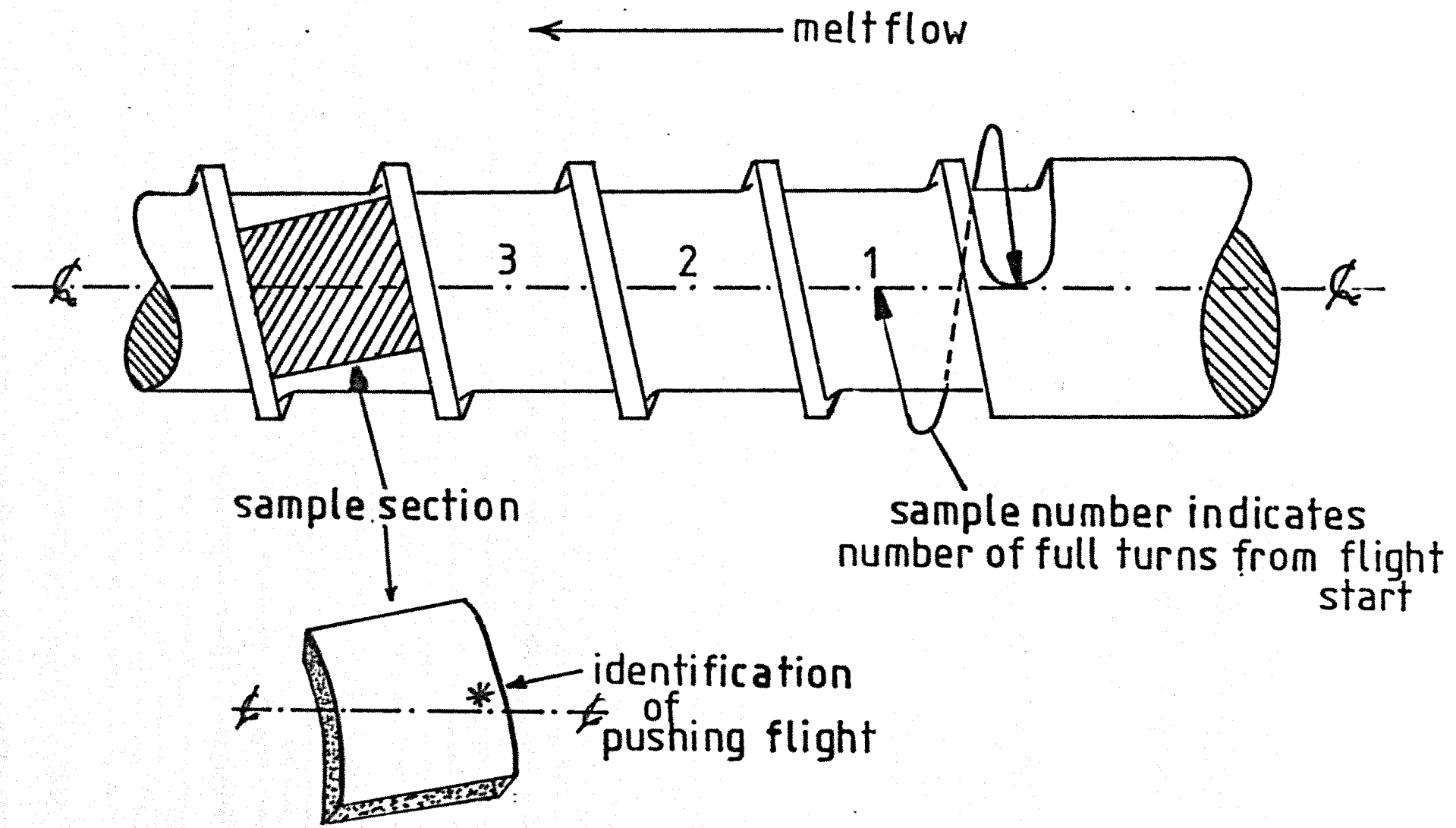
Figure 2.21 sample removal from extracted screw
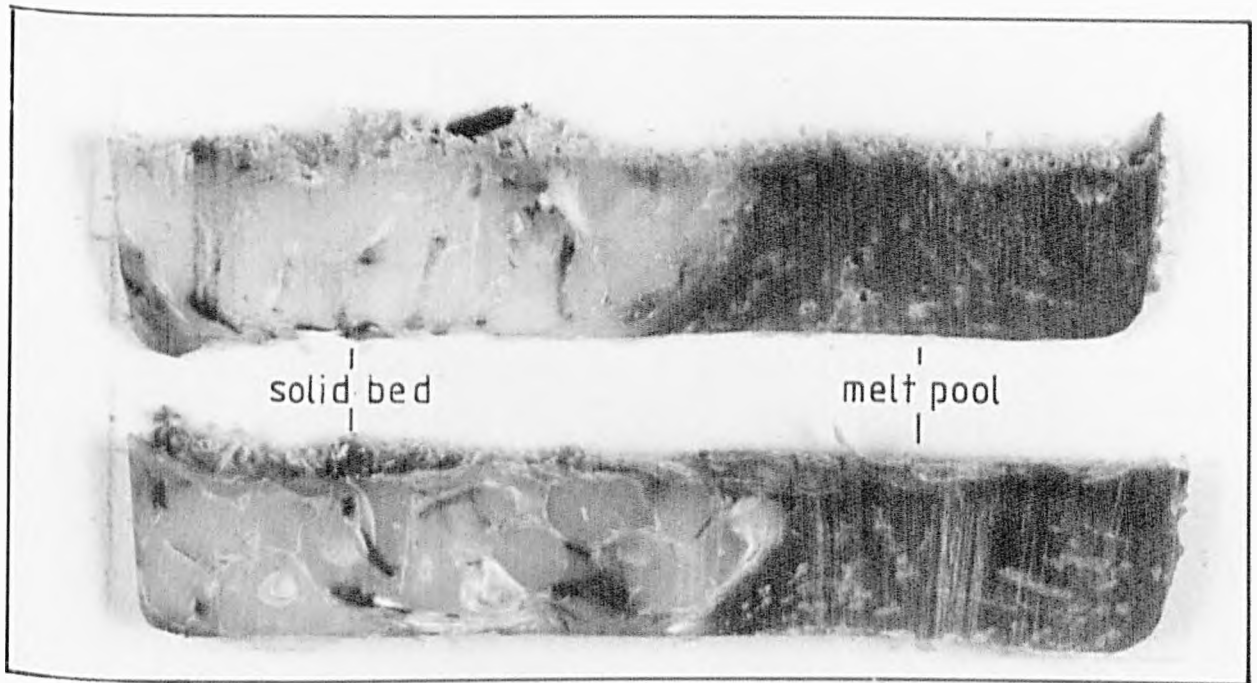
OPTICAL PHOTOGRAPH OF MELTING SECTION
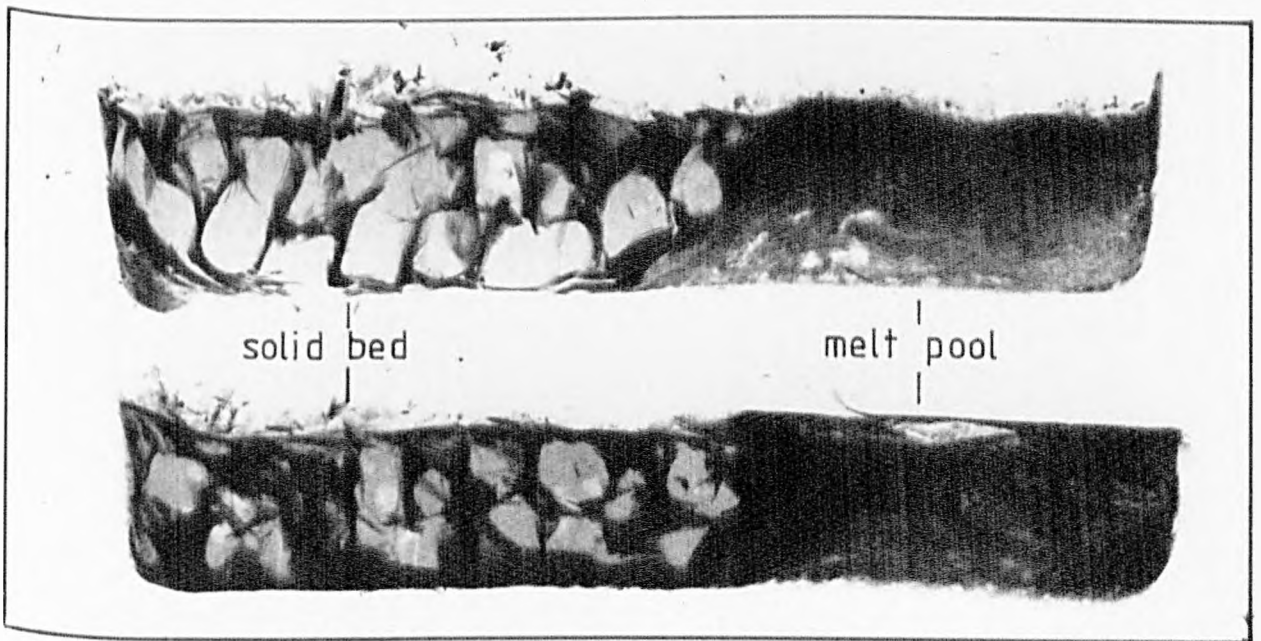
X-RAY POSITIVE PRINT OF MELTING SECTION

FIGURE 2.22 COMPARISON OF OPTICAL AND X-RAY TECHNIQUES

Fig. 2.23 melt pool-**zy** section.

Fig. 2.24 melt pool-xy section

Fig. 2.25 melt pool-xz section

Fig. 2.26 solid bed – melt pool interface-xy section
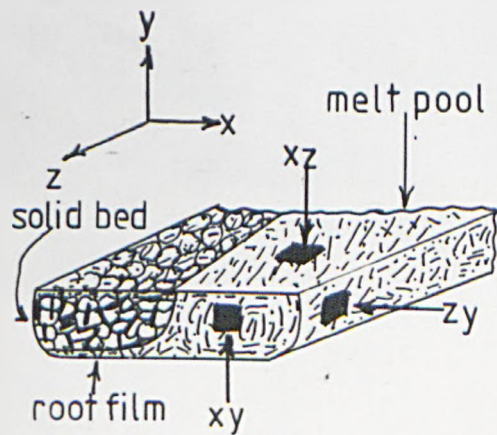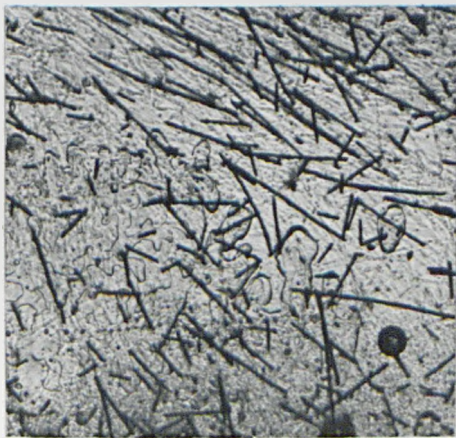
Fig. 2.27 root film-xy section

magnification = 62×

Figure 2.28 150 tex F.G.C.S. 1640
mean = 10·7
σ = 1·39

Figure 2.29 190 tex F.G.C.S. 1640
mean = 11·4
σ = 1·59

Figure 2.30 306 tex F.G.C.S. 1640
mean = 13·5
σ = 1·88
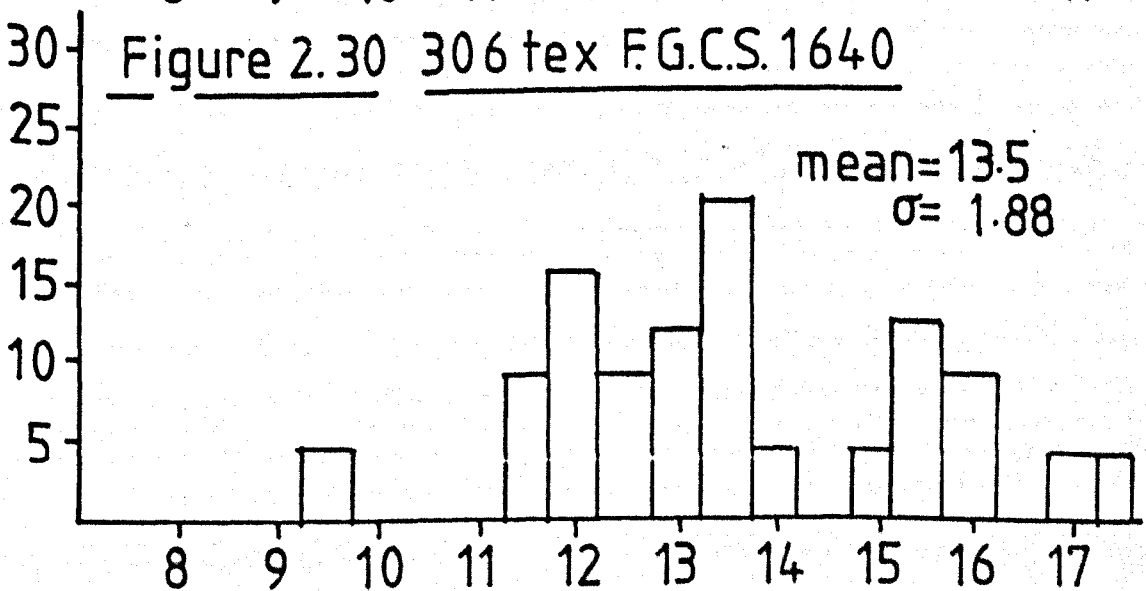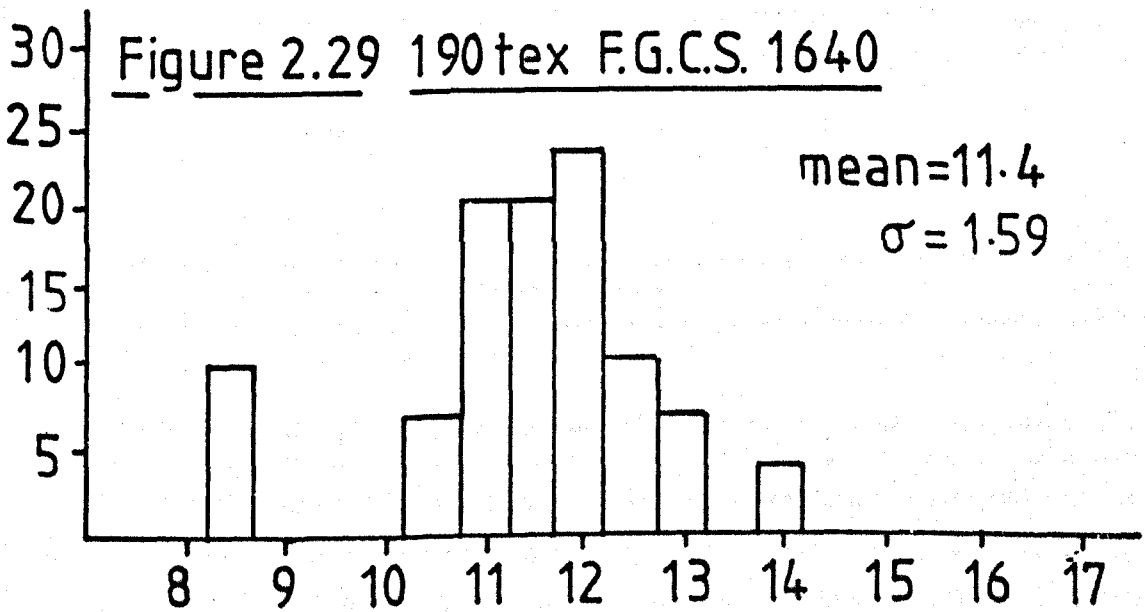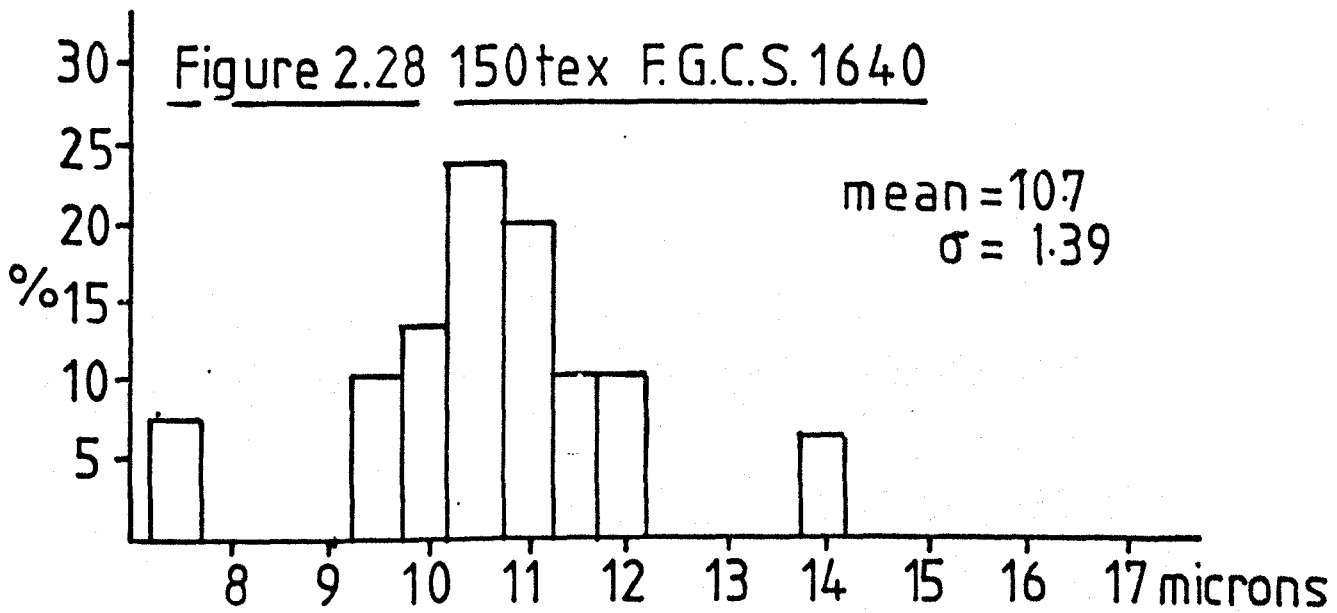
Filament diameter distributions

fibre type	break force N	strand tex gm./km.	strand solids %	actual glass wt gm/km	strand area m²	strand strength GN/m²	mean strength GN/m²
FGCS 1640 190 tex 2 split	75.2	(i) 88.1 } 187.6	1.41	86.9 } 185	34.2×10^{-9}	2.2	
	81.1	(2) 99.5	1.41	98.1	38.6×10^{-9}	2.1	
	74.4	(i) 87.1 } 188.3	1.41	85.9 } 186	33.8×10^{-9}	2.2	2.2
	90.4	(2) 101.2	1.41	99.8	39.3×10^{-9}	2.3	
	78.9	(i) 88.3 } 188.7	1.41	87.1 } 186	34.3×10^{-9}	2.3	
	78.0	(2) 100.4	1.41	99.0	39.0×10^{-9}	2.0	
XS 929 190 tex 2 split	66.0	(1) 90.0 } 192.1	2.0	88.2 } 188	34.7×10^{-9}	1.9	
	94.6	(2) 102.1	2.0	100.1	39.4×10^{-9}	2.4	
	73.4	(1) 95.0 } 193.0	2.0	93.1 } 189	36.7×10^{-9}	2.0	2.1
	64.3	(2) 98.0	2.0	96.0	37.8×10^{-9}	1.7	
	85.4	(1) 92.1 } 193.8	2.0	90.3 } 190	35.6×10^{-9}	2.4	
	86.5	(2) 101.7	2.0	99.7	39.3×10^{-9}	2.2	

Table 2.6 glass strand strengths

CHAPTER 3 RESULTS

3.1 The single screw plasticating extrusion process

The glass fibres are introduced through the feed port as an intimate physical blend with the polymer granules. The ensuing processes of solids conveying, melting, mixing and pressurisation, combine to produce molten material suitable for extrusion. The overall stability of the compounding operation and the degree of fibre fracture will be dictated by the interelation between the above functions and design, processing and material parameters. The results discussed relate to a 30% by weight blend of F.G.C.S. 1640 3 mm chopped strands and Maranyl A100 unless specifically stated to be otherwise.

3.1.1 Design variables

Extrusion processing studies utilised the two Betol extruders which were equipped with two stage screws of different compression and length to diameter ratios - Table 2.1, screws 1, 2 and 3. The 25 mm extruder differed from the larger machine in that it was not of the almost standard 'square pitch' design. In addition, the very low compression and pump ratios produced trends in processing and fibre degradation studies which set this machine apart from the larger commercial extruder. However, the results obtained serve to emphasise the importance of correct screw design for the successful extrusion of glass fibre filled thermoplastics. The influence of screw geometry on processing and fibre fracture under equivalent processing conditions is illustrated in Table 3.1. Changes in specific power consumptions are mirrored in the mean fibre lengths of the resultant extrudate. However, as indicated in Figure 3.1 such differences in the recovered fibre lengths occur primarily by changes in the fraction of undispersed fibre bundles rather than shifts in the fibre distribution as a whole. A significant proportion of undispersed

strands is observed in the extrudate produced on the lowest compression ratio machine.

3.1.2 Processing variables

3.1.2.1 Pressure control

Variations in back pressure, achieved by restrictions at the die, are used to control the output and degree of mixing occurring in single screw extruders. For two stage machines such effects are generally not observed for the reasons discussed in Section 2.3.2.1. However, increases in discharge pressure are often desirable and lead to an overall improvement in the stability of the process by 'damping' out any fluctuations occurring in the feeding or melting processes.

Pressure changes were produced in this study by using dies of different diameters. The pressure-output relationships for the three screws are illustrated in Figures 3.2(a) to 3.2(c). The discharge pressure obviously increases with reduction in die diameter and increased screw speed. The curved characteristics of these plots reflect the reduction in melt viscosity which accompanies an increase in shear for pseudoplastic materials.

As expected no significant change in output occurred for the larger machine although for both screws the output stability of the system was significantly improved when using the smaller diameter dies. In contrast the output of the 25 mm extruder proved to be extremely sensitive to imposed back pressure due to the extremely low pump ratio. During 'normal' operation polymer would exude from the barrel vent under all but the lowest pressures if the vent was not kept sealed. Tables 3.2 and 3.3 contain the relevant processing results and associated fibre length changes for the various combinations covered.

For a set screw speed the insensitivity of output to die

restriction for the larger machine is observed in the recovered fibre lengths. For the 25 mm extruder differences in the extrudate fibre lengths accompany the changes in output produced by changing the die diameter. The actual fibre length distributions are re-produced in Figure 3.3. Systematic reduction in the die size produces an unexpected increase in the fraction of undispersed fibre bundles although a significant quantity of degraded material is still present. The explanation for such behaviour lies in the melting and mixing processes and is discussed in Section 3.1.9.3.

3.1.2.2 Screw speed

As described in Tables 3.2 and 3.3 increases in all the dependent processing parameters accompany increased screw speeds. Again, examination of residual fibre lengths indicated significant quantities of undispersed material at the lowest screw speed, the fraction of dispersed material increasing at the expense of such fibre bundles with increasing screw speed and compression ratio. Screw number 1 produced no undispersed fibres at speeds in excess of 30 r.p.m. The observed increase in the recorded melt temperature with increased screw speed indicates the growing importance of viscous heat dissipation produced by energy input through the screw shaft. Heat is produced in the polymer melt by shearing of thin films of molten material both in the melting region and subsequent melt conveying processes. This viscous energy input often supplements the thermal energy supplied through the barrel wall, whilst the increased shear promotes mixing of the molten material leading to improved thermal homogeneity of the extrudate. The ratio of the above two heat sources will be dictated by machine size and geometry, operating conditions, and the polymer rheology - shear/ temperature relationships.

Accelerated fibre fracture would be predicted from the

heightened shear stresses which accompany increases in shear rate. This effect, however, will be somewhat lessened by the pseudoplastic nature of the polymer melt, temperature increases and the interelation between screw speed and length of the melting zone. Whilst the rate of melting is generally proportional to N^2 (where N = screw speed) improvements are generally reduced by the increased throughput rates which accompany such a change (93). Subsequent studies will indicate the complicating influence of the melting region when studying fibre degradation in plasticating extruders.

3.1.2.3 Barrel temperature

The total energy requirements of the extrusion process are dictated by the thermal properties of the material being processed. The temperature in the melt will be controlled by the barrel heaters and the viscous heat generated by shear. Elevated barrel temperatures increase the heat supplied by conduction through the barrel walls although the associated reduction in melt viscosity lowers the viscous energy input. Thus, there will be an optimum barrel temperature for a particular machine and operating condition. For a set screw speed of 60 r.p.m., barrel temperatures were varied between $300^{\circ}C$ and $260^{\circ}C$ for each machine. The resulting processing and fibre degradation trends are described in Table 3.4. Significant differences in the dependent processing parameters are observed whilst the influence of such temperature changes on the extrudate fibre length distribution is extremely slight. Comparison with Tables 3.2 and 3.3 indicates that screw speed exerts a greater influence on the recovered fibre lengths than alterations in the extruder set temperatures. Additionally, operation at the lowest temperature was only possible after running the machines at $280^{\circ}C$ for approximately 30 minutes. Output and pressure variations, however, were pronounced under these conditions.

3.1.3 Material parameters

3.1.3.1 Glass fibre variables

The influence of size type, initial strand length, tex and glass content on the processing requirements and degree of fibre fracture are described by Figures 3.4 and 3.5 and Tables 3.5 to 3.8. These studies were carried out on the 45 mm extruder. Preliminary studies with the 25 mm machine yielded unexpected fibre length trends when the glass loadings were varied - Figure 3.6 and, as indicated in Table 3.9, the processing results exhibit significant differences. The pronounced discordance between these distributions and the increased fibre fracture which accompanies increased glass levels for the larger machine is considered to originate in the melting processes occurring and is discussed in Section 3.1.9.

Increased throughputs and specific power consumptions accompany increases in the apparent bulk density of the polymer-glass fibre blend achieved by reductions in initial fibre length or improved strand integrity - Table 3.10 and Table 2.2. However, such changes probably reflect the efficiency of the solids conveying region which is dependent on the frictional force exerted against the barrel walls arising from compaction of the solid material (20). Fibre length analyses determined for this region indicate little significant fibre fracture (Section 3.1.6). The inadequacy of the specific power requirement in predicting the resultant fibre degradation is evident from Figure 3.5 and Table 3.5 in which increased fibre fracture is observed for the more filamentised material. Obviously such correlations are only relevant if material parameters remain unchanged.

Processing of the higher glass content materials on the larger extruder produced significant increases in melt temperature, pressure and specific power consumption - Table 3.8, in spite of the reduction in bulk density which accompanied such changes. These results are

consistent with an increased melt viscosity for the highly filled

materials and as might be expected the resultant fibre length

distributions reflected the above trends. Problems of feeding the

higher glass content materials can be related to the apparent bulk

densities and increased frictional coefficients -Table 3.10 and Figure

3.7. Flow disturbances in the gravitational discharge from bins and hoppers

have been discussed by Johanson (94) and suitable designs are outlined to

alleviate such problems.

3.1.3.2 Matrix polymer

The results of processing-fibre degradation studies for the

Maranyl range of polymers listed in Table 2.3 incorporating 30%

by weight of F.G.C.S. 1640 strands are given in Table 3.11. The

physical and thermal properties of these blends were identical and

thus the observed differences can be attributed to the melt viscosity

changes occurring.

3.1.4 Recycling studies

Most commercial manufacturers minimise wastage in the compounding

operation by recycling processed material after drying and granulation.

The actual levels of 'regrind' used are generally determined by the end

product requirements. Material for reprocessing is normally metered

into the feed pocket at levels ranging from one to five percent

although increasing quantities are being used as raw material costs

increase. It was of interest, therefore, to examine the influence of

successive extrusion operations upon the processing and retained

fibre length distributions. Both F.G.C.S. 1640 and XS 929 30% by

weight extrudates were recycled twice through the 45 mm machine using

screw number 1. The processing performance and fibre length trends

are described in Table 3.12 and Figure 3.8. Fibre degradation increases

with each successive cycle as observed by several workers (95), (96), (43).

However, the original advantages of the cationic sized fibres in terms

screw / operating results	1	2	3
melt pressure [†]s. d. (σ) MN/m^2	13.3 0.7	16.2 1.8	7.5 2.0
output (kg./hr. s.d. (σ).	10.6 0.3	16.3 0.6	3.9 1.0
dimensionless output (π_Q).	0.34	0.38	0.09
mean specific power (kW.hr/kg)	0.306	0.250	0.078
melt temperature (°C)	263	262	-
shear rate (sec^{-1}) primary metering section	99.0	71.6	13.4
wt. av. fibre lth.(μm) no.av. fibre lth.(μm)	442 336	593 407	650 450

material: 30% b.w. F.G.C.S.1640/Maranyl A100
screw speed: 60 r.p.m.
die size: 2mm.
barrel temperature: 280°C

† indicates variation in mean pressure over ten screw revolutions

Table 3.1 influence of screw geometry on processing and fibre fracture
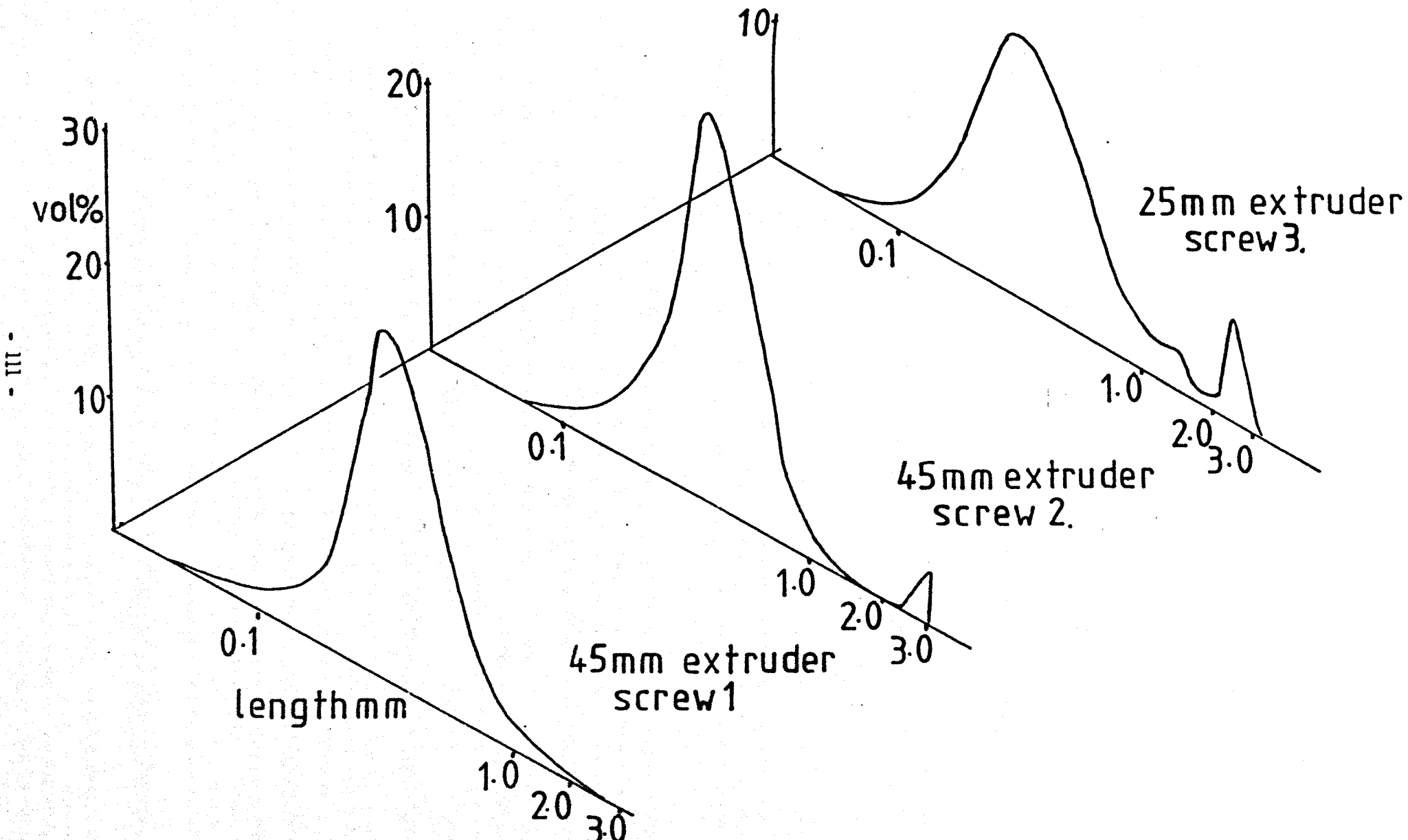
Figure 3.1 influence of screw geometry on fibre fracture
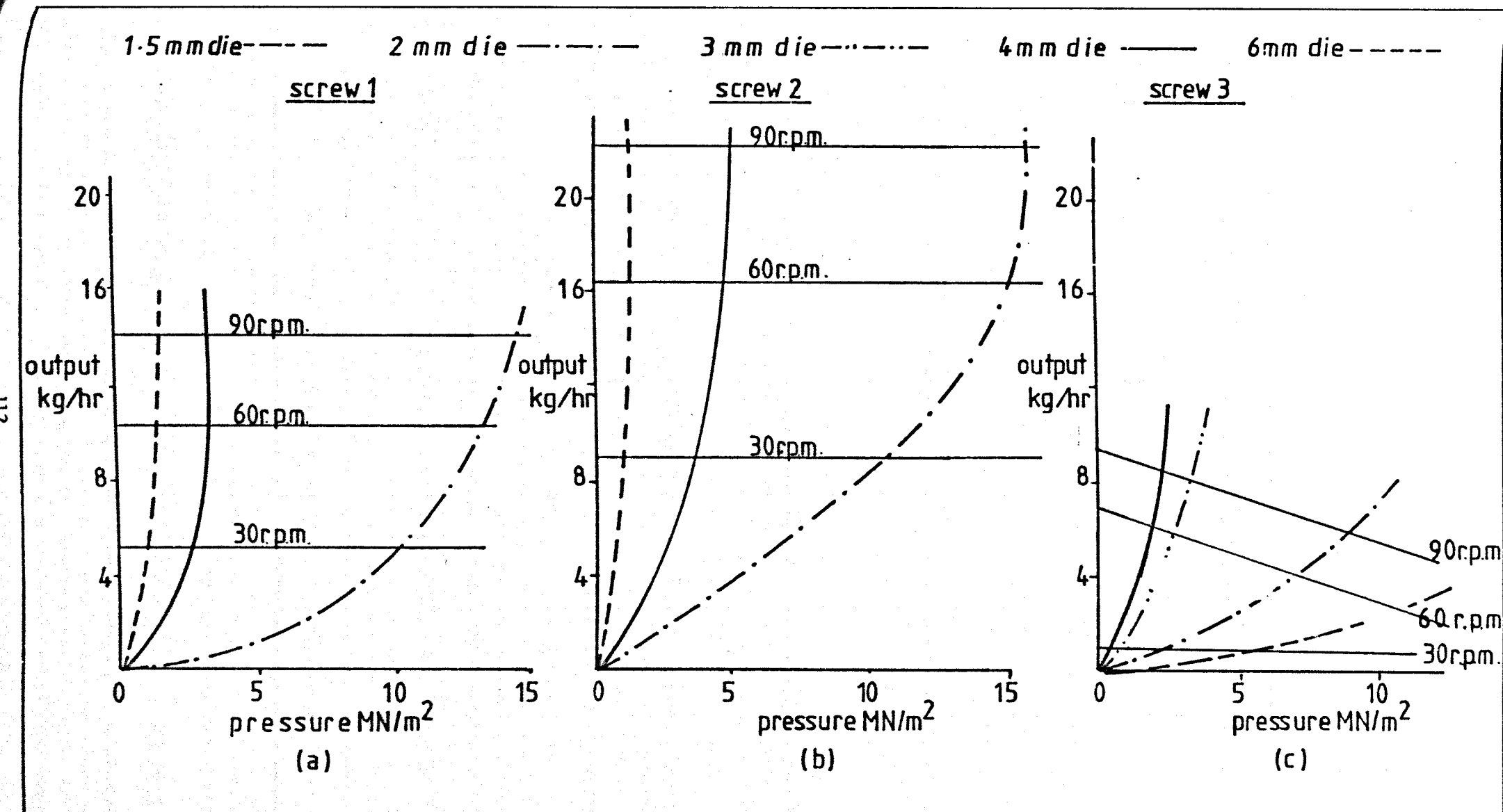
Figure 3.2. pressure-output relationships

SCREW	DIE DIAM. mm	SCREW SPEED r.p.m.	MELT PRESS. MN/m²		SP POWER KWhr/Kg	OUTPUT Kg/hr		MELT TEMP °C	π_Q	FIBRE LENGTHS microns	
			mean	s.d.		mean	s.d.			no. av.	wt. av.
1	2	30	9.7	0.3	0.29	5.21	0.2	262	0.35	401	542
		60	13.3	0.7	0.31	10.59	0.3	263	0.34	336	442
		90	14.5	1.0	0.36	14.27	0.2	267	0.31	304	412
	4	30	2.5	0.3	0.26	5.86	0.2	262	0.35	390	540
		60	3.2	0.4	0.30	10.57	0.2	263	0.34	340	442
		90	3.6	0.5	0.35	14.42	0.6	267	0.31	302	420
	6	30	1.3	0.2	0.28	6.08	0.2	262	0.35	400	544
		60	1.8	0.3	0.30	10.76	0.4	264	0.34	338	438
		90	2.0	0.3	0.34	14.43	0.8	266	0.31	301	422
2	2	30	10.3	0.6	0.18	9.0	0.4	261	0.42	459	738
		60	16.2	1.8	0.25	16.3	0.6	262	0.38	407	593
		90	16.6	1.7	0.29	21.7	0.6	266	0.28	384	437
	4	30	3.1	0.4	0.17	9.0	0.4	261	0.42	450	720
		60	4.1	0.5	0.23	16.0	0.8	262	0.38	414	615
		90	4.8	0.5	0.28	21.8	1.0	265	0.28	380	438
	6	30	1.0	0.3	0.18	9.2	0.3	260	0.42	453	721
		60	1.2	0.3	0.24	16.4	0.8	263	0.38	409	598
		90	1.3	0.3	0.29	22.0	1.5	265	0.28	386	440

Table 32. processing performance and fibre fracture v extrusion parameters 45mm extruder

SCREW	DIE DIAM. mm	SCREW SPEED r.p.m	MELT PRESS MN/m^2 mean	s.d.	SP. POWER KWhr/Kg.	OUTPUT Kg/hr mean	s.d.	MELT TEMP. °C	π_Q	FIBRE LENGTHS microns no. av.	wt. av.
3	1·5	30	5·0	0·8	0·06	1·2	0·1	—	0·06	550	1040
		60	9·5	1·1	0·09	2·3	0·4	—	0·05	405	680
		90	14·0	2·0	0·10	4·0	0·4	—	0·06	310	390
	2·0	30	2·5	0·7	0·07	1·5	0·1	—	0·07	565	111 0
		60	7·5	2·0	0·08	3·9	1·0	—	0·09	450	650
		90	8·8	2·1	0·10	5·4	1·8	—	0·09	360	580
	3·0	30	1·2	0·2	0·07	1·6	0·6	—	0·08	620	1350
		60	2·0	0·4	0·08	4·0	1·5	—	0·09	340	520
		90	3·2	0·8	0·08	8·0	2·3	—	0·13	320	500
	4·0	30	0·8	0·1	0·05	1·7	0·6	—	0·08	900	1900
		60	1·5	0·4	0·07	6·0	1·6	—	0·16	420	900
		90	2·3	0·8	0·08	8·7	2·5	—	0·14	370	600

Table 3.3. processing performance. and fibre fracture v extrusion parameters 25mm extruder
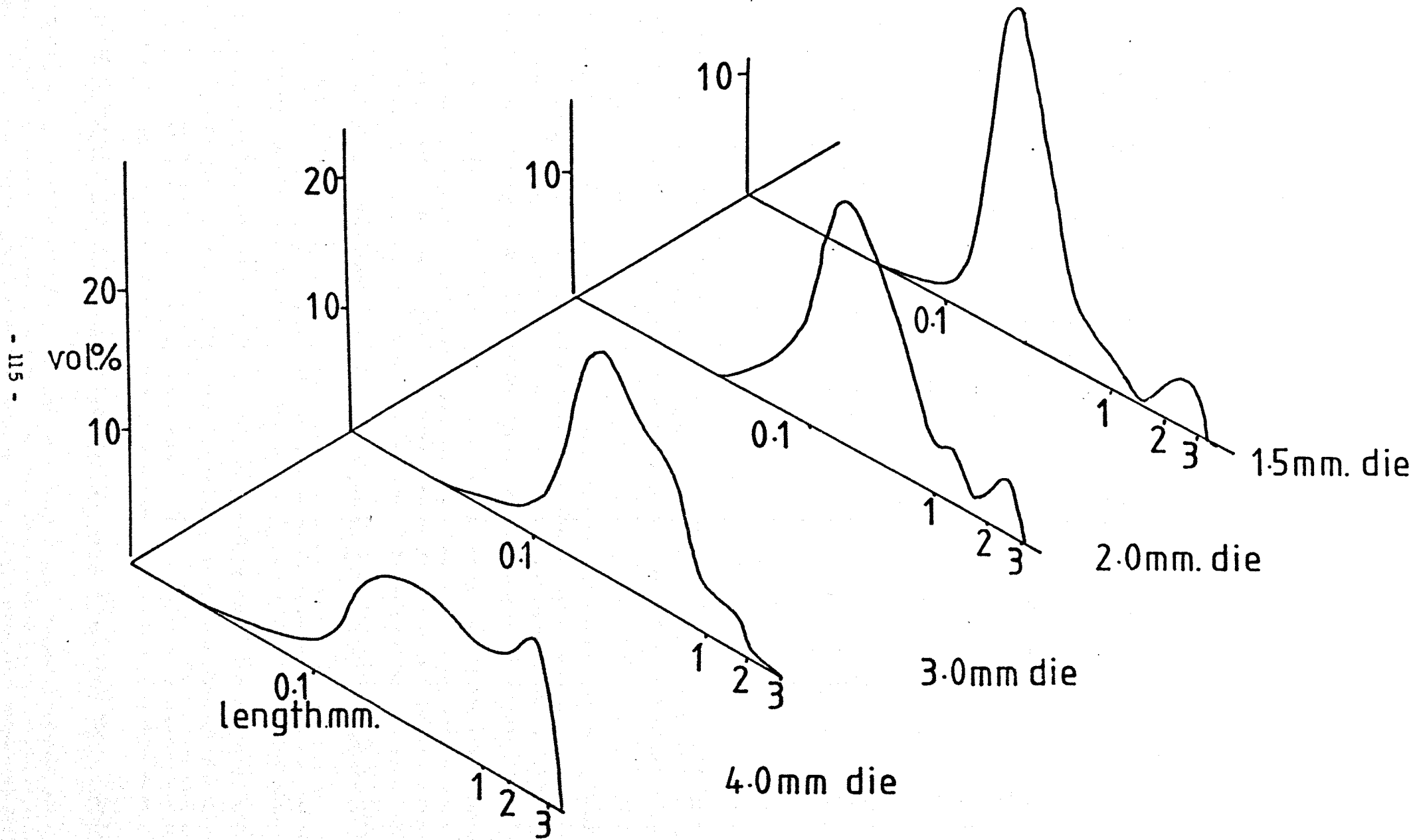
Figure 3.3. extrudate fibre length distributions - 2.5mm. extruder

SCREW	BARREL TEMP °C	MELT PRESS. MN/m²		SP. POWER KW.hr./Kg	OUTPUT Kg/hr.		MELT TEMP °C	π_Q	FIBRE LENGTH microns	
		mean	s. d		mean	s. d			no.av.	wt. av.
1	260	13·4	2·0	0·42	9·04	0·8	256	0·29	343	437
	280	13·3	0·7	0·31	10·59	0·3	263	0·34	336	442
	300	12·1	0·4	0·29	10·59	0·2	277	0·35	362	472
2	260	17·3	2·5	0·30	13·8	1·0	256	0·32	399	479
	280	16·2	1·8	0·25	16·3	0·6	262	0·38	407	593
	300	13·3	1·0	0·19	16·8	0·5	276	0·39	390	595
3	260	8·9	2·7	0·17	3·0	1·7	—	0·07	444	641
	280	7·5	2·0	0·08	3·9	1·0	—	0·09	450	650
	300	4·2	1·0	0·07	4·2	0·6	—	0·10	470	662

die diameter = 2mm   screw speed = 60.r.p.m.

Table 3.4 processing performance and fibre fracture v barrel temperature
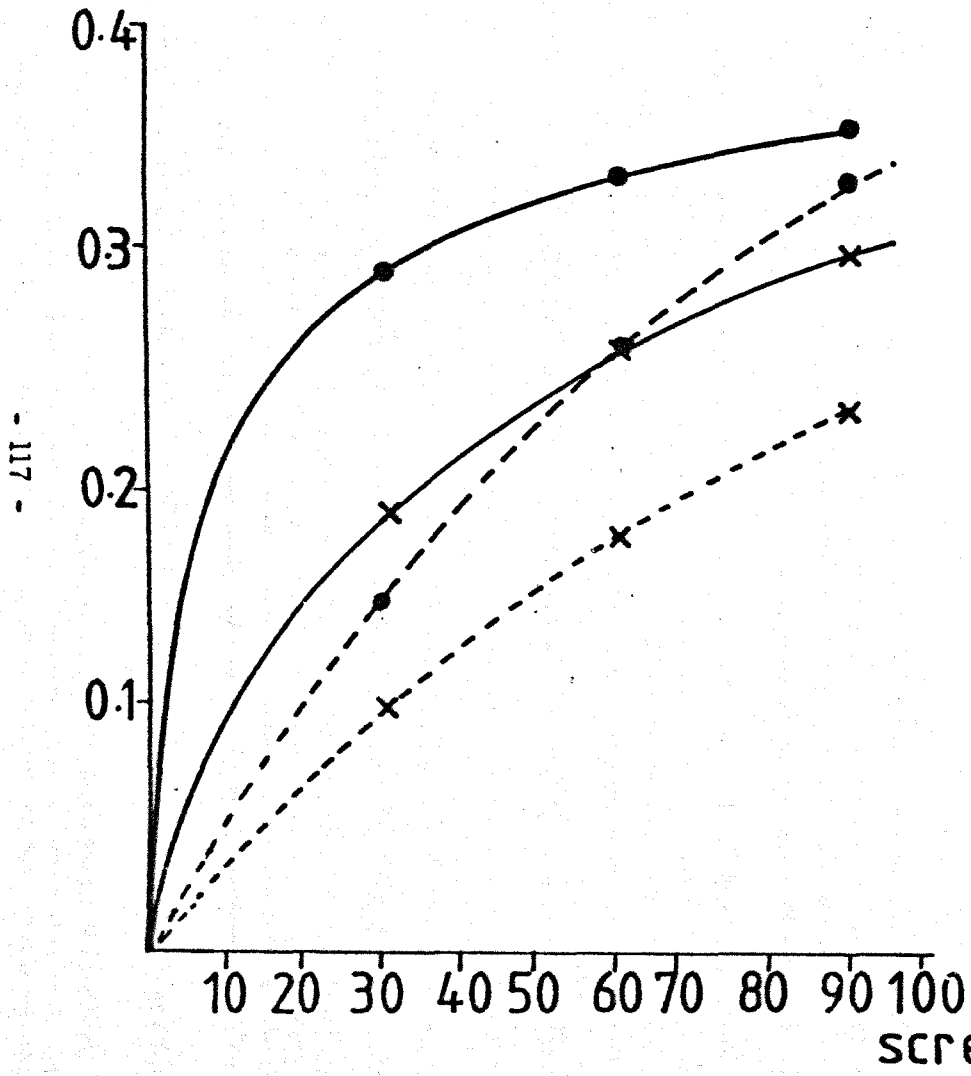
Figure 3.4(a) influence of size type on specific power consumed
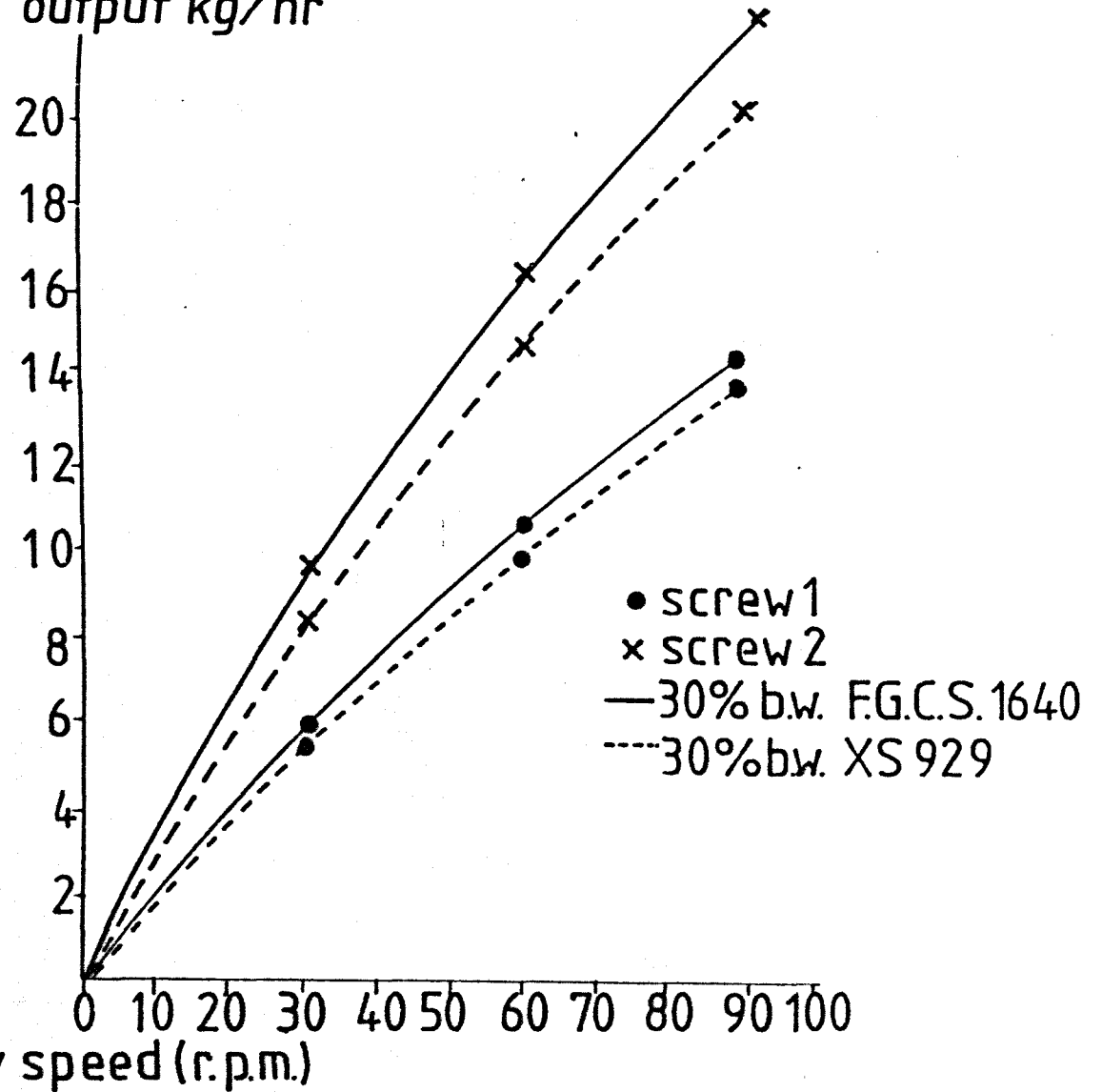
Figure 3.4(b) influence of size type on output

screw speed (r.p.m.)

Legend:
- screw 1
- × screw 2
- —30% b.w. F.G.C.S. 1640
- ---30% b.w. XS 929
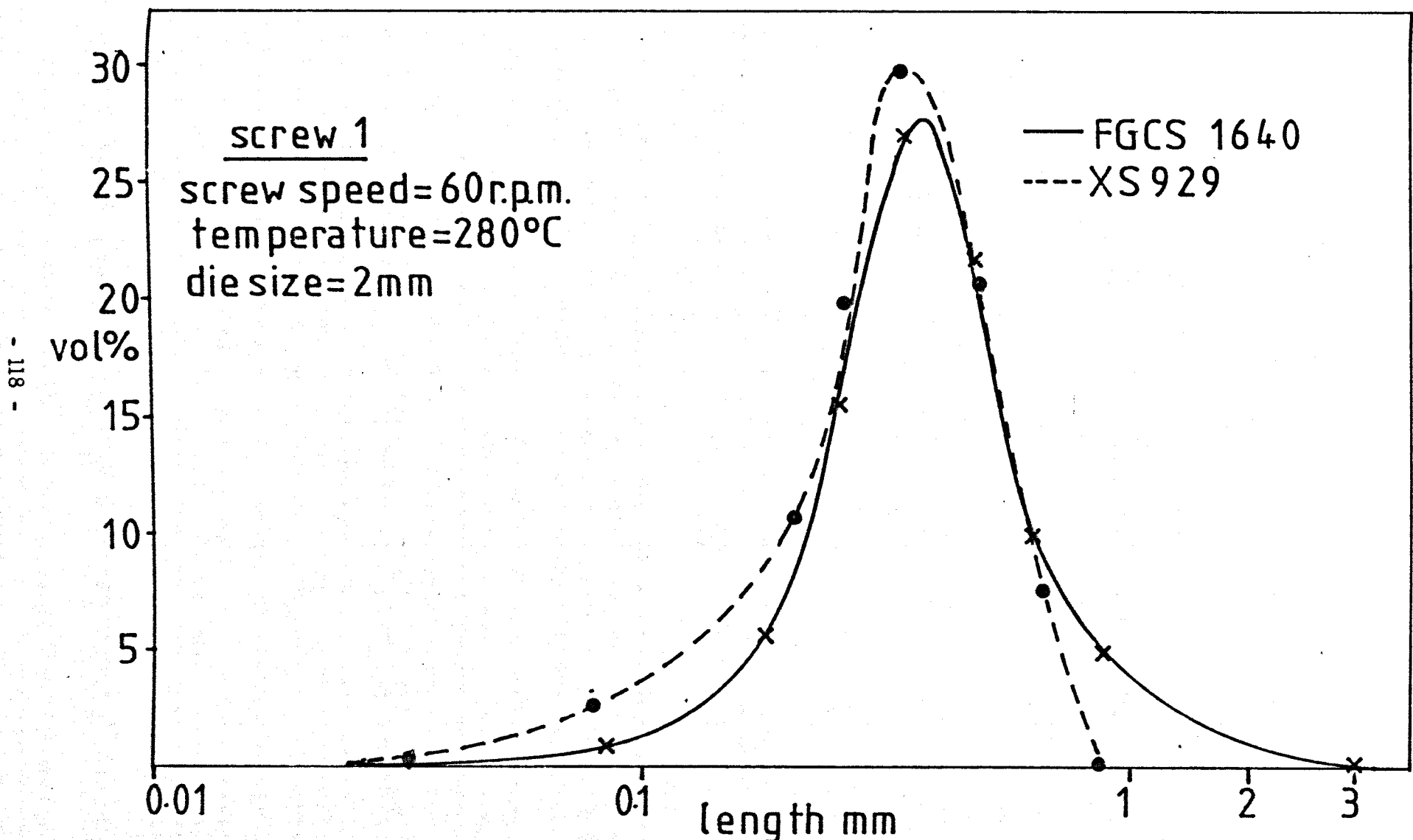
Figure 3.5. extrudate fibre length distributions v fibre type

die size = 2 mm
screw speed = 60 r.p.m.
45 mm. extruder 280 °C

screw	fibre type	melt pressure MN/m²		specific power KWhr/Kg	output Kg/hr.		π_Q	melt temp. °C	fibre lths. microns	
		mean	s.d.		mean	s.d			no.av.	wt.av.
1	F.G.C.S. 1640	13.3	0.7	0.31	10.59	0.3	0.34	263	336	442
	XS 929	9.3	0.2	0.26	9.50	0.2	0.31	263	302	363
2	F.G.C.S. 1640	16.2	1.8	0.25	16.30	0.6	0.38	262	407	593
	XS 929	12.1	0.3	0.16	14.10	0.4	0.33	262	317	380

Table 3.5. processing and fibre fracture v fibre type

screw	initial strand length mm	melt pressure MN/m² mean s.d.		specific power KWhr/Kg.	output Kg/hr. mean s.d.		π_Q	melt temp. °C	fibre lths. microns no.av. wt.av.	
1	1.5	14.10	0.9	0.34	11.02	0.2	0.36	265	315	375
	3.0	13.30	0.7	0.31	10.59	0.3	0.34	263	336	442
	5.0	12.90	0.5	0.30	10.10	0.1	0.33	263	330	432
2	1.5	18.00	2.0	0.29	17.10	0.7	0.40	263	321	399
	3.0	16.20	1.8	0.25	16.30	0.6	0.38	262	407	593
	5.0	15.40	0.9	0.23	15.80	0.4	0.37	262	411	595

die size=2mm screw speed=60r.p.m. temp.=280°C. 30% b.w. F.G.C.S. 1640/A100

Table 3.6. processing and fibre fracture v initial strand length

screw	fibre diam. µm	split	melt pressure MN/m²		specific power KWhr/Kg	output Kg/hr.		π_Q	melt temp. °C	fibre aspect ratio	
			mean	s.d.		mean	s.d			no.av.	wt.av.
1	10	2	13.6	0.4	0.31	10.62	0.1	0.34	264	33.4	40.0
	11	2	13.3	0.7	0.31	10.59	0.3	0.34	263	29.4	38.1
	13	2	13.8	1.0	0.30	10.70	0.1	0.35	263	25.1	33.3
	13	1	13.3	1.0	0.31	10.60	0.2	0.34	263	25.0	33.0
	13	4	13.4	0.5	0.31	10.71	0.1	0.34	263	25.4	33.5
2	10	2	16.4	1.6	0.25	16.42	0.4	0.38	262	38.1	54.4
	11	2	16.2	1.8	0.25	16.30	0.6	0.38	262	35.7	52.0
	13	2	16.0	2.0	0.24	16.35	0.6	0.38	262	30.9	44.0
	13	1	16.3	1.9	0.25	16.31	0.5	0.38	262	32.0	46.4
	13	4	16.1	1.9	0.25	16.61	0.4	0.39	262	28.4	41.0

Table 3.7. processing and fibre fracturev bundle tex

SCREW	GLASS CONTENT VOL.%	MELT PRESS. MN/m²		SP. POWER KWhr/m³	OUTPUT m³/hr. ×10³		π_Q	MELT TEMP. °C	FIBRE LENGTHS microns	
		mean	s.d.		mean	s.d.			no. av.	wt. av.
1	0	1.72	0.4	311	8.36	2.2	0.33	261	—	—
	2.3	1.90	0.5	355	7.92	0.5	0.32	262	599	7.93
	4.7	2.40	0.5	362	8.06	0.5	0.32	262	496	774
	16.2	3.20	0.4	378	8.59	0.2	0.34	263	340	442
	23.0	3.80	0.3	390	8.04	0.2	0.32	265	304	380
	31.0	4.14	1.4	436	7.98	0.4	0.32	268	262	319
	40.2	6.20	1.5	511	8.30	0.4	0.33	275	195	235
2	0	2.00	0.7	290	12.60	1.0	0.36	260	—	—
	2.3	2.60	0.9	281	13.20	0.8	0.38	261	601	895
	4.7	3.31	0.7	281	13.30	0.7	0.38	262	490	773
	16.2	4.14	0.5	308	13.20	0.5	0.38	262	414	615
	23.0	4.80	0.4	312	13.41	0.5	0.39	263	371	540
	31.0	5.20	1.6	333	13.50	0.6	0.39	266	328	504
	40.2	5.90	1.6	361	13.90	0.7	0.40	274	244	324

die size = 4mm   screw speed = 60 r.p.m.   temperature = 280°C

Table 3.8. processing performance and fibre fracture v glass content
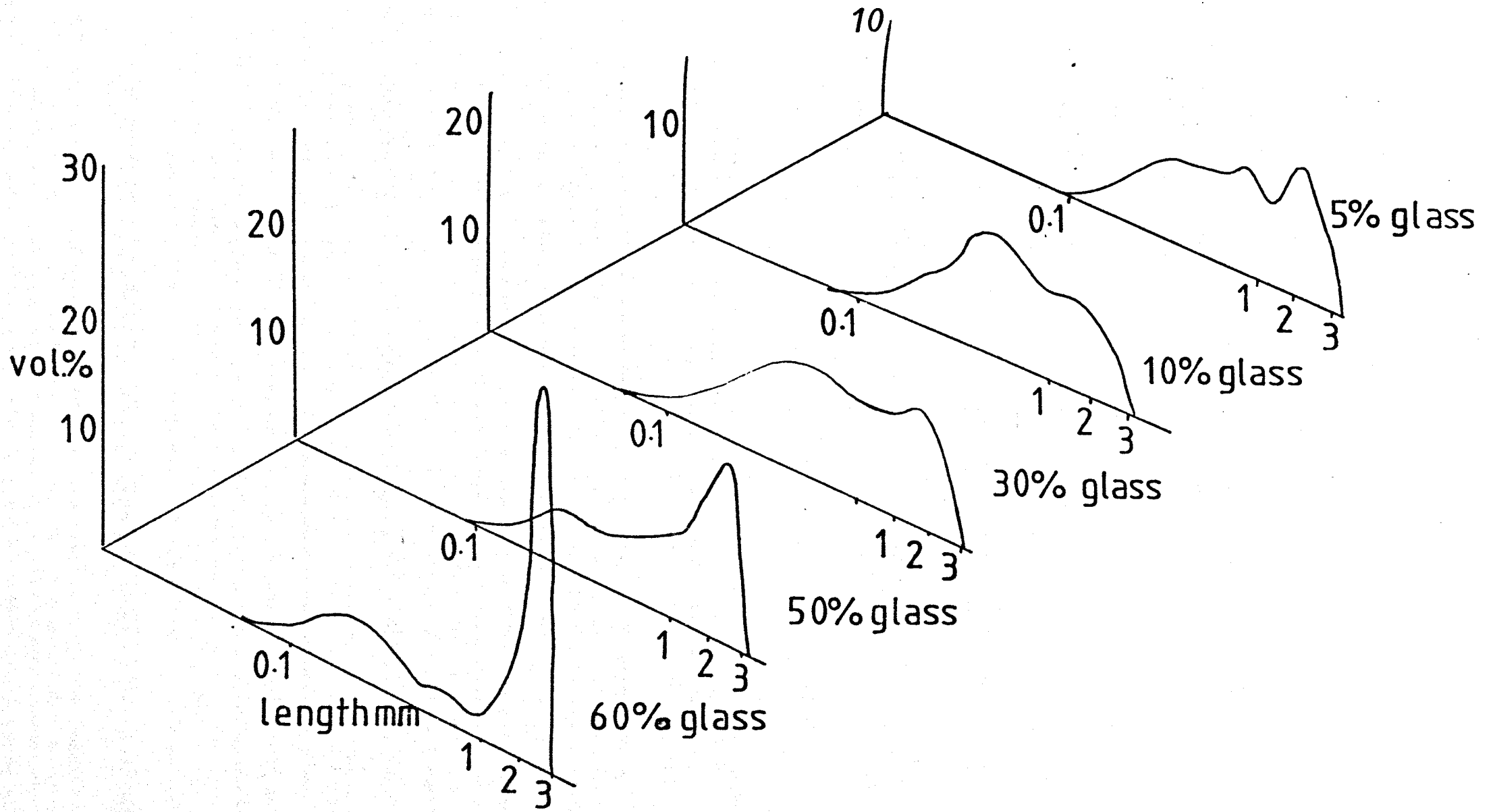
Figure 3.6 variation in glass content-extrudates 25mm extruder

screw	glass content vol.%	melt pressure MN/m² mean s.d.		specific power KWhr/m³	vol. output m³/hr×10³ mean s.d.		π_Q	melt temp. °C	fibre lths. microns no.av.	wt.av.
	0	0.34	0.6	75.0	3.51	1.0	0.10	—	—	—
	2.3	0.55	0.5	76.0	3.84	1.0	0.11	—	601	900
	4.7	1.03	0.4	78.5	4.01	1.1	0.12	—	504	804
3	16.2	1.50	0.4	86.3	4.87	1.3	0.16	—	420	900
	23.0	2.07	0.4	85.7	5.70	0.9	0.17	—	490	980
	31.0	4.82	0.5	88.0	6.05	1.5	0.18	—	448	1100
	40.2	8.27	0.5	88.5	6.15	1.7	0.18	—	630	1500

die size = 4mm screw speed = 60 r.p.m. temp. = 280 °C

Table 3.9. processing and fibre fracture v glass content 25mm extruder

fibre characteristics		volume % of fibres to polymer (A100)	apparent bulk density (Kg/m³)
3mm F.G.C.S. 1640 190 tex. 2split		0	711
		2·3	706
		4·7	695
		16·2	660
		23·0	590
		31·0	557
		40·2	500
		100	423
190 tex 2split	1·5mm	16·2	750
	5·0mm	16·2	460
3mm 306 tex	1split	16·2	696
	2split	16·2	694
	4split	16·2	681
150 tex. 2split		16·2	661
3mm XS929 190 tex. 2split		16·2	610

Table 3.10 influence of fibre parameters on the apparent bulk density of glass fibre-polymer blends.

30% b.w. F.G.C.S 1640/Maranyl A100

Maranyl A100

temperature °C
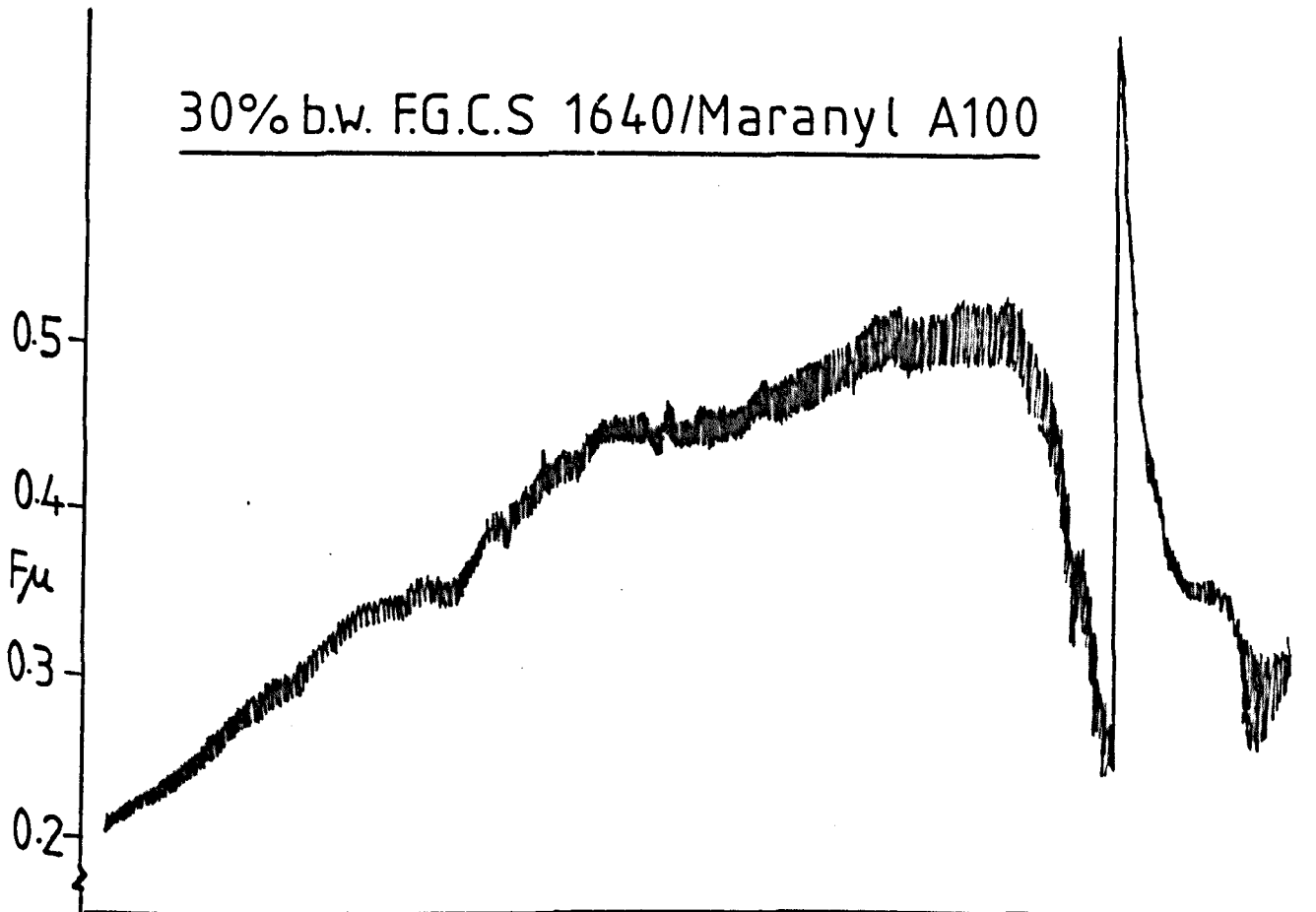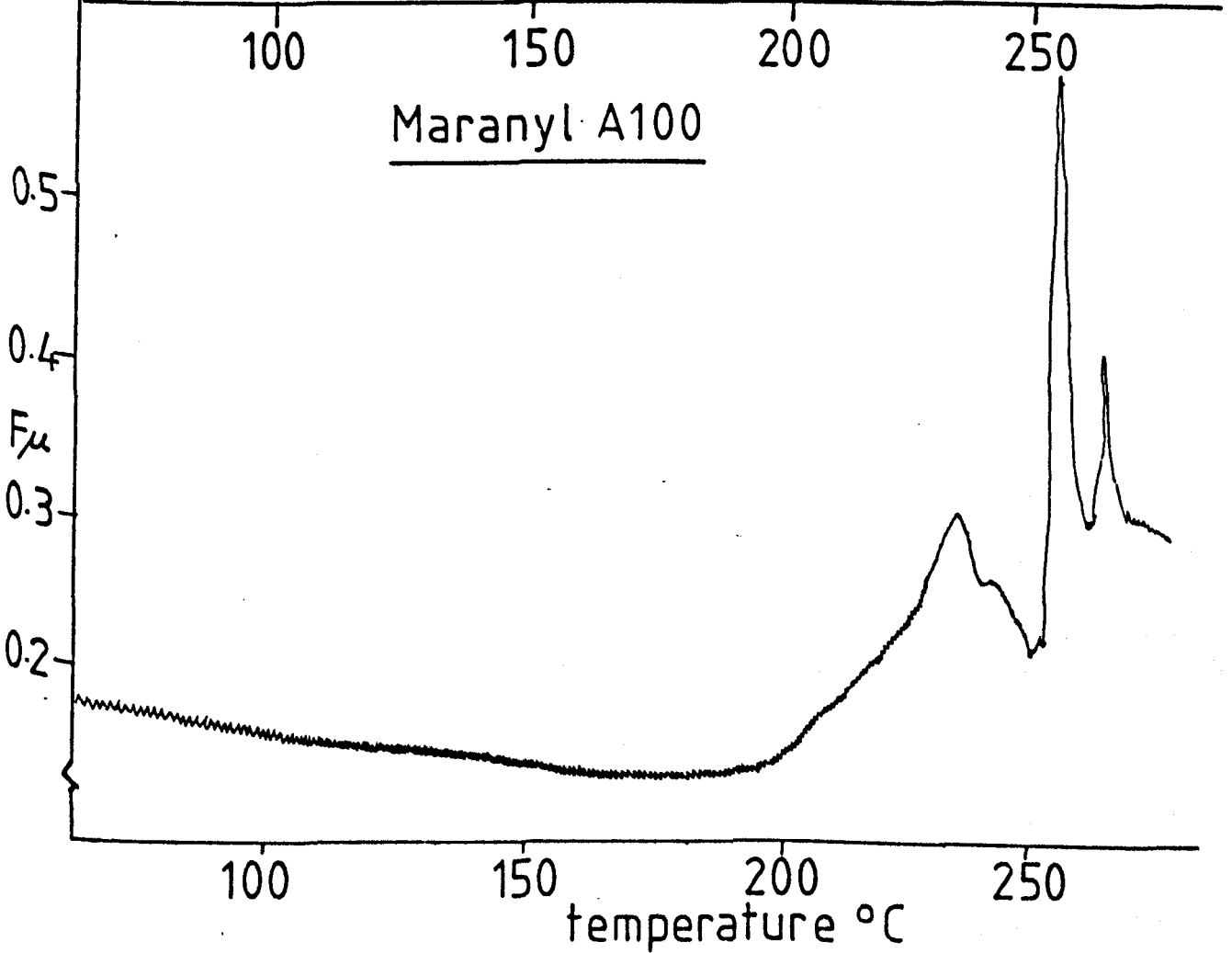
Figure 3.7 Frictional forces against steel

screw	matrix material	melt pressure MN/m² mean	s.d.	specific power KWhr./Kg	output Kg/hr. mean	s.d.	π_Q	melt temp. °C	fibre lths. microns no. av.	wt. av.
	A100	13.3	0.7	0.31	10.59	0.3	0.34	263	336	442
	A144	14.6	0.6	0.32	10.30	0.5	0.33	263	310	378
1	A146	16.9	0.5	0.34	10.56	0.3	0.34	266	267	327
	A148	18.4	0.4	0.42	11.00	0.3	0.35	267	260	317
	A150	21.1	0.5	0.53	10.60	0.2	0.34	268	252	298

die size = 2mm. screw speed = 60 r.p.m. . temperature = 280°C

glass fibres = F.G.C.S. 1640

Table 3.11. processing and fibre fracture v polymer molecular weight

material	number of processing cycles	melt pressure MN/m² mean s.d.	specific power KWhr/Kg.	output Kg/hr mean s.d.	π_Q	melt temp. °C	fibre lths. microns no.av. wt.av.
30% b.w. F.G.C.S.1640 Maranyl A100	1	13.3 0.7	0.31	1059 0.3	0.34	263	336 442
	2	12.41 0.5	0.42	10.80 0.1	0.35	262	219 272
	3	12.44 0.5	0.39	10.80 0.1	0.35	263	201 251
30% b.w. XS 929 Maranyl A100	1	9.30 0.2	0.26	9.50 0.2	0.31	263	302 363
	2	9.03 0.2	0.36	9.21 0.1	0.30	262	241 305
	3	8.27 0.1	0.33	9.04 0.1	0.29	262	216 264

die size = 2mm. screw speed = 60 r.p.m. temp. = 280 °C. screw no. 1

Table 3.12. processing and fibre fracture v number of processing cycles
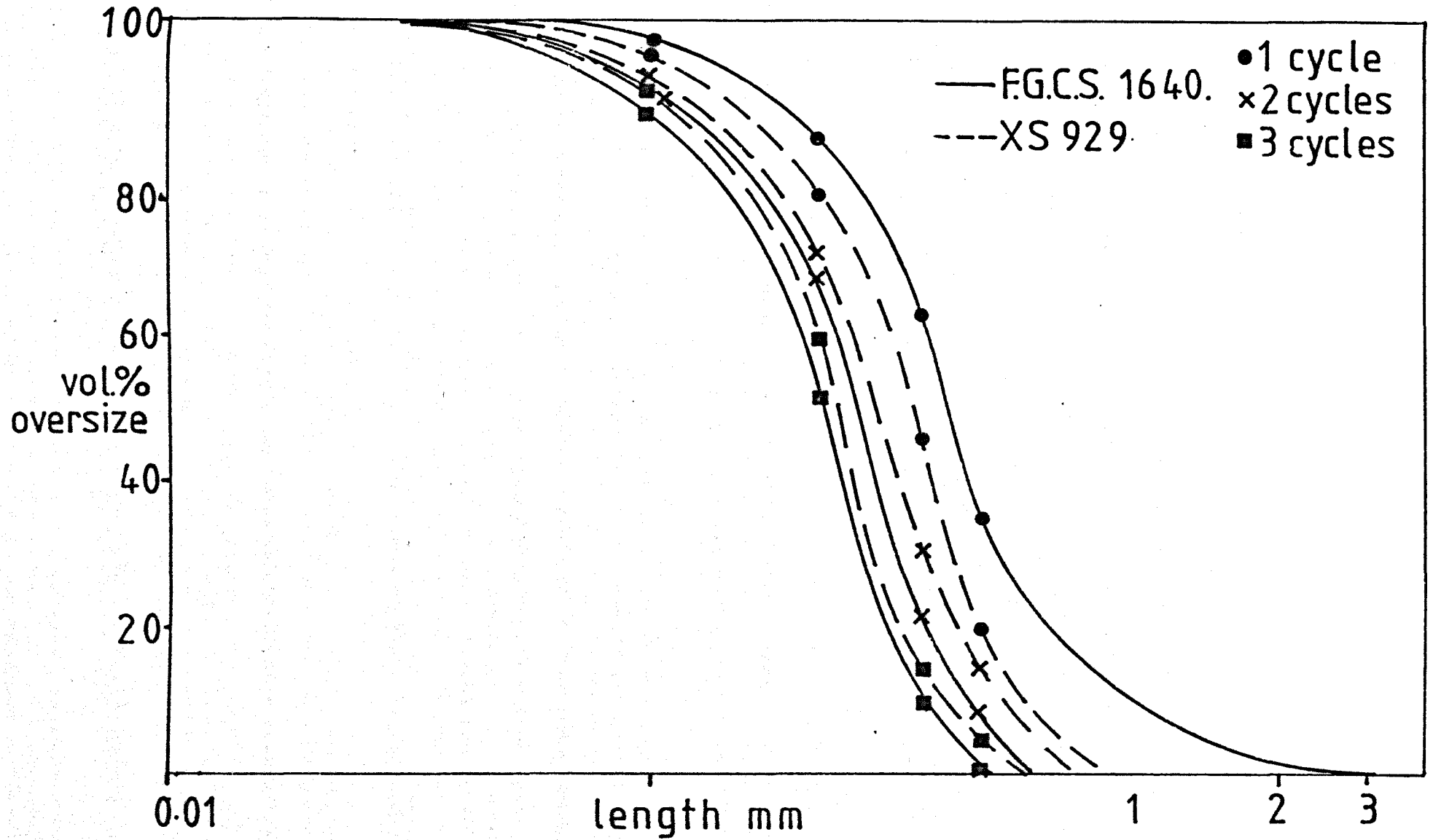
Figure 3.8. cumulative fibre lengths v number of extrusion cycles

of residual fibre lengths are not maintained in the subsequent reprocessing operations, presumably due to the diminished fracture which accompanies the reduced melt viscosity of the polyvinyl acetate sized material. This reduced melt viscosity is discussed in Section 3.3.1.

3.1.5 Screw extraction experiments

Fibre samples obtained from the Betol extruders for screw numbers 1 and 3 provide a partial explanation for the pattern of fibre fracture observed in the extruded compounds analysed in Sections 3.1.1 and 3.1.2. Such extracted screw samples were produced under equivalent processing conditions using the standard 30% by weight blend. Cross channel fibre length distributions (x-y samples) determined for selected sections are illustrated in Figures 3.9 and 3.10. Moving along the screw from the feed section produces a decrease in the fraction of 3 mm strands whilst the secondary distribution becomes more pronounced. The mode length of this dispersed material is approximately 350 microns and remains unaltered on passing through the various functional zones of the extruder. Differences in the mode length for each machine are slight although the accuracy of the fibre length measurements is limited by the interval sizes of the counter and hence slight shifts will not be detected. Similar fibre fracture processes appear to be occurring in each machine despite the relatively large differences in dimensionless outputs and extruder size. The process of fibre degradation is, however, considerably retarded for the 25 mm machine as indicated by the relative proportions of undispersed fibres for comparative channel sections - Figure 3.11. Significantly, this undegraded material is present almost exclusively as integral fibre bundles, indicating that these strands have not been subjected to the same shear regime as the dispersed filaments.

Figures 3.9 and 3.11 indicate that pronounced fibre breakage has occurred in the feed section of the 45 mm extruder. Simliar results were obtained by Pennington (45) during the processing of Sheet Moulding Compounds and was attributed to the crushing of the fibres achieved by material passing over the screw flights. No evidence of such a process was found in these studies. Analysis of unmelted material directly below the feed entrance showed little fibre degradation indicating that the tumbling of the fibres with the polymer pellets and the subsequent feeding operation were not responsible for significant fibre diminution. Very fine material was detected in the solids conveying region prior to the formation of the barrel melt film, indicating some frictional damage. However, the overall extent of fibre fracture in the feed section cannot be accounted for solely by damage due to contact abrasion, especially in view of the formation of the barrel melt film some three turns into the feed section.

For the 45 mm machine little additional fibre length reduction occurs beyond the primary metering section. Such a result is consistent with the previous observation of the insensitivity of extrudate fibre length to imposed back pressure. Obviously such pressure will only act over the length of the secondary metering section as long as the decompression zone is incompletely filled. Thus, in the absence of output changes the influence of increased die pressure is not felt in the region of predominant fibre fracture. The observed pattern of fibre breakage for both machines is considered to be related to the melting process occurring as the fibre-polymer mixture passes through the extruder.

3.1.6 The melting process

Following the experimental techniques of Maddock (34) and Street (29) observations of the melting process occurring in the

50 mm extruder were carried out for 30% by weight blends of F.G.C.S.
1640 and XS 929 Strands with Maranyl A100.

3.1.6.1 F.G.C.S. 1640 - Maranyl A100

Figure 3.12 shows cross channel sections removed at one half
turn intervals from the extracted screw, the first section illustrated
representing 3 full turns into the feed zone. Comparison with the
idealised cross-section presented in Figure 1.10 indicates that
the melting mechanism, prior to the primary compression step, resembles
that observed by the above workers and subsequently by Tadmor (23)
and Fenner et. al (24) for unfilled nylon and polypropylene.

Fibre length analyses were carried out for the solid bed and
melt pool regions existing in the feed zone samples. The distributions
for channel six are illustrated in Figure 3.13. Little significant
fibre degradation has occurred in the solid filled region of the
channel, this picture continuing as the material advances in the down
channel direction. The small quantity of dispersed material originates
from frictional damage prior to formation of the barrel melt film
coupled with molten material, containing dispersed fibres, penetrating
the interstices of the solid bed. The latter process occurs in the delay
zone which separates the solids conveying and steady state melting
regions. The explanation for the overall lack of fibre fracture in
the solid bed lies in the early compaction of the solid material into
a 'plug' which thereby hinders any relative displacement of the solid
pellets and fibre bundles. Solids conveying in an extruder is provided
by a drag aided particulate flow mechanism (93) in which the frictional
force between the moving barrel wall and the solids produces a forward
dragging motion. This force can be divided into two components,
comprising the down channel and cross channel forces, respectively. It
is this latter component which provides the mechanism by which
compaction of the solid blend occurs.

The fibre length distribution in the melt pool is a direct consequence of the melting process. Melting occurs in a single screw extruder by virtue of a 'drag induced conduction melting mechanism' (93). Initiation of melting is marked by the formation of a thin film of molten material produced both by heat conducted through the barrel and by frictional heating. The relative motion of the barrel to the solid bed, in the cross channel direction, drags the formed melt into the melt pool region. This rapid removal of molten material generates a steady melting process in which the material melted at the barrel surface is continuously transferred to a melt pool located at the pushing edge of the screw flight. The pressure exerted by this melt pool causes solids to be continuously supplied to the melting interface and also produces segregation of the solid bed at the trailing flight.

The continuous removal of the upper melt film aids the heat transfer rate and accelerates the melting process due to the heat generated by viscous dissipation. Additionally, heat is generated in this thin film under the intense shear and together with heat conducted from the barrel surface, raises the temperature of the solid at this solid bed-melt interface to the melting temperature.

Since in the initial stages of melting all the material in the melt pool has its origins in the barrel melt film then the source of fibre fracture is obviously located in this region. Under steady state conditions the thickness of this film will approximate to the clearance between the flight land and the barrel (27). The mean shear rates existing in this region and in the metering sections for the various operating conditions are given in Table 3.13. V_r is the relative velocity in the upper film and is obtained from the relative velocities of the barrel and solid bed in the downstream direction and transverse directions respectively - equation 3.5 in

section 3.1.8. V_z is the downstream velocity in the melt filled regions and H_c and H_m are the flight land-barrel clearance and metering section depths respectively. The shear stresses in these regions will be dictated by the shear rate - temperature/viscosity relationships for the material being extruded. As indicated in the above table the severest shear conditions exist in the upper melt film region.

As melting progresses, conduction melting at the radial interface of the solid bed and melt pool, initially negligible due to the small contact area and lower polymer conductivity, may become significant when the solid bed width is sufficiently reduced. In addition, the gradual increase in the solid bed temperature will assist the above secondary melting process as will processing conditions which favour an increased contribution from conductive thermal energy input i.e. low throughput rates and low melt viscosities - see Section 3.1.9.3. Evidence of such conduction melting is confirmed by the presence of a small fraction of undispersed fibre bundles in the melt pool region of channel number 10 - Figure 3.14.

In addition to the above melting regions, examination of section 9 in Figure 3.12 indicates the formation of a melt film along the screw root. This film is presumably formed much earlier in the process since after channel 5 samples could be removed from the screw without loss of fibres and unmelted polymer. Examination under the microscope showed that fibres in this region had been severely degraded - see Figure 2.27, although due to the extremely small area exact analysis was impossible. This lower melt film is only formed when the screw temperature exceeds the polymer melting point and arises either from penetration of the melt pool or by conduction from the screw surface. The contribution of the existence of such a film to the overall degree of fibre attrition is relatively unimportant in view of the retention

of all melted material. However, in terms of solid bed fracture
its presence can have important consequences - Section 3.1.9.1.

Under the extrusion conditions imposed, melting for this material
was not completed by the end of the feed section. Cross channel
fibre length distributions were determined immediately prior to and
after the primary compression step and are described by Figure 3.15.
Further fibre fracture occurs in the transition region. Microscopic
examination indicated that samples removed after the transition
contained small fragments of unmelted material confirming the occurence
of solid bed fracture. Melting appeared to be finally completed by
channel 16, the fibre length distribution at this point showing little
change from that of the previous sample - Figure 3.15. Such behaviour
is in accordance with the melting pattern observed by Martin (25) the
residual fibre lengths indicating that melting after solid bed break-up
is achieved primarily by conduction.

Subsequent to the melting process little significant fibre length
changes occur reflecting the reduced shear stress in the melt conveying.
region. The gradual removal of undispersed fibre bundles indicated in
Table 3.14 is controlled by the overall mixing performance of the
remaining screw length and will obviously be related to the residence
time and shear stresses existing in this section. Further confirmation
of the role of the melting process in largely determining the resultant
fibre length distribution is provided by the similiarity of the
extrudate and melt pool distributions illustrated in Figure 3.14.

3.1.6.2 XS 929 - Maranyl A100

Extracted screw samples for this material are illustrated in
Figure 3.16. A similar melting pattern to the F.G.C.S. 1640 sized
material is evident although several significant differences are
observed:-

(a) The melting process is extremely variable, presumably due to
     the poor feeding performance of this blend as a result of the
     reduced bulk density which accompanies the increased
     filamentisation of the fibres.

(b) The overall melting rate is slower leading to reduced fibre
     fracture in the feed section - Table 3.15. In addition, no root
     film is detected although samples could be removed without damage
     after channel number 8.

(c) Fibre length analysis of the melt pool of channel 10 indicated
     the absence of undispersed fibres, the actual distribution being
     superimposable with that of the resultant extrudate. Subsequent
     X-ray analysis confirms these observations - see Figure 3.20.

(d) No fracture of the solid bed is observed in the transition region.
     Consequently the increased melting rate leads to melting being
     completed by channel 12.

     Once again no significant fibre breakage is observed in the
melt conveying regions. The observed differences between the two
fibre types is attributal to the lower compaction of the latter
material which arises from the reduced bulk density. Since the
thermal conductivity of air is considerably lower than most polymeric
materials (93), such changes would lead to a significant reduction in
the rate of the secondary melting processes; hence the delay in the
formation of the root film and absence of undispersed material in the
melt pool. The absence of solid bed fracture is in accordance with
the work of Edmondson (27) who observed that such fracture only
occurred in the presence of the melt film at the screw root. Finally,
Figure 3.17 indicates the resultant extrudate fibre length distributions
for both materials.

   3.1.7 Determination of solid bed profiles

   3.1.7.1 Melting sections

   The most obvious change in successive cross sections removed

from the melting region is in the relative proportions of solid and melt, the melt pool increasing in width at the expense of the solid bed. The ratio of solid bed width to channel width at any particular location is often used to express the degree of melting which has occurred (97), (28). However, due to circulation in the melt pool, the solid bed width at the screw root is less than at the melt film and thus the mean width is often used. An alternative criterion which is often easier to apply, particularly in the early stages of melting, is that of relative cross-sectional areas. Such measurements were applied to the samples illustrated in Figures 3.12 and 3.16 and are reproduced in Figure 3.18. Values were obtained from the above sections using the MOP/ AMO3 modular pen system described in Section 1.6 or by projection of the images onto paper which was subsequently cut into the relevant sections and weighed. The solid and melt boundaries in the above sections are clearly marked by the carbon fibres included as tracers in the glass fibre - polymer blend.

The observed increase in the relative cross-sectional area of the solid in the primary compression step arises from the reduction in channel depth occurring faster than the rate of melting. The initial effect of this increased interface is to accelerate the rate of melting and hence fibre degradation due to the increased shear. However, such a situation will only lead to the completion of the melting process if fracture of the solid does not occur.

3.1.7.2 X-ray radiographic analyses

Samples removed from the extracted screws for the above materials were X-rayed to enable observation of the glass fibres in the matrix polymer - Figure 3.19. Photographic enlargement of the radiographs for the melting region clearly indicate the areas of undispersed fibre bundles and dispersed material respectively. Examples of such enlargements are provided in Figures 2.22 and 3.20. The excellent agreement
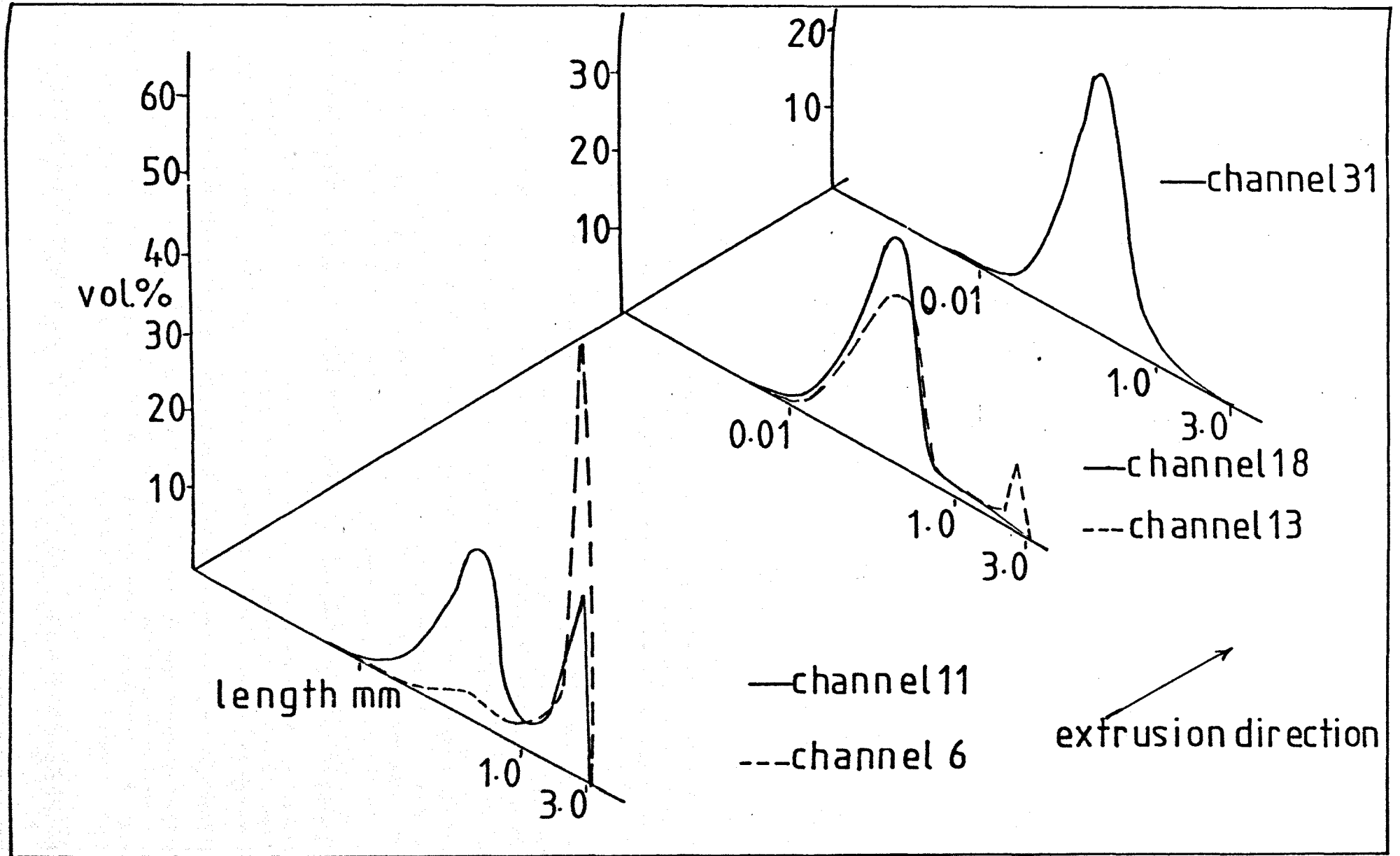
Figure 3.9   cross channel fibre length distributions-screw 1 (45mm)
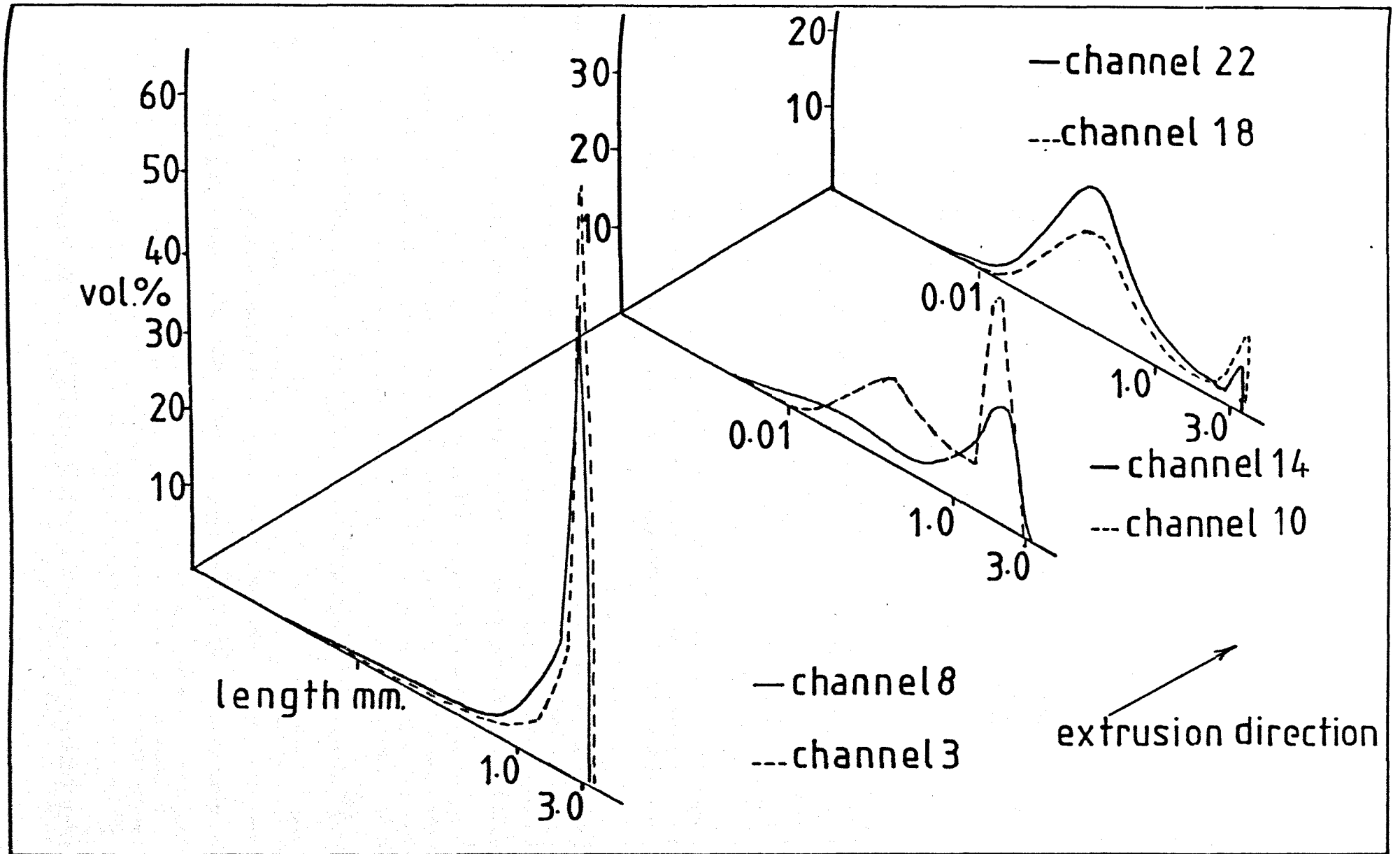
Figure 3.10 cross channel fibre length distributions - screw 3 (25mm)
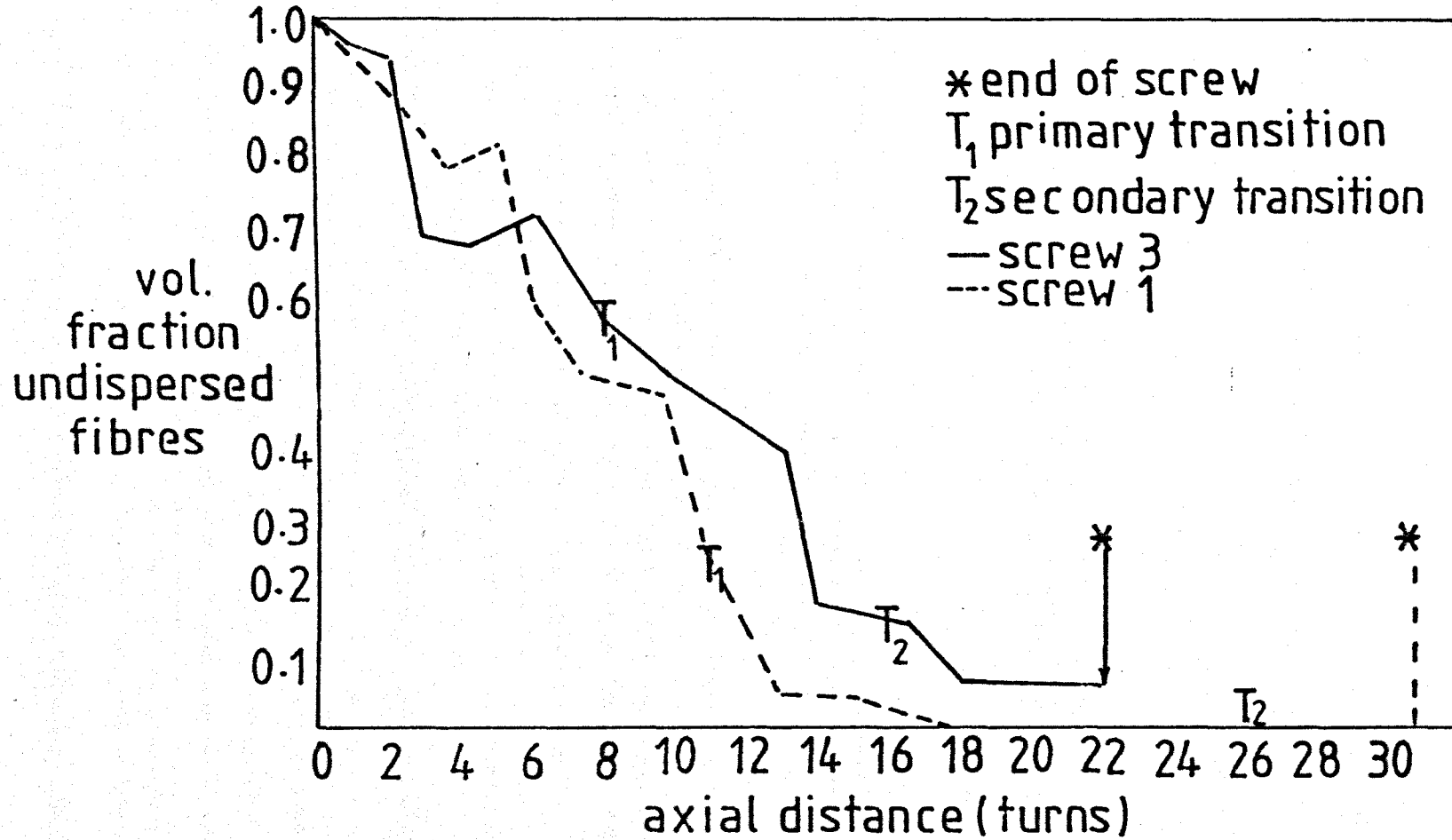
Figure 3.11 fraction of undispersed fibre bundles v axial distance

FIGURE 3.12 MELTING SECTIONS F.G.C.S 1640/A100

Figure 3.13 channel 6 fibre length distributions
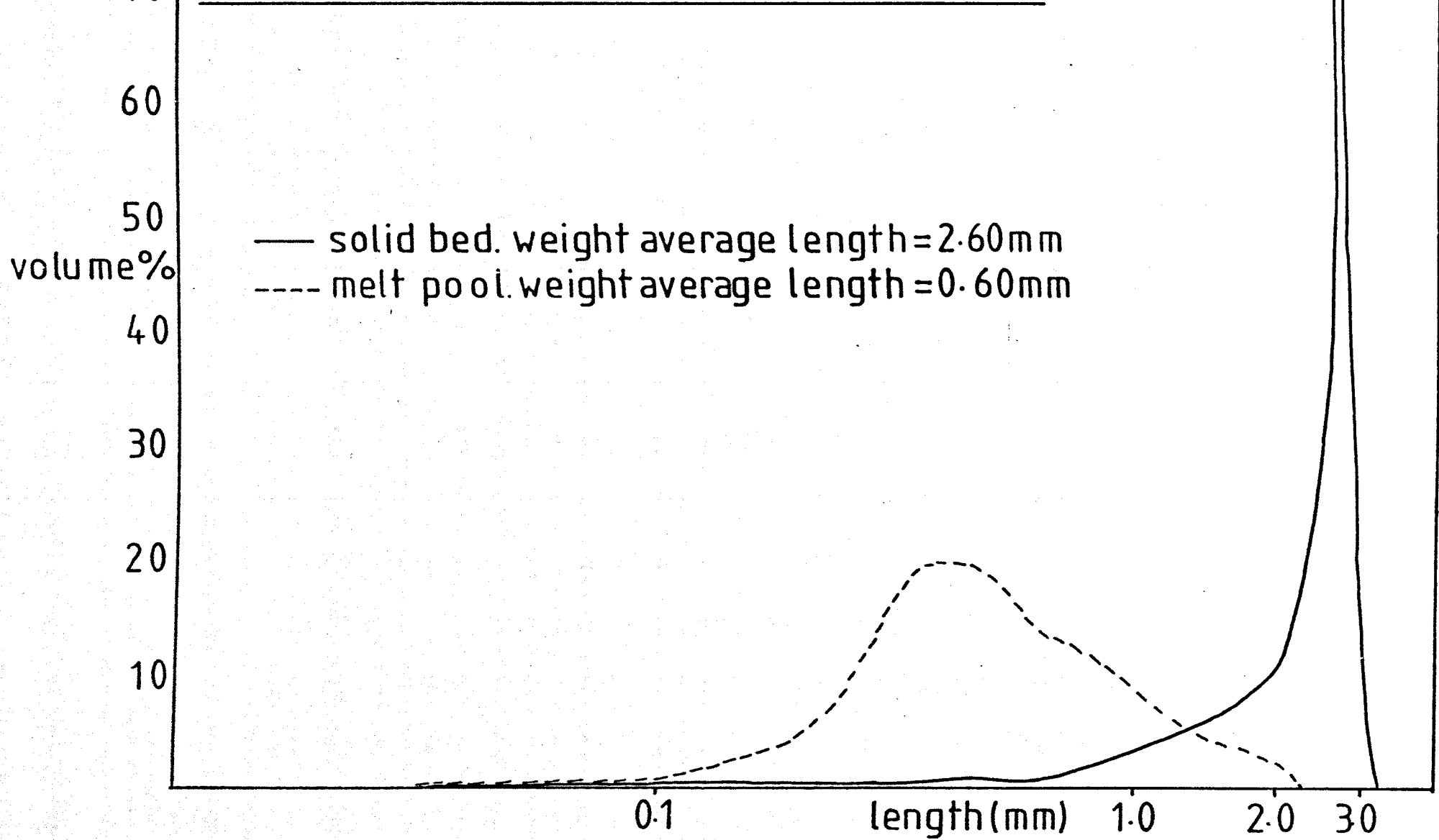
——— solid bed. weight average length = 2·60 mm
----- melt pool. weight average length = 0·60 mm

volume%

length (mm)

Qvol. cm^3/sec.	screw speed (N) rev/sec.	$V=\pi DN$ cm/sec	$V_x=V\sin\theta$ cm/sec	$V_z=V\cos\theta$ cm/sec.	$V_{sz}=\dfrac{Q_{vol.}}{XH_f}$ cm/sec.	$V_r=[(V_z-V_{sz})^2+V_x^2]^{\frac{1}{2}}$ cm/sec.	mean shear rate sec^{-1}		
							feed zone V_r/H_c	1st met. V_z/H_{m_1}	2nd met. V_z/H_{m_2}
4.40	0.5	8.0	2.45	7.6	1.11	6.94	279	39.5	27.8
7.48	1.0	16.0	4.90	15.26	1.89	14.24	570	79.1	55.7
9.85	1.5	24.0	7.35	22.89	2.48	21.70	868	119.0	83.6

actual barrel diameter = 51.0 mm

H_c = flight land–barrel clearance = 0.25 mm

H_{m_1} = primary metering zone channel depth = 1.93 mm

H_{m_2} = secondary metering zone channel depth = 2.74 mm

Table 3.13 comparative shear rates 50mm extruder

50mm extruder
screw number 4
screw speed = 60 r.p.m.
barrel temperature = 290°C
material: 30% b.w. F.G.C.S.1640/A100

melt pool
channel 10 wt. av. lth. = 0.670 mm

extrudate wt. av. lth. = 0.665 mm.
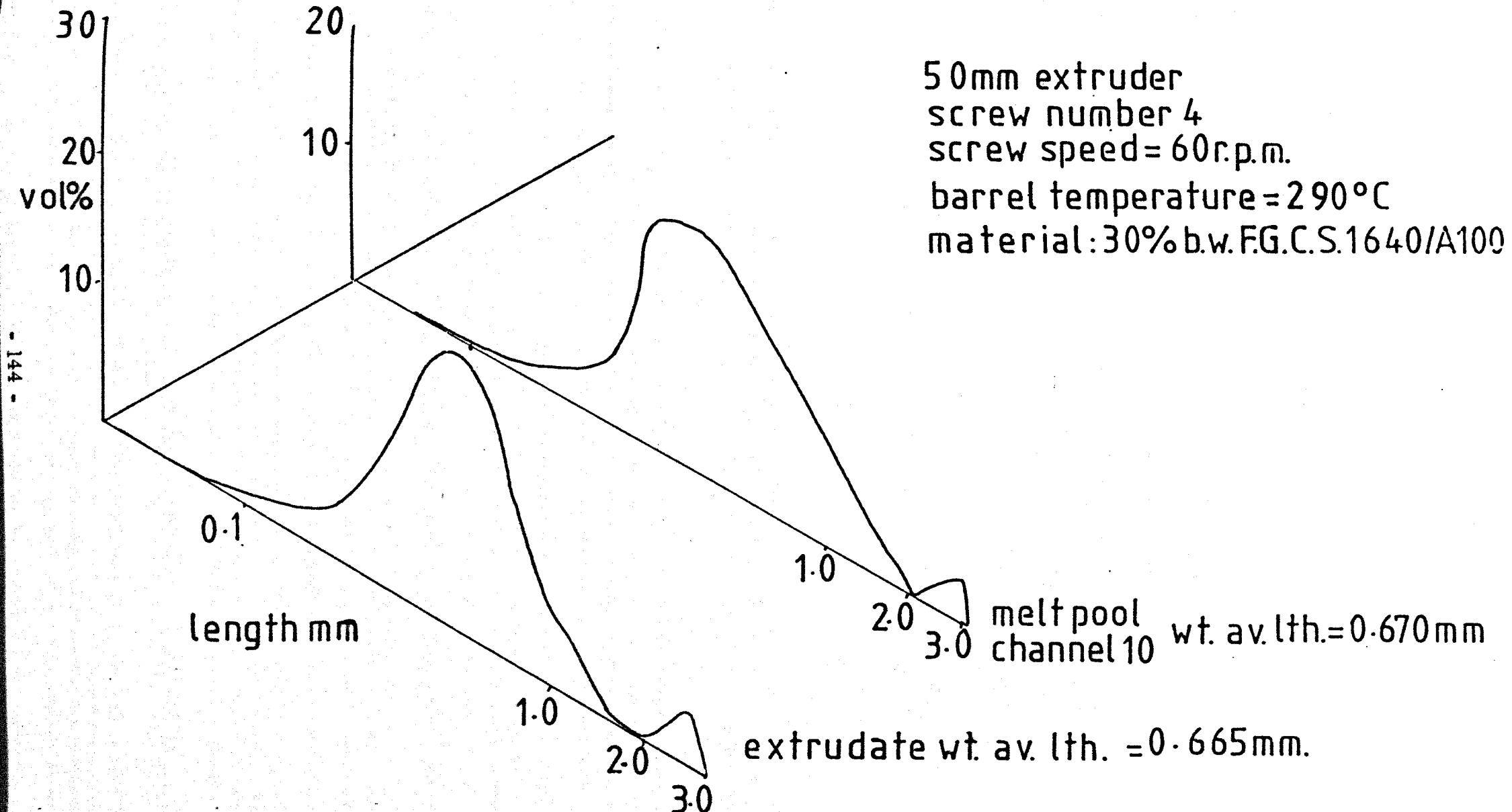
Figure 3.14 melt pool fibre length v extrudate

primary transition=10.75D

vol%

0.04

0.1

length.mm.

section 16
wt. av. lth.=0.777mm.

section 12
wt. av. lth.= 0·879 mm.

section 10
wt. av. lth.= 1·75 mm.
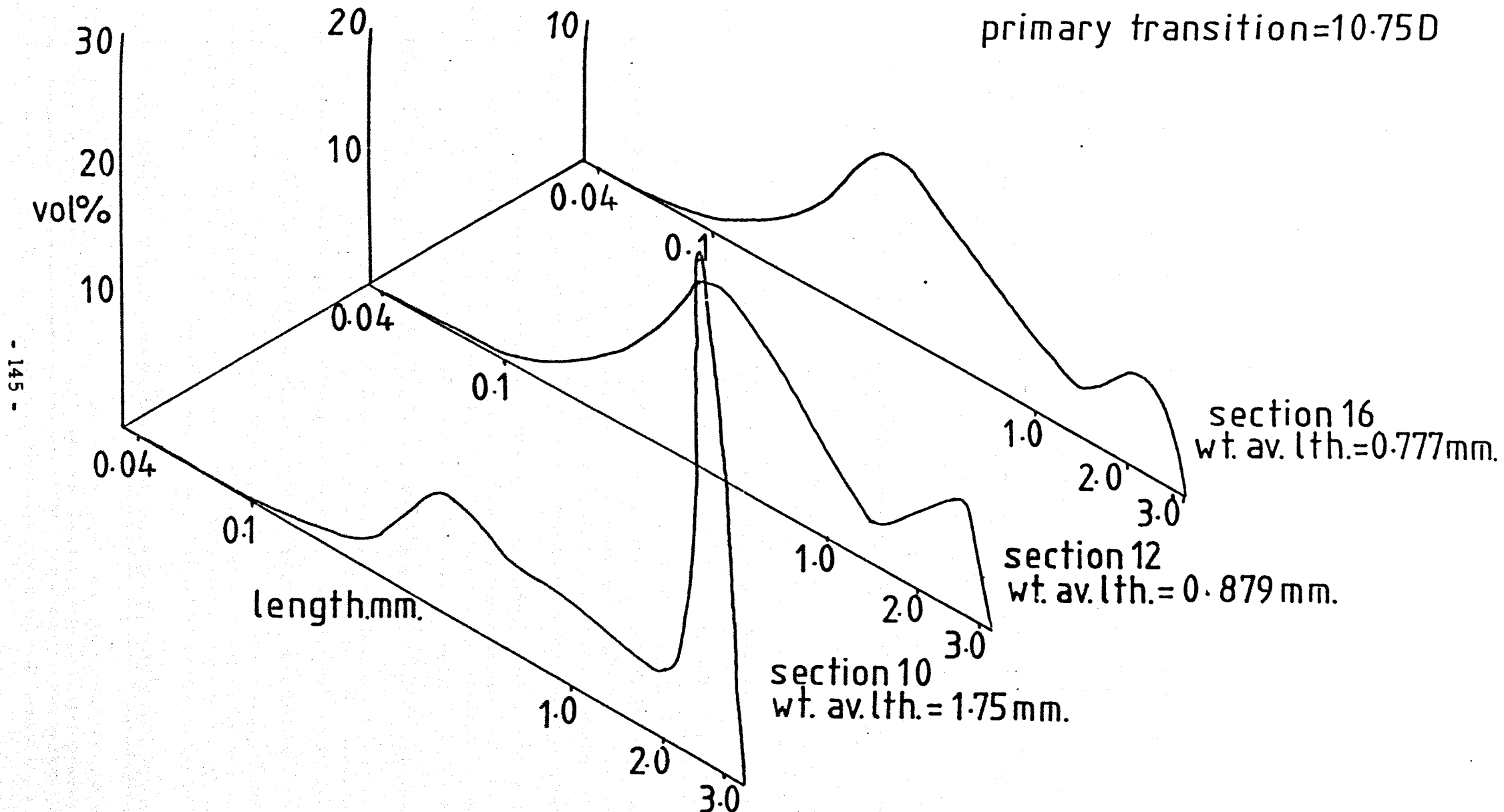
Figure 3.15 cross channel fibre lengths, primary screw – 50mm extruder

section number	vol.% fibre bundles	wt.av. fibre length mm
18	4.8	0.750
23	3.0	0.680
32	2.8	0.665

Table 3.14 vol.% fibre bundles.v axial position
50mm extruder

section number	weight average fibre lth. mm	
	F.G.C.S.1640/A100	XS 929/A100
1	2.70	2.63
2	2.64	2.72
3	2.48	2.22
4	2.40	1.94
5	1.95	1.89
6	2.16	1.98
7	1.78	2.35
8	1.76	2.08
9	1.38	1.75
10	1.75	1.76
11	1.50	2.21
12	0.88	0.64

Table 3.15 fibre fracture in the feed zone-screw 4
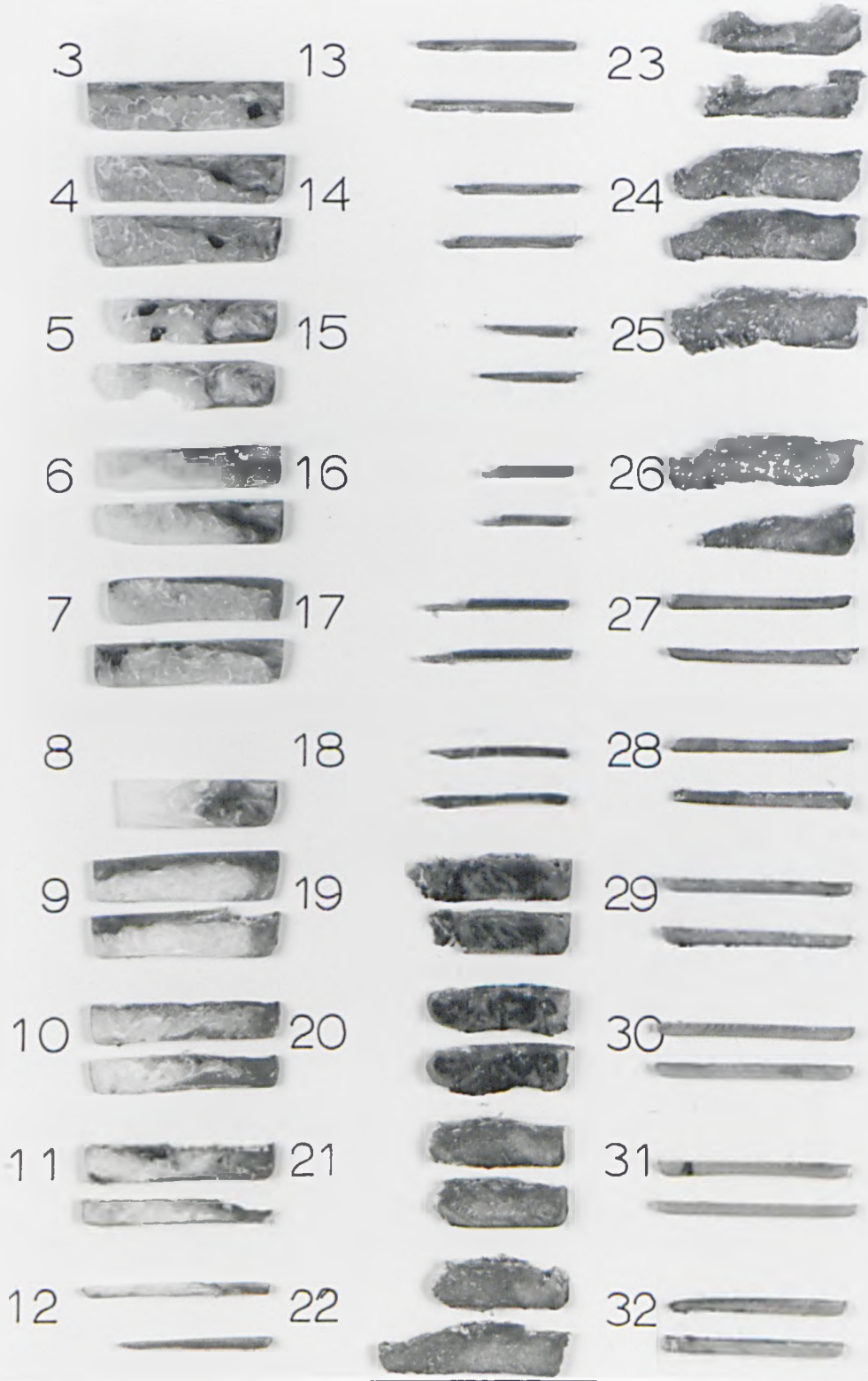
FIGURE 3.16 MELTING SECTIONS-XS 929/A100
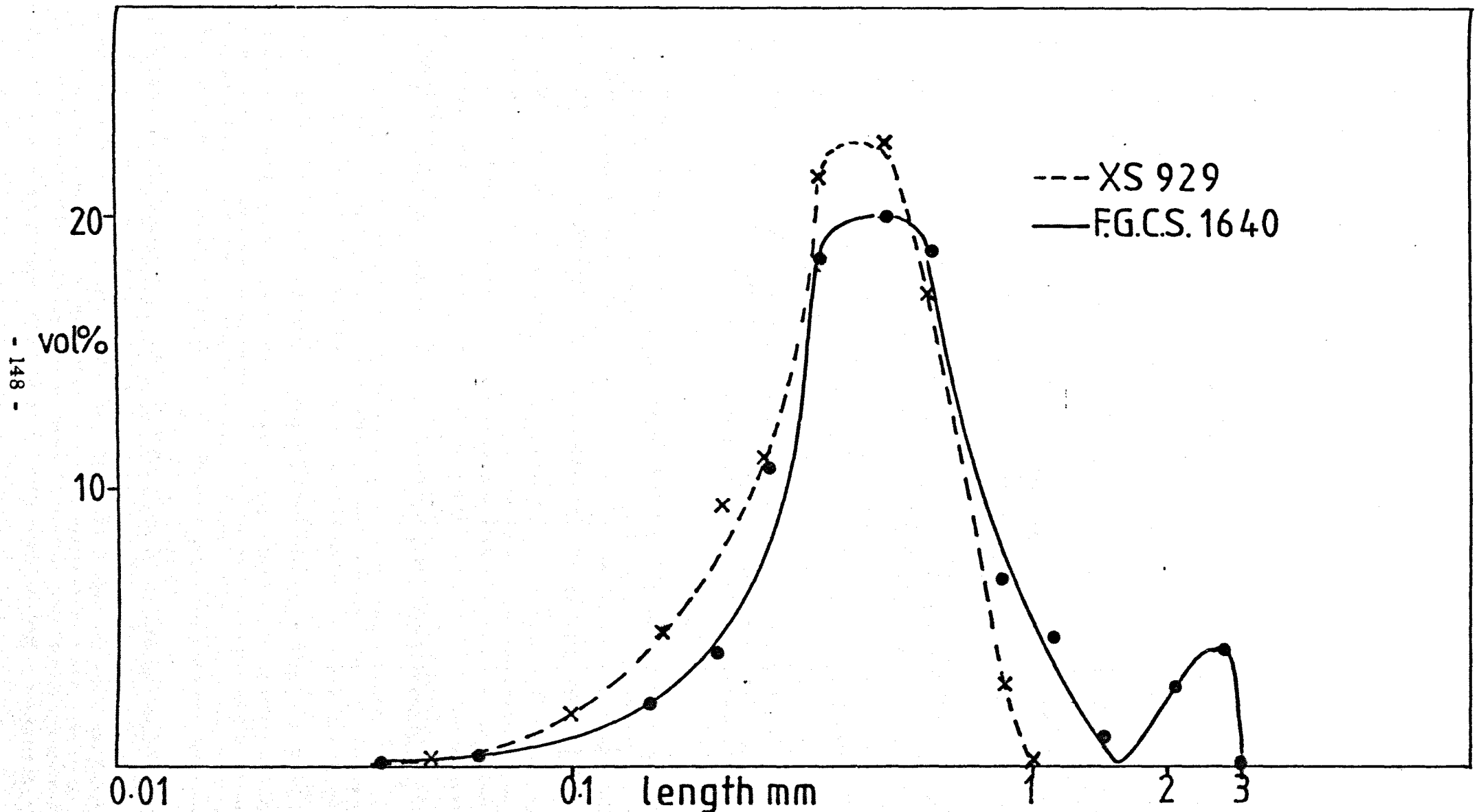
Figure 3.17. extrudate fibre length distributions–screw 4
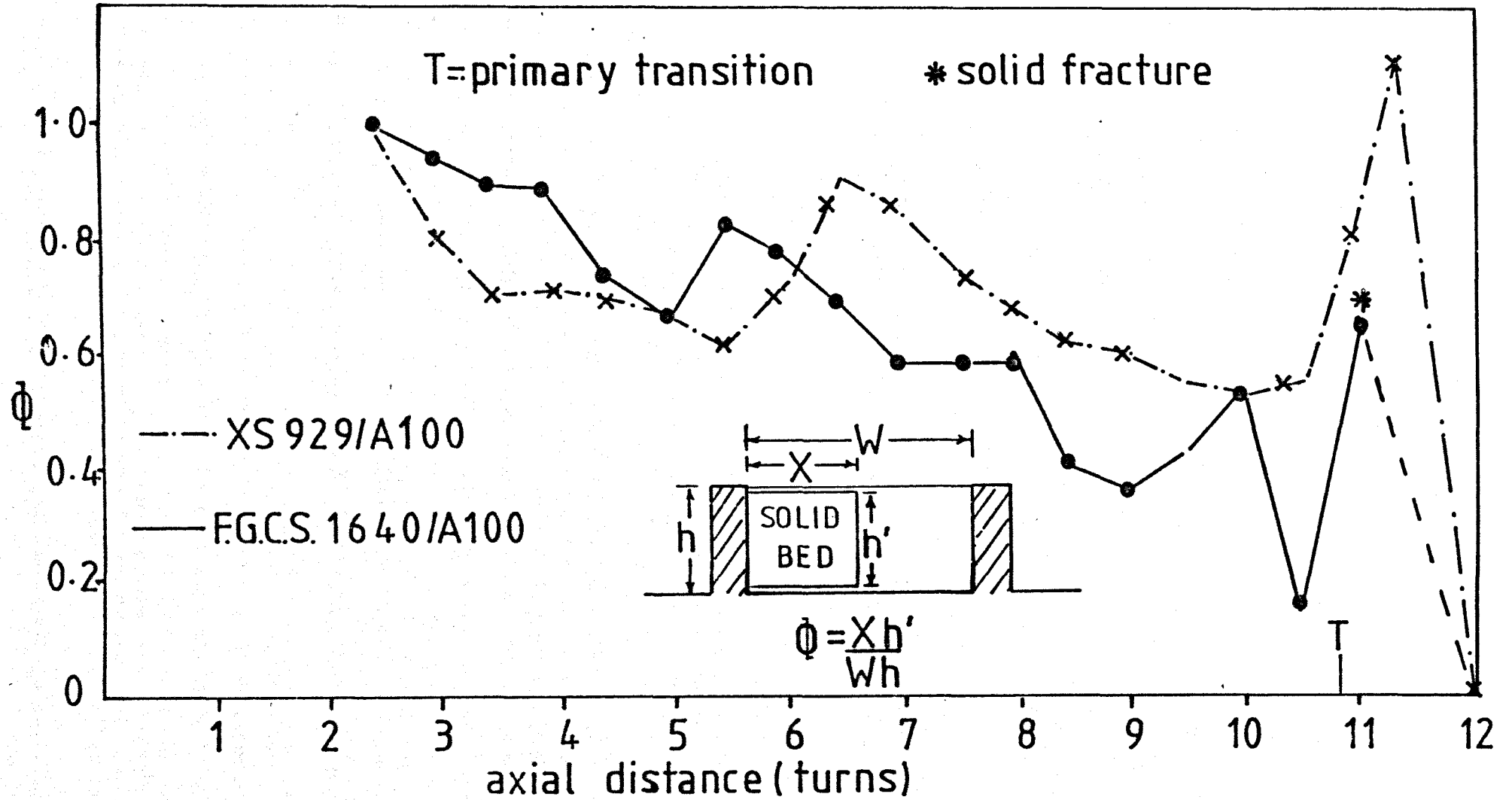
Figure 3.18. measured solid bed profiles 50mm extruder

T=primary transition   * solid fracture

$$\phi = \frac{Xh'}{Wh}$$

axial distance (turns)

-149-

F.G.C.S.1640/MARANYL A100

$T_b = 290°C$ $N = 60$ r.p.m.
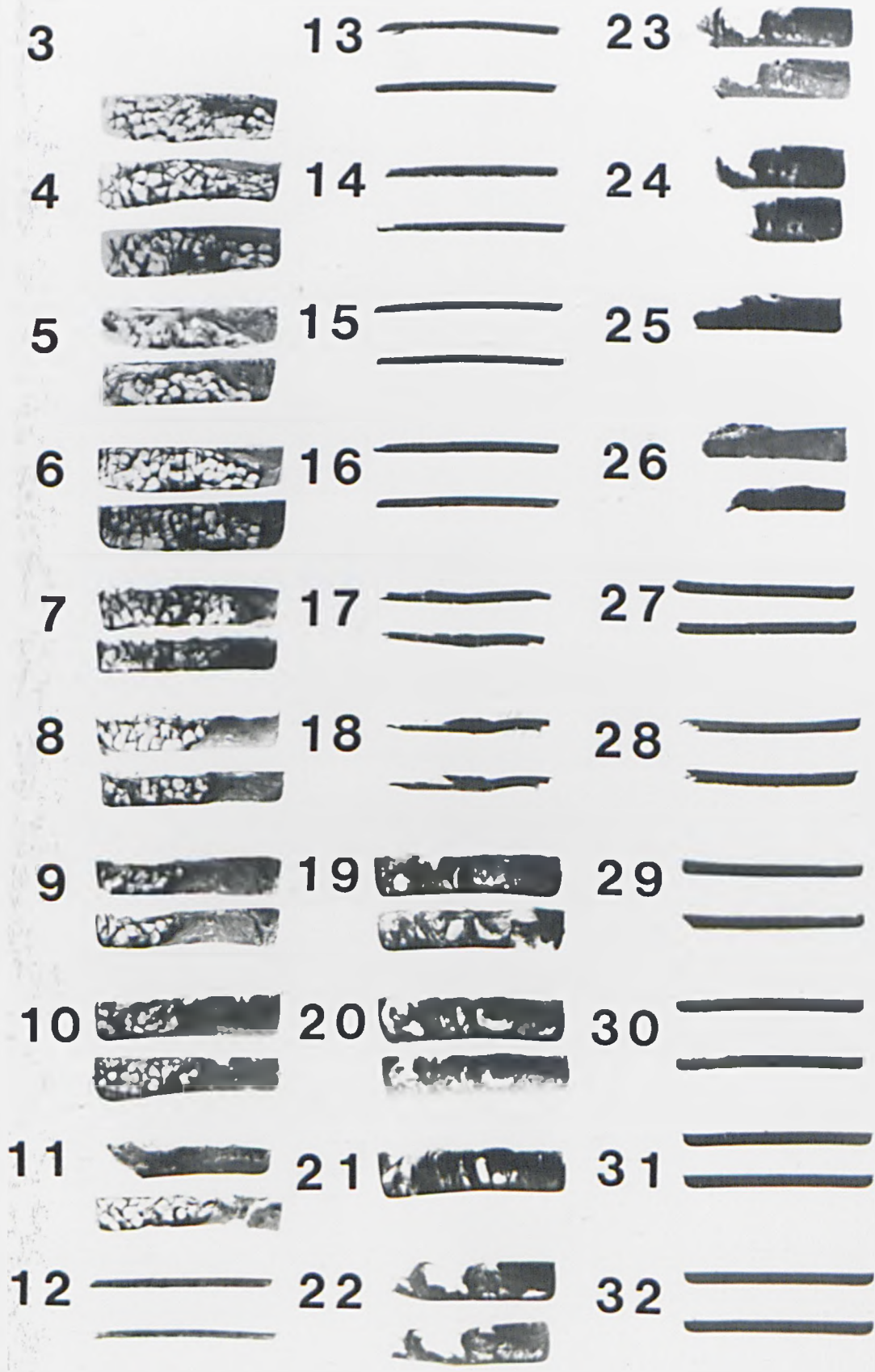
FIG. 3.19 X-RAY POSITIVE PRINTS - MELTING ZONE

solid bed   melt pool

Figure 3.20 X-ray radiograph P.V.A. sized fibres channel 10 screw 4
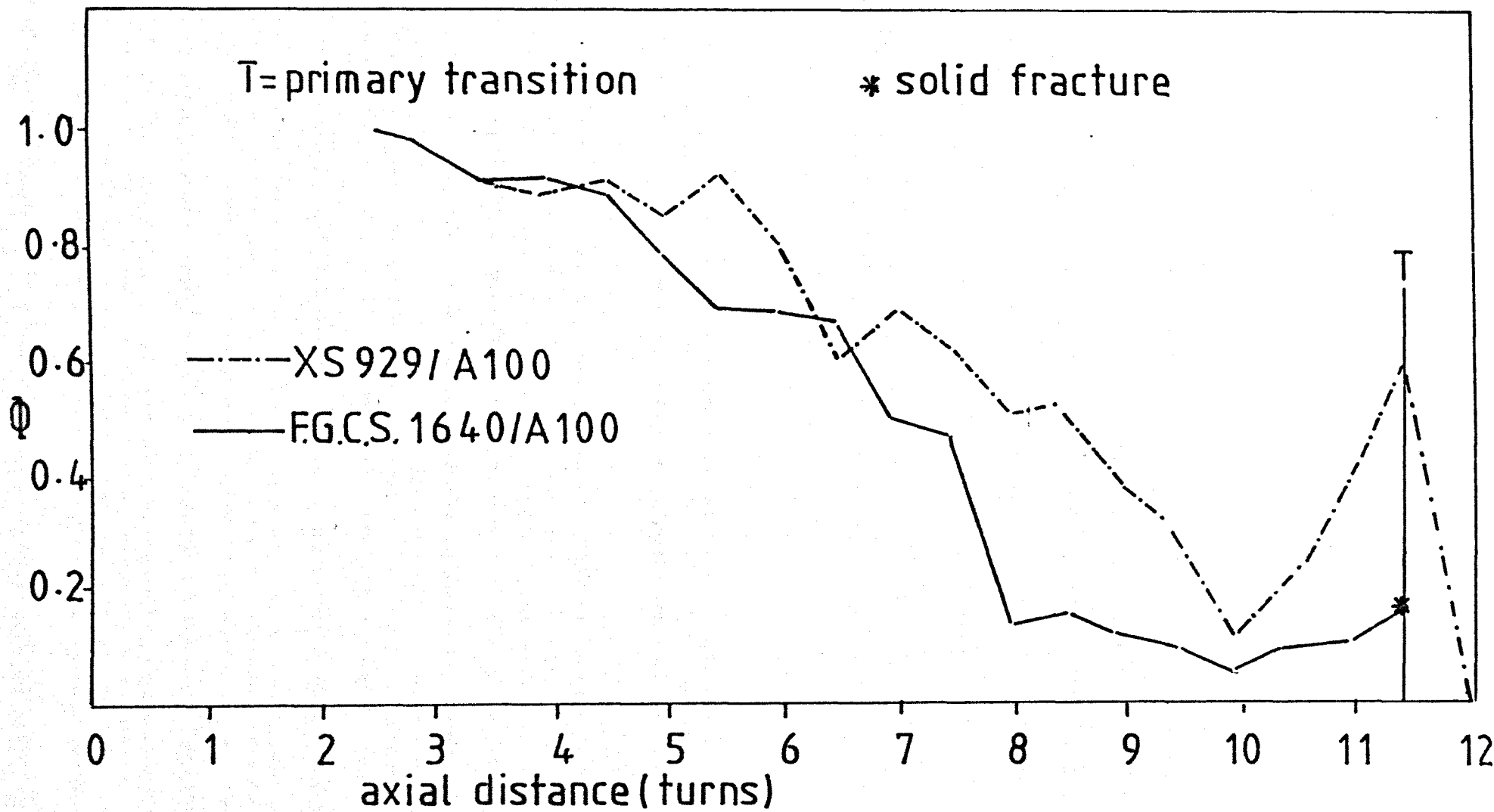
Figure 3. 21 measured solid bed profiles 45mm extruder screw 1

In the figure:

T=primary transition   * solid fracture

−·−·−XS 929/ A100

——F.G.C.S. 1640/A100

axial distance (turns)

between the relative areas obtained from such radiographs and the
previously determined solid bed profiles, provided the means of
assessing the melting pattern occurring in the 45 mm Betol extruder
- Figure 3.21.

3.1.8 Modelling of the melting process

3.1.8.1 The Tadmor model

The earliest theoretical attempt to describe the melting process
of the type observed in these studies was by Tadmor in 1966 (93).
In addition to the geometric simplifications described in Section 1.1
the following assumptions were introduced:-

(a) Although the density of the melt (ρ_m) is dependent on both
the temperature and pressure, density is considered to be effectively
constant at a particular location.

(b) The melting process is steady state.

(c) Thermal conductivities (K) and specific heats at constant
pressure (C_p), are locally constant.

(d) The solid bed is treated as a homogeneous semi infinite solid
whose temperature varies through the channel depth (y direction)
only.

(e) The velocity of the solid bed, (V_{sz}) in the downstream direction
is independent of Z i.e. velocity is constant and given by the
required mass flow rate along the channel calculated from the
velocity of the solid bed prior to melting.

(f) Melting occurs in the upper melt film only and the thickness of
this film (∂_1) is independent of the cross channel distance, x .

(g) Flow and temperature profiles in the melt film are fully developed.

(h) Viscosity in the melt film is not shear rate dependent, i.e. the
material is Newtonian.

Assumptions (e) and (f) dictate the motion of the solid bed.
The supposition of fully developed temperature profiles in the melt
film ignores the considerable changes in melt viscosity which can
accompany variations in temperature through the film thickness.
Thermal boundary condition of T_b and T_m are established at the barrel
and solid surfaces, respectively, the need to specify boundary conditions
for the screw temperature being avoided by assumption (d).

The mathematical analysis involves the calculation of mass
and energy transfers occurring in the solid bed and upper melt film,
respectively. Analysis of flow in the melt pool is not required since
it is implicit in the model that the flow rate in this region is balanced
with the sum of the flow rates in the former two regions, to provide the
total downstream flow rate.

Equations for the conservation of mass can now be stated. For the
upper melt film:-

$$m_{1Z} = \omega_1 X = \tfrac{1}{2} V_x \, \partial_1 \, \rho_m _____ 3.1$$

where, X = width of solid bed

m_{1Z} = downstream flow rate per unit bed width

ω_1 = melting rate/unit area

For the solid bed:-

$$\frac{d\, M_{SZ}}{dz} = -\omega_1 X \_\_\_\_\_ 3.2$$

and

$$M_{SZ} = \rho_s \, V_{SZ} \, X \, H_S$$

where M_{SZ} = downstream mass flow rate in solid bed

H_S = depth of solid bed

Assuming $H_S = H \left(\text{since } \partial_1 \leqslant H \right)$

then

$$\frac{d}{dz} \left(\rho_s \, V_{SZ} \, X \, H \right) = -\omega_1 X \_\_\_ 3.3$$

- 154 -

Determination of melting rate

The melting rate at the solid bed/melt film interface is calculated from a heat balance in this region

i.e.
$$\omega_1 \lambda = K_m \left(\frac{dT}{dy}\right)_m - K_s \left(\frac{dT}{dy}\right)_s$$

where λ = Latent heat of fusion

K_m, K_s = Thermal conductivities of melt and solid respectively

and m, s refer to gradients at the interface of melt and solid.

$\left(\frac{dT}{dy}\right)_m$ = Rate of heat conducted into the interface per unit surface area

$\left(\frac{dT}{dy}\right)_s$ = Rate of heat conducted out of interface per unit surface area

The rate of heat conducted into the interface per unit surface area is determined by the temperature profile existing in the melt film.

For a Newtonian fluid, this profile is given by:-

$$K_m \frac{d^2 T}{dy^2} = -\mu_1 \left(dV_r / dy\right)^2 \text{ -------3.4}$$

where μ_1 = constant melt viscosity

and V_r = relative velocity in upper film

This relative velocity is at an angle β to the downstream direction as shown in Fig. 3.22. The velocities of the barrel relative to the solid bed are given by $(V_z - V_{sz})$ in the downstream direction and V_x in the transverse and thus V_r is obtained from:-

$$V_r = \left[\left(V_z - V_{sz}\right)^2 + V_x^2 \right]^{1/2} \text{ -----3.5}$$

Now for a constant shear rate in the melt film equation 3.4 becomes:-

$$K_m \frac{d^2 T}{dy^2} = -\mu_1 \left(V_r / \partial_1\right)^2$$

Imposing the boundary conditions $T = T_m$ at $y = 0$

and $T = T_b$ at $y = \partial_1$
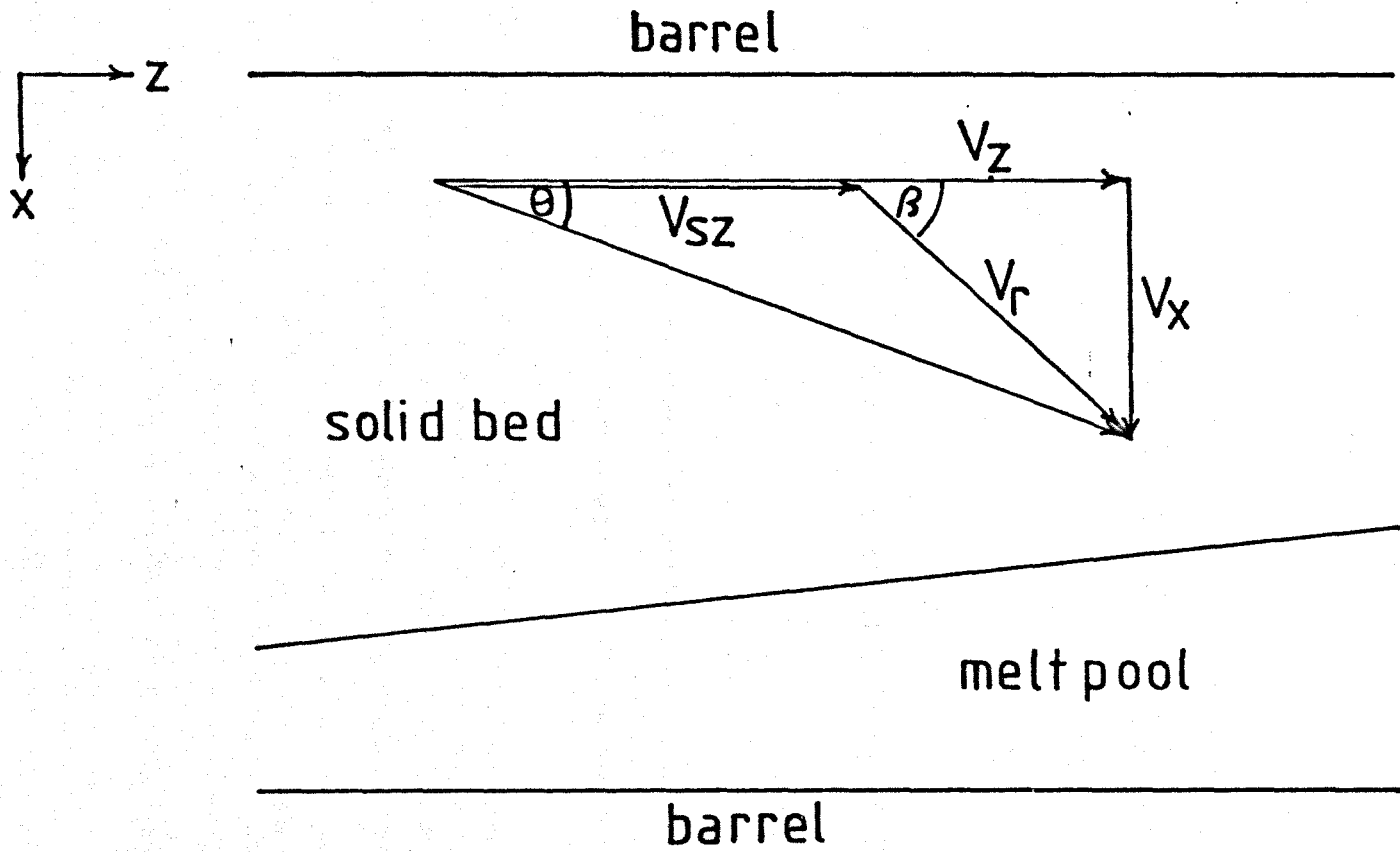
Figure 3.22. relative velocity diagram for the solid bed (97)

and integrating gives:-

$$T_b - T_m = \frac{\mu_1 V_r^2}{2 K_m} \cdot \frac{y}{\partial_1}\left(1 - \frac{y}{\partial_1}\right) + \frac{y}{\partial_1}\left(T_b - T_m\right) \text{---} 3.6$$

The first term on the R.H.S. of equation 3.6 represents the heat input due to viscous dissipation and the second from thermal conduction. Thus the heat flow per unit area into the solid bed is:-

$$K_m\left(\frac{dT}{dy}\right)_{y=0} = \frac{\mu_1 V_r^2}{2 \partial_1} + \frac{K_m}{\partial_1}\left(T_b - T_m\right)$$

Neglecting the heat required to raise the bulk temperature of the solid bed (assumption d) the rate of melting/unit area is given by:-

$$\omega_1 = \frac{1}{\lambda \partial_1}\left[\frac{\mu_1 V_r^2}{2} + K_m\left(T_b - T_m\right)\right] = \frac{C_1}{\lambda \partial_1} \text{---} 3.7$$

Combining equations 3.1 and 3.7 produces values for the melt film thickness (∂_1) and rate of melting/unit area (ω_1) namely:-

$$\partial_1 = \left(\frac{2 C_1}{\lambda \rho_m V_x}\right)^{1/2} \cdot X^{1/2} \quad \text{and} \quad \omega_1 = \left(\frac{C_1 \rho_m V_x}{2 \lambda}\right)^{1/2} \cdot X^{-1/2} \text{---} 3.8$$

Thus the melt film thickness is directly proportional to the square root of the solid bed width whilst the rate of melting is inversely proportional to this width.

Combining equations 3.3 and 3.7 gives:-

$$\frac{d}{dz}\left(\rho_s V_{sz} X H\right) = -\left(\frac{C_1 \rho_m V_x}{2 \lambda}\right)^{1/2} X^{-1/2} \cdot X$$

therefore $\quad \rho_s V_{sz} \, d/dz\left(X H\right) = \left(-\frac{C_1 \rho_m V_x}{2 \lambda}\right)^{1/2} X^{1/2} = -C_2 X^{1/2} \, .3.9$

For a constant channel depth section of depth H, solution of equation 3.9 gives:-

$$\frac{X}{W} = \left(1 - \frac{C_2 z}{2 \rho_s V_{sz} H W^{1/2}}\right)^2 \text{---} 3.10$$

$\frac{X}{W}$ = reduced solid bed width

Obviously the reduced solid bed area will be given by:

$$\boxed{\Phi = \frac{X H_s}{W H} = \frac{H_s}{H}\left(1 - \frac{C_2 z}{2 \rho_s V_{sz} H W^{1/2}}\right)^2 \text{---} \quad} \text{---} 3.11$$

where $Z = O$ when $X = W$ i.e. at the commencement of melting.
Equations 3.10 and 3.11 can also be solved for a tapering channel
when X is a linear function of Z.

Good qualitative agreement between predicted and measured
reduced solid bed widths was reported by several workers (98),
(99), (16), using the above melting model. However, Tadmor et. al.
(23) performed detailed comparisons for a wide variety of experimental
data using several commercial amorphous and semi-crystalline thermo-
plastics. Discrepancies between the observed and theoretical solid bed
profiles at high barrel temperatures were observed. Such deviations
were attributed to the non-Newtonian nature of polymeric materials and
also the temperature dependence of viscosity. Both the above effects
will produce a non linear velocity profile in the melt film, resulting
in a reduced melting rate or larger solid bed width at any cross-section
(c.f. equation 3.4). Additionally convection of heat into the molten
film was neglected. However, at the solid-melt interface, flow of newly
melted polymer at its melting point into the melt film produces a reduction
in the temperature of the melt. Consequently the temperature profile in
this film is changed causing a decrease in the rate of heat flow from the
film into the interface.

Marked improvements to the original model were achieved by
allowing for the above effects (23). Additional modifications were
incorporated by several workers, the most significant of which are
listed below:-

(a) The heat required to raise the temperature of the newly melted
    material to the mean temperature of the molten film was accounted
    for by defining an effective latent heat of fusion.

i.e. $$\lambda_{eff} = \lambda + C_{pm}\left(\overline{T_i} - T_m\right)$$

where λ_{eff} = effective latent heat of fusion

λ = measured latent heat of fusion

C_{pm} = specific heat of melt

$\overline{T_1}$ = mean melt temperature

T_m = melting point of polymer

(b) Correction factors to allow for channel curvature and flow in the flight clearance were introduced by Tadmor and Klein (16). The latter modification alters the mass balance expressed in equation 3.1 to:- $\omega_1 X = \frac{1}{2} V_x \partial_1 \rho_m - \frac{1}{2} V_x C_{pm}$ The second right hand term gives the leakage mass flow rate and is derived by assuming a linear velocity profile and pure drag flow conditions in the clearance.

(c) Correction factors for curvature and leakage flow were also derived by Hinrichs and Lilleleht (100) who also introduced a more sophisticated calculation for the solid bed velocity.

(d) All prior improvements have still maintained the assumption of constant melt film thickness across the channel. According to Tadmor and Klein, however, ∂_1 should increase in thickness towards the melt pool. Vermeulen et. al (101) allowed the melt film thickness to increase with x and developed a suitable model.

(e) Perhaps the most significant improvements to the Tadmor model were introduced by Donovan (26). Specific modifications based on experimental observations were:-

(i) The assumption of constant downstream velocity for the solid bed was removed. The solid bed was allowed to accelerate by the introduction of a 'solid bed acceleration parameter'.

(ii) The presence of a lower melt film was accounted for by introducing the screw boundary condition of $T = T_m$

(iii) An allowance for downstream convection was introduced enabling the average solid bed temperature to increase in the melting process.

(iv) The upper melt film thickness was considered to vary linearly across the width of the solid bed, initially equalling the flight clearance at the trailing edge.

The above modifications formed the basis of a modified melting model. However, the results achieved indicated that whilst the solid bed velocity does vary, its velocity cannot be easily stipulated. Subsequently Shapiro (102) treated V_{sz} as an unknown quantity and proposed a melting model which was then developed by Pearson and Halmos (103). A somewhat elementary version of this model was used by Edmondson and others and correlation with experimental results found to be reasonable for a wide variety of polymers (27), (28). The ability of this refined model to predict the experimentally observed solid bed fracture was demonstrated.

3.1.8.2 The modified melting model

Examination of Figure 1.10 indicates up to four distinct regions in the channel cross-section for which mass balances are required:-

(i) Upper melt film

$$\left[\begin{array}{l} \text{Rate of change} \\ \text{of downstream} \\ \text{mass flow rate} \end{array} \right] = \left[\begin{array}{l} \text{Rate of melting} \\ \text{over interface} \\ \text{with solid bed} \end{array} \right] - \left[\begin{array}{l} \text{net transverse} \\ \text{flow rate} \\ \text{out of melt film} \end{array} \right]$$

$$\frac{d}{dz}\left(m_{1z} X \right) = \omega_1 X - \left(m_1 x - m_f x \right)$$

where m_{1z} = downstream mass flow rate/unit width of solid bed in the upper film

$m_1 x$ = transverse mass flow rate/unit width of solid bed

$m_f x$ = leakage mass flow rate/unit length of flight

Note:- $m_f x = \frac{1}{2} V x \, C \rho m.$

(ii) Lower melt film

This is assumed to be of uniform thickness at a particular channel cross-section. All molten material is retained in this film and the mass balance conditions are:-

$$\frac{d}{dz} m_{2z}(X + H_s) = \omega_2 (X + H_s)$$

where $m_{2z}(X + H_s)$ = downstream mass flow rate/unit width of solid bed in the lower film and $H_s = H - d_1 - d_2$

(iii) Solid bed

The downstream mass flow rate for the solid bed will decrease due to loss of material by melting into the surrounding melt films:-

$$\frac{d}{dz}(\rho_s V_{sz} X H_s) = -\omega_1 X - \omega_2 (X + H_s)$$

The above mass balance neglects melting at the interface of the melt pool and solid bed, which appears to occur in the later stages of melting - Section 3.1.6.1. This omission, however, is not considered serious and at most should represent a slight underestimation of the degree of melting in the final stages of the melting process.

(iv) Melt pool

Since it is assumed that the total mass flow rate remains constant and is also a known quantity, then the mass change in the melt pool may be obtained from an overall mass balance:-

$$M_T = m_{1z} X + m_{2z}(X + H_s) + M_{mz} + M_{sz} - \frac{1}{2} \rho_m W V_{zc} \qquad 3.12$$

where M_T = total mass flow rate

M_{mz} = downstream mass in melt pool

In addition to the mass balances a relationship may be established between the forces due to the pressure gradient acting on the solid bed and the shear forces acting on its surfaces, for the bed to be in equilibrium.

i.e. $$P_z H_s X = T_1 z X - T_2 z (X + H_s) \qquad - - - - - 3.13$$

where P_z = downstream pressure gradient

τ_{1z}, τ_{2z} = downstream shear stresses in the upper and lower melt

films

The much reduced shear stresses acting on the solid due to the melt

pool are neglected. Equation 3.13 indicates that the dragging force,

produced by the relative motion of the barrel and solid bed, acts

in the downstream direction towards the die and is opposed by the

shear force in the lower melt film. Such a situation can only exist

when $V_{sz} \leqslant V_z$ and in practice the ratio of V_{sz}/V_z is relatively small.

Values of $m_{1z}, m_{2z}, \omega_1, \omega_2, \tau_{1z}, \tau_{2z}$ and M_{mz}

are obtained from analyses of flow and heat transfer in the

four regions.

(a) Analysis of the melt films

Non-Newtonian, non-isothermal analyses are used to calculate

flow and heat transfer rates in these regions. The presence of

pressure gradients are considered to be too small to significantly

influence the velocity profiles and thus drag flow is assumed. The

molten polymer is treated as a power law fluid for which shear stress

is shear rate dependent and also an exponential function of temperature.

i.e. $$\tau = \frac{\mu_o}{\gamma_o^{n-1}} \left(\frac{dv}{dy} \right)^n exp \left[-b(T - T_o) \right]$$

where μ_o = effective viscosity at a reference shear rate γ_o and

temperature T_o.

The temperature profile may be obtained from equation 3.4 by

substitution of the constant melt viscosity term for the effective

viscosity and assuming boundary conditions of:-

$$V = O, \ T = T_m \quad \text{at} \quad y = O$$

and $\quad V = V, \ T = T_w \quad \text{at} \quad y = \partial_1$

where T_w = boundary wall temperature

Such a technique was used by Edmondson and Fenner (24) who, by adapting

the largely analytical technique developed by Martin (104), derived values

for flow rate, shear stress and temperature gradients for a given film thickness and relative velocity. Since for the upper melt film the relative velocity is V_r , the required mass flow rates and shear stress in this direction were obtained as:-

$$m_1 x = m_1 \sin \beta$$

$$m_1 z = m_1 \cos \beta + \rho_m \partial_1 V_{sz}$$

$$\tau_{1z} = \tau_1 \cos \beta$$

where $\beta =$ the angle between V_r and the Z axis - Figure 3.22.

For the lower melt film the relative velocity, V_{sz} , is in the downstream direction and thus similar solutions can be obtained.

(b) Analysis of the solid bed

Heat transfer in the solid bed is due to a combination of thermal conduction through the bed thickness and thermal convection in the downstream direction. Temperature is assumed to be independent of x and the resultant heat transfer is governed by the energy conservation equation:-

$$\rho_s C_{ps} V_{sz} \frac{dT}{dz} = K_s \frac{d^2 T}{dy^2}$$

with $T = T_m$ and ambient temperature throughout at the commencement of melting. Convection of material into the melting interface is accounted for in the melting rate equations given below.

(c) Determination of melting rates

The melting rates at the solid and melt interfaces are determined from the known temperature gradients:-

$$\omega_1 \lambda_1 = K_m \left(\frac{dT}{dy}\right)_m - K_s \left(\frac{dT}{dy}\right)_s \qquad \text{for the upper film}$$

$$\text{and} \quad \omega_2 \lambda_2 = K_m \left(\frac{dT}{dy}\right)_m - K_s \left(\frac{dT}{dy}\right)_s \qquad \text{for the lower film}$$

The use of effective latent heats of fusion described previously allows for thermal convection which occurs in the y direction:-

i.e. $\quad \lambda_1 = \lambda + C_{ps} \left(T_m - \bar{T}_s\right) + C_{pm}\left(\bar{\bar{T}}_1 - T_m\right)$

and $\quad \lambda_2 = \lambda + C_{ps} \left(T_m - \bar{T}_s\right) + C_{pm}\left(\bar{T}_2 - T_m\right)$

where $\overline{T_S}$, $\overline{T_1}$, and $\overline{T_2}$ are the bulk mean temperatures in the solid bed and upper and lower films respectively:-

(d) Analysis of the melt pool

To prevent the analysis for this region dominating the overall solution procedure which would be extremely expensive in computing time, a very simple Newtonian analysis is used to describe flow in the melt pool. The total mass flow rate is given from the drag flow rates arising from the relative motion of the barrel and solid bed to the screw, and the pressure flow originating from the downstream pressure gradient.

Thus:-

$$M_{mz} = \rho_m W_m H \left\{ \frac{1}{2} V_z F_0 \left(\frac{H}{W_m} \right) + \frac{1}{2} V_{sz} F_0 \left(\frac{W_m}{H} \right) - H^2 \left(\frac{dp/dz}{12\overline{\mu}} \right) F_\rho \left(\frac{H}{W_m} \right) \right\}$$

where $F_0(\frac{H}{W_m})$ and $F_\rho(\frac{H}{W_m})$ are the drag and pressure flow shape factors (15) for flow in a rectangular channel of Width W and depth H. The mean viscosity $\overline{\mu}$, is evaluated from the mean shear rate and bulk mean temperature of the melt in this region.

Solution of the modified melting model described above requires the use of a high speed digital computer. A set of algebraic and differential equations for ∂_1, ∂_2, V_{sz}, X and the downstream pressure gradient, P_z, are derived from the mass and force balances. Given the operating conditions, the values of the above variables can be obtained for a particular channel cross-section. The calculation is terminated when either the width or depth of the solid bed approaches zero. Rapid increases in the velocity of the solid bed towards the end of melting often cause the calculation scheme to become unstable. Thus the calculation is performed in small downstream increments to eliminate or delay this instability. Typically 150 steps along a screw are appropriate, although up to 300 steps may sometimes be required.

At the commencement of melting initial values of V_{SZ} and X are required. V_{SZ} is obtained from equation 3.11, assuming only solid is present and X is therefore the channel width. Precise location of the start of melting is often difficult. Cooling of the feed pocket reduces both the screw and barrel temperatures below the polymer melting point and prevents the formation of melt films. Usually the upper film is formed after three or four screw turns - see Section 3.1.6. The lower film is generally formed one or two turns later for a neutral screw. Obviously the screw and barrel temperature profiles must be established to enable exact location of these two points. While the barrel temperature profile is usually set and thus presumably known the screw temperature profile is often unknown. However an empirical profile of the following form has been found to be satisfactory (27).

$$T_{S}(z) = T_{b} \left\{ 1 - exp(\lambda z) \right\} + T_{SO} \, exp(\lambda z)$$

where $\quad \lambda = \ln \left\{ (T_{S}(z) - T_{b}) / (T_{SO} - T_{b}) \right\} / z_{2}$

and $\quad T_{b}$ = barrel temperature

$\quad T_{SO}$ = material feed stock temperature

z_{2}, $T_{S}(z_{2})$ are the position and temperature at which the screw film is formed.

3.1.9 Application of the melting models to glass fibre - nylon 6.6 blends

3.1.9.1 50 mm extruder melting sections

Comparison of the predicted and measured solid bed profiles using the standard 30% B.W. blend of F.G.C.S. 1640 chopped strands and Maranyl A.100 is given in Figure 3.23. As expected improved agreement is achieved using the modified melting model. The observed fracture of the solid bed coincides with a predicted increase in solid bed velocity as illustrated in Figure 3.24. As observed experimentally by Edmondson such solid bed break-up only

occurred in the presence of a lower root film. Figures 3.25 and 3.26 indicate the predicted effect of delaying the formation of this lower film on the solid bed velocity (V_{SZ}) and solid bed profile (ϕ) respectively. The early formation of this film can be prevented in practice by cooling of the screw (15) or as observed in this study by reducing the bulk density of the feedstock material. However, in both instances reductions in output are observed.

Extending the axial length of the screw prior to forming this lower film reduces the initial rate of melting. The delayed occurence of predicted solid bed fracture, however, can result in an increased melting rate in the compression section. Such observations are in agreement with the observed melting and fibre fracture trends for the polyvinyl acetate sized fibres.

Physical, thermal and rheological property data used in the above melting simulations are given in Table 3.16. Values for the solid density were taken as the apparent bulk densities determined in section 3.1.3.1. However, since the actual density may be quite different it is instructive to observe the sensitivity of the predicted melting performance to variations in solid density - Figure 3.27. Other possible sources of error are in the solid thermal conductivity data, due to the uncertainty in the density values and the input barrel temperatures. The predicted influence of these variables is examined in Figures 3.28 and 3.29 respectively. The greatest sensitivity is shown by changes in barrel temperature. Although a "flat" temperature profile is assumed the measured temperatures during processing showed considerable deviation from the set points as indicated in Figure 3.30.

The ability of the modified melting model to successfully reflect the melting process occurring in these extrusion studies has been illustrated. The influence of the various design, processing and fibre
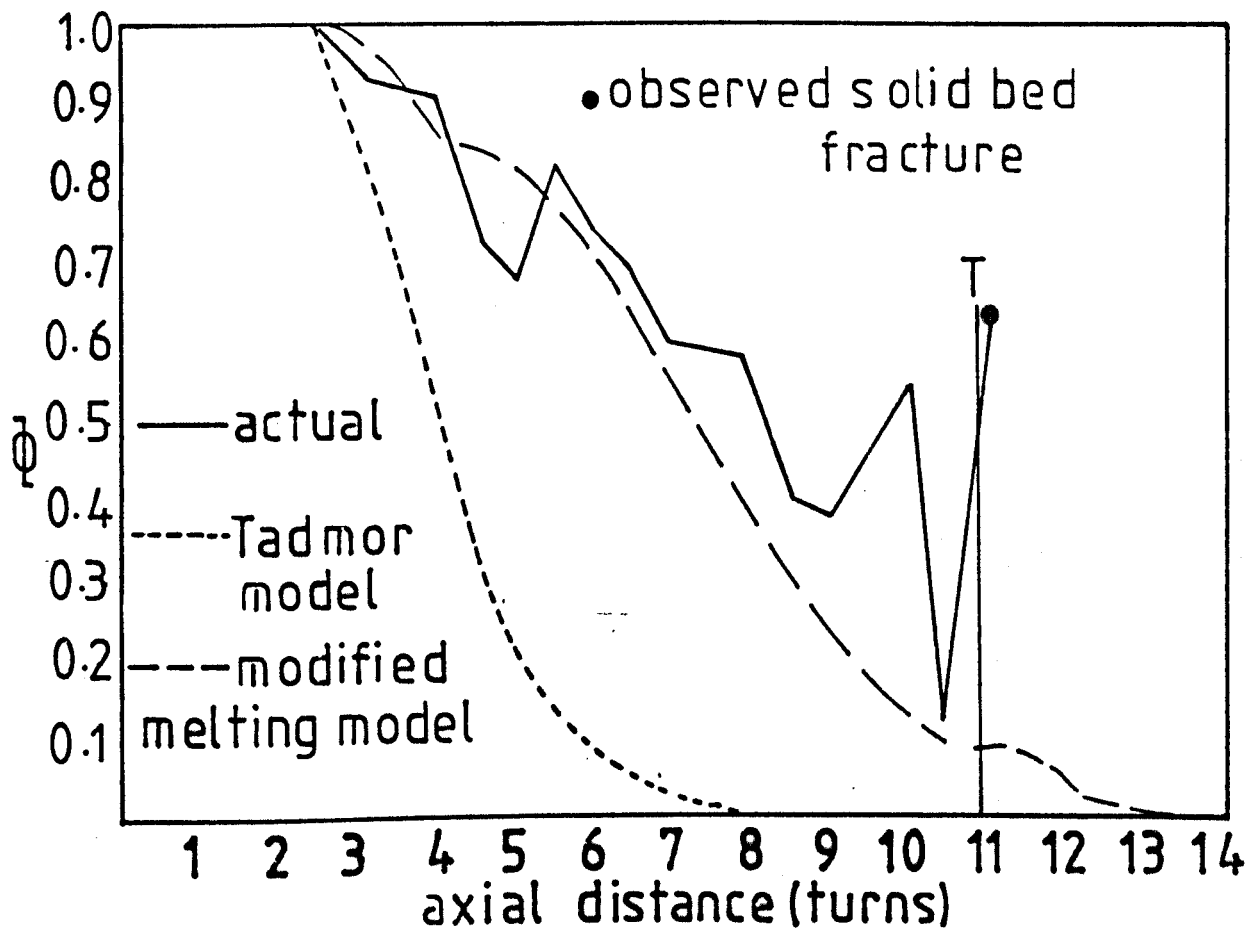
Figure 3.23. predicted v actual solid bed profiles
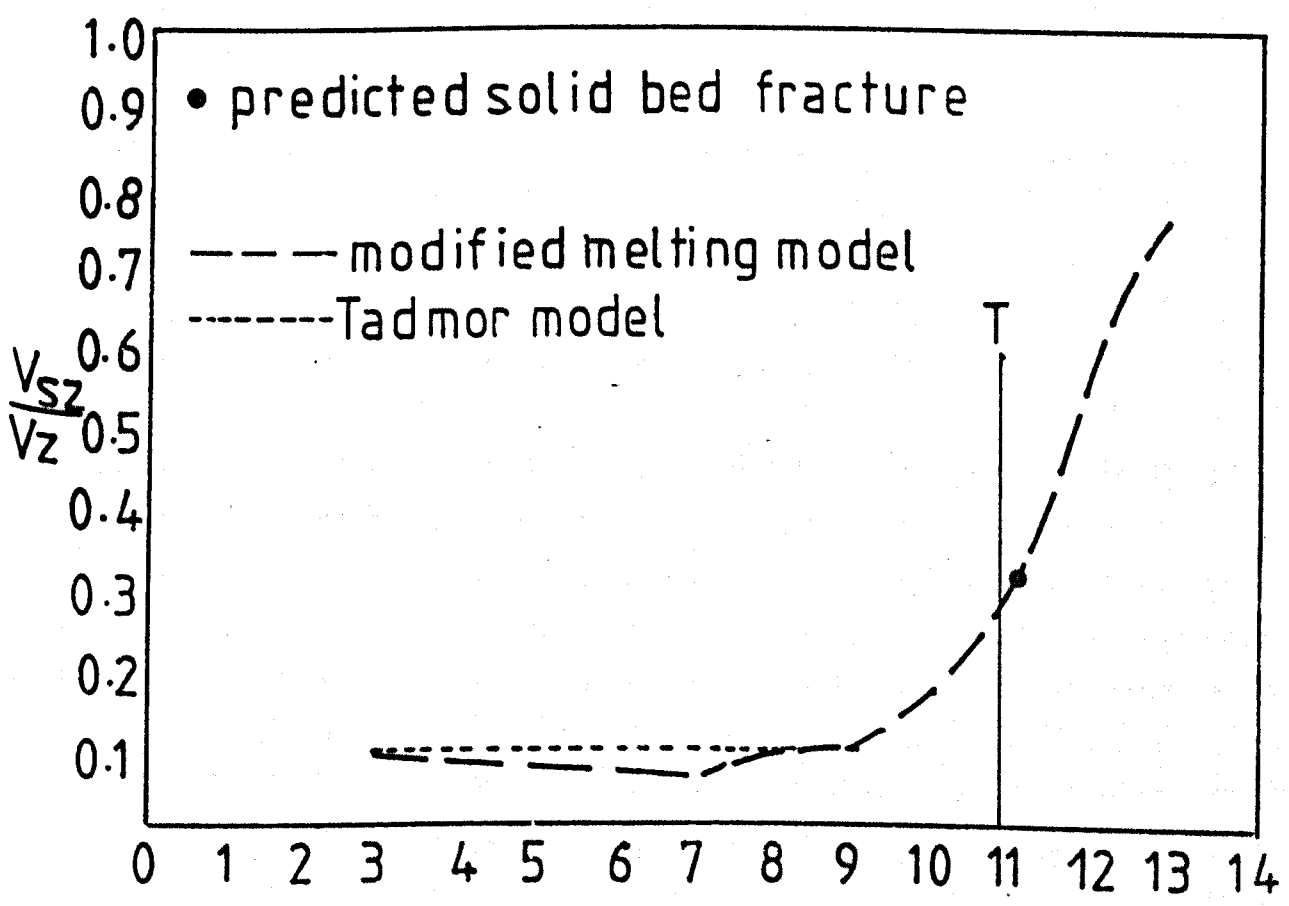
Figure 324 predicted solid bed velocities
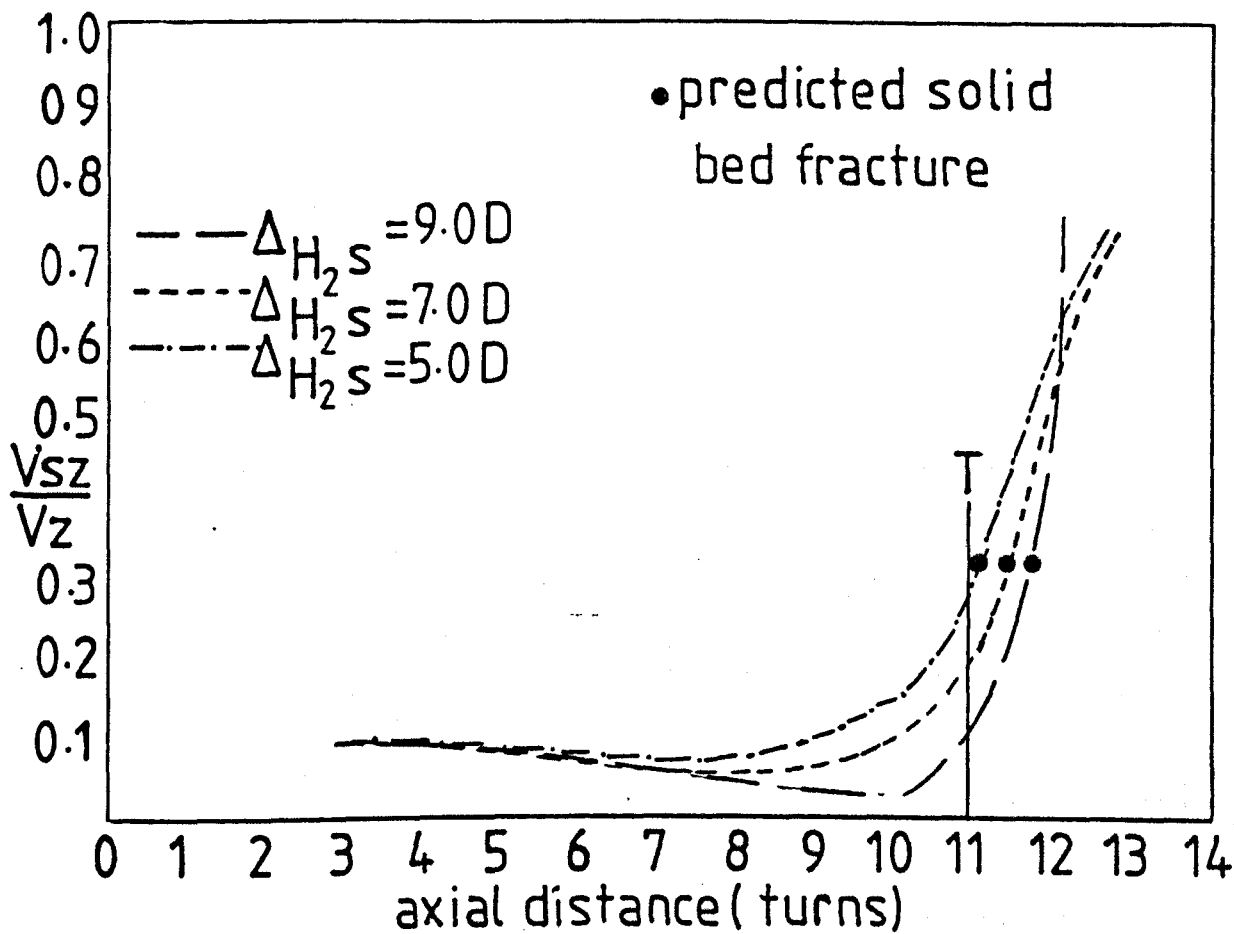
Figure 3.25. solid bed velocity v $\Delta H_2 s$
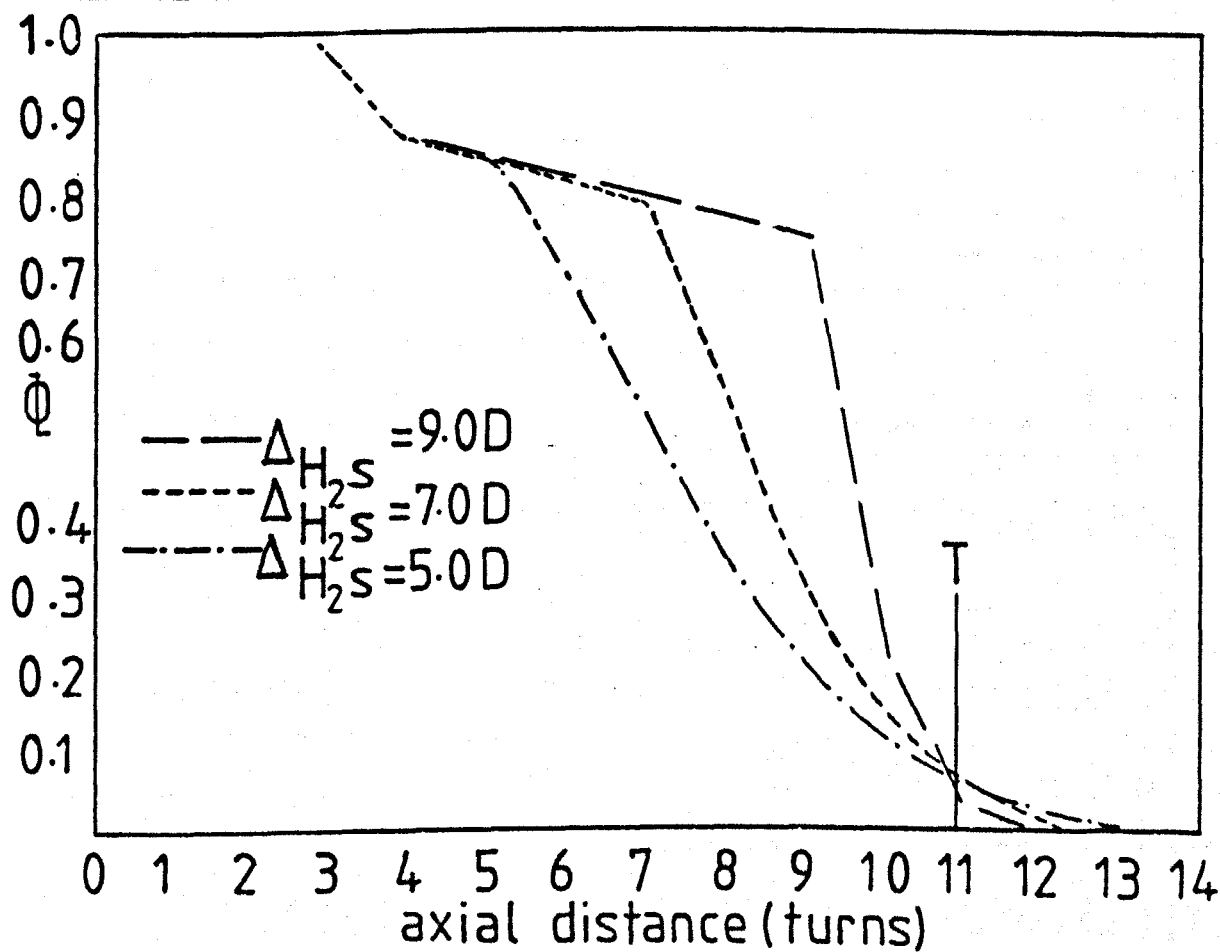
Figure 3.2 6. melting rate v $\Delta H_2 s$

material	density solid / melt	specific heat solid / melt	melting point	thermal conductivity solid / melt	latent heat of fusion	'n'	viscosity at 1sec^{-1} (apparent)	temp. coeff. of viscos.
30% b.w. FGCS 1640/ A100	660 (a) 1230 (c) Kg/m³	1300 (c) 2200 (c) J/Kg/°C	258 (c) °C	0.15 (e) 0.33 (c) W/m°C	123 (d) KJ/Kg	0.55 (a)	800 (a) N.s./m²	0.011 (a) °C-1

(a) measured values   (b) calculated values   (c) suppliers values – ex I.C.I. (d) R.A.P.R.A. (e) assumed

Table 3.16. material data –30% b.w. F.G.C.S. 1640/Maranyl A100

material	density Kg/m³ solid / melt	specific heat J/Kg/°C solid / melt	melting point	thermal conductivity W/m.°C solid / melt	latent heat of fusion KJ/Kg	'n'	viscosity at 1sec^{-1} (apparent) N.s/m²	temp. coeff. of viscos. °C-1
Maranyl A100	711 (a) 1010 (c)	1700 (c) 2600 (c)	258 (c)	0.15 (e) 0.28 (c)	175 (d)	0.89 (a)	170 (a)	0.02 (a)
10% b.w. F.G.C.S. 1640/A100	695 (a) 1210 (b)	1610 (c) 2420 (c)	258 (c)	0.15 (e) 0.29 (c)	158 (d)	0.65 (a)	450 (a)	0.013 (a)

Table 3.17. material data for different glass contents
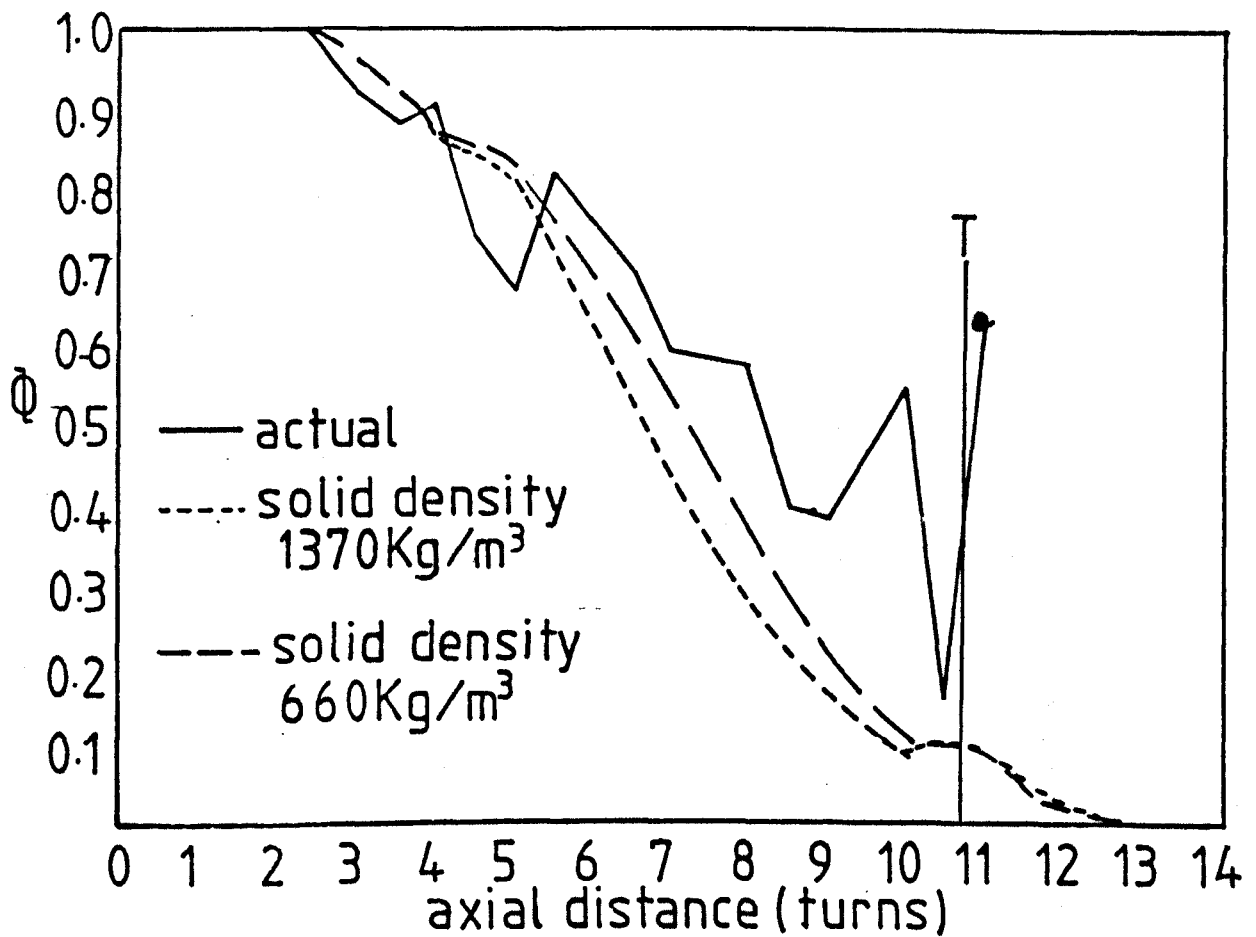
Figure 3.27. influence of solid density on melting.
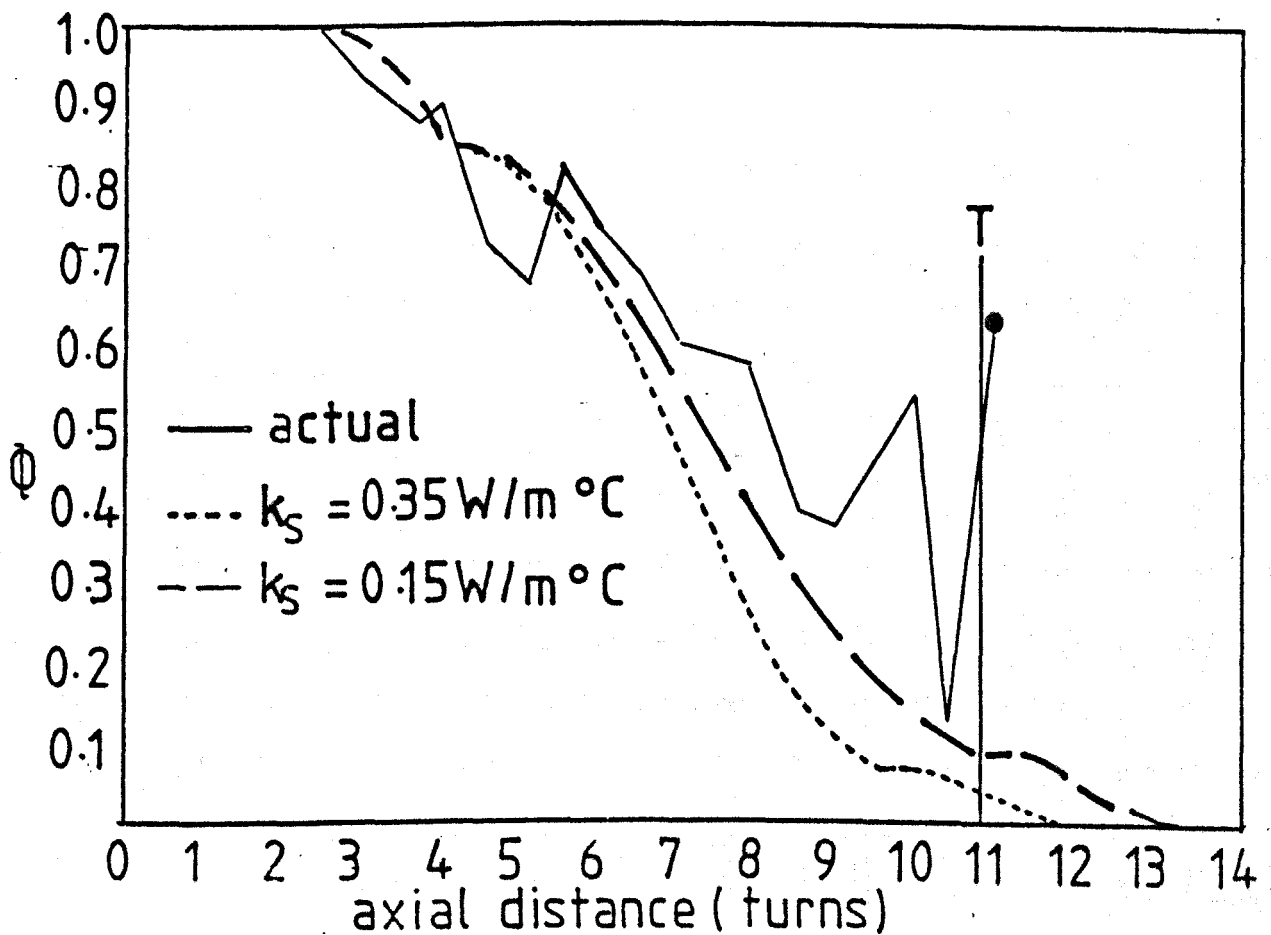
Figure 3.28. influence of solid thermal conductivity on melting
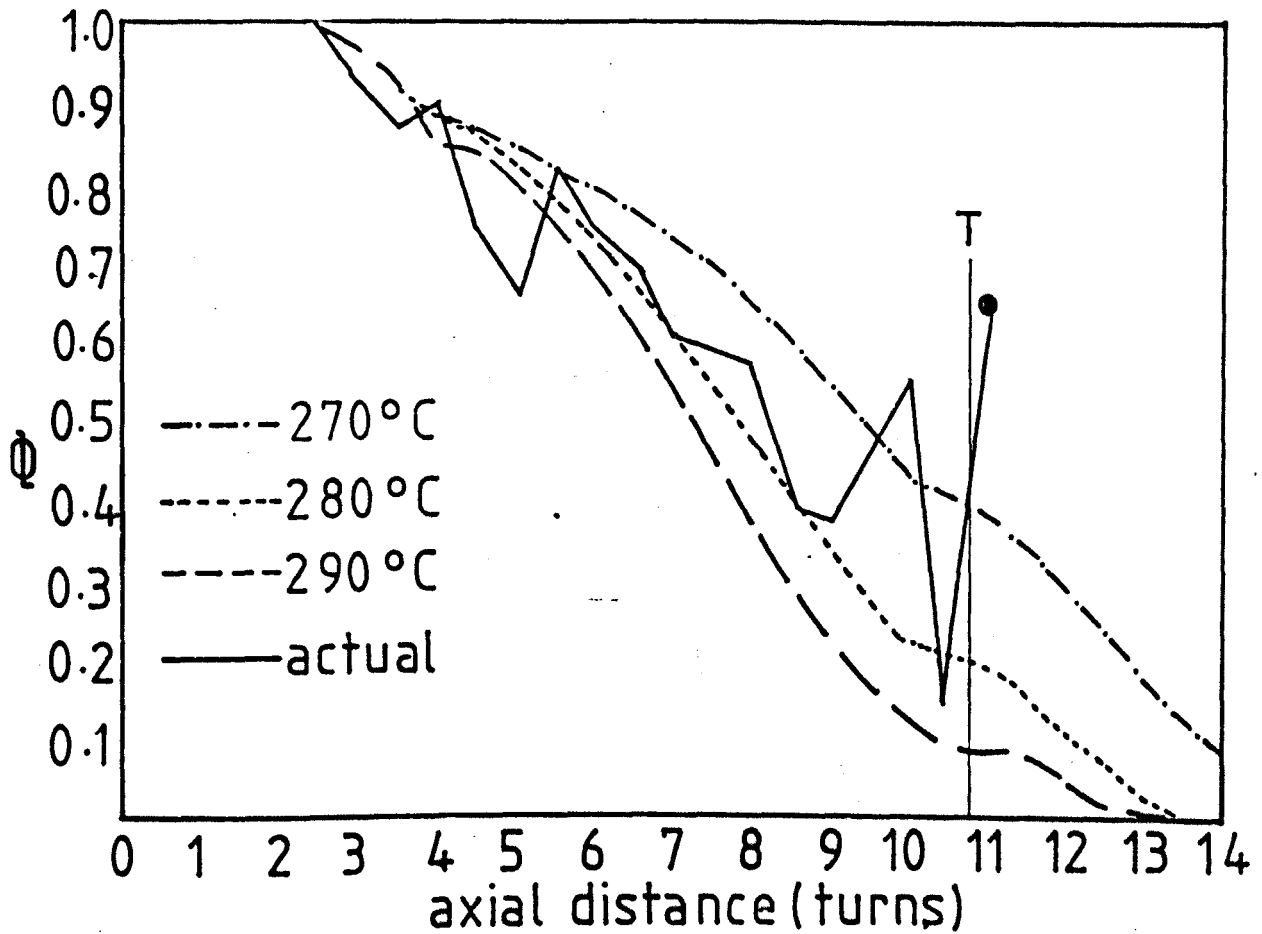
Figure 3.29. influence of barrel temperature on melting.
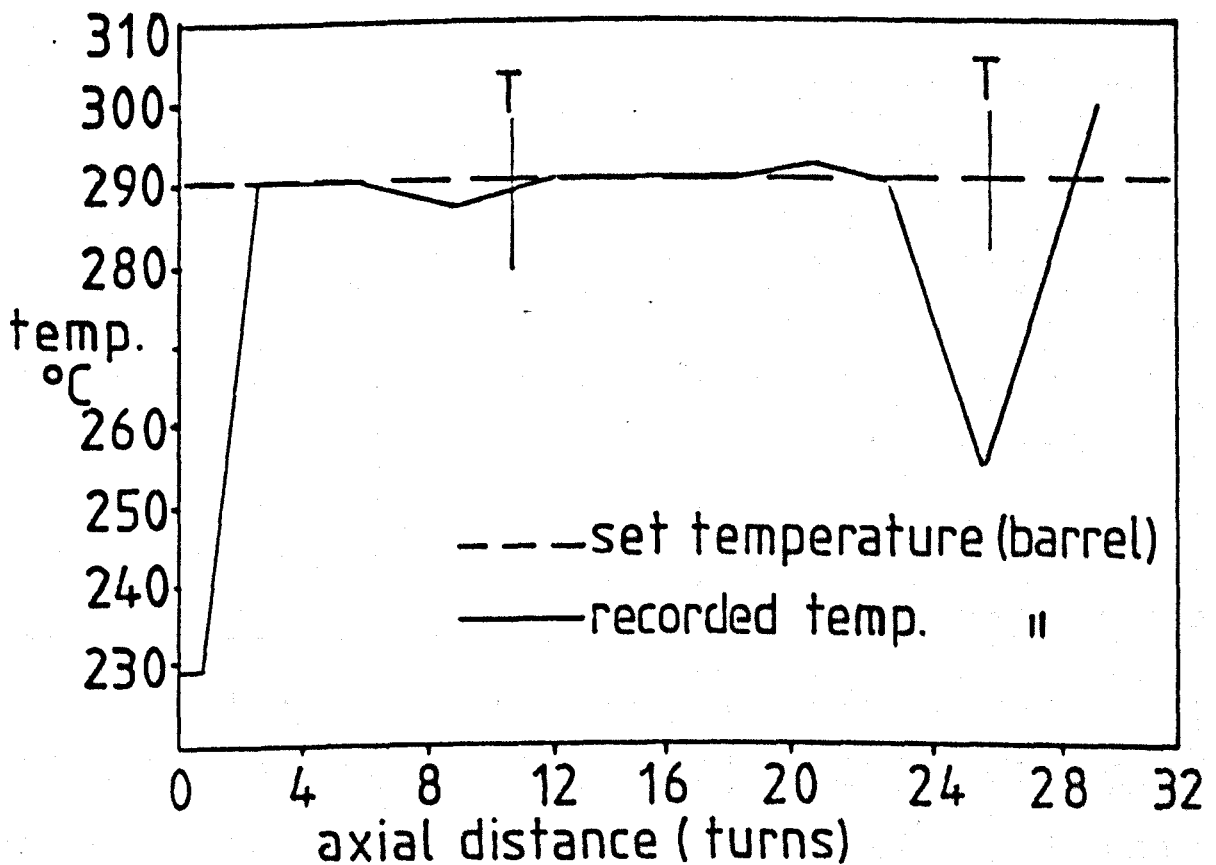
Figure 3.30. recorded temperature profile

variables upon the melting behaviour and the ensuing fibre fracture can therefore be demonstrated by computer modelling.

3.1.9.2 Interaction of geometrical design parameters and the melting process

The experimental solid bed profile obtained by x-ray analysis of samples obtained from screw 1 for the 45 mm extruder is compared with the computer prediction in Figure 3.31 and shown to give satisfactory agreement. In addition comparison of the predicted melting performance of screws 1 and 2 is given in Figure 3.32. A reduced melting length, arising primarily from the reduced throughput of the higher compression screw, is predicted. The corresponding solid bed velocities shown in Figure 3.33 indicate that fracture of the solid bed should occur in both instances. However, the predicted onset of solid bed acceleration occurs when melting is 99% completed for screw 1 as opposed to 83% for screw 2. Examination of the residual fibre length distributions produced by these screws, as indicated in Figure 3.1, is in accordance with such a melting pattern. Indirect evidence of solid bed fracture for screw 2 is provided by the increased scatter in the measured outputs and recorded melt pressures. The influence of other geometrical variables such as helix angle, flight clearance and number of parallel channels on the resultant fibre length distribution have not been studied although their effects on melting are well known (16).

3.1.9.3 Influence of operating conditions on the melting process

The dependency of the predicted solid bed profile and velocity on the operating variables of screw speed and barrel temperature is described by Figures 3.34 to 3.37 for screw 1.

Increased screw speed extends the melting region due to the higher throughput. However, as discussed in Section 3.1.2.2

the actual melting rate is accelerated due to the concomitant increases

in the cross-channel velocity component of the barrel and the rate

of melt film removal. Both of the above processes generate heat by

viscous dissipation. Evidence for this enhanced mechanical energy

input is provided by the elevated extrudate melt temperatures - Table

3.2 and the increased fibre breakage. This improved melting rate

which arises from increased screw speeds, will be somewhat lessened by

the non-Newtonian, temperature dependent behaviour of the polymer

melt. Ultimately, the increased output which accompanies faster screw

speeds will result in incomplete melting or solid bed fracture unless

matched by the improved melting rate. The likely consequence of such

melting deficiencies would be undispersed fibre bundles in the resultant

extrudate. No such effects were observed over the range of speeds

utilised in this study. However, parallel studies carried out for

directly injection moulded glass fibre blends provided confirmation of

such a trend - Section 3.3.2.7.

The predicted effect of barrel temperature on melting is described

by Figures 3.36 and 3.37. Reductions in the set temperature extend

the melting zone although this effect is somewhat diminished by

the increased viscous energy input which accompanies the increased

melt viscosity. The predicted solid bed fracture at the lowest barrel

temperature correlates with the observed instability of the extrusion

process under these conditions. However, recovered fibre lengths do

not reflect these pronounced changes, no undispersed material being

detected in the final extrudate. However, it is probable that the

increased shear stress in the melt conveying region, which accompanies

the higher melt viscosity, serve to disperse any fibre bundles prior to

extrusion through the die.

The predicted melting changes, achieved by throughput variations

occurring as a result of die restriction, are illustrated for the 25 mm

extruder in Figure 3.38. The improved stability of the compounding operation correlates with the faster melting rate for the smaller dies. However, the expected increase in fibre fracture is not realised - Figure 3.3. The proportion of undispersed fibre bundles is seen to initially decrease with reduction in die diameter and then increase with further reductions. Consideration of the dimensionless outputs given in Table 3.3 are consistent with a melting restricted process. Such inefficient melting coupled with the low specific power consumptions is indicative of a melting operation dominated by thermal energy input from the barrel heaters. As discussed in Section 3.1.6 the likely consequence of such a situation is the survival of a significant quantity of undegraded fibres either as a result of incomplete melting or melting which is completed under conditions of low shear stress.

3.1.9.4 Influence of material variables on the melting process

The influence of size type has been discussed in Section 3.1.9.1.

For screw 1 the predicted melting and solid bed velocity trends which accompany increased glass loadings are described in Figures 3.39 and 3.40. The associated physical, thermal, and rheological data for these materials is given in Tables 3.16 and 3.17. Computer simulations were restricted to 0%, 10% and 30% by weight blends due to practical difficulties in determining accurate rheology data for the higher glass content materials. Such difficulties have been observed by other workers (105) (106) and could be attributed to plugging of the capillary die by the glass fibres leading to erratic readings. Also degradation of the nylon matrix occurred which produced spurious results when using wider diameter capillaries (107).

Improvements in the melting rate and stability of the solid bed are predicted with increased glass contents. These improvements arise from the reduced latent heat of fusion and increased melt
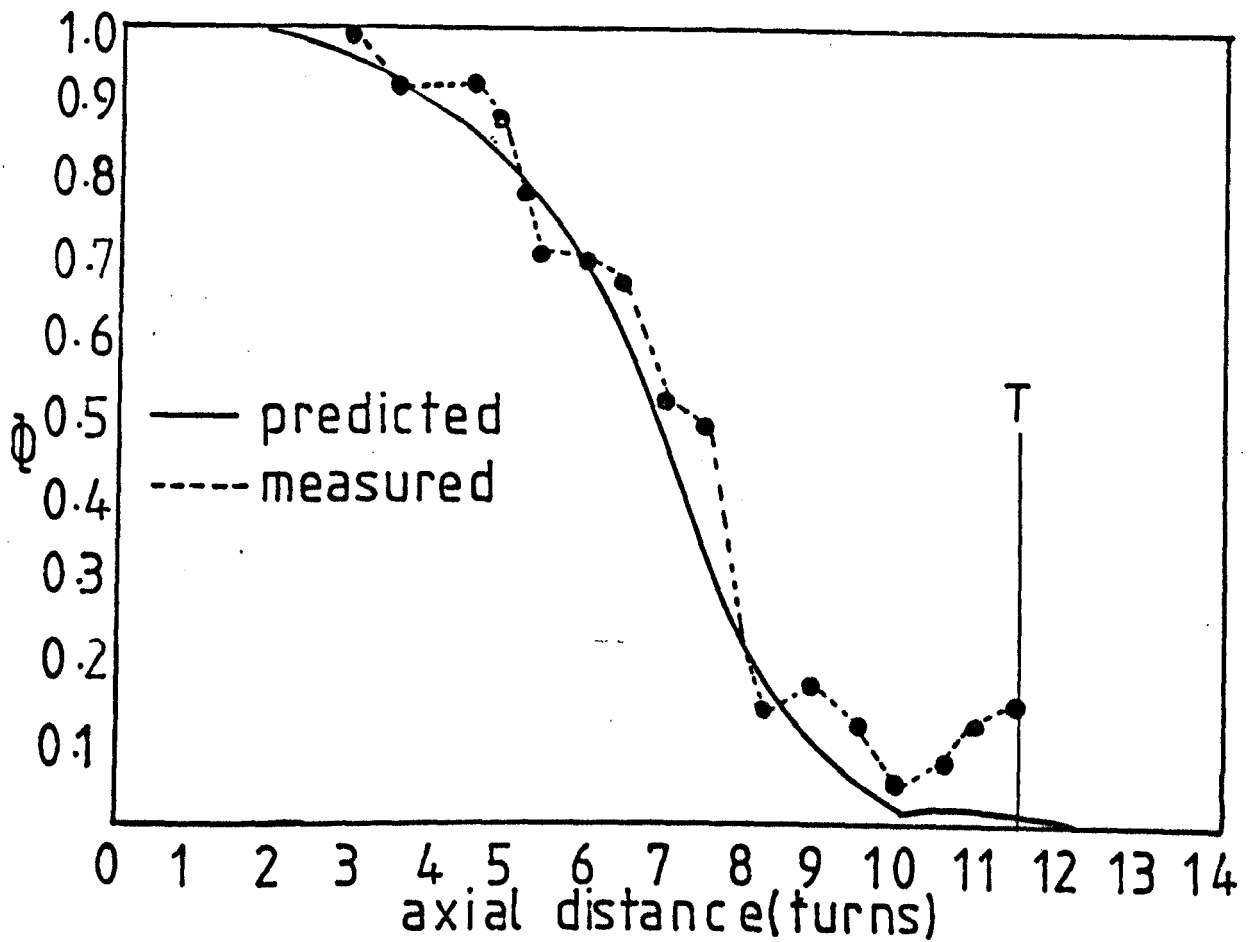
screw number: 1
material: 30% b.w. F.G.C.S. 1640/A100
screw speed: 60 r.p.m.
barrel temp.:   280°C
lower film start: 5·0D ($\Delta H_2 s$)
upper film start: 2·0D ($\Delta H_1 s$)
dimensionless
throughput (π_Q): 0·343

Figure 3.31. predicted v measured solid bed profiles
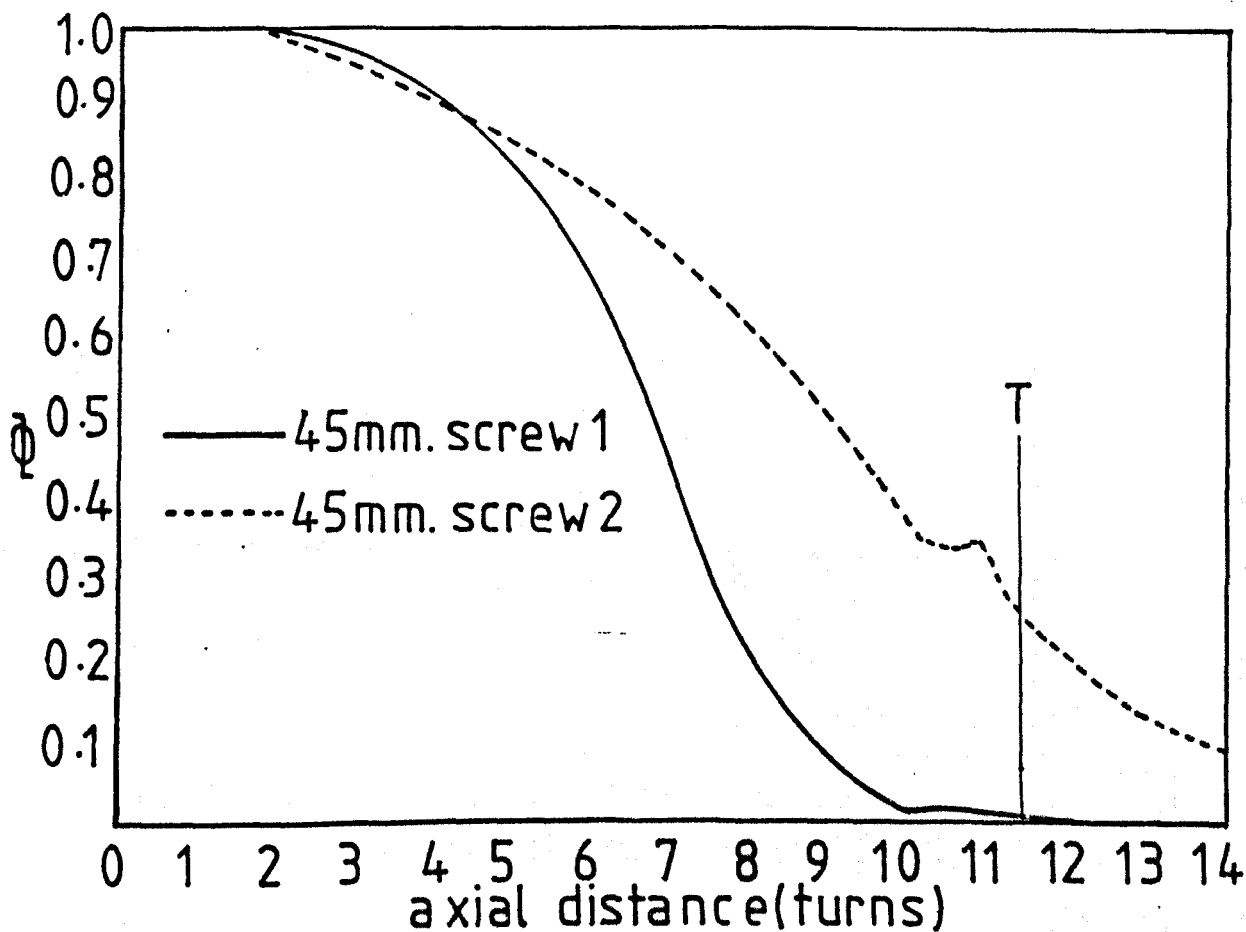
Figure 3.32 influence of screw geometry on melting
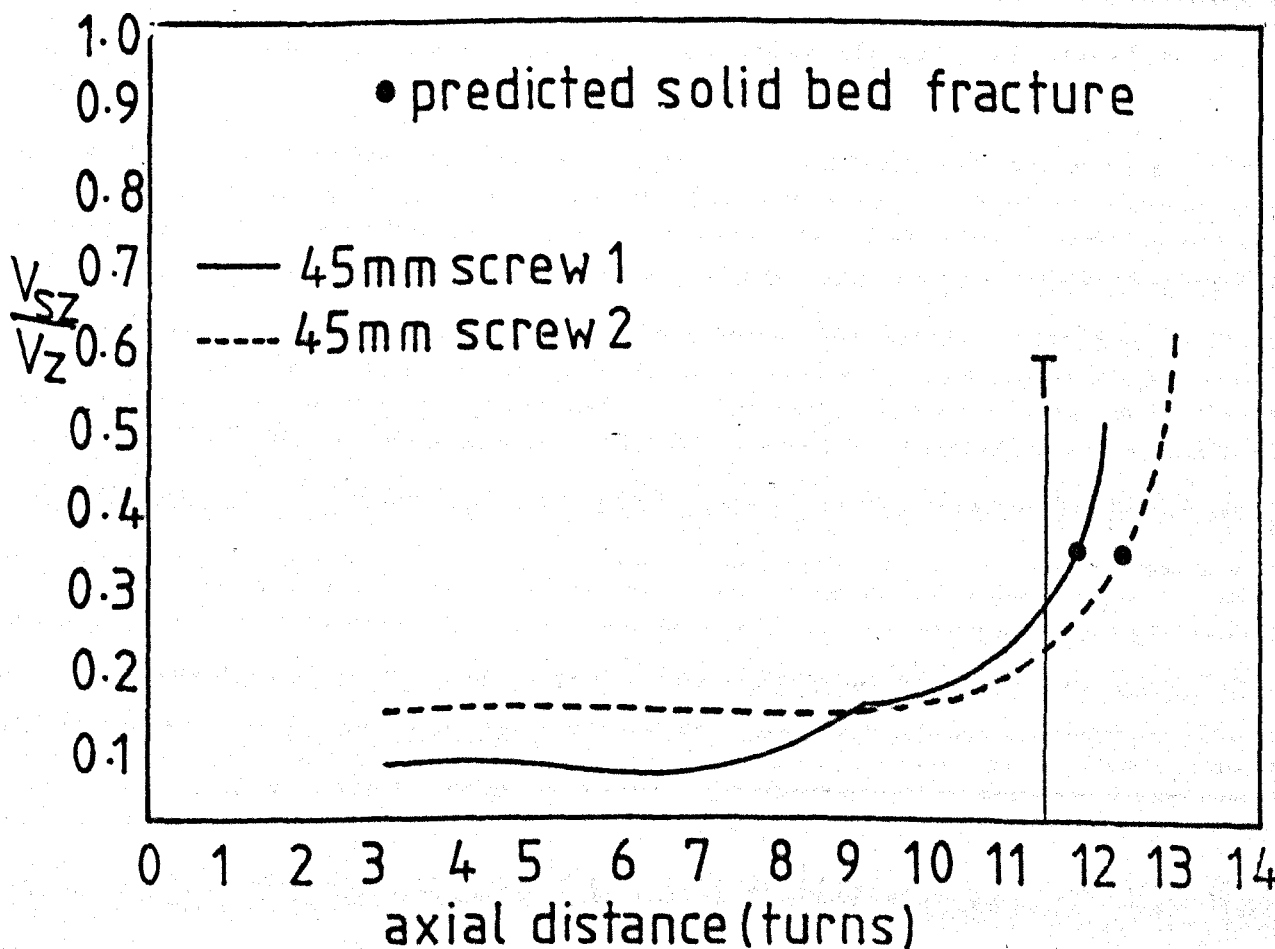
Figure 3.33 influence of screw geometry on solid bed velocity
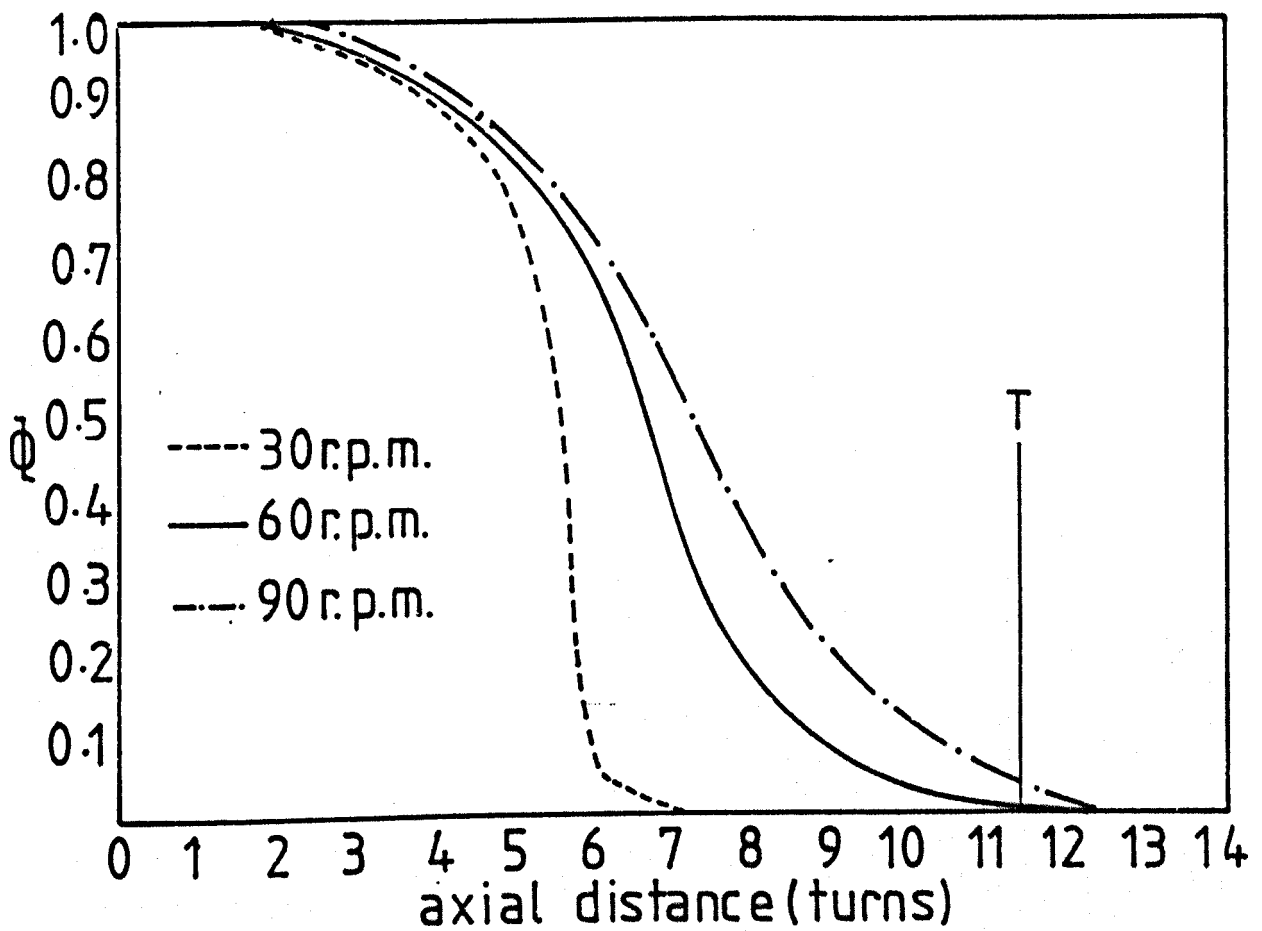
Figure 3.34. predicted influence of screw speed on melting
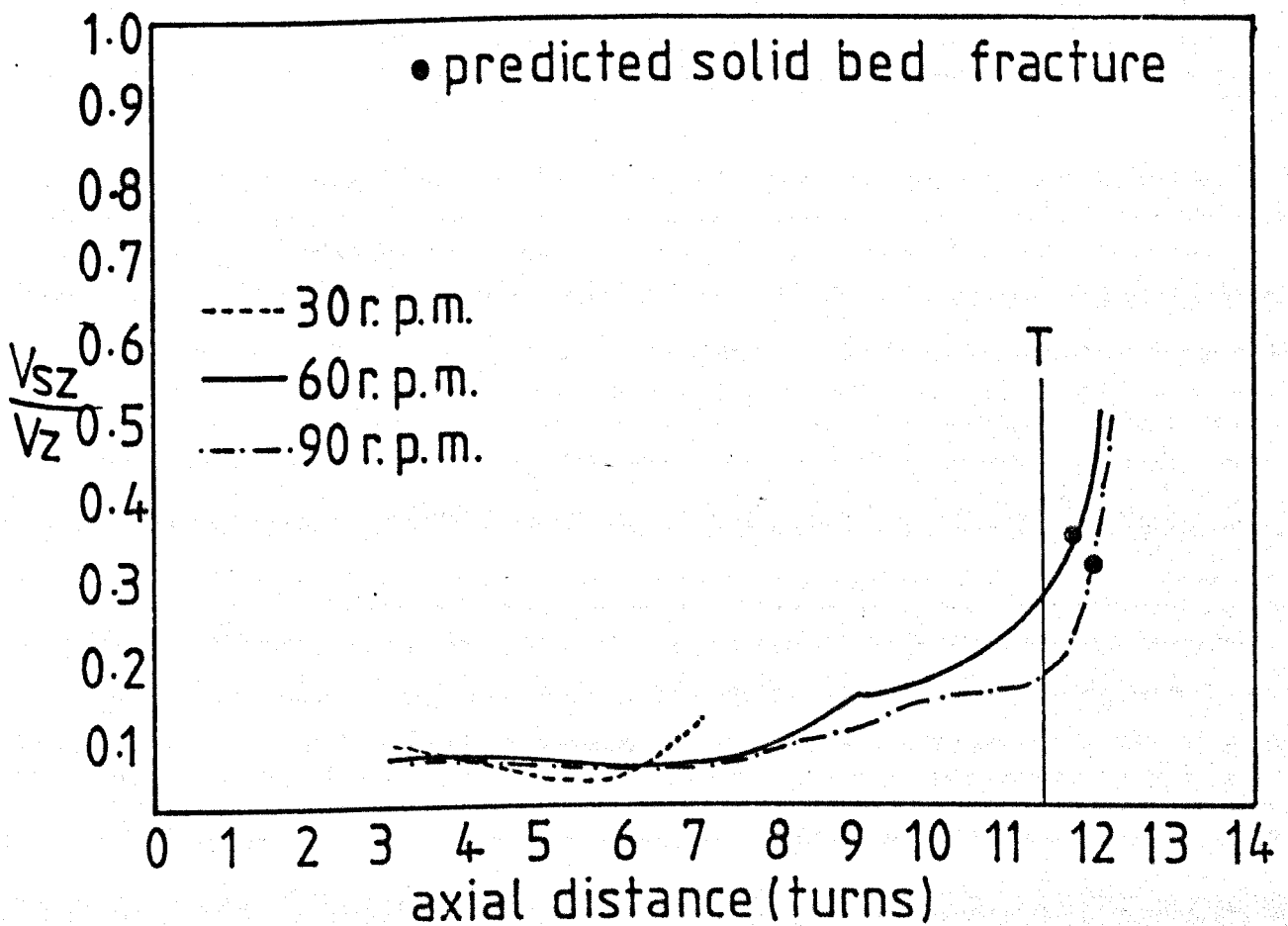
Figure 3.35. predicted influence of screw speed on solid bed velocity
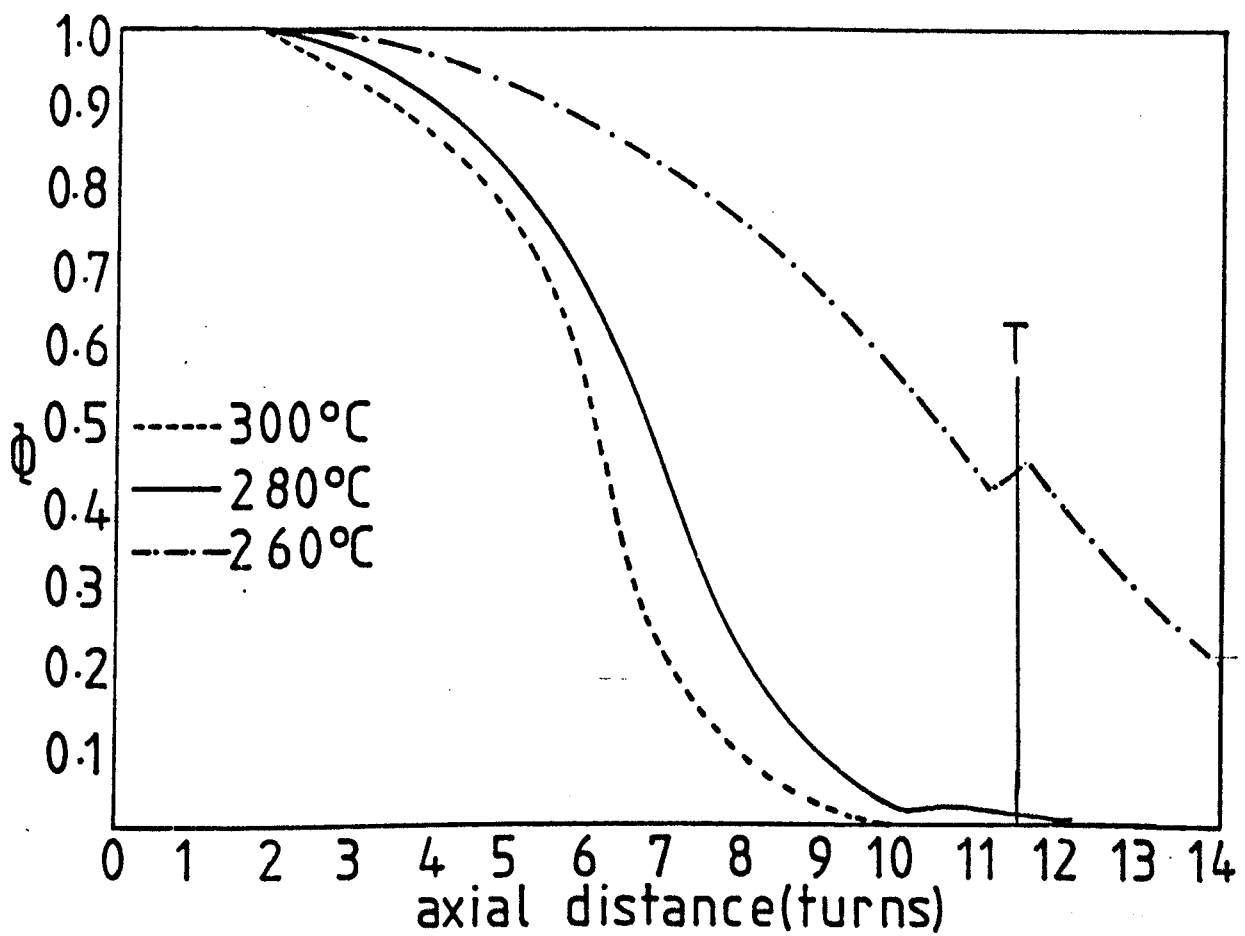
Figure 3.36 influence of temperature on melting - screw 1
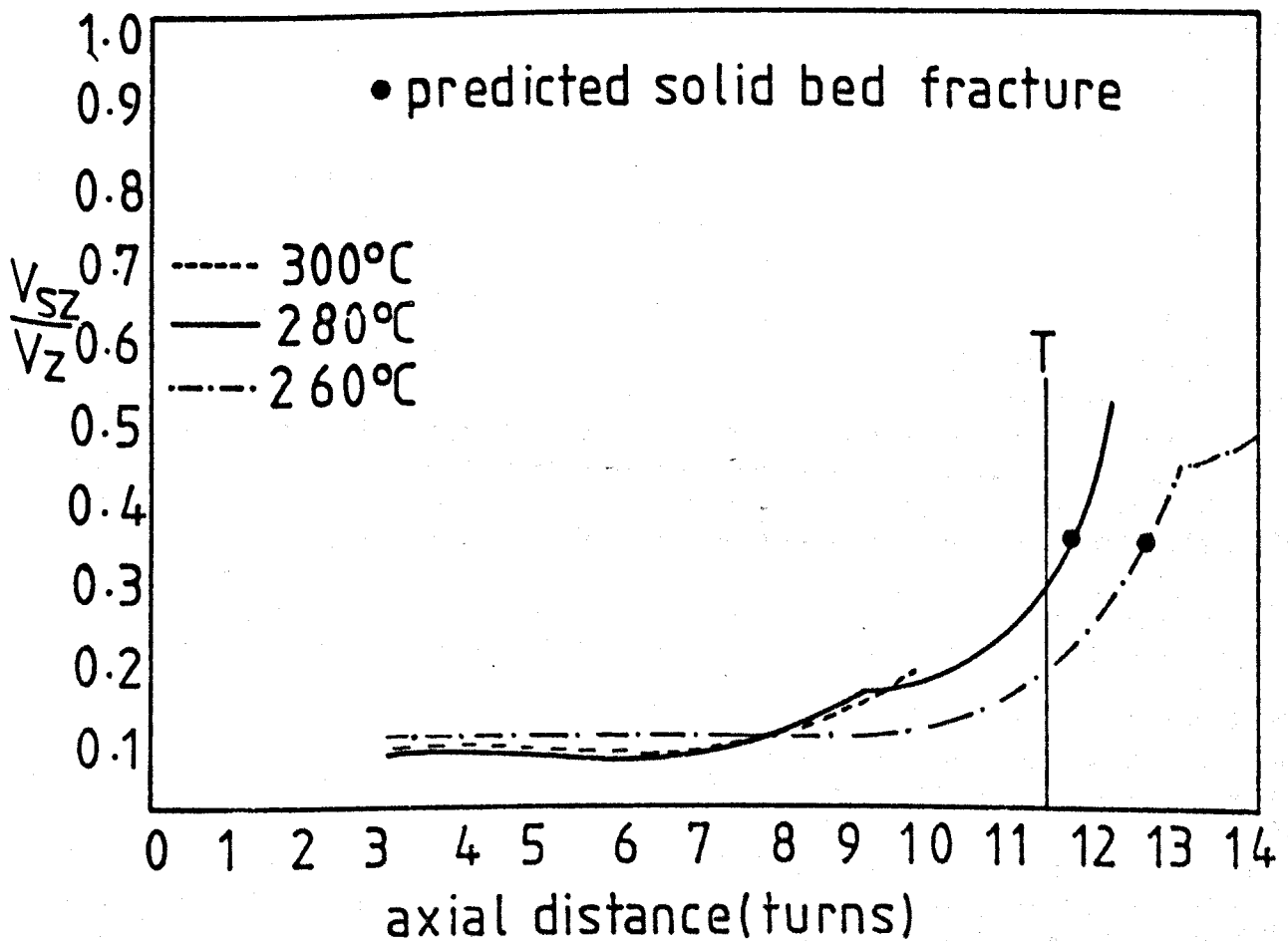
Figure 3.37.influence of temperature on solid bed velocity-screw 1
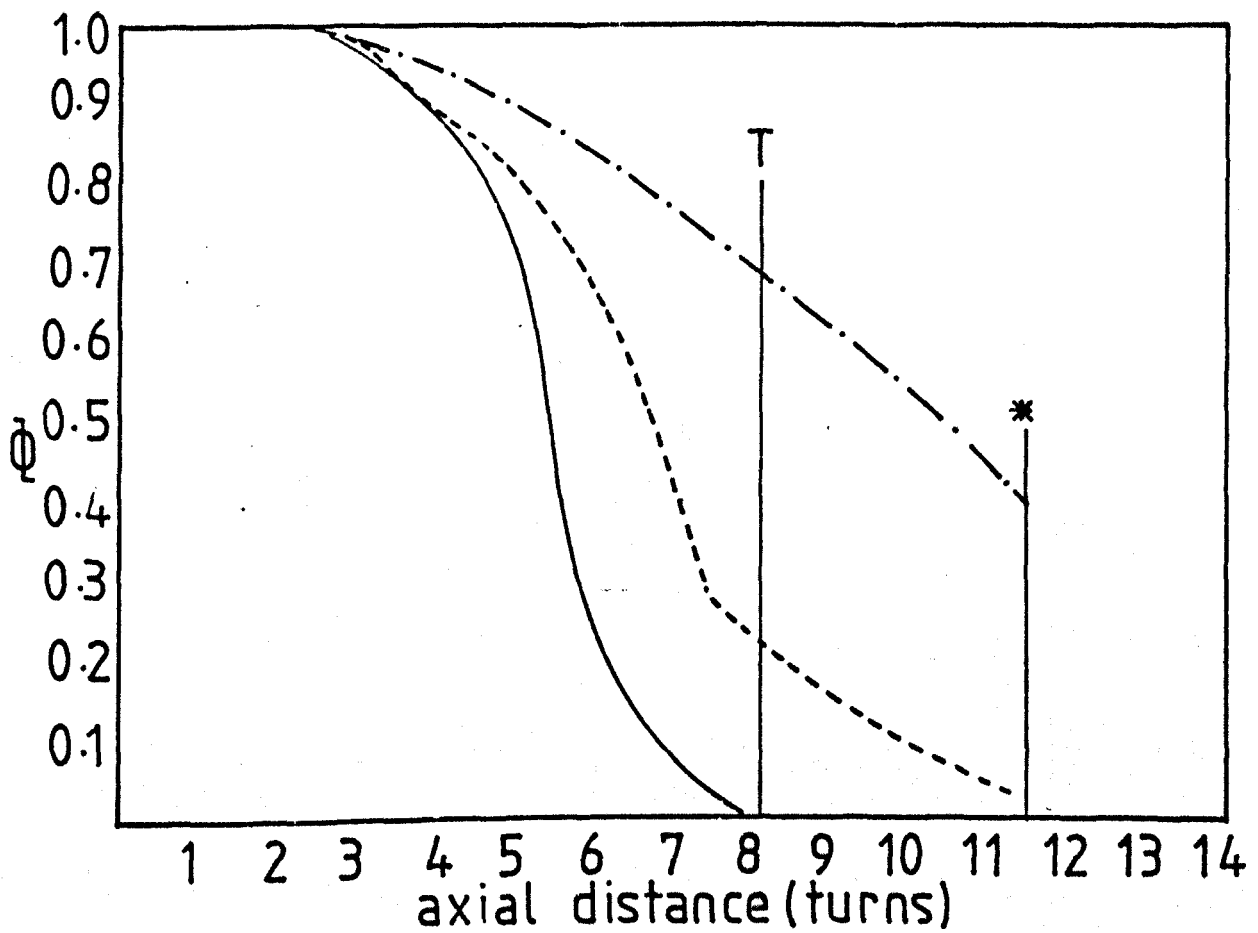
* end of primary screw

—— 1.5 mm die $\pi_Q = 0.053$

----- 2.0 mm die $\pi_Q = 0.090$

—·—· 4.0 mm die $\pi_Q = 0.161$

Figure 3.38. influence of die size on melting performance-25mm extruder
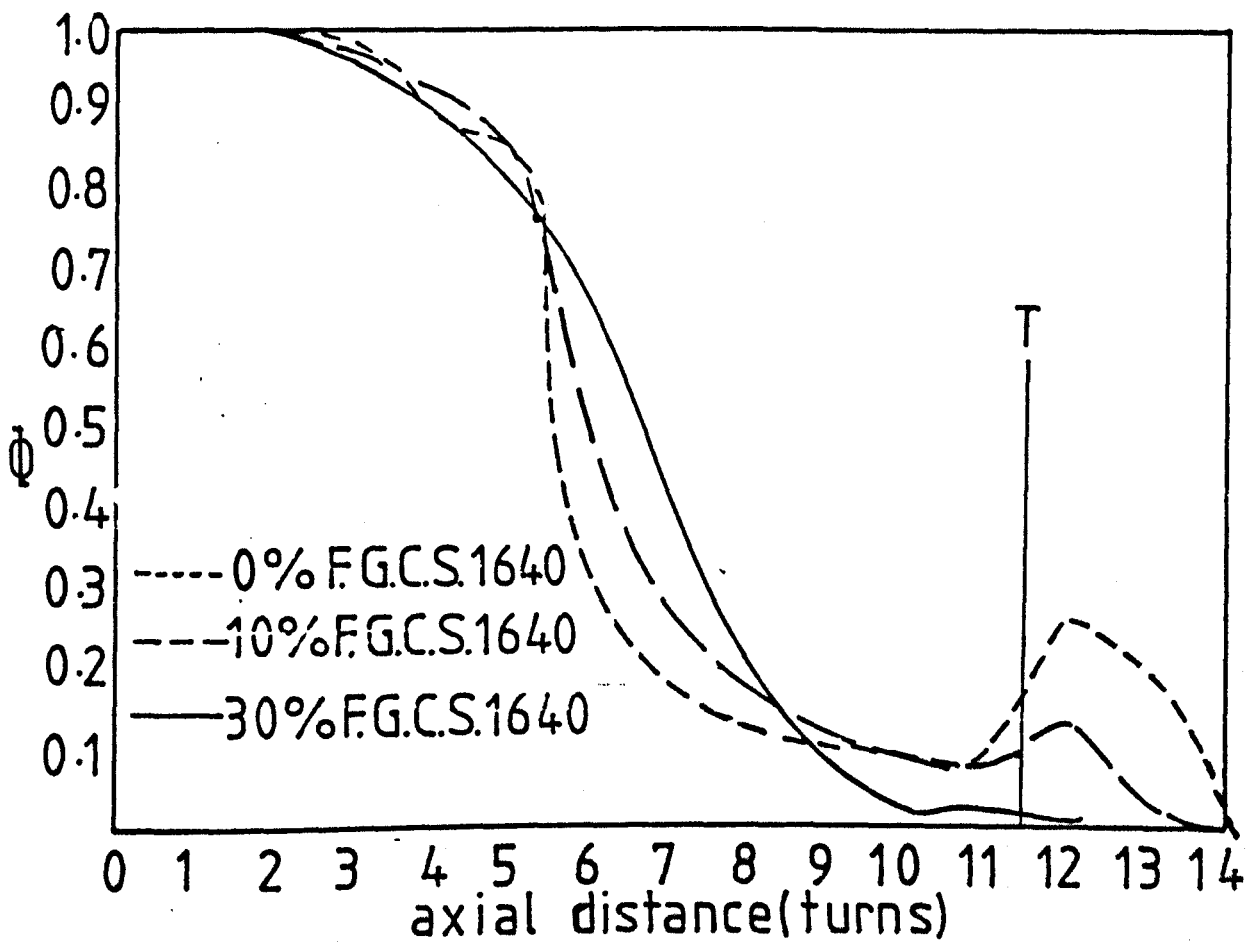
Figure 3.39. influence of glass content on melting
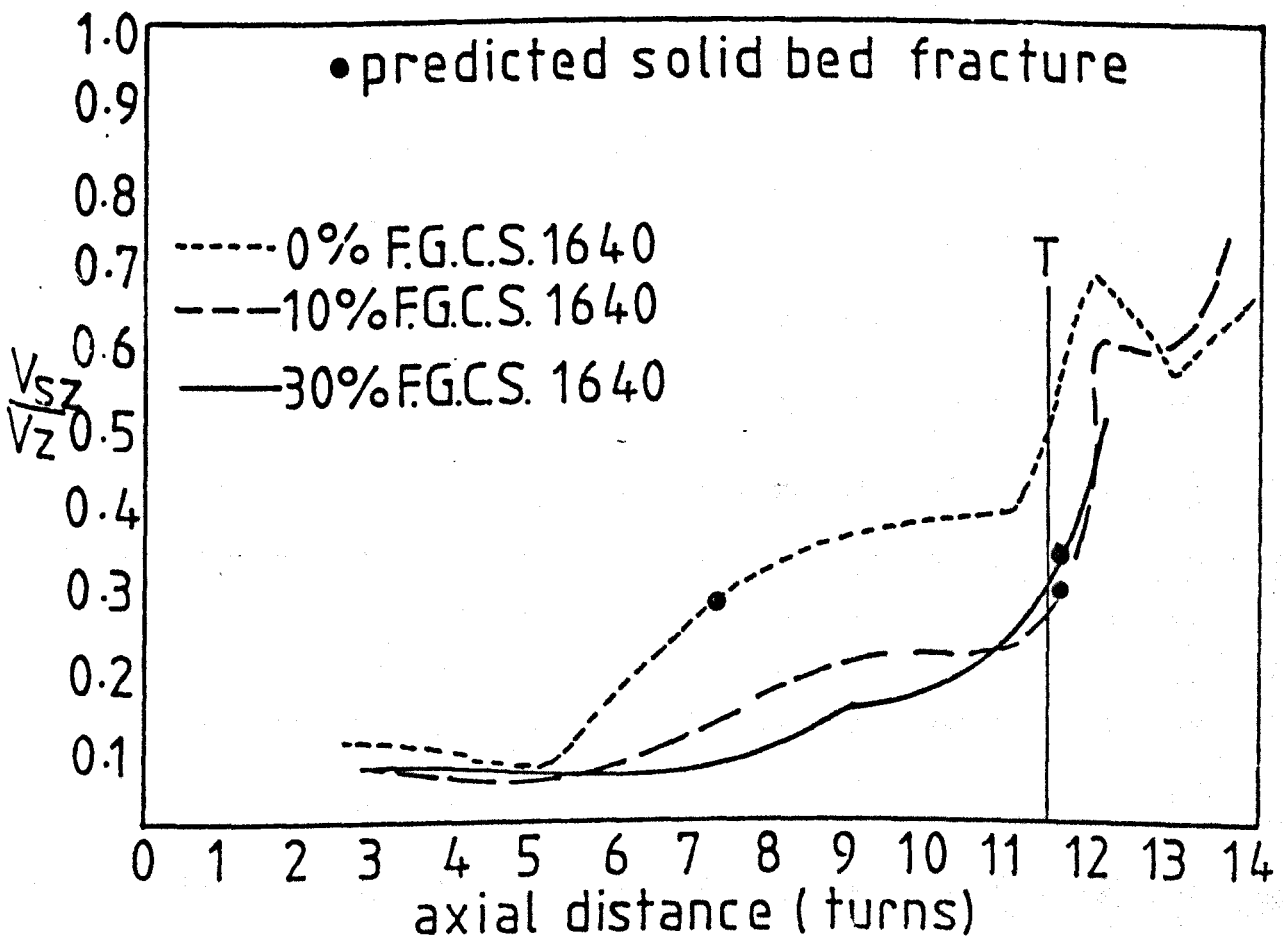
Figure 3.40. influence of glass content on solid bed velocity
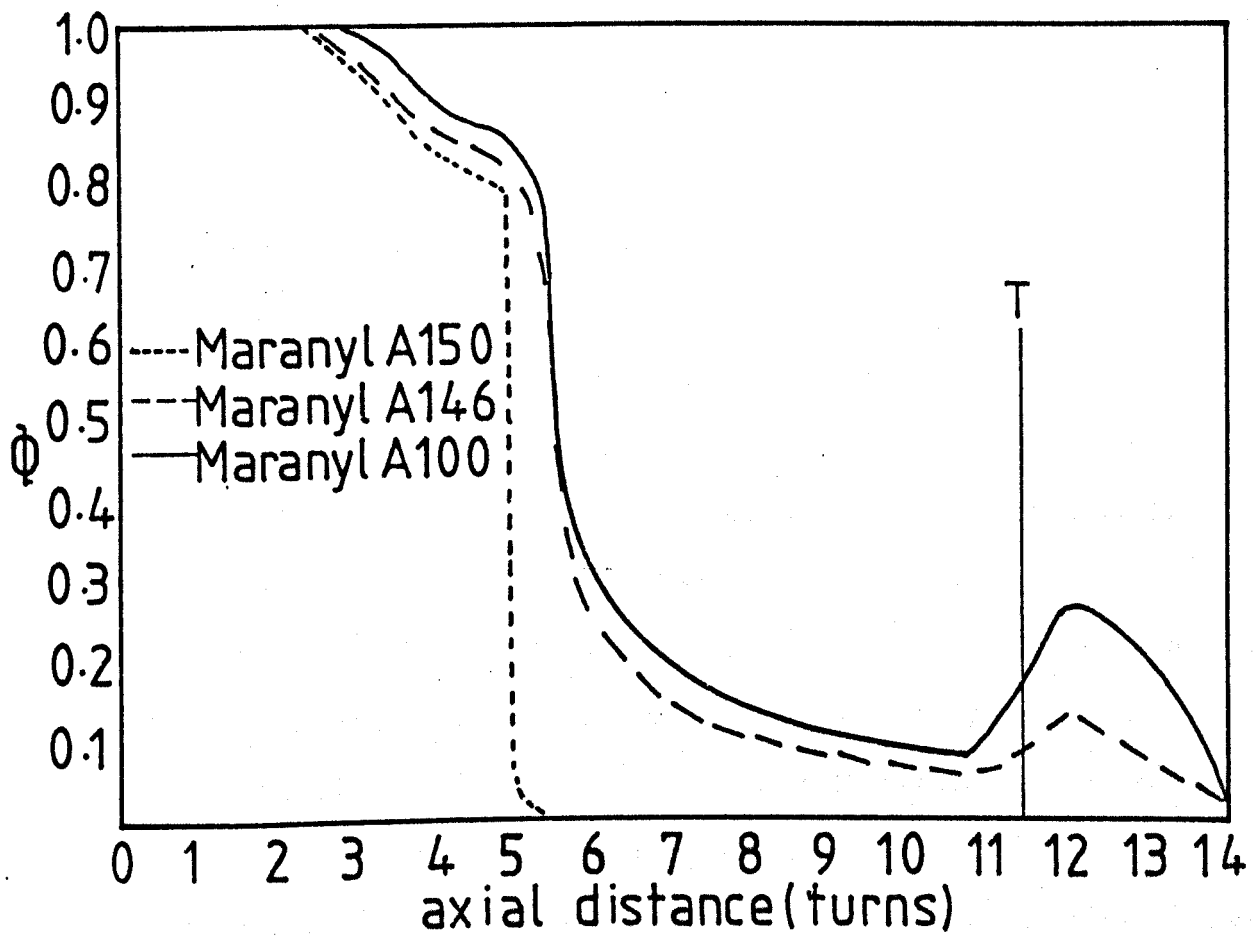
Figure 3.41 influence of molecular weight on melting

viscosities. The expected increase in thermal conductivity of the solid blend will, however, be offset by the reduced bulk density which accompanies such increases in glass levels. The increased viscous energy input is evidenced by the melt temperatures and measured fibre length changes - Table 3.8. Similar trends were observed for screw number 2 although undispersed fibre bundles were detected in the resultant extrudate produced from the lower glass content materials.

The performance of the 25 mm machine was again noted to differ from that above - Figure 3.6. The generated fibre length distributions are a direct consequence of the extremely poor melting performance of this machine especially when using the 4 mm die. Again erratic operation was observed indicating probable melting instabilities.

As expected increases in melt viscosities produced by molecular weight changes for the base polymer are mirrored in the improved melting performance - Figure 3.41 and the resultant fibre length distributions - Table 3.11 for screw number 1.

3.2 The melt feeding process

The evidence presented in the preceeding sections locates the melting region as the major source of fibre degradation. Obviously introduction of the fibres into the melt filled region downstream of this zone should improve the residual fibre lengths although this approach is not without difficulties. Two conflicting requirements emerge:-

(i) To adequately disperse the fibre bundles under the low stress conditions normally existing in this region requires strands which filamentise readily and are easily 'wetted' by the matrix polymer. Both of the above conditions are most easily satisfied by reducing the size level in the fibre manufacturing process and/or employing softer size coatings.

(ii) Introduction of the fibres is generally achieved via a side mounted screw feeder. Such a system is only successful if the fibres are

integral and free flowing. This combination is generally achieved by using hard size coatings and a relatively high size pick-up.

A possible solution is to utilise rovings instead of chopped strands and to feed these through the decompression vent and indeed such a system is commonly used for twin screw compounding processes (6). Control of glass content is achieved by the number of "ends" fed into the machine. Attempts to duplicate such a process using the 50 mm extruder were, however, unsuccessful due to lack of control over the actual cut length of strand which produced blocking of the die. The free flowing nature of the F.G.C.S 1640 chopped strands enabled the use of the side screw feeder as discussed in section 2.6. Dispersion of these integral fibres was provided by an Egan mixing section. Fibre length analyses and specific power consumptions for the various extrudates produced are given in Table 3.18. In addition, comparison of the cumulative fibre length distributions for materials prepared at 60 r.p.m. by both processes are illustrated in Figure 3.42. A significant improvement in the retained fibre lengths is observed which results in improved properties for the final composite - Section 3.3.2.6.

3.3 Injection moulding studies

Tensile and impact specimens, both unreinforced and fibre reinforced, were prepared under the conditions described in Section 2.10. For the reinforced mouldings fibre length analysis revealed further fibre breakage - Figure 3.43 confirming the work of others (108) (10). However, differences in fibre lengths produced at the extrusion stage were maintained in the final moulding albeit at a reduced level.

3.3.1 Matrix properties

Mechanical properties for the various grades of nylon 6.6 are

given in Table 3.19. The observed differences in un-notched Izod impact strength (U.N.I.S.) arise from the interdependence of moisture content, molecular weight and crystallinity (84). The polycondensation of adipic acid and hexamethylene diamine to form nylon 6.6 is an equilibrium reaction in which increases in molecular weight result from the continuous removal of by-product water. The linear homopolyamides such as nylon 6 and 6.6 have been shown by X-ray analysis to be partially crystalline, typical degrees of crystallinity generally being less than 50% (77). Increases in the degree of crystallinity which accompany reductions in molecular weight or changes in the polymerisation conditions have been shown to produce brittle behaviour for these materials (109).

It is evident from the foregoing discussion that factors, either chemical or thermal, which produce reductions in molecular weight will additionally lead to embrittlement of the polyamide. The observations of matrix cracking observed in the region of the fracture zone of tensile specimens by Bader et. al (96) are consistent with a brittle behaviour of the matrix. Such embrittlement observed by the above workers is considered to be induced by the elevated temperatures required to mould the highly filled materials. Additionally, Curtis (110) confirms these observations and also postulates that moisture present on the fibre surface can interact with polymer adjacent to the fibre to produce hydrolysis and subsequent increased crystallisation in the interfacial region.

Moulding conditions for unreinforced and reinforced materials were accurately controlled in this study with the base polymer, moulded under identical conditions, exhibiting ductile behaviour. However, extended cycle times and the recycling of moulded specimens did produce embrittlement (111). In addition, for the high volume fraction filled materials, the increased melt viscosities could result in higher melt temperatures arising from viscous heat generation -

material	screw speed r.p.m.	glass content % b.w.		specific power KWhr./Kg.	extrudate fibre lengths. microns	
		nominal	actual		no.av.	wt. av.
	30	30.0	33.0	0.16	577	917
	60	30.0	29.4	0.24	414	673
	90	30.0	27.2	0.28	420	654
F.G.C.S. 1640/	150	30.0	27.6	0.31	426	626
Maranyl A 100	90	40.0	34.0	0.30	415	630
	90	10.0	11.3	0.12	718	920

Table 3.18. processing and fibre fracture:melt fed materials
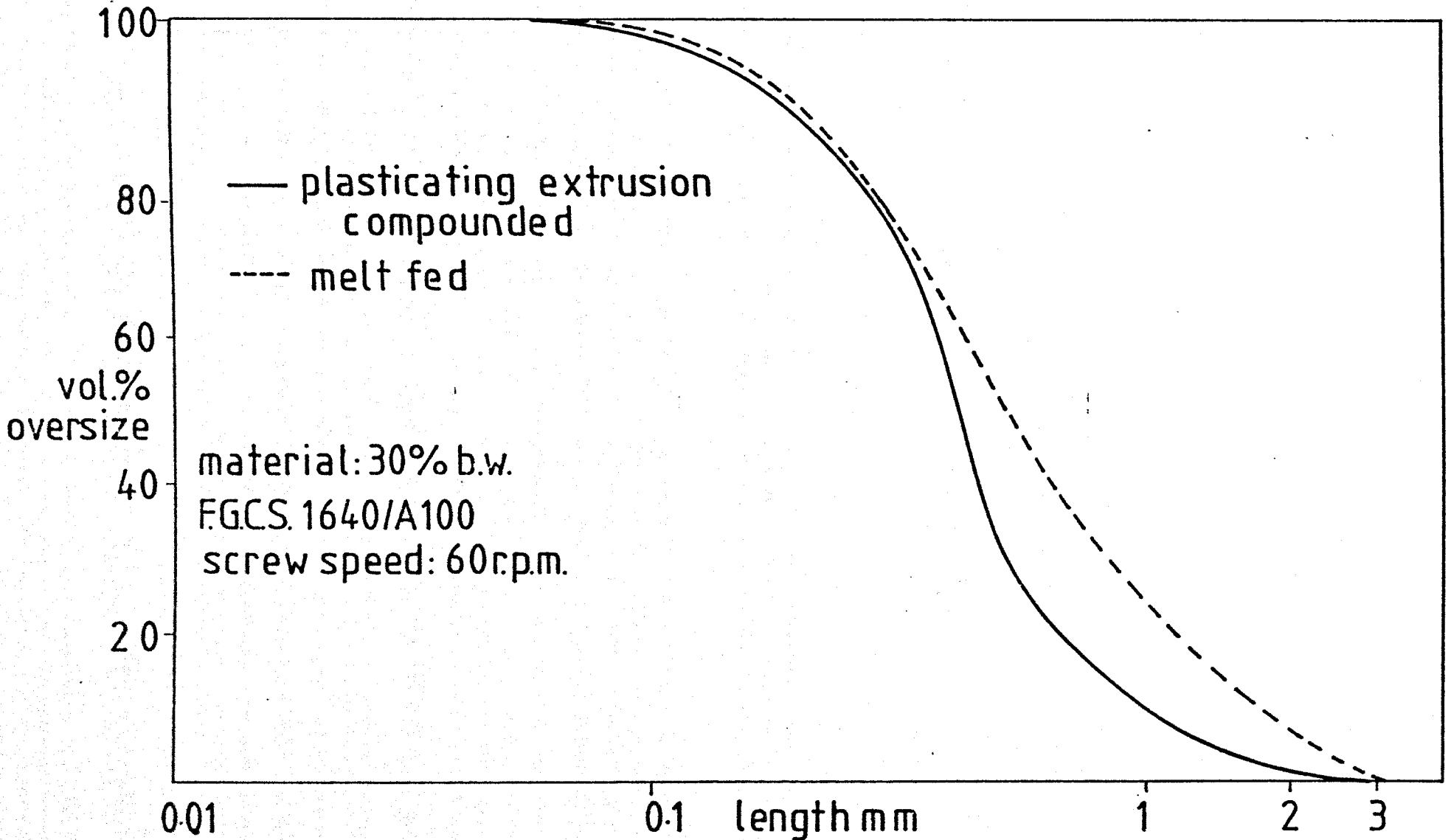
Figure 3.42. cumulative fibre lengths. tumble blended material v melt fed.
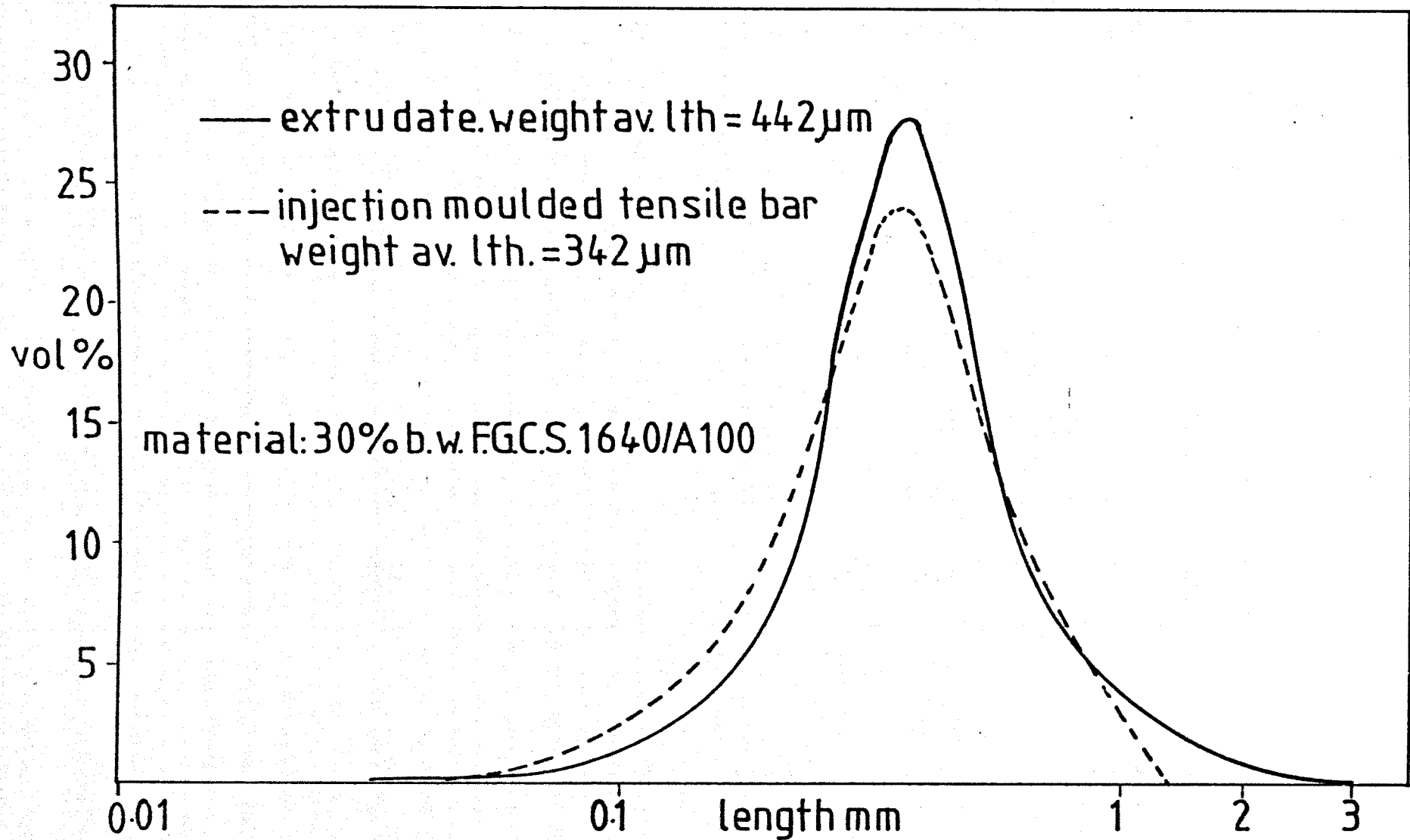
Figure 3.43. fibre length distributions. extrudate.v.injection moulded material

polymer grade	tensile st. MPa+		impact st. U.N.I.S. KJ/m.		tensile modulus G.Pa.		failure strain %		interlaminar shear stress MPa.	
	v. dried m. s.d.	boil. m. s.d	v. dried m.s. d.	boil* m.s.d	v. dried. m.s.d.	boil. m. s.d.	v. dried	.boil.	v. dried. m.s.d.	boil. m. s.d
A 100	81 0.7	30 0.4	1.06 0.3		3.01 0.02	0.54 0.03	c.60	>200	67 0.2	35 0.2
A 144	82 0.7	30 0.4	1.23 0.1		3.02 0.02	0.53 0.02	c.80	>200	67 0.1	35 0.2
A 146	81 0.5	30 0.2	2.54 0.07		3.0 0.02	0.61 0.06	c.90	>200	66 0.1	35 0.1
A 148	81 0.7	30 0.3	2.58 0.08		3.01 0.01	0.55 0.05	c.120	>200	66 0.2	35 0.2
A 150	82 0.6	31 0.4	2.59 0.05		3.0 0.02	0.50 0.05	c.180	>200	66 0.1	35 0.2

* samples unbroken

+ yield strengths

Table 3.19. mechanical properties of maranyl polymers

SIZING MATERIAL	SIZE CONC^n BY WEIGHT %	ULTIMATE TENSILE STRENGTH MPa.		UN-NOTCH. IZOD IMPACT STRENGTH KJ/m		0.5% TANGENT MODULUS GPa		FAIL. STRAIN %
		mean	s.d.	mean	s.d.	mean	s.d.	
XS 929	0.5	81	0.6	0.74	0.3	3.01	0.04	6.1
	1.0	81	0.7	0.58	0.25	3.03	0.04	5.8
	3.0	81	0.7	0.29	0.08	3.06	0.06	4.8
M.S.S.1640	0.5	82	0.6	1.03	0.30	3.01	0.04	c 40
	1.0	81	0.7	1.08	0.20	3.01	0.05	c 40
	3.0	81	0.7	0.82	0.20	3.02	0.05	6.8

Table 3. 20 influence of size chemicals on the mechanical properties of vac. dried nylon 66

SIZING MATERIAL	SIZE CONC^n BY WEIGHT %	MELT FLOW INDEX (gms/10 min)					
		initial residence time (mins)					
		5		15		30	
		mean.	s.d.	mean.	s.d.	mean.	s.d.
XS 929	0.5	4.90	0.1	5.20	0.1	5.90	0.3
	1.0	6.86	0.1	8.47	0.11	8.73	0.08
	3.0	8.73	0.5	12.20	0.40	20.13	0.60
M.S.S.1640	0.5	4.50	0.3	3.37	0.24	3.20	0.20
	1.0	3.89	0.6	3.91	0.50	3.25	0.20
	3.0	1.61	0.03	1.48	0.04	1.05	0.04
———	0	4.54	0.2	3.86	0.07	3.48	0.12

Table 3.21 influence of size chemicals on the melt flow index of vac. dried nylon 66
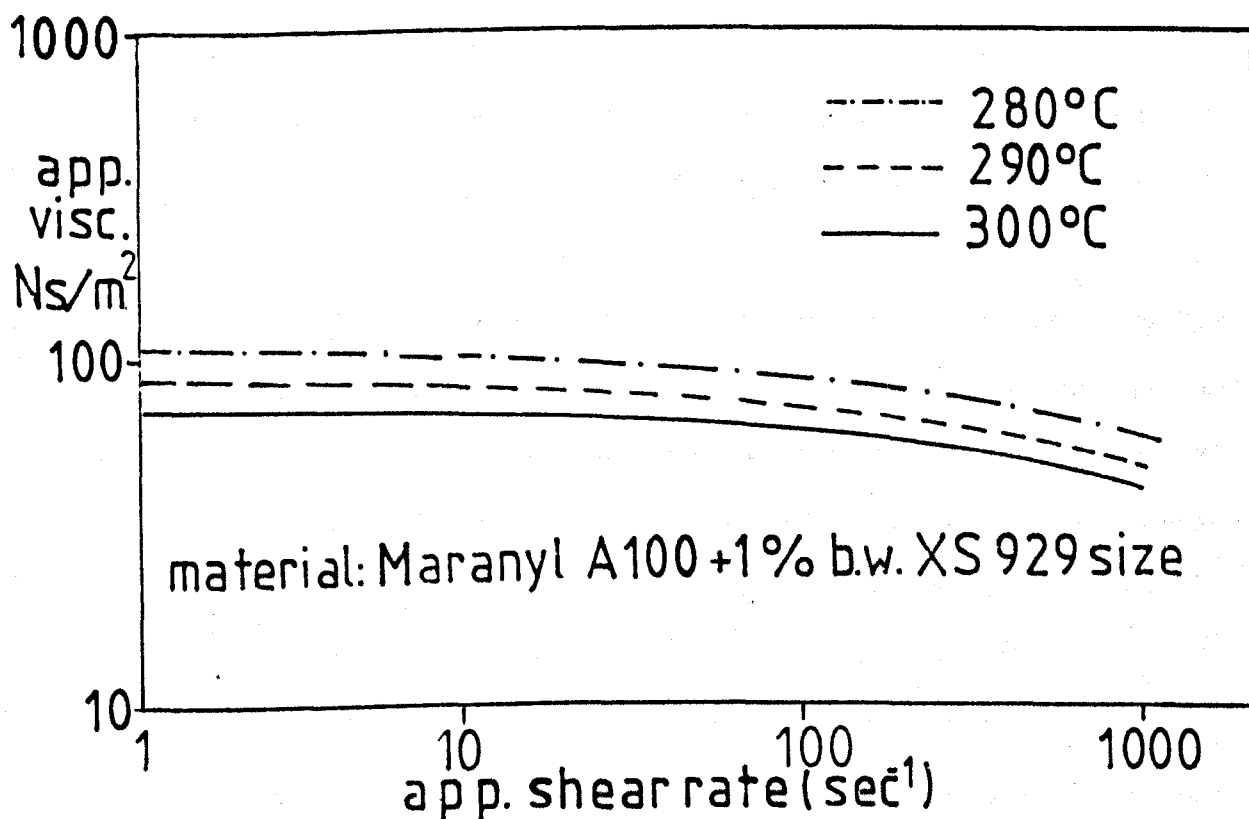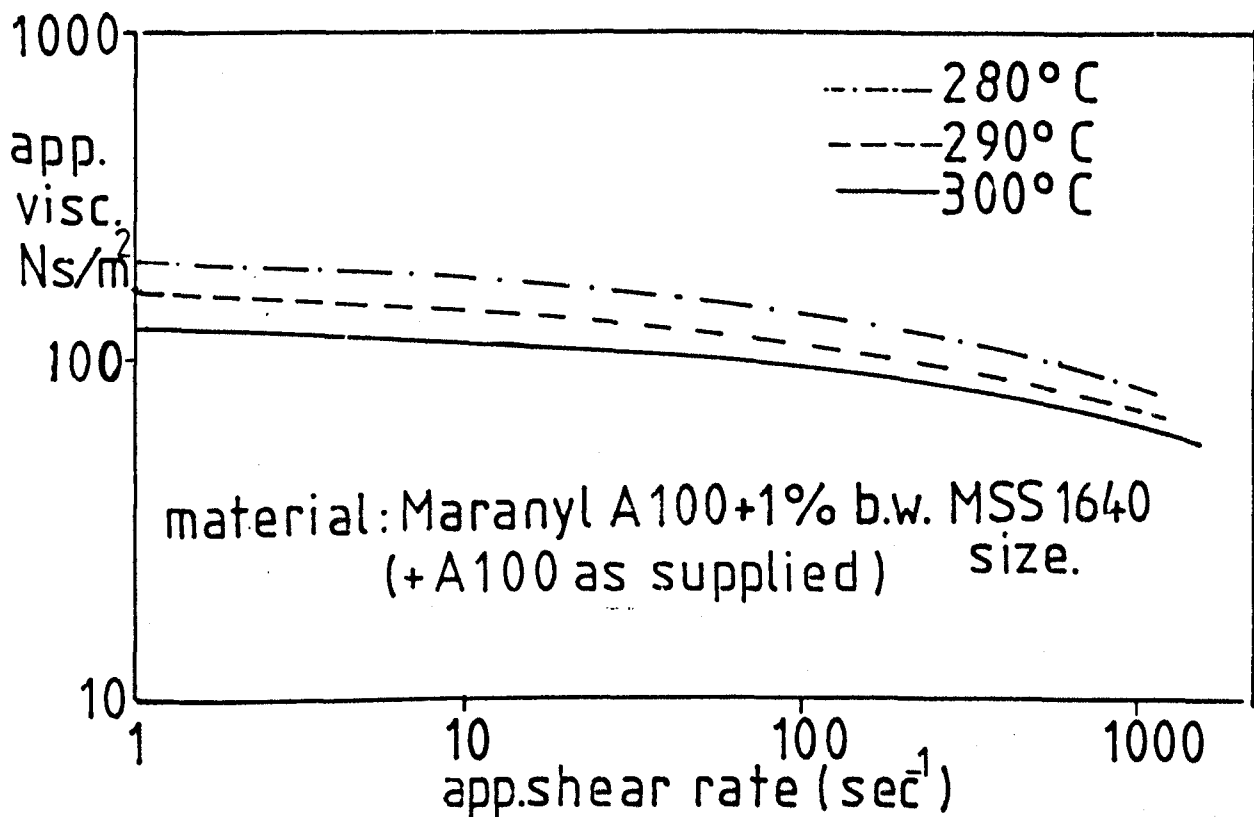
Figure 3.44 influence of size chemicals on the rheology of A100

see Section 3.1.3. One other alternative which was discussed by Bessel and Shortall (112) is that of interaction of the sizing material and the matrix polymer in the interfacial region. Such interactions are possible under the severe conditions existing in the extrusion compounding and injection moulding processes and indeed chemical reaction of the two materials is considered a pre-requisite for good adhesion.

The polymeric materials used in this study were coated onto Maranyl A100 pellets prior to extrusion and injection moulding to produce tensile and impact specimens. In addition, the extruded materials were granulated and Melt Flow Indices and shear rate - viscosity relation-ships determined as described in Section 2.9.1. The relevant results are presented in Tables 3.20 and 3.21 and Figure 3.44. The presence of the polyvinyl acetate is observed to have a pronounced effect on viscosity and mechanical properties at all levels of addition, the severity of the viscosity changes increasing with extended residence times and size levels. For the cationic size significant increases in melt viscosity are observed at the 3.0% level, the mechanical property changes being less pronounced. The reasons for the reduced melt flow index for the latter material are not obvious and embrittlement would not be expected from an increase in molecular weight. It is possible, however, that the reaction occurring is one of crosslinking as observed by Kamerbeck et. al (113). The presence of free amine in both the size polymer and matrix material being known to produce such an effect. At the 1.0% and 0.5% levels no definite effects could be attributed to the presence of this material in the matrix.

3.3.2 Reinforced composite properties

3.3.2.1. Reinforcement efficiency factor

Composite properties for these short fibre reinforced materials are largely determined by the interelation between orientation, fibre

bonding and fibre length (114). Whilst orientation can reasonably be assumed to be effectively constant for similar materials produced under identical moulding conditions, interfacial bonding and fibre length are often related (115). During this study extruded materials often contained undispersed fibre bundles, many of which survived the subsequent injection moulding process. It is to be expected that those bundles which are dispersed in this secondary moulding stage will possess reduced adhesion to the matrix polymer and hence behave as inefficient reinforcing elements. Changes in fibre length therefore, are unlikely to completely dominate composite performance unless sufficient work has been performed to ensure equivalent adhesion of all the fibres for the matrix polymer. The use of a 'reinforcement efficiency factor' provides a means of observing the influence of both fibre length and interfacial bond strength on ultimate composite performance.

Equation 1.10, derived by Bader and Bowyer, has been shown to provide a reasonable estimate of composite tensile strength for these materials. The value of τ in this study was initially assumed to be 60 MN/m^2 based on the work of Burns et.al. (71) although this has subsequently been shown to be optimistic - Section 3.5. The orientation constant C was assumed to be 0.825 although again results presented in Table 3.32 show this to be unrealistic. Calculation of composite strength is performed using the measured fibre length distribution and the stress in the fibre at the composite breaking strain. Changes in the ratio of the measured composite strength to the calculated values indicate variations in interfacial bonding, assuming C is unaltered.

3.3.2.2 Machine and operating variables

Extrudates prepared in section 3.1.1 and 3.1.2 differ in their mechanical properties - Tables 3.22 and 3.23. The low reinforcement

efficiencies for the 25 mm compounded materials, using the narrower dies, reflect the overall poor dispersion and 'wetting' of the fibres by the matrix polymer. Many of the undispersed fibres present in the 1.5 mm and 2.0 mm die extrudates are observed in the subsequent mouldings - Figure 2.17, and result in further reduced performance over their counterparts in which the fibres are completely dispersed. Fibre bundles are invariably found to be present in the fracture surface of such composites - Figure 3.45. Increasing screw speeds improve the wetting of the fibres although the reinforcing effect is somewhat lessened by the increased fibre fracture which occurs. For the larger machine, the reduced fibre fracture which accompanies lower screw speeds and compression ratio is mirrored by the composite properties. However, since as discussed in Section 3.1.1, these original fibre length differences occur by changes in the fraction of undispersed material, then subsequent improvements are again lessened by the reduced adhesion of the longer filaments.

3.3.2.3 Glass fibre variables

Changes in bundle tex produced by varying the degree of split of the strands and variations in initial strand length do not produce any significant changes in the resultant composite performance. Reduction in fibre diameters produces definite improvements in mechanical properties arising from the more favourable aspect ratio distribution for the smaller diameter fibres. These changes are expressed in Table 3.24 and Figure 3.46.

The established differences in fibre length which accompany size chemistry and fibre concentration changes are maintained in the final injection moulded articles - Tables 3.25 and 3.26. The reduced average fibre lengths of the polyvinyl acetate sized material are reflected in the lower composite performance for both vacuum dried and boiled samples. The reduced interfacial bonding expected from the poor

surface protection - Figure 1.2 and lack of chemical functionality
are confirmed by the diminished reinforcement efficiencies and the low
calculated $\top$ value (Section 3.5). In addition, the poor impact
performance and low tensile failure strain is the probable result
of matrix embrittlement, achieved by thermal degradation of the
polyvinyl acetate size under the high temperature regimes existing in
the extrusion and moulding processes.

Increases in the level of glass fibres produce corresponding
improvements in tensile performance and low strain stiffness. The
actual level of property enhancement is, however, dictated partly
by the previous extrusion process, which largely controls the fibre
length distribution, and by the significant reduction in failure
strain which accompanies such increased fibre loadings. Similar
trends have been observed by previous workers (69) (96). Both tensile
strength and 0.5% tangent moduli show a non linear dependence on
volume fraction of fibres as seen in Figure 3.47. Such trends arise
from the changes in fibre length and failure strain described
in Table 3.26, and the apparent increase in fibre alignment predicted
with increasing fibre concentrations - Figure 3.48. The values of the
orientation factor C, are obtained from the modified law of
mixtures approach described by Bader et. al. (116) in which equation
1.2.3.is modified to allow for fibre misalignment i.e.

$$E_c = C E_f V_f + (1-V_f) E_m.$$

The changes in un-notched Izod impact which accompany variations
in fibre volume fraction are illustrated in Figure 3.49. Dry impact
performance shows an initial dramatic decrease with the addition of low
low levels of glass fibre followed by a gradual non-linear increase,
ultimately reaching a maximum at approximately 40% b.w. (0.23 Vf) of
fibres. The original 'tough' behaviour of the unreinforced matrix is,
however, not regained, all the fibre reinforced materials failing in a
brittle manner. In contrast, the 72 hour boil samples indicate a
continuous reduction in impact performance with increasing volume

fraction of fibres. These results illustrate the marked dependence of composite performance on moisture content and to some extent explain the conflicting observations of other workers (110) (117).

Processing of these high glass content materials presented no practical problems under the extrusion and moulding conditions selected. However, for both extrudate and mouldings pronounced discolouration was observed, presumably reflecting increased matrix degradation arising both from the increased heat generation and high size levels present. Further evidence of the increased fibre fracture which accompanies higher glass levels is provided by the results presented in Table 3.27. The original extrudates were diluted with Maranyl A100 and injection moulded to produce specimens containing 30% by weight of reinforcement. The reduced mechanical performance of these materials over the standard specimens is evident. Additionally, comparison of the average lengths of these diluted materials with those found in the moulded parent compounds indicates the reduced levels of fibre fracture found in these mouldings. Such trends are consistent with the interdependence of fibre concentration, melt viscosity and fibre fracture observed in the previously described extrusion compounding studies. Again the final composite performance reflects the previous compounding history of the undiluted materials.

3.3.2.4 Matrix polymer variations

Results for the range of Maranyl polymers listed in Table 2.3 reinforced with 30% by weight of F.G.C.S. 1640 strands are presented in Table 3.28. The increased fibre degradation observed in the extrusion process to attend increased melt viscosities is also found in the injection moulded materials. Wet and dry impact strengths increase with increasing molecular weight although again a net reduction is observed after conditioning by boiling in water

for 72 hours. Tensile property differences are marginal despite the significant changes in retained fibre lengths. Although increased fibre alignment could be postulated to explain the high tensile strengths, the measured moduli do not support such a supposition. However, the enhanced strain to failure which accompanies improvements in the molecular weight of the base polymer would suggest increased ductility in the interfacial region. This improved ductility would preclude the premature failure observed by other workers (96) and discussed further in Section 3.4. Such enhanced failure strains would therefore extend the permissible stress levels prior to composite failure.

3.3.2.5 Recycling studies

Extrudates produced in Section 3.1.4 were subsequently injection moulded. The decreased rate of fibre fracture for the polyvinyl acetate sized material observed in these reprocessing studies is confirmed in the final composites - Table 3.29. However, the embrittled nature of the matrix polymer which results from the interaction of these two materials is manifested in the reduced impact performance and low failure strains. The trends in failure strains are consistent for both wet and dry samples being seen to increase with reductions in fibre length. The divergence in impact performance with absorbed moisture observed in Section 3.3.2.3 is again noted for these materials.

3.3.2.6 Melt fed materials

The significant improvements achieved in retained fibre lengths and composite properties over test coupons obtained from conventional extruded materials are illustrated in Figures 3.50 to 3.53. The overall property enhancement is, however, limited by the reduced failure strains confirming the results of Bader et. al (96). The reduced wet impact performance is to be expected from the previous

SCREW	EXTRUSION CONDITIONS TEMP °C	DIE.S mm	SPEED r.p.m	TENSILE ST. MPa. DRY mean s.d.		WET mean s.d.		IZOD IMPACT ST. U.N.I.S. J/m DRY mean s.d.	WET mean s.d.	0.5% TAN. MODULUS GPa. DRY mean s.d.		WET mean s.d.		FAILURE % DRY	WET	REINFORCE. EFFICIENCY DRY
1	280	2	30	190	2.0	79	1.0	940.120	880.160	9.01	0.4	4.3	0.2	3.0	3.3	0.86
	280	2,4,6	60	187	1.8	77	0.8	888.100	860.170	9.00	0.4	4.2	0.2	2.9	3.4	0.87
	280	2	90	184	2.0	76	1.0	839.90	830.170	8.80	0.3	4.0	0.3	3.0	3.8	0.90
	260	2	60	186	1.5	77	1.0	894.100	864.90	9.0	0.7	4.1	0.1	3.1	3.8	0.89
	300	2	60	187	1.0	77	0.6	910.95	875.100	9.03	0.4	4.3	0.1	2.8	3.3	0.88
2	280	2	30	198	2.5	82	1.1	960.120	920.150	9.3	0.2	4.4	0.3	2.7	3.2	0.78
	280	2,4,6	60	194	1.3	80	1.0	920.95	870.80	9.0	0.3	4.4	0.2	2.8	3.3	0.79
	280	2	90	190	1.0	78	1.0	870.80	860.100	9.0	0.5	4.2	0.3	2.9	3.3	0.79
	260	2	60	188	1.0	77	0.8	900.110	870.100	9.0	0.2	4.1	0.2	2.8	3.5	0.77
	300	2	60	194	2.0	78	0.6	930.70	878.90	9.2	0.4	4.2	0.2	2.7	3.1	0.77

Table 3. 22. influence of extrusion history on composite performance – 45 mm extruder

SCREW	EXTRUSION CONDITIONS			TENSILE ST. MPa				IZOD IMPACT ST. U.N.I.S. J/m				0.5% TAN. MODULUS GPa.				FAILURE %		REINFORCE EFFICIENCY
	TEMP °C	DIE mm	S.SPEED r.p.m.	DRY mean	s.d.	WET mean	s.d.	DRY mean	s.d.	WET mean	s.d.	DRY mean	s.d.	WET mean	s.d.	DRY	WET	DRY
3	280	1.5	60	171	4.0	76	2.0	660	100	650	60	8.5	0.6	3.6	0.2	2.6	3.1	0.78
	280	2.0	30	164	5.0	74	2.0	600	80	590	90	8.11	0.5	3.51	0.1	2.3	3.0	0.71
	280	2.0	60	166	3.0	77	1.3	718	95	700	70	8.51	0.4	4.00	0.2	2.4	3.1	0.75
	280	2.0	90	181	2.0	78	1.0	710	80	690	75	8.92	0.2	4.11	0.1	2.8	3.3	0.78
	290	2.0	60	166	2.1	77	1.1	710	76	700	65	8.54	0.2	4.07	0.1	2.6	3.2	0.75
	300	2.0	60	167	2.0	78	2.0	725	90	710	84	8.53	0.3	4.03	0.2	2.3	3.3	0.75
	280	3.0	60	179	2.0	83	1.0	750	95	730	90	9.01	0.2	4.10	0.1	2.9	3.3	0.87
	280	4.0	60	187	1.5	85	1.0	816	80	810	75	9.03	0.2	4.11	0.1	2.7	3.2	0.89

Table 3.23. influence of extrusion history on composite performance – 25 mm extruder

Figure 3.45   fracture surface containing fibre bundles mag.=80 ×

SCREW	FILAMENT DIAMETER MICRONS	TENSILE ST. MPa				IZOD IMPACT ST. U.N.I.S. J/m				0.5% TAN. MODULUS GPa.				FAILURE %		FIBRE ASPECT RATIOS	
		DRY		WET		DRY		WET		DRY		WET		DRY	WET	NO. AV.	WT. AV.
		mean	s.d.	mean	s.d.	mean	s.d.	mean	s.d.	mean	s.d.	mean	s.d.				
	10.7	190	2.0	84	1.0	1040.	120.	978.	100.	9.54	0.4	4.46	0.2	2.9	3.7	27.1	33.2
1	11.4	187	1.7	77	0.8	888	100	860	170	9.00	0.4	4.20	0.2	2.9	3.4	24.3	29.9
	13.5	177	2.0	76	0.8	732	90	870	90	8.98	0.3	4.10	0.2	3.1	3.8	19.5	23.4

Table 3.24. influence of fibre diameter on composite performance

SCREW	MATERIAL	TENSILE ST. MPa.				IZOD IMPACT ST. U.NIS J/m				0.5% TAN. MODULUS GPa.				FAILURE %		REINFORCE EFFIC.	FIBRE LENGTHS MICRONS	
		DRY		WET		DRY		WET		DRY		WET		DRY	WET		NO. AV	WT. AV
		mean	s.d.	mean	s.d.	mean	s.d.	mean	s.d.	mean	s.d.	mean	s.d.					
1	F.G.C.S.1640	187	1.8	77	0.8	888	100	860	170	9.00	0.4	4.20	0.2	2.9	3.4	0.87	278	342
	XS 929	173	2.0	64	0.9	692	160	629	100	9.06	0.3	4.30	0.1	2.2	2.7	0.79	260	313
2	F.G.C.S. 1640	194	1.3	80	1.0	920	95	870	80	9.00	0.3	4.4	0.2	2.8	3.3	0.79	320	384
	XS 929	177	1.9	68	2.0	722	79	734	90	9.08	0.1	4.4	0.3	2.1	2.5	0.71	294	352

Table 3.25. influence of size type on composite performance
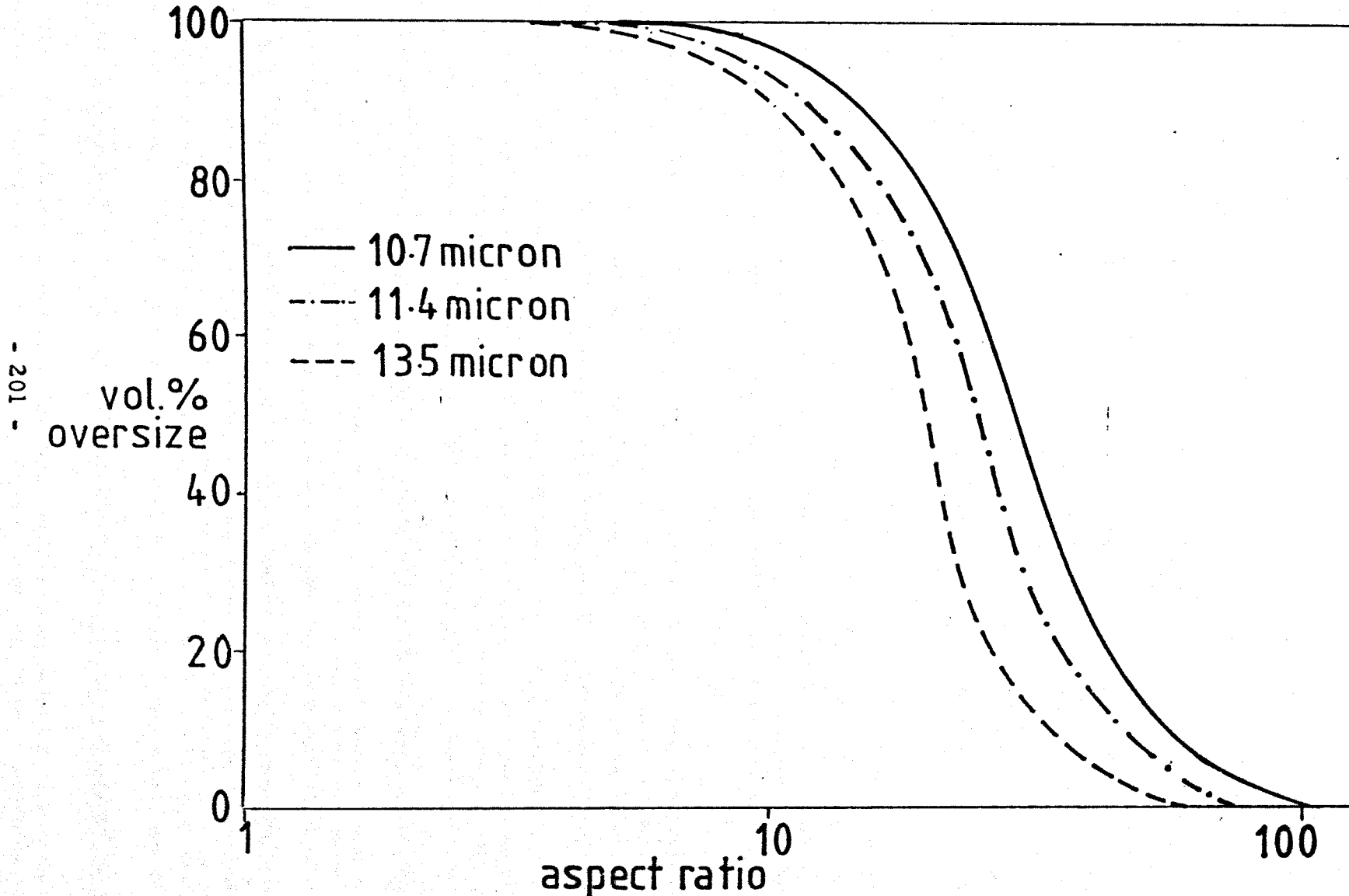
Figure 3.46 cumulative aspect ratio distributions- tensile bars

SCREW	GLASS CONTENT VOL.%	TENSILE ST. MPa. DRY		WET		IZOD IMPACTST. U.N. I.S. J/m DRY		WET		0.5% TAN. MODULUS GPa DRY		WET		FAILURE % DRY	WET.	FIBRE LENGTHS. MICRONS NO. AV.	WT. AV.
		mean	s.d.	mean	s.d.	mean	s.d.	mean	s.d.	mean	s.d.	mean	s.d.				
1	2.3	81	8.0	40	4.0	341	80	2330	200	3.82	0.5	1.63	0.2	3.7	15	407	535
	4.7	102	8.0	45	4.1	349	90	1615	200	4.64	0.6	2.37	0.3	3.0	11	394	516
	16.2	187	1.8	77	0.8	888	100	860	170	9.00	0.4	4.20	0.2	2.9	3.4	278	342
	23.0	218	2.1	87	4.0	1158	120	717	140	11.73	0.8	6.80	0.6	2.6	2.5	203	260
	31.0	225	39	91	4.0	1087	140	697	180	15.59	1.0	11.16	0.5	2.2	1.7	184	234
	40.2	229	4.1	101	7.0	606	100	461	140	20.81	0.8	15.65	0.7	1.7	1.4	151	196
2	2.3	82	8.0	41	3.0	349	75	2300	210	3.79	0.6	1.60	0.2	3.1	8.0	427	589
	4.7	101	7.9	44	4.0	353	90	1595	190	4.69	0.5	2.40	0.3	2.9	8.0	369	498
	16.2	194	1.3	80	1.0	920	95	870	80	9.00	0.3	4.40	0.2	2.8	3.3	320	384
	23.0	220	2.0	98	2.0	1300	140	200	100	12.64	0.9	7.40	0.6	2.5	2.4	270	350
	31.0	235	5.0	107	3.0	1220	160	200	90	16.69	0.8	12.00	0.5	2.3	1.6	203	249
	40.2	239	5.0	111	4.0	1000	100	140	60	22.00	0.9	18.10	0.6	1.6	2.0	180	233

Table 3.26. influence of glass content on composite performance – 45 mm extruder
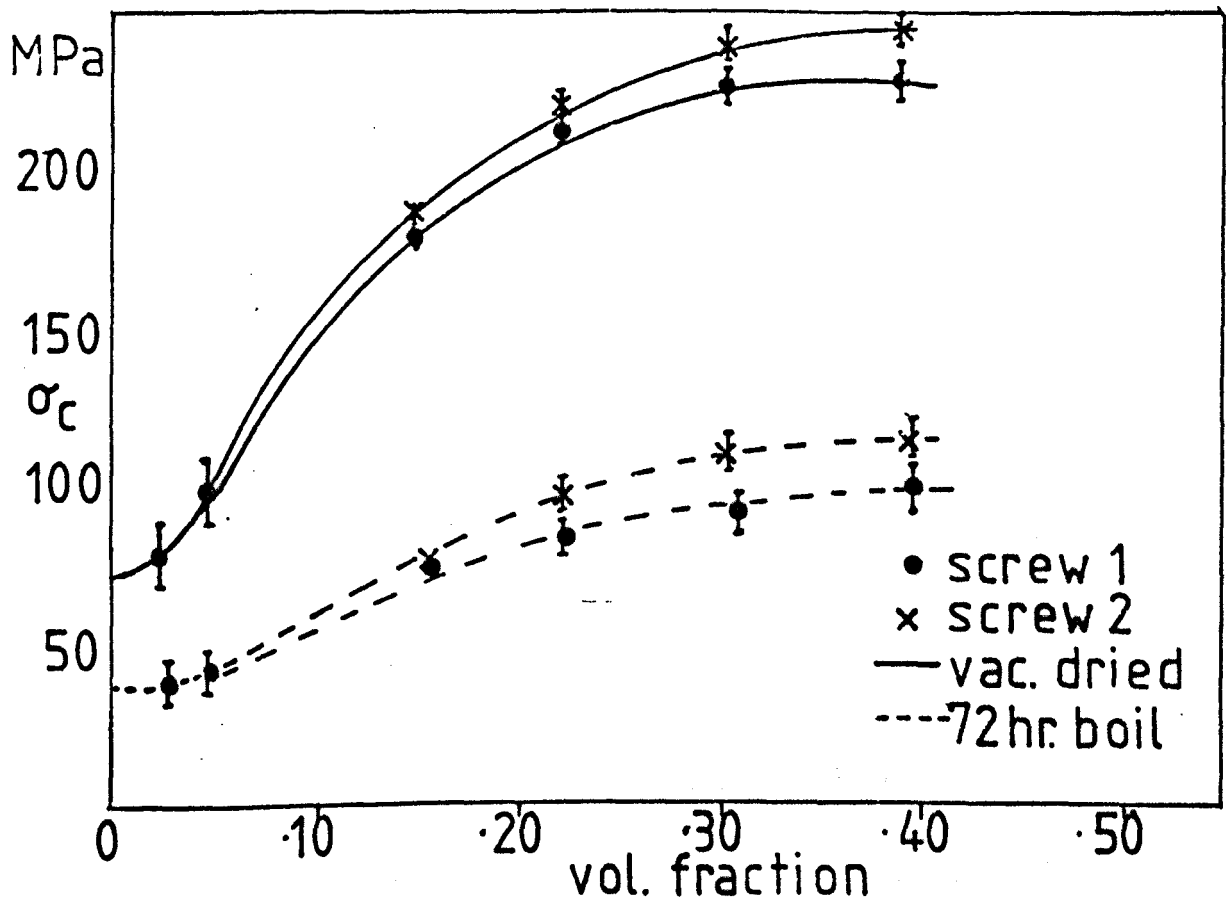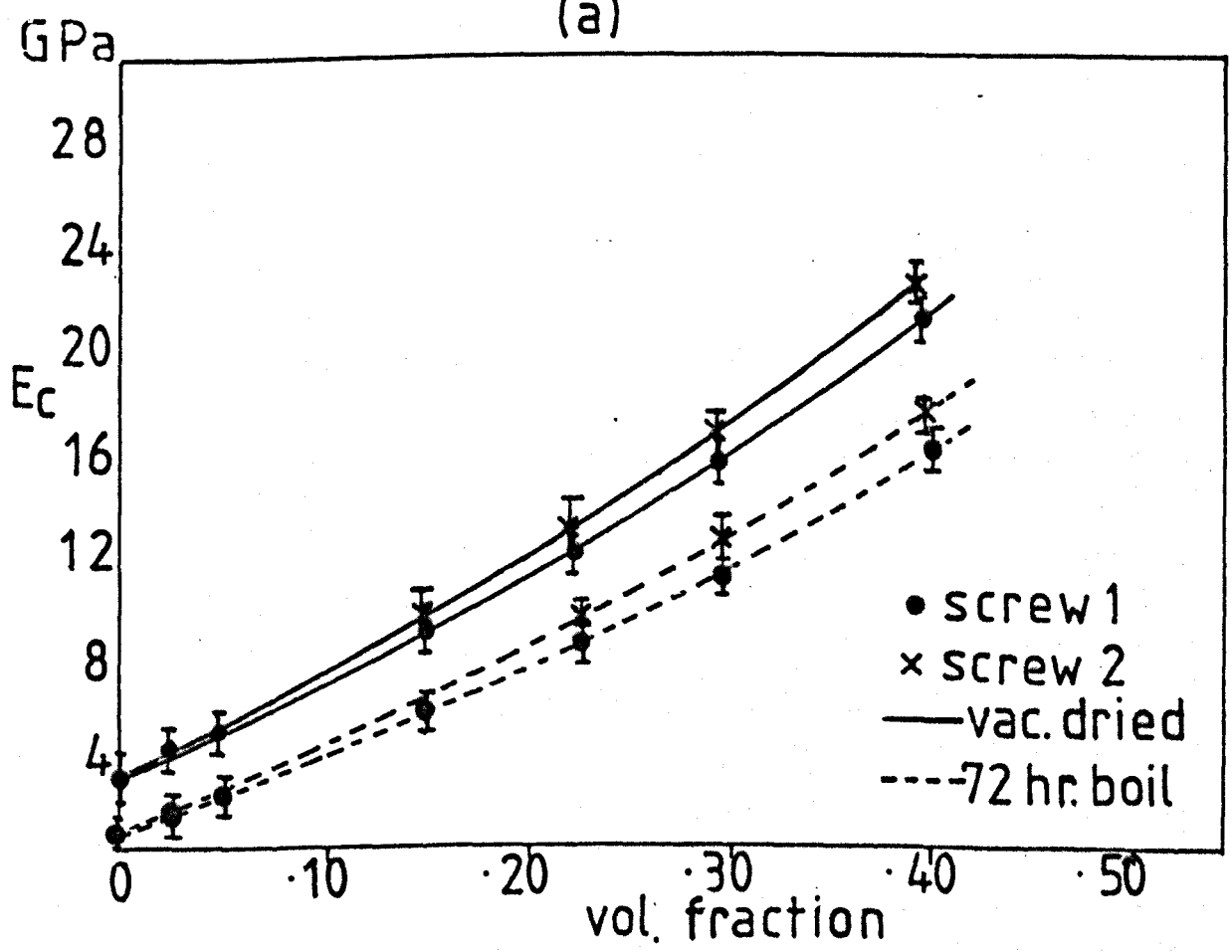
Figure 3. 47 (a)   tensile strength v fibre conc[n]

Figure 3. 47 (b)   0.5% tangent moduli v fibre conc[n]
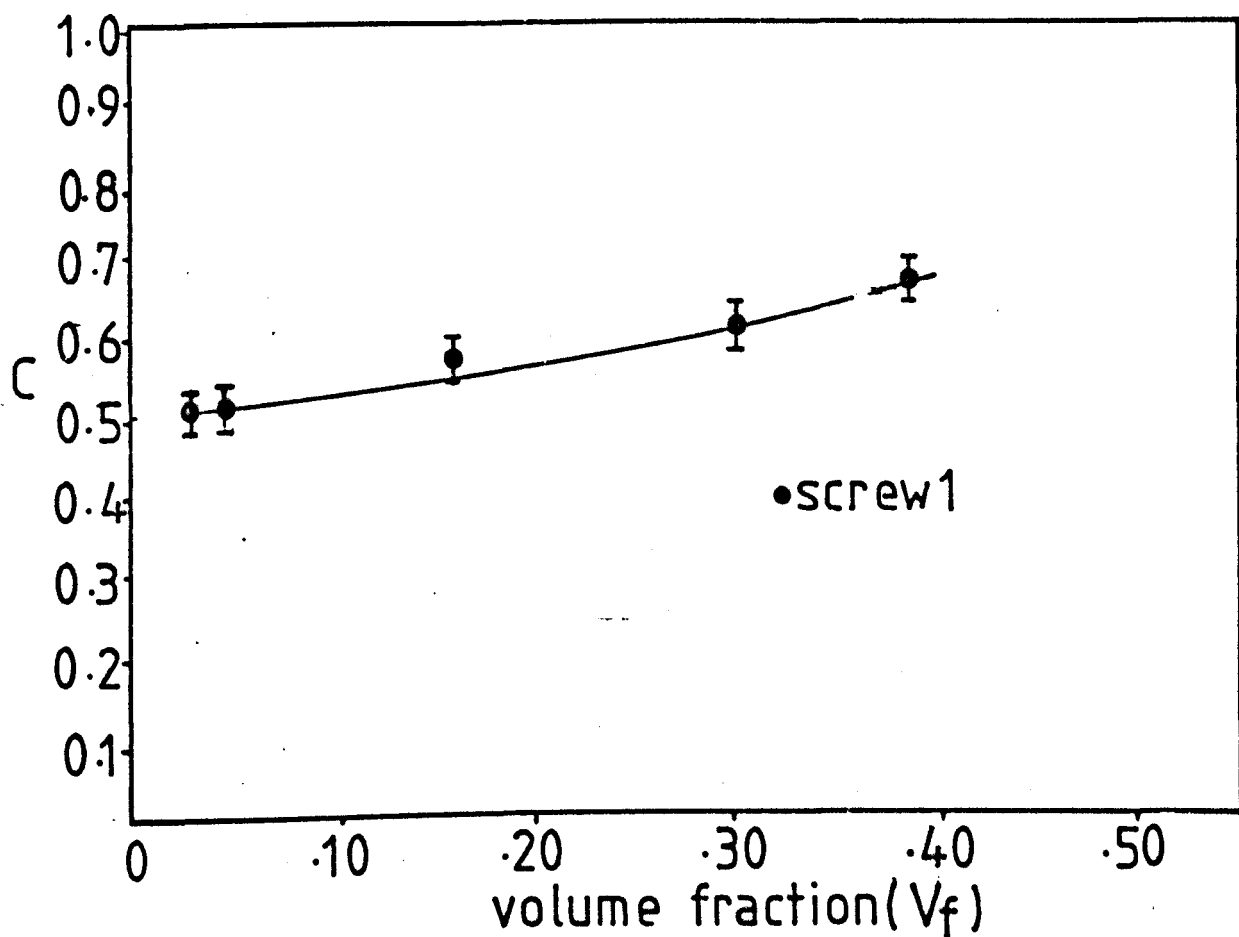
Figure 3.48 variation in orientation constant with V_f
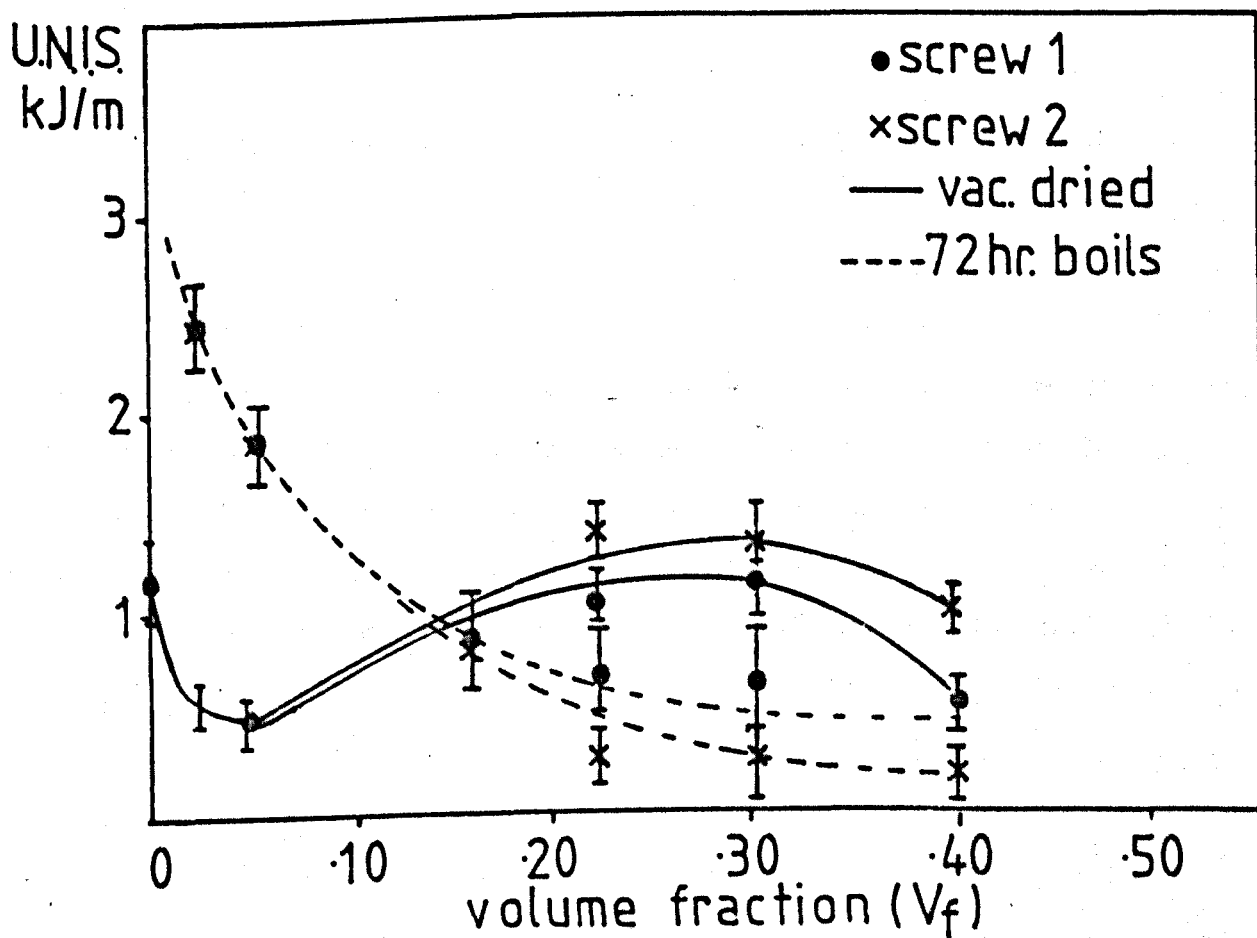
Figure 3.49 variation in IZOD impact with V_f

SCREW	EXPERIMENT CONCⁿ WT.% F.G.C.S.1640	TENSILE ST. MPa. DRY		WET		IZOD IMPACT ST. U.N.I.S. J/m DRY		WET		0.5% TAN MODULUS GPa DRY		WET		FAILURE % DRY	WET	FIBRE LENGTHS MICRONS NO.AV.	WT. AV.
		mean	s.d.	mean	s.d.	mean	s.d.	mean	s.d.	mean	s.d.	mean	s.d.				
1	30% as made	187	1.8	77.	0.8	888	100	860.	170	9.0	0.4	4.2	0.2	2.9	3.4	278	342
	40%→30%	185	1.0	73	0.7	821	90	826.	95	8.9	0.3	4.1	0.3	3.0	3.9	236	286
	50%→30%	176	1.1	66	0.5	740	88	828.	100	8.7	0.5	3.7	0.2	3.1	4.1	199	254
	60%→30%	164	1.0	62	0.5	726	78	838.	100	8.4	0.3	3.5	0.3	3.1	4.5	184	229
2	30% as made	194	1.3	80	1.0	920	95	870.	80	9.0	0.3	4.4	0.2	2.8	3.3	320	384
	40%→30%	188	2.0	78	0.7	890	90	860.	95	9.0	0.2	4.2	0.3	2.9	4.0	280	364
	50%→30%	180	3.0	73	0.6	800	80	879.	90.	8.9	0.3	3.92	0.3	2.9	4.0	226	308
	60%→30%	173	2.0	67	1.0	760	75	900	80	8.7	0.5	3.62	0.2	3.0	4.6	206	253

Table 3. 27. extrudate dilution experiments

SCREW	MATERIAL.- 30% B.W. F.G.C.S. 1640 BLENDS	TENSILE ST. MPa				IZOD IMPACT ST. U.N.I.S. J/m				0.5% TAN. MODULUS GPa.				FAILURE %		FIBRE LENGTHS MICRONS	
		DRY mean	s.d.	WET mean	s.d.	DRY mean	s.d.	WET mean	s.d.	DRY mean	s.d.	WET mean	s.d.	DRY	WET	NO. AV.	WT. AV.
1	A100	187	1.8	77	0.8	888	100	860	170	9.00	0.4	420	0.2	2.9	3.4	278	342
	A144	187	2.0	77	0.7	1020	120	940	100	9.20	0.3	430	0.2	3.1	3.9	254	330
	A146	186	1.8	77	0.8	1093	105	982	70	9.20	0.2	4.20	0.3	3.7	4.1	203	274
	A148	184	1.6	76	0.5	1141	90	1036	90	9.10	0.5	4.50	0.2	4.0	4.3	199	258
	A150	185	2.0	76	0.3	1240	100	1102	70	9.10	0.3	4.70	0.2	4.1	4.4	197	243

Table 3.28 composite performance v polymer molecular weight

SIZE TYPE	NUMBER + OF PROCESSING CYCLES	TENSILE ST. MPa				IZOD IMPACT ST. U.N.I.S. J/m				0.5% TAN. MODULUS GPa				FAILURE %		FIBRE LENGTH MICRONS	
		DRY mean s.d.		WET mean s.d		DRY mean s.d.		WET mean s.d		DRY mean s.d.		WET mean s.d.		DRY	WET	NO. AV.	WT. AV.
MSS.1640	1	187	1.8	77	0.8	888	100	860	170	9.00	0.4	4.20	0.2	2.9	3.4	278	342
	2	180	1.0	69	1.0	787	110	868	105	8.80	0.3	3.80	0.2	3.0	3.7	201	263
	3	164	2.0	64	0.9	627	90	872	80	8.40	0.3	3.60	0.2	3.1	4.2	185	235
XS 929	1	173	2.0	64	0.9	692	160	629	100	9.06	0.3	4.30	0.1	2.2	2.7	260	313
	2	165	1.9	57	0.9	687	140	640	80	9.03	0.2	3.70	0.1	2.5	3.2	223	282
	3	157	1.6	57	0.7	650	120	744	95	8.70	0.2	3.2	0.2	2.7	3.8	206	252

+ SCREW 1 EXTRUDATES

Table 3.29 influence of number of extrusion processing cycles on composite performance
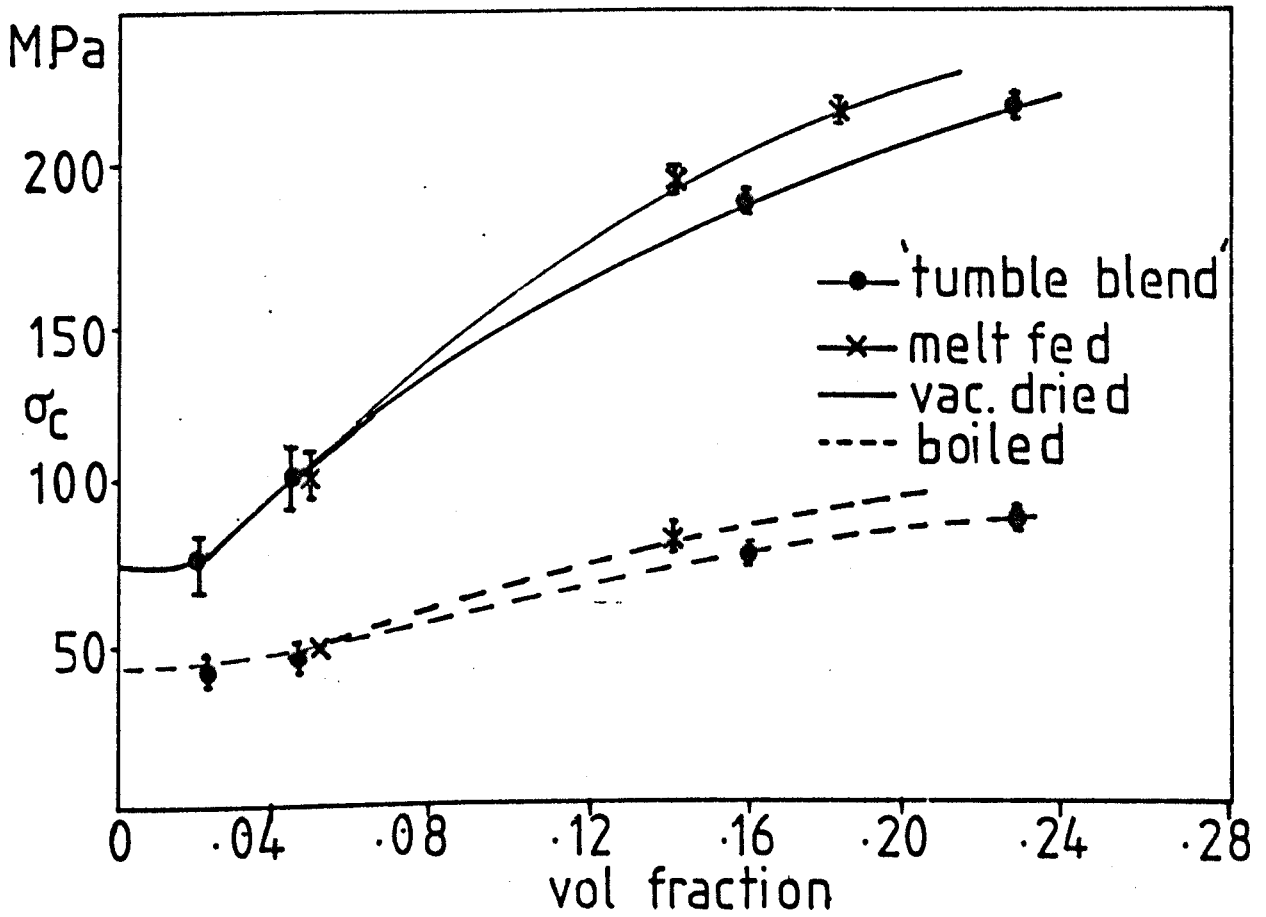
Fig. 3.50 tensile strength v extrusion method
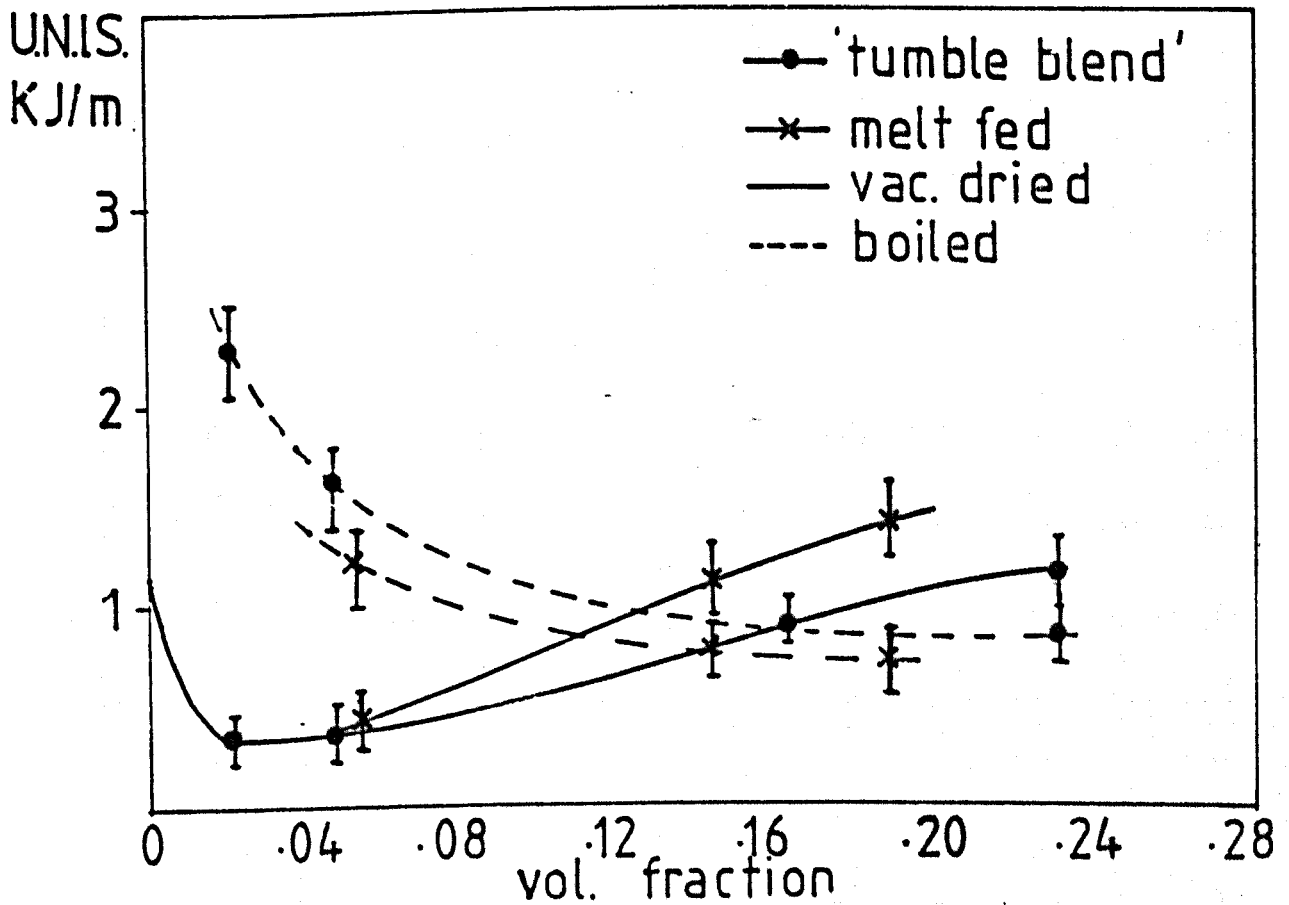
Fig. 3.51 impact strength.v. extrusion method
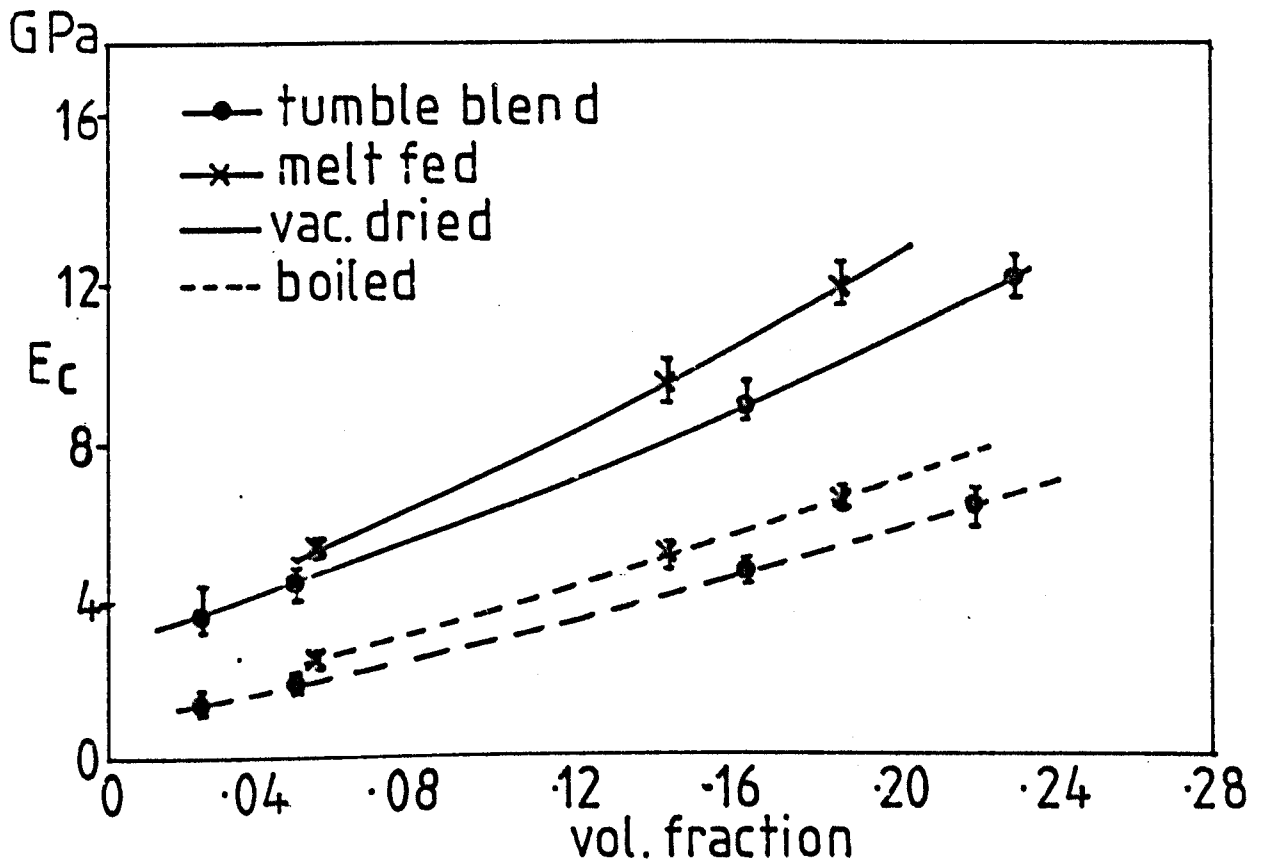
Fig. 3.52 tangent modulus v extrusion method
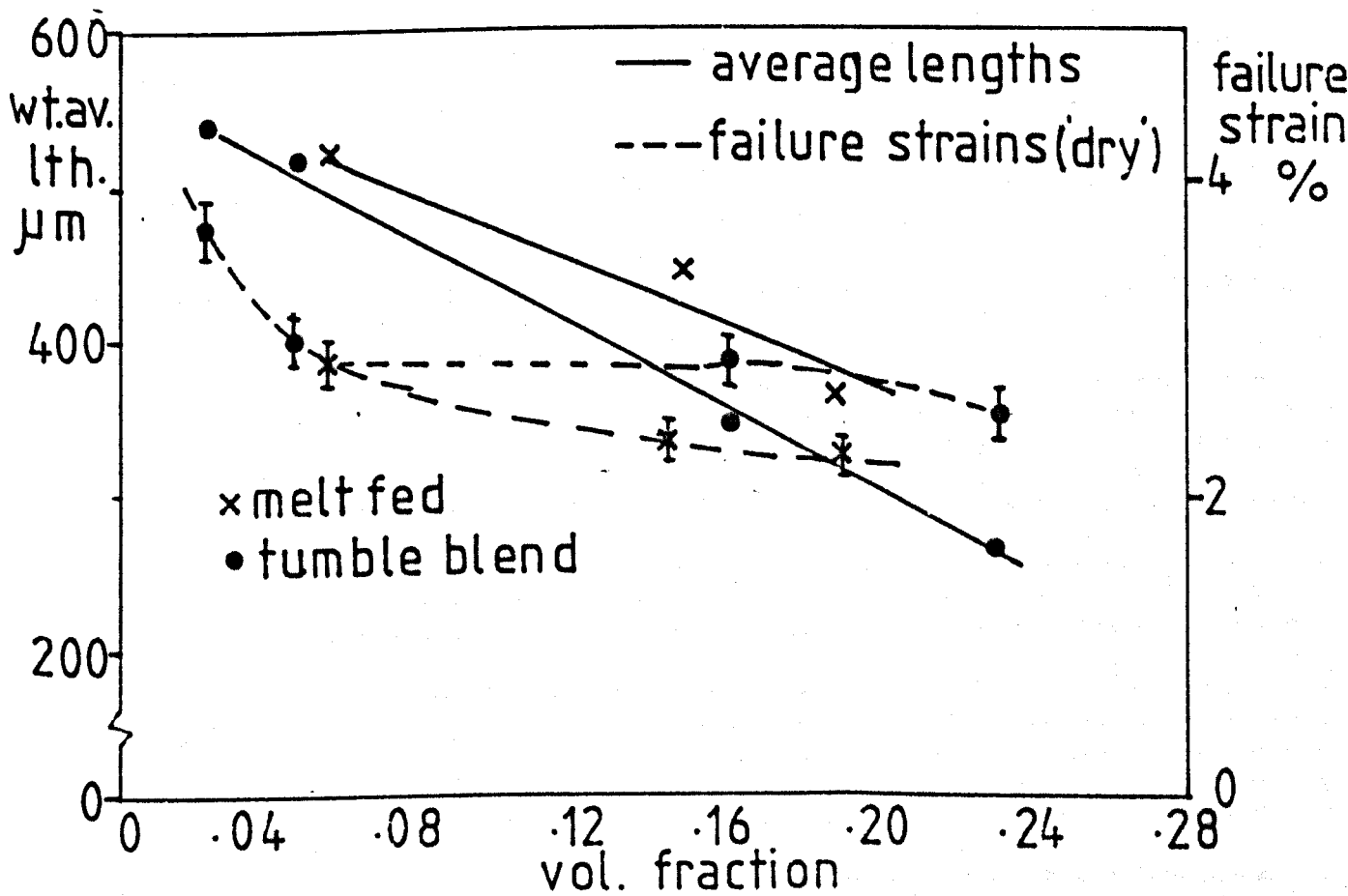
Figure 3.53 mean fibre lths. and failure strains
                                v extrusion method.

sample position	fibre lengths microns	
	no. av.	wt. av.
feed port	336	442
nozzle	292	350
sprue	284	353
runner	287	351
tensile bar	278	342

nozzle diameter = 6mm.
sprue diameter = 6mm ➔ 8mm.
runners (½ round) radius = 3mm

Table 3. 30 <u>fibre fracture during injection moulding</u>

machine conditions				dispersion	talysurf
s.speed r.p.m.	s.r.p. MN/m²	in. press. MN/m²	s.r.t. sec.	% bundles	c.l.a. microns
71	0	6·1	6	22·5	53
71	1·01	6·1	10	5·5	49
71	1·51	6·1	15	1·1	40
71	1·82	6·1	21	0·5	33
71	2·42	6·1	*	—	—
127	1·82	6·1	7	1·9	47
127	2·42	6·1	26	0·17	31
127	3·03	6·1	*	—	—

* screw stalled

Table 3.31. <u>fibre dispersion and surface finish</u>
<u>v injection moulder conditions</u>

material: 30% b.w. F.G.C.S. 1640/Maranyl A100
weight average length = 1.12 mm
number average length = 0.52 mm
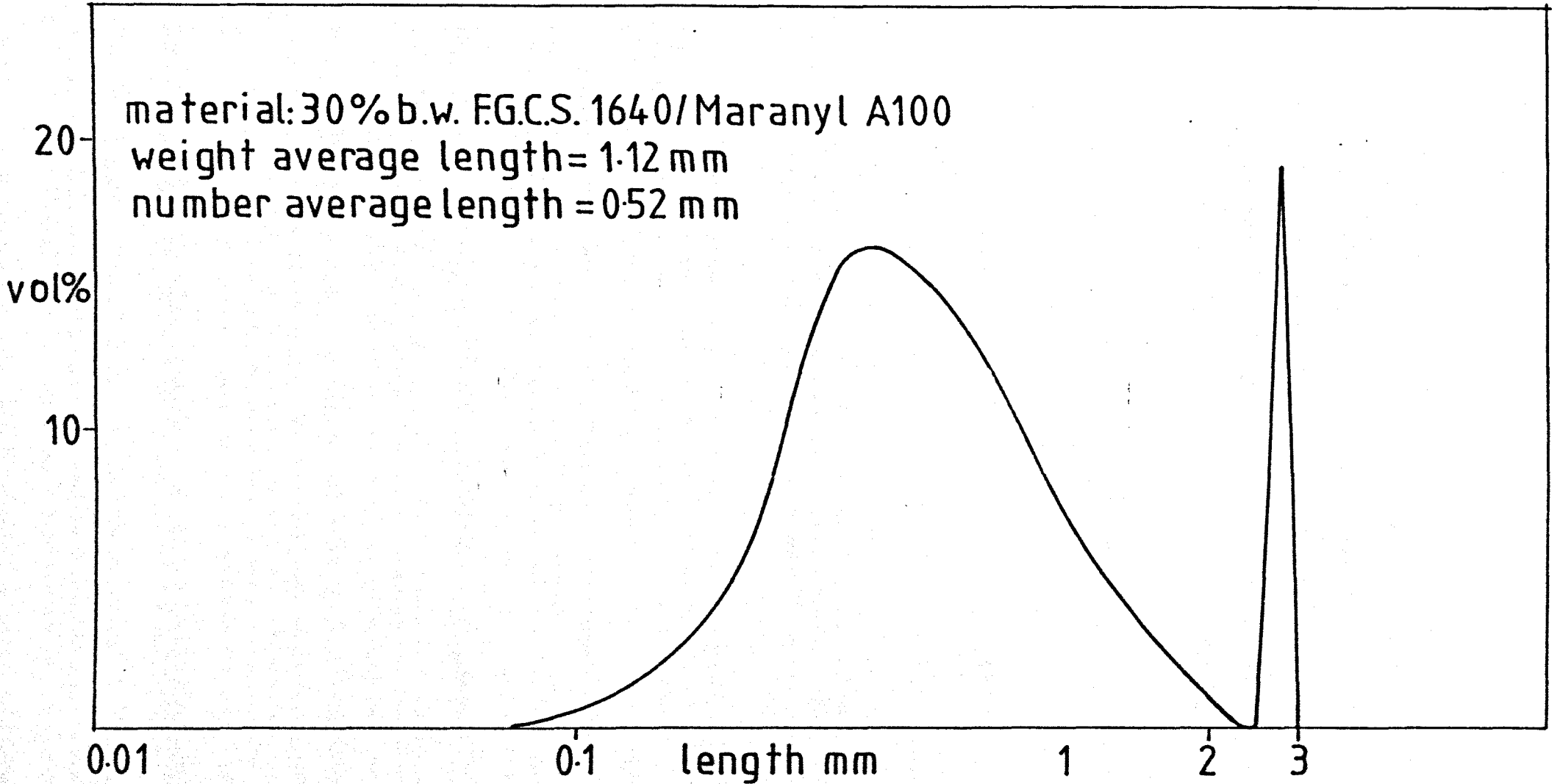
Figure 3.54 fibre length distribution— direct injection moulding
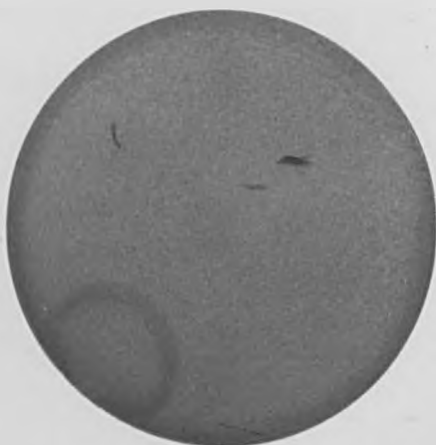
FIG. 3.55 INFLUENCE OF MOULDING VARIABLES ON FIBRE DISPERSION

trends of increasing wet impact with reduced fibre lengths - Tables 3.27 and 3.29.

3.3.2.7 Fibre fracture in sprues and runners

Fibre length analyses carried out for these regions indicate little significant fibre degradation over that measured at the nozzle - Table 3.30. These results appear to conflict with the work of others (118) (119), although in each case no evidence is produced to support such observations. However, it is possible that the lack of fibre fracture observed in this study arises from the large nozzle, sprue, and runner dimensions respectively.

Direct injection moulding of a 30% by weight blend of F.G.C.S. 1640/Maranyl A100 under standard conditions produced a significant quantity of undispersed fibre bundles in the resultant composite. The resultant fibre length distribution for this material is illustrated in Figure 3.54. The pattern of fibre breakage is consistent with the melting studies described in Section 3.1.6. The melting process occurring in reciprocating screw injection moulders has been studied by Fenner et. al. (120) and shown to possess all the elements of the melting mechanism occurring in plasticating extruders. The intermittent nature of the former process, however, produces less severe shear conditions for the glass-polymer blend during its transport from the feed port to the injection point. Variations in screw speed and back pressures are found to significantly effect the level of dispersion achieved - Figure 3.55 and Table 3.31. Such results confirm the work of Filbert et. al (42). However, it is to be noted that improvements in dispersion are only achieved if the screw return pressure is raised to reduce the higher throughput which accompanies increased screw speeds and reduced screw return times.

3.4 Composite failure modes

As discussed in Section 2.13.3 pronounced matrix crazing was observed immediately prior to failure for boiled tensile specimens containing relatively low volume fractions of reinforcement. Microscopic examination of ground and polished sections revealed that such crazing seemed to originate from matrix cracking and fibre debonding. Photographic evidence of such effects could not be obtained although examination under the stereoscan indicated the presence of such cracks in the surface region - Figure 3.56 (a). Closer observation revealed fibres bridging these surface cracks - Figure 3.56 (b). The above observations are consistent with a failure process controlled by fibre debonding and matrix cracking. Such effects arise from plasticisation of the matrix and degradation of the interfacial region due to moisture attack (121). Further evidence is provided by measurements of the fibre length distributions before and after tensile testing which indicate no significant changes Figure 3.57. Observation of the resulting fracture surface also illustrates the reduced bonding between the fibres and matrix polymer - Figure 3.58 Similar arguments for such a failure mechanism have been advanced by Jackson (111) and Ramsteiner et. al. (70) based on acoustic emission and fracture surface studies respectively.

For the higher volume fraction materials ($V_f > 0.23$) no matrix crazing is observed prior to tensile failure, although after fracture pronounced surface cracks are observed in both vacuum dried and boiled specimens. The reduced failure strains for these composites could be explained by diminished fibre strengths due to surface damage in the compounding operations. Alternatively, premature failure could arise from matrix cracking originating at points of stress concentrations. The former hypothesis is

considered unlikely in that flawed fibres would be broken into
shorter lengths during processing resulting in presumably an enhanced
strength for the remaining fragments in accordance with statistical
fibre strength theories (122) (123). Support for the latter
supposition is widespread for brittle matrices reinforced with short
fibres (124) (125). Again the similarity of recovered fibre lengths
for stressed and unstressed composites lends support to a failure
mechanism dominated by matrix failure and confirms the work of others
(110).

3.5 Application of the Bader-Bowyer equation to injection moulded composites

Typical force-strain curves for vacuum dried nylon 6.6
composites containing different levels of short glass fibres are
described by Figure 3.59. For those composites which fail below
the mean fibre fracture strain equation 1.10 is considered to be
applicable. By analogy with the work of Kelly and Tyson (53),
the value of the critical length at composite failure is given by
equation 1.3, i.e.

$$l_c = \frac{\sigma_f D}{2\tau} = \frac{\varepsilon_c E_f D}{2\tau}$$

where $\sigma_f =$ stress in the fibre at composite failure.

However, for any value of composite strain, prior to fracture,
there will be a similar critical length, l_ε given by:-

$$l_\varepsilon = \frac{E_f \varepsilon_c D}{2\tau} - - - - - - 3.14$$

For fibres shorter than this critical length the mean stress in
the fibre is given by:-

$$\bar{\sigma}_f = {}^{L\tau}/_D - - - - - 3.15$$

For fibres above this critical length, the mean fibre stress
is given by:-

$$\bar{\sigma}_f = E_f \varepsilon_c \left(1 - \frac{E_f \varepsilon_c D}{4\tau L}\right) - - - 3.16$$

Incorporating the above equations into equation 1.10 gives:-

$$\sigma_c = C\left[\sum_{l_i=0}^{l_i=l_z} \frac{\tau l_i V_i}{D} + \sum_{l_j=l_z}^{l_j=\infty} E_f \varepsilon_c \left(1-\frac{E_f \varepsilon_c D}{4\tau l_j}\right)V_j\right] + E_m \varepsilon_c (1-V_f) \quad -- 3.17$$

For the above composites E_f, E_m and D are known and σ_c and ε_c can be readily obtained. Thus, by making the assumption that orientation is independent of strain and fibre length, the above model allows calculation of both C and τ for a known fibre length distribution. A computer programme was established by the above workers (116) which used the following computing procedure:-

(i) Using the fibre modulus obtained from single strand tests, values of ε_1, and ε_2 were selected so that $\varepsilon_2 = 2\varepsilon_1$.

(ii) The corresponding stresses at the above two strains were determined from the measured stress-strain curve.

(iii) The matrix contribution at these strains was calculated from $E_m \varepsilon_c (1-V_f) = Z_1$, and the ratio of the fibre reinforcement calculated, i.e. $R = \dfrac{\sigma_1 - Z_1}{\sigma_2 - Z_2}$

(iv) Using an assumed value for τ the corresponding values of l_{ε_1}, and l_{ε_2}, were determined.

(v) Using the measured fibre length distributions the fibre contribution terms were determined using equations 3.15 and 3.16 summed over the spectrum of fibre lengths.

(vi) A second ratio was determined:-

$$R' = \frac{X_1 + Y_1}{X_2 + Y_2}$$

where X and Y are the fibre contributions above and below the critical length for the two strains.

(vii) The assumed value of τ was adjusted until $R' = R$.

(viii) Having obtained τ the value of C is obtained from equation 3.17.

Values of Υ obtained were compared with previous results obtained from fracture surface studies and shown to give good agreement (96).

Values of Υ and C obtained for the two fibre types used in this study are given in Table 3.32. The reduced bonding of the polyvinyl acetate sized material is confirmed.

Fibre Type	Υ	C
F.G.C.S. 1640	45.0 MPa	0.63
XS 929	32.0 MPa	0.61

Table 3.32 calculated values for interfacial bond strengths and orientation constants.
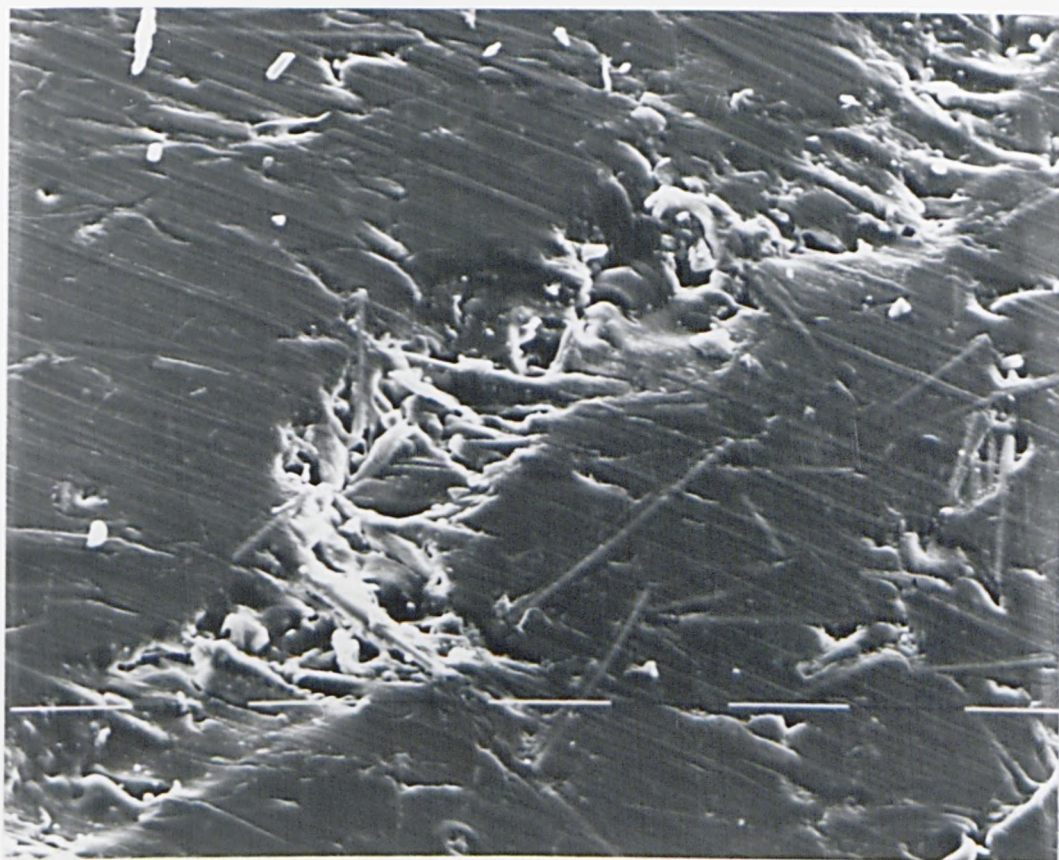
Figure 3.56(a) surface cracks 'boiled' A.S.T.M. bar
magnification 160×
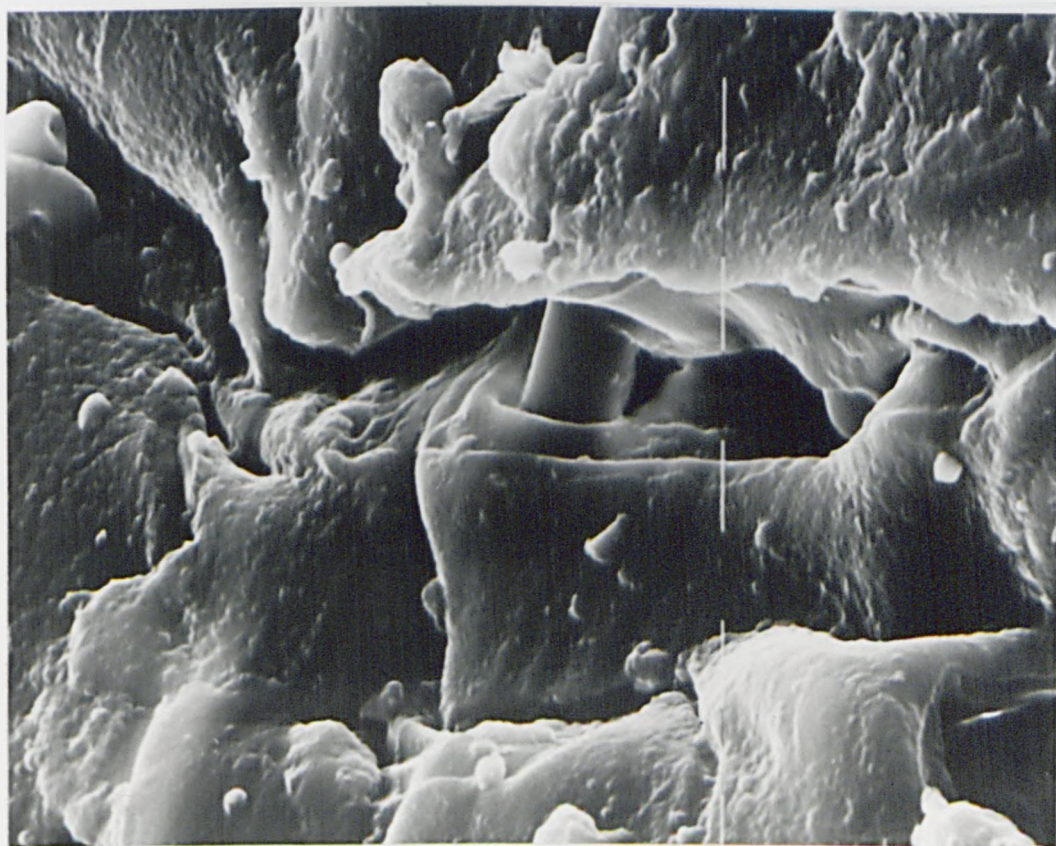
Figure 3.56(b) surfacecracks 'boiled'A.S.T.M bar mag.1200×
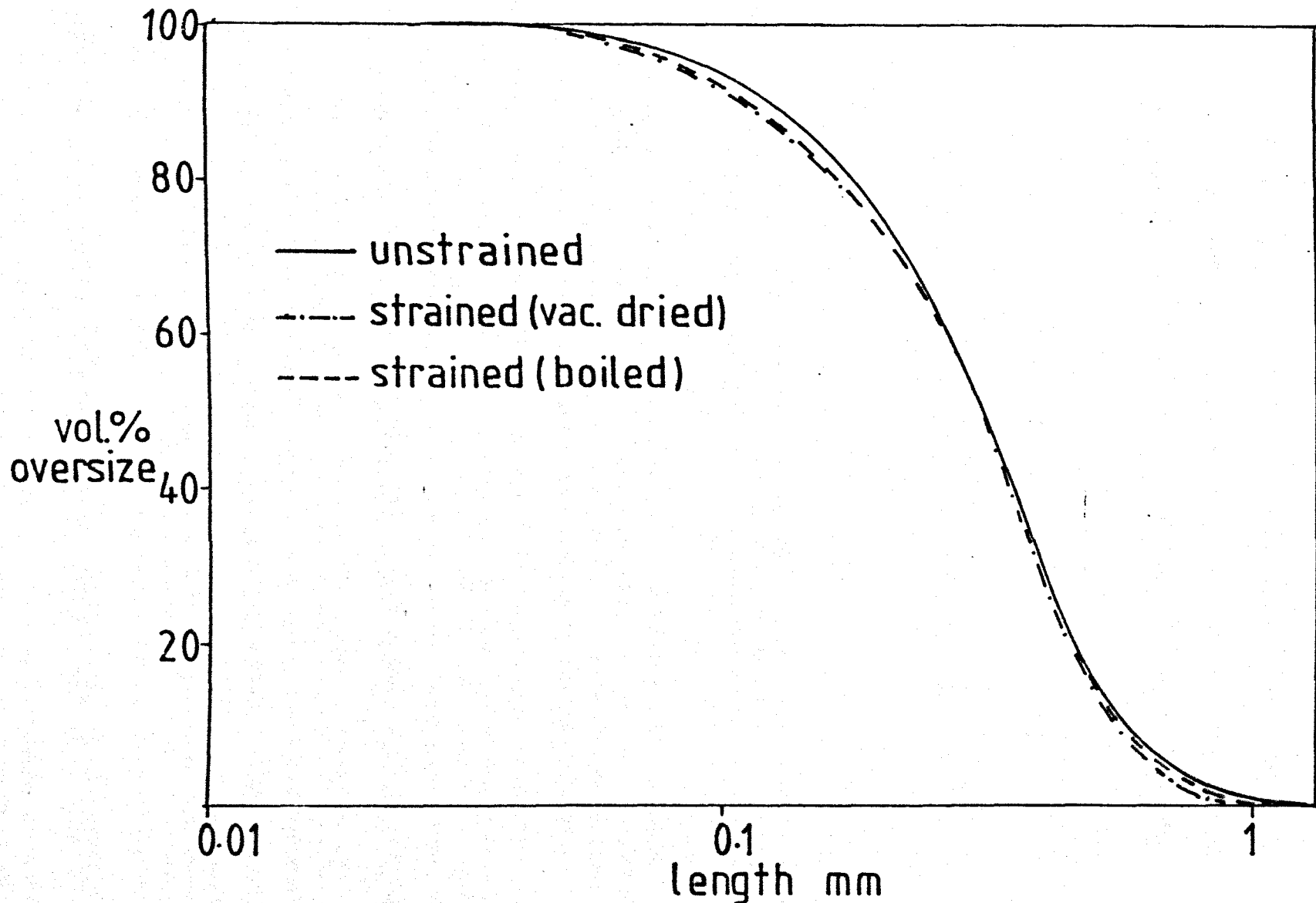
Figure 3.57 cumulative fibre length distributions for strained and unstrained tensile bars

Figure 3.58. stereoscan photograph of 'boiled' fracture surface mag.=768x

– MSS 1640 sized fibres
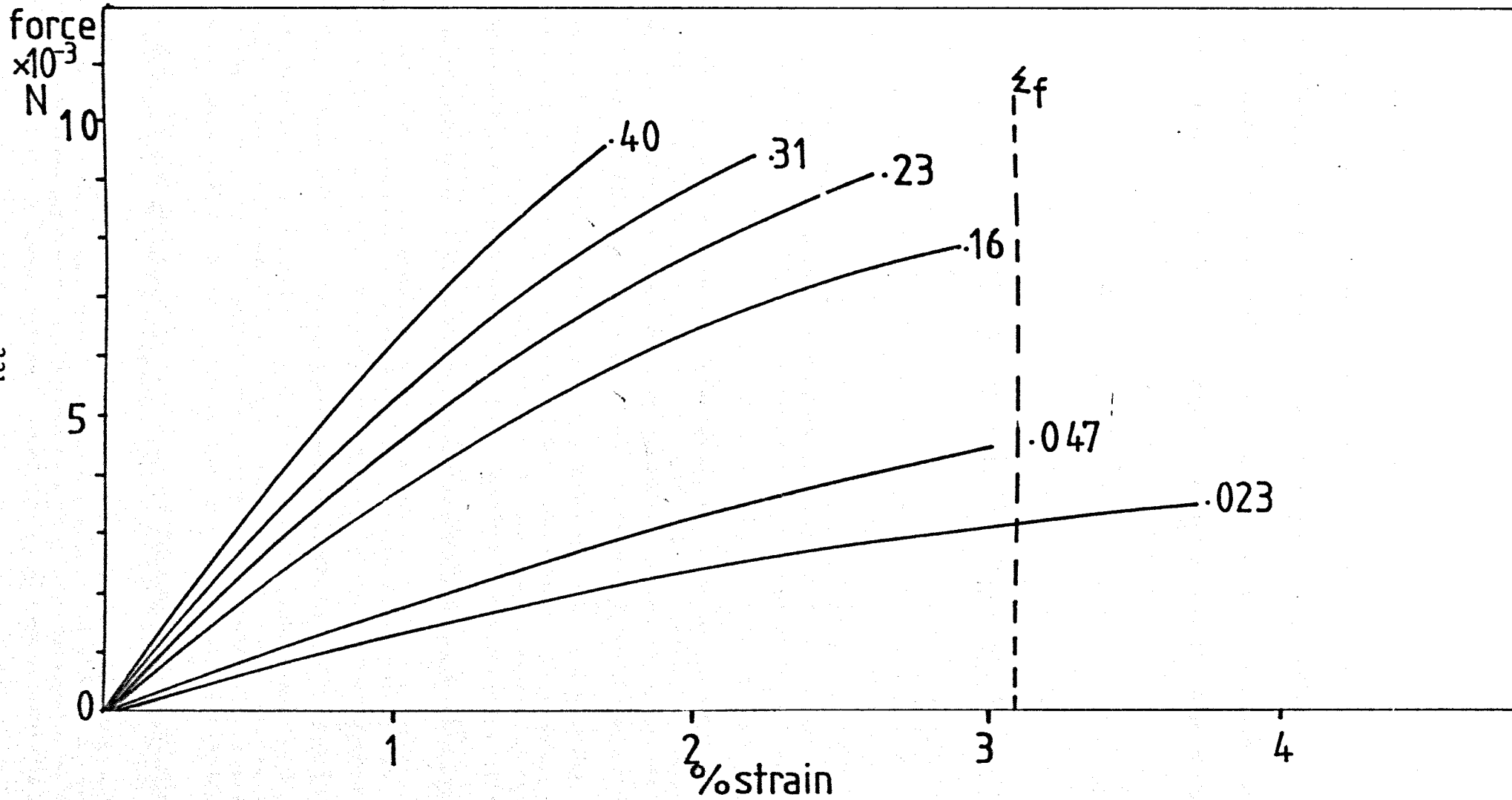
Fig. 3.59 typical force-strain curves. v. vol. fraction for vac. dried tensile bars

CHAPTER 4   DISCUSSION AND SUMMARY

4.1 Introduction

The total mechanical property enhancement achieved by the incorporation of short glass fibres into a thermoplastic matrix results from the complex interaction of several factors. Prominent dependent variables discussed in the literature sources examined are orientation, fibre matrix adhesion, and fibre length. Obviously, significant composite improvements will accrue from greater alignment of the fibres in the test direction. Similarly, optimisation of residual fibre lengths and matrix-fibre adhesion are accepted to be a pre-requisite for efficient fibre utilisation in even the most complex mouldings. The calculated interfacial bond strengths, determined in section 3.5 after the method of Bader et. al. (116), would suggest that cationic size coatings of the type used in this study provide excellent bonding to the polyamide matrix in the dry state. Evidence of such adhesion is seen in the stereoscan photograph provided - Figure 4.1. However, a similar photograph of a boiled sample - Figure 3.58, indicates the extremely poor adhesion existing after such conditioning and would suggest a deficiency in the sizing materials presently used.

In both the above cases, improved fibre length in the moulded article produces benefits in tensile performance and low strain stiffness. Typical results for compounds manufactured in this study are provided by Figures 3.50 and 3.52. The literature contains several references to practical routes by which such fibre length improvements can be achieved (41) (110) (127). Of the methods proposed,the technique utilised by Bader and Bowyer offers the greatest promise. Such a process is used to produce compounds containing long fibres suitable for processing on conventional reciprocating screw injection moulding machines. A possible disadvantage of this method lies in the low size levels required

to obtain adequate impregnation of the fibre tow as it passes through the extruder cross-head. Such reduced size levels can lead to abrasion damage of the fibres, resulting in fibre breakage and blockage of the die, unless lubricants are incorporated to maintain the strand integrity and surface protection required.

Over 80% of all short fibre reinforced polyamides are pre-compounded in single screw plasticating extruders whereby the fibre, in the form of short chopped strands, is tumble blended with the polymer pellets prior to extrusion. This study has thus concentrated on the influence of the various processing, design and fibre parameters on the pattern and degree of fibre fracture occurring. The subsequent processing and composite trends are also highlighted.

Principal literature sources for the composite studies were RAPRA abstracts and the various S.P.I. Conference publications and plastics journals. Processing and melting references were obtained from RAPRA computer searches and processing journals. Computer searches of the Mechanical Engineering indexes also provided useful information for the extrusion and melting studies.

4.2 Extrusion processing of glass fibre - polyamide blends

4.2.1 The plasticating extrusion process

The processing of short glass fibre-polyamide 'tumble' blends is marked by increases in melt temperatures, die pressures and specific power consumptions over the unreinforced material - Tables 3.8 and 3.9. The magnitude of such effects is related to the glass fibre loading and fibre properties, subject to the influence of design and processing variables. The success of such a mode of processing largely rests with the improved fibre properties which allow 'flood' feeding of blends containing fibre volume fractions of up to 0.23. However, even with the highly integral cationic sized fibres used in this study, which possess good static attraction for the polymer pellets, the free feeding

properties deteriorate rapidly above this level. In addition,
increases in filamentisation or initial strand lengths can so reduce
the feeding performance that stable operation with fibre volume
fractions above 0.05 is impossible, without expensive modifications to
hopper and feed throat designs. Such effects are related to the
changes in bulk density and frictional coefficients which accompany
alteration in the fibre properties and addition levels - Figure 3.7
and Tables 2.2 and 3.10. Obviously changes in the physical form of
the polymer would also be expected to influence the feeding performance.
Milling of the polymer pellets to produce a fine powder is reported to
lead to improvements (68), although this is obviously not a practical
proposition due to the additional cost involved.

Increased differential friction at the screw-solid and barrel-
solid interfaces is beneficial to the solids conveying efficiency
of the single screw extruder. It is to achieve this aim that grooved
feed sections are being introduced for unreinforced materials (128).
Such a technique, however, increases the mechanical energy requirement
of the extrusion process. The relative motion of the screw and
barrel provides the means of introducing such energy, both in the solid
filled and melt conveying regions. Changes in frictional coefficients,
temperatures, screw speed and bulk densities will alter the relative
energy balance of the system, in that changes in the heat generated by
mechanical work will be compensated for by the thermal energy supplied
by the barrel heaters. The importance of the former energy source
under various conditions is indicated by the specific power consumptions
and the measured melt temperatures discussed in sections 3.1.1 to 3.1.4.
The recorded temperatures were always lower than the barrel heater
settings indicating the poor thermal conductivity of these polymeric
melts. Increases in melt temperatures, however, accompany increased

specific power consumptions - Tables 3.2. 3.8 and 3.11.

Changes in the specific power consumption have been used to assess fibre fracture during the processing of glass filled thermoplastics (33), increases in this parameter being considered synonymous with increased fibre degradation. However, such correlations are only valid in the absence of melting changes introduced by variations in material parameters. Consideration of Figure 3.4 (a) and Tables 3.5 and 3.10 indicates a reduced specific power requirement for the more filamentised, lower bulk density material. However, recovered fibre lengths - Figure 3.5, show increased fibre fracture for this material when processed on the 'high shear' screw. Recovered fibre lengths for the lower compression ratio screws - screws 2 and 3 in Figure 3.1, indicate that undispersed fibre bundles have survived the extrusion process for the higher bulk density blend. This co-existence of significantly degraded monofilaments and integral fibre bundles provides an insight into the fibre breakage process occurring. Fibre length analyses for extracted screw samples are represented in Figures 3.9 to 3.11 and Figures 3.14, 3.15 and Table 3.15. The observed fibre length trends can be related to the melting mechanism occurring in these single screw plasticating extruders.

4.2.1.1 The melting process

The physical picture of the melting process occurring is provided by Figures 3.12 and 3.16. Fibre length analyses carried out for the solid bed and melt pool regions of these sections are typified by Figures 3.13 and 3.14 and confirm the location of this melting region as the source of predominant fibre breakage. Further evidence of the presence of fibre bundles and dispersed fibres, in the solid bed and melt pool regions respectively, is provided by the X-ray radiographs presented in Figures 2.22 and 3.20. Specifically, fibre fracture occurs under the high shear conditions existing in the melt film at the solid bed-melt film interface

- see Table 3.13. The rapid removal of this molten material, containing degraded fibres, generates a highly efficient melting process in which small amounts of molten material are subjected to transient high temperatures and shear stresses. Such a dynamic melting equilibrium reduces the probability of polymer degradation which can arise from the prolonged high temperature exposure of these temperature sensitive materials. Obviously, a stable melting process in which no fracture of the solid bed occurs is the preferred mode of operation, provided melting is completed before the die. However, for glass fibre filled materials, such a situation is likely to produce severely degraded fibres as illustrated in Figure 3.17 for the lower bulk density polyvinyl acetate sized fibres. Paradoxically, the higher outputs achieved by blending of the more integral MSS 1640 sized fibres with the polymer pellets, can generate instabilities in the melting process which arise from fracture of the solid bed. Evidence of such fracture is presented in Figures 3.12 and 3.18 and, as discussed in Section 3.1.6.2, occurs under the influence of the secondary melt film formed at the screw root. The occurrence of such solid bed fracture terminates the steady state melting process and leads to the survival of undegraded strands which remain trapped in unmelted polymer, until melting is finally completed by thermal conduction from the surrounding melt films. As discussed in Section 3.1.6.1 integral fibre bundles are also produced by conduction melting at the radial interface of the melt pool and solid bed, which occurs prior to solid fracture for the more compacted fibre polymer blends.

As discussed in Section 3.1.9 the extent of stable melting prior to the onset of such fracture is dictated by screw geometry, throughput rate, processing and fibre parameters. Although screw extraction experiments of the type carried out in this study provide the means of studying this melting process, such experiments are extremely time

consuming. In addition, the reduced thermal contraction and brittle nature of these glass filled, semi-crystalline polymers create difficulties in obtaining adequate samples. An alternative procedure lies in computer modelling. The efficiency of melting and hence the degree of fibre fracture can be predicted by utilisation of the computer model established for unfilled thermoplastics which is discussed in Section 3.1.8.2. Figures 3.23 and 3.31 illustrate good agreement between the predicted and measured melting rates for extracted screw samples obtained in these studies. The ability of this computer model to accurately predict the process of solid bed acceleration, which preceeds solid bed fracture, is illustrated in Figure 3.24. The fibre length distributions indicated in Figure 3.15 are seen to be in accordance with these melting predictions. Explanations of the influence of the various parameters on melting stability and fibre fracture are provided by the use of this melting model and the results are discussed in Section 3.1.9.

The physical, thermal and rheological data required for these studies is given in Tables 3.16 and 3.17. Problems of determining accurate rheological data for glass contents in excess of 16% by volume are discussed in section 3.1.9.4 and are likely to limit the application of such a model. Additionally, uncertainties in the thermal conductivities of these blended materials leads to errors, although, as indicated by Figure 3.28, such discrepancies are not large. Typical literature values for the thermal conductivities of these fibre filled materials range from 0.33 W/m$^{\circ}$C to 0.39 W/m$^{\circ}$C (95), depending on the fibre loading. In addition, since such values are invariably obtained on injection moulded disc specimens (88), the results obtained vary significantly due to the anisotropic nature of these materials. For the uncompacted materials existing in the solids conveying and melting regions of the extruder,

the actual thermal conductivity would be expected to be considerably lower than the values given above. Typical values calculated by the method of Yagi and Kunii (129) for a 30% by weight blend of glass fibres and nylon 6.6, having bed 'porosities' of 0.3 to 0.5, are 0.17 to 0.09 W/m$^{\circ}$C. These values are in the region occupied by cellular plastics, whose conductivities are generally determined by a guarded hot plate method (88). Such a method is obviously worthy of consideration for future determinations of the thermal conductivities of these polymer-fibre blends.

The use of realistic raw material data will enable accurate simulation of the suitability of envisaged screw profiles and processing conditions, in producing stable melting conditions for these glass fibre filled thermoplastic materials. However, the evidence presented in Section 3.1 indicates that significant improvements in retained fibre lengths, for extrudates prepared by the above process, are unlikely to be achieved. Reductions in compression ratio and screw speed have been illustrated to be unsatisfactory in that undispersed fibre bundles survive the extrusion process, either due to solid bed fracture or increases in the thermal energy input from the barrel heaters. Additionally, the throughput and operating stability is often so affected as to render the process impractical. Obviously, improved dispersion of the fibres can be achieved by reducing the size levels, although the concomitant reduction in the bulk density leads to poor feeding properties. This dicotomy can be resolved by introducing the fibres into the molten polymer, downstream of the melting section.

4.2.2 The melt feeding process

The glass fibres are introduced directly into the molten polymer as described in Section 2.6. Whilst significant improvements in retained fibre lengths are achieved - see Figure 3.42 and Table 3.18, extensive fibre fracture is still evident. The shear conditions

in this process are, however, still quite severe and are at a maximum over the Egan section. It is anticipated that distributive mixing sections of the types illustrated in Figure 2.10 will offer additional improvements in residual fibre lengths during this initial processing stage, and this avenue remains a worthwhile area for further reseach.

4.3 The injection moulding process

Undispersed fibre bundles found in extruded compounds often survive the subsequent injection moulding process, as illustrated in Figure 2.17. Variations in machine conditions, in the manner described in Section 3.3.2.7, could be used to remove these integral strands as observed in Figure 3.55. However, comparison with materials moulded under the conditions described in Section 2.10 would no longer be valid. The moulding conditions used in the standard experiments were selected as being typical of those used commercially to manufacture such materials. Moulding of the glass fibre filled extrudates produced in this study presented no practical problems, although the 0.4 vol. fraction materials are considered to be the practical upper limit. These high volume fraction fibre reinforced composites showed pronounced discolouration and excessive fibre breakage throughout the compounding operations - Tables 3.8 and 3.26. Further evidence of this severe fibre fracture is provided by the results presented in Table 3.27, in which the higher glass content materials were diluted to 0.16 vol. fraction blends with Maranyl A100, prior to injection moulding. The fibre length trends for different glass content extrudates produced on the smaller 25 mm extruder show the reverse trend to the materials evaluated above, see Fig. 3.6. However, extrudates produced at glass contents higher than the 0.16 vol. fraction material were unsuitable for further processing due to the inability to process and chop the resultant extrudate lace. Such difficulties were caused by the pronounced "swelling" and aeration of the extruded material. Composite performance for the lower glass content materials is similar to that achieved on the larger extruder.

Processing of the higher molecular weight reinforced nylon 6.6 grades produces composites containing severely degraded fibres - Table 3.28. However, the pronounced matrix discolouration, which accompanies the viscosity increases associated with increased glass loadings, is not observed. The size levels in these materials are approximately 0.5% by weight in contrast to 1.2% by weight in the 0.40 fibre vol. fraction composites. Therefore, it is the fibre sizing component which is presumably responsible for the poor colour in these higher glass content materials. These cationic sizing polymers, however, provide enhanced adhesion to the matrix polymer in the dry state as indicated in Table 3.32. Therefore, if high glass contents are a requirement, coupled with an aesthetic appearance, then degradation of these size materials must be prevented. In processing terms, the melt feeding process possibly provides the solution to such problems due to the lower residence times and reduced shear conditions prevailing. The observed divergence in the recovered composite fibre lengths with increasing glass levels is illustrated in Figure 3.53. These trends apply to extruded materials previously processed by the two routes and would suggest the possibility of achieving more efficient fibre utilisation in these higher glass content composites. However, it is unlikely that such glass levels could be introduced via the side screw arrangement discussed in Sections 2.6 and 3.2 and thus alternative techniques of introducing the fibres are probably required.

4.4 Composite properties

4.4.1 Tensile failure modes

In addition to the variables discussed in Section 4.1, the chemical interaction of the fibre sizing components and the matrix polymer introduces a further complication. The changes in melt viscosity, discussed in Section 3.3.1 and illustrated in Table 3.21

and Figure 3.44, indicate significant reductions in molecular weight for the polymer containing the polyvinyl acetate sized material, at all levels of addition. In contrast, reduced melt flow properties accompany the presence of relatively high levels of the cationic poly-electrolyte. In both instances, however, severe embrittlement of the matrix is observed, although as indicated in Table 3.20, the polyvinyl acetate size produces the more significant changes. Such embrittled behaviour of the polyamide matrix is in accord with the observations of other workers (96) (110). The fibre sizing materials used by Bader et. al. (96) are chemically similar to those used in this study and thus, whilst a thermal degradative mechanism is a distinct possibility for the base material, chemical degradation appears a more credible alternative for the glass filled systems.

Vacuum dried test coupons, containing fibre volume fractions in excess of 0.047, possess tensile failure strains below those of the matrix material or the as made glass fibres - see Table 3.26 and Figure 3.59. The actual failure strain is seen to decrease with progressive increases in the fibre loading. Consideration of Table 3.25 indicates that composites reinforced with the polyvinyl acetate sized fibres show significantly reduced strains to failure over equivalent composites prepared from the cationic sized fibres. Materials possessing such reduced failure strains are considered to fail by a matrix cracking mechanism arising from stress intensification at fibre ends or cross-over points (96) (114). For low volume fractions of fibre, increased failure strains and ductile behaviour are observed and thus fibre fracture is possibly responsible for composite failure, particularly for those materials containing cationic sized fibres in which the interfacial bond strength is relatively high.

For composites conditioned by immersion in boiling water for 72 hours, two distinct failure processes again appear to be operative:-

(i) $V_f < 0.23$

Composite failure strains for the cationic sized fibres invariably exceed the fibre breaking strain, - Table 3.26. Immediately prior to failure pronounced matrix crazing is observed as illustrated in Figures 3.56 (a) and (b). Such effects, coupled with the observed poor adhesion illustrated in Figure 3.58, would seem to support a fibre debonding - matrix cracking mechanism. Confirmation of fibre debonding was obtained by microscopic examination of ground and polished sections.

(ii) $V_f \geqslant 0.23$

Failure strains are again below the fibre breaking strain and thus the effects of matrix plasticisation, resulting from absorbed water, would appear to be offset by the severe matrix embrittlement which accompanies such high fibre and size levels.

4.4.2 Ultimate tensile strengths

Both vacuum dried and 72 hour boil samples show improvements in tensile strengths with increasing fibre lengths and concentration. The overall property improvement is, however, controlled by the previous extrusion operation, coupled with the reduced failure strains which accompany increased fibre lengths and the matrix embrittlement discussed in the previous section. The presence of undispersed fibre bundles, in composites produced from extrudates prepared on the smaller extruder, cause a reduction in tensile strength for these materials. Considerable reductions in tensile strength also accompany the recycling of extrudates and the use of polyvinyl acetate sized fibres. These composite trends are discussed in Section 3.2 and are illustrated in Tables 3.22 to 3.29 and Figures 3.47 and 3.50.

4.4.3 Impact performance of reinforced composites

Impact strengths were determined using a Tinius Olsen impact machine. Specimens were tested in the Izod mode and were unnotched.

Typical results for vacuum dried and boiled samples are given in the above Tables and Figures 3.49 and 3.51.

For vacuum dried samples improvements in impact performance accompany increased fibre lengths for both fibre types. Composites containing the polyvinyl acetate sized fibres, however, show considerably lower impact strengths although for recycled materials such property differences are less pronounced - see Table 3.29. Improvements in aspect ratio, produced by reductions in filament diameters, are illustrated in Figure 3.46 and produce corresponding increases in both tensile and impact properties.

Increases in the level of glass fibres produce an initial reduction in impact performance, for vacuum dried materials, followed by an increase, ultimately reaching a maximum at a fibre volume fraction of approximately 0.23. For 72 hour boiled samples, however, the trend is quite different, a continuous reduction in impact performance occurring with increased glass additions. This divergence in impact performance after conditioning in boiling water is also observed for the 0.16 volume fraction materials. In these instances, increases in impact strength are observed for reductions in fibre length, although impact levels are generally reduced over the vacuum dried materials. However, for the recycled materials and composites produced by dilution of the original high glass content extrudates, boiled impact values are generally higher than the original dry specimens.

Definite improvements in dry impact values are achieved for the melt fed materials although, as expected from the above discussion, wet impact properties are reduced over the conventional extruded materials.

4.4.4 0.5% Tangent moduli

Values obtained in this study are presented in Tables 3.22 to 3.29 and Figures 3.47 and 3.52. The trends are similar to those

observed for the ultimate tensile strengths discussed in Section
3.2 and 4.4.2. Definite improvements in dry and wet values are
again achieved for the melt fed materials. The slight upward
curvature for the moduli plots presented in the above Figures can
be explained by the increase in fibre alignment predicted in Figure
3.48.

4.5 Conditioning of composites prior to testing

The dependence of mechanical properties on absorbed moisture
content highlights the requirement for accurate conditioning of
these hygroscopic materials. Composites prepared during this
study were tested under two environmental extremes which, while
accentuating property differences, are highly unlikely to be
encountered in actual use. However, the time span required for
equilibration of atmospherically conditioned specimens is of such
a magnitude as to render a systematic study of this type impractical
(130). Typical results obtained by the above author for reinforced
nylon 6.6, containing 0.16 volume fractions of MSS 1640 sized fibres,
are illustrated in Figure 4.2. Obviously, the total absorbed
moisture level and equilibration time will vary with the relative
humidity, specimen dimensions, glass fibre levels and orientation
respectively.
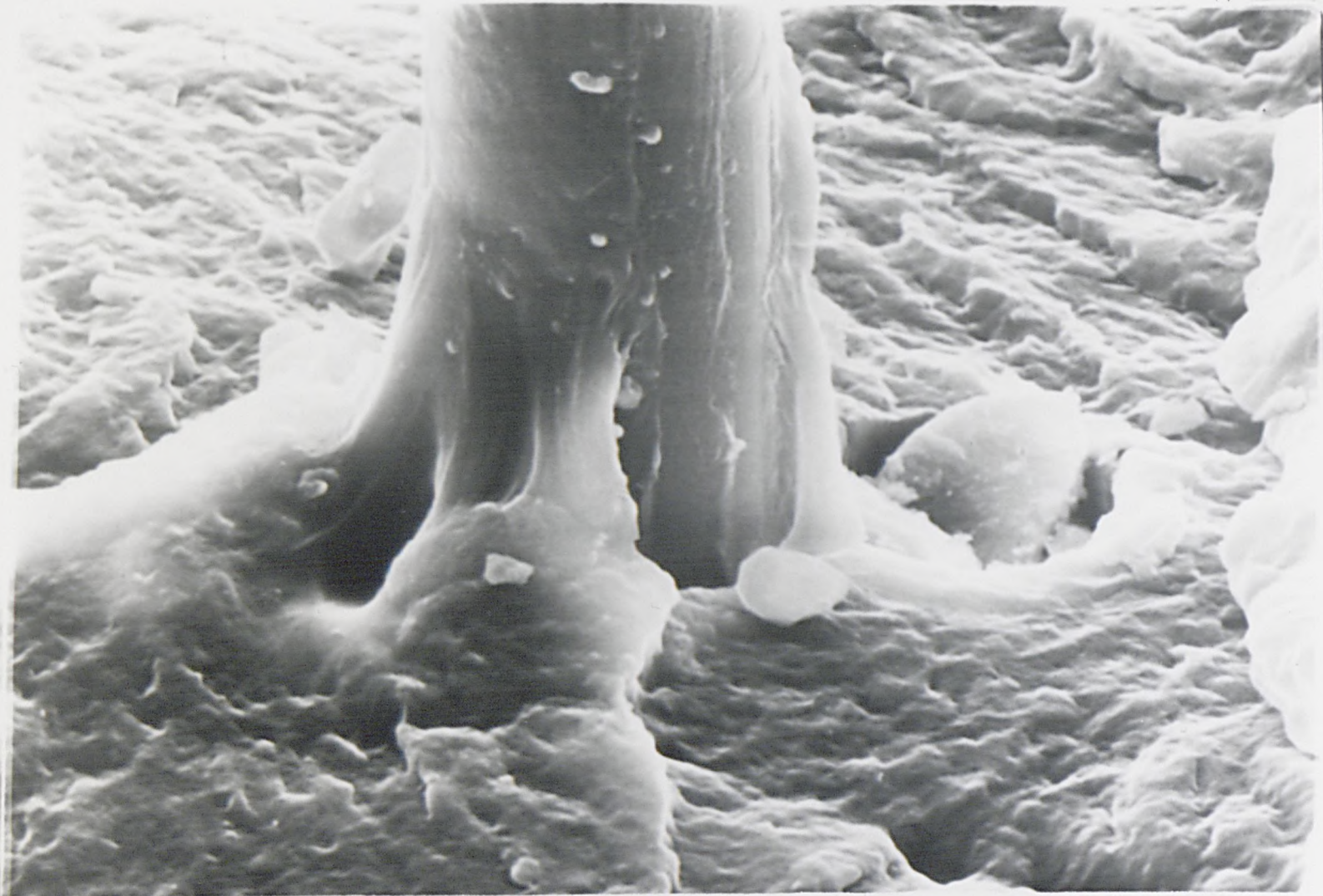
Figure 4.1 fibre-matrix adhesion in vacuum dried composites
mag.=5000×
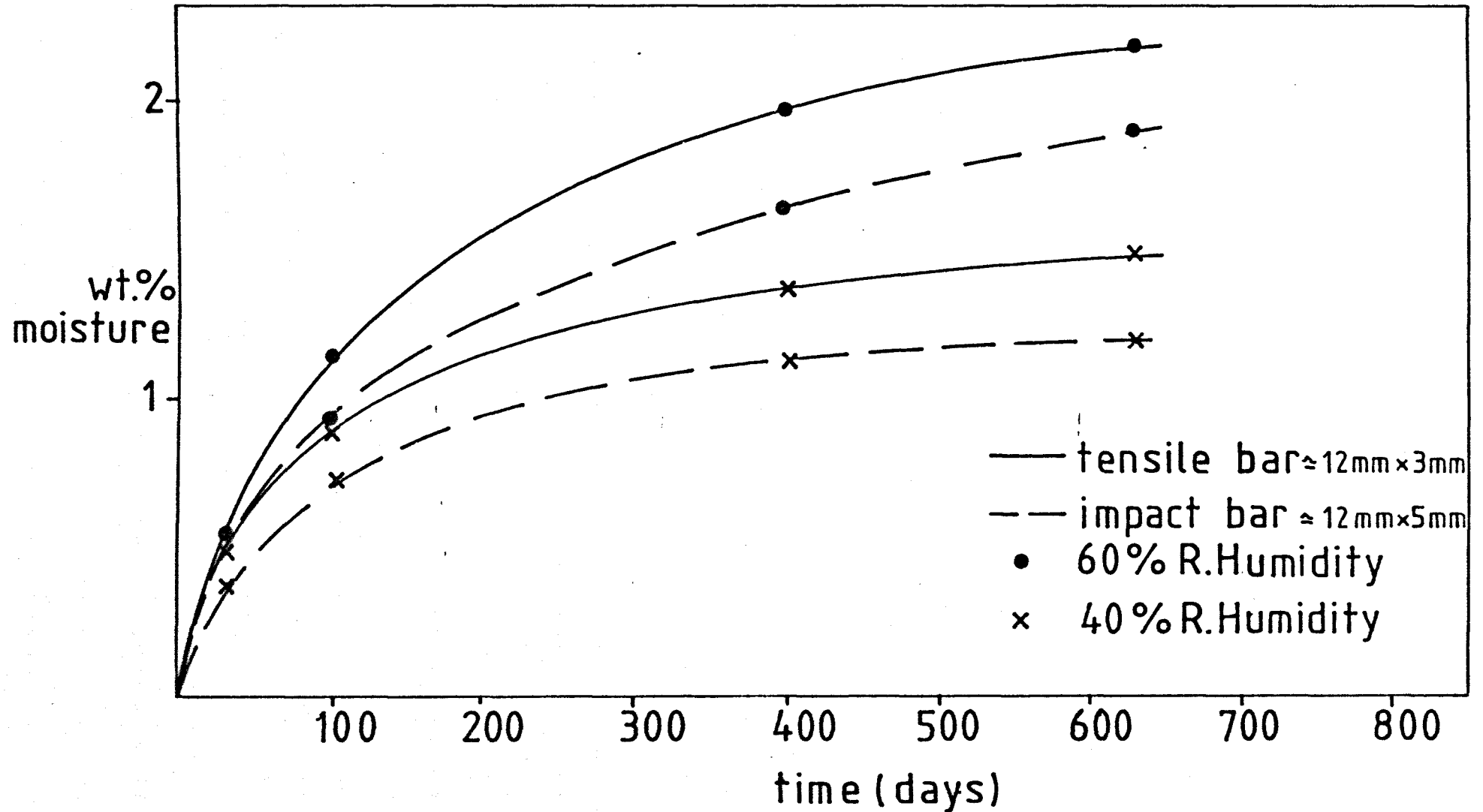
Figure 4.2 wt.% moisture absorbed v relative humidity

CHAPTER 5   CONCLUSIONS AND SUGGESTIONS FOR FUTURE WORK

5.1   Conclusions

5.1.1   Considerable fibre fracture occurs during the extrusion compounding and injection moulding processes used to manufacture short fibre reinforced nylon 6.6 composites.

5.1.2   Design, processing and material variables show significant effects on the extrusion compounding performance and degree of fibre fracture observed in this initial processing stage. Fibre breakage increases with screw speed, compression ratio and melt viscosity. Increases in melt viscosity are achieved by increased fibre loadings or by the use of higher molecular weight grades of nylon 6.6.

5.1.3   The melting region is shown to be the source of predominant fibre fracture in the single screw plasticating extrusion process used to compound short glass fibre - nylon 6.6 'tumble' blends. This melting stage commences approximately three to four turns into the feed zone and, under optimum conditions, is completed at the primary compression step for the rapid transition screws used in this study. The solid and molten materials existing in the screw channels are observed to segregate and hence occupy precise locations relative to the screw flights. Fibre length and X-ray analyses indicate the presence of undispersed fibre bundles in the solid bed region of the channel. The melt pool region, however, contains largely dispersed monofilaments, the fibre length distribution being almost superimposable with that of the resultant extrudate. The observed occurence of solid bed fracture, which occurs in the vicinity of the primary transition step, leads to undispersed fibre bundles in the resultant extrudate and generates instabilities in the extrusion process.

5.1.4   Different fibre types influence the processing stability and resultant fibre dispersion, due to the change in bulk density which accompanies variations in strand integrity.

5.1.5 Undegraded fibre bundles produced in this process often survive the subsequent injection moulding operation leading to surface imperfections and reduced mechanical performance of the resultant composite.

5.1.6 The use of a melting model, developed for unreinforced thermoplastics, enables correlations between melting performance and fibre fracture to be established. Ultimately, such a model can be used to design screw geometries suitable for the processing of a particular fibre - polymer blend. However, since efficient melting of the thermoplastic is the prime requirement of these machines, then excessive fibre fracture is unavoidable if the glass fibres are present in this melting stage.

5.1.7 X-ray radiographic analysis enables the observation of undispersed fibre bundles in extruder channel melting sections and injection moulded composites. For the latter materials a Quantimet image analysing computer provides a means of assessing the fibre dispersion.

5.1.8 A wet sieving technique is described which provides improvements in the classification of fibre lengths. Such a technique enables the observation of fibre length changes which occur during the extrusion and injection moulding processes.

5.1.9 The use of a modular pen counting system facilitates the rapid measurement of fibre length and largely removes the tedium usually associated with such measurements.

5.1.10 Introduction of the glass fibres into the molten polymer produces significant improvements in retained fibre lengths. The presence of undispersed fibre bundles is prevented by the inclusion of a standard mixing element into the extruder screw profile.

5.1.11 Mechanical properties of the injection moulded composites reflect the previous extrusion history and fibre parameters.

Improvements in tensile strength and modulus for both vacuum dried and 72 hour boiled materials, accompany increased glass loadings and fibre aspect ratios. Reductions in the primary compression ratio of the extruder screw can produce composite improvements if the residual fibre bundles can be dispersed without increasing the severity of the subsequent moulding process.

Impact performance is seen to be dependent on the conditioned state of the specimen. Dry impact strengths increase with increased fibre aspect ratio and glass content, after a significant reduction at low glass levels. Maximum properties are achieved at a fibre volume fraction of 0.23. However, all the fibre containing materials fail in a brittle manner at values generally below that of the matrix polymer. Wet impact strengths indicate a continuous fall with increasing glass concentration and increased fibre length. Melt fed materials exhibit an overall dry property enhancement over conventionally extruded compounds although again wet impact performance is reduced for these longer fibre length materials.

5.1.12 Chemical interaction of the fibre sizing materials with the matrix polymer produces embrittlement and reduced impact performance in the unreinforced matrix. Such embrittlement would explain the reduced failure strains in the glass fibre reinforced materials. For both dry and boiled specimens, composite tensile failure strains are below those of the as made glass fibres, at fibre volume fractions in excess of 0.16. Failure strains decrease with increased fibre length and increased fibre volume fractions. These effects tend to limit the tensile property improvement which would be expected from improved fibre lengths in the moulded materials.

The improved ductility of the composites produced from the higher molecular weight grades of nylon 6.6 leads to enhanced failure strains

and improved impact properties. The loss in tensile performance expected from the increased fibre fracture is partially offset by the increased failure strains which extend the permissible stress levels prior to composite failure.

5.2 Suggestions for future work

5.2.1 The suitability of the various distributive mixing elements, presently supplied for the low shear mixing of unreinforced polymers, should be assessed for fibre reinforced materials.

5.2.2 The chemistry of the interaction of fibre sizing polymers and the matrix polymer should be established and alternative systems developed.

5.2.3 The fibre length techniques developed are already finding application in other materials such as Reinforced Reaction Injection Moulded compounds. These studies should be extended to ascertain the best fibre sizing materials required to maintain optimum fibre length, whilst still providing adequate adhesion in these liquid monomer and thermoplastic polymer melt compounding processes.

REFERENCES

1. Milewski, J.V., and Katz, H.S., Handbook of Fillers and Reinforcements for Plastics. p. 468-469, Van Nostrand Reinhold Company, 1978.

2. Rapra Survey March 1978, European Plastics News.

3. Ogoriewicz, R.M., Thermoplastics, Properties and Design, John Wiley & Sons, London 1974.

4. Quinn, J.A., Fibreglass Limited, Design Data for Composites.

5. Johnson, A.E., and Lunt, J.M., New Coupling Concepts for Glass-Reinforced Nylon. Modern Plastics, July 1976.

6. Werner and Pfleiderer, K.S., Information Brief Report, No. 8.

7. Fisher, E.G., Extrusion of Plastics. Plastics & Rubber Inst. Monograph 1976.

8. Gray, M., Br. Patent, 5056 (December, 1879).

9. Menges, G., and Lutterbeck, J., Plastics & Rubber Int. March/April, 1979.

10. Richards, R.W., and Sims, D., Composites, December, 1971.

11. British Patent 618094.

12. U.S. Patent 2,877,501.

13. Dr. Ing. Wolf-Dietrich Mahler, Darmstadt Kunststoffe, 67 (1977), 4 p. 224-226.

14. Bernhardt, E.C., Processing of Thermoplastic Materials, Reinhold, New York, S.P.E. Monograph (1959).

15. Fenner, R.T., Extruder Screw Design, Plastics Inst. Monograph, 1970.

16. Tadmor, Z., and Klein, I., Engineering Principles of Plasticating Extrusion. Van Nostrand Reinhold, 1970.

17. Irvin, I., Rubin, Injection Moulding Theory and Practice, John Wiley & Sons, 1972.

18. Fenner, R.T., Developments in the Analysis of Steady Screw Extrusion of Polymers. Polymer, 1977, Vol. 18.

19. Fenner, R.T., Computer Aided Design of Extruder Screws. Plastics & Rubber International January/February, 1978.

20. Broyer, E., and Tadmor, Z., Solids Conveying in Screw Extruders. Polymer Engineering and Science, January, 1972, p. 12-24.

21. Tadmor, Z., Duvdevani, I.J., and Klein, I., Ibid., 7, 198 (1967).

22. Kaoir, L., and Tadmor, Z., Solids Conveying in Screw Extruders, Part III, The Delay Zone, Polymer Engineering and Science, September 1972.

23. Edmondson, I.R., and Fenner, R.T., Polymer, 16, 49 (1975).

24. Fenner, R.T., Principles of Polymer Processing, Macmillan, London (1979).

25. Martin, G., The Determination of Melting Zone Length in a Single Screw Extruder, Kunststoffe Technik, 7, 238 (1969) Rapra Translation No. 1716.

26. Donovan, R.C., Pressure Profiles in Plasticating Extruders, Polymer Engineering and Science, 11, 484, (1971).

27. Edmondson, I.R., Ph.D. Thesis, London University 1973.

28. Fenner, R.T., Cox , A.P.D., and Isherwood, D.P., Surging in Screw Extruders, Polymer 1979, Vol. 20.

29. Street, L., Extrusion Plastification, International Plastics Eng. 1, 289, (1961).

30. Menges, G., and Klenk, P., Kunststoffe, 1967, 57, 598.

31. Gale, G.M., Plast. Polymer, 1970, 38, 183.

32. Lindt, J.T., Polymer Engineering and Science, 1976, 16, 284.

33. Moskal, E.A., Interaction of H.D.P.E. and Discontinuous Fibreglass Reinforcement during Extrusion Processing, Fiberglas Canada Limited.

34. Maddock, B.H., Modern Plastics, April 1957, 34, 123.

35. Danckwerts, P.V., Appl. Sci., Res.(A) 1953, 3, 279.

36. McKelvey, J.M., Polymer Processing, Wiley, New York 1962.

37. Maddock, B.H., SPE J., 1967, 23, 23.

38. Braun, K.J., and Helmy, H.A., Single Screw Extruder - Developments, Design Trends and Limitations, International Conference of Polymer Extrusion, P.R. I., 27/28 June, 1979.

39. Mohr, W.D., Saxton, R.L., and Jepson, C.H., Ind. Eng. Chem. 49, 1855 (1957).

40. Schumann, The Glass Fibre Reinforced Thermoplastics Market in Europe:- Volume and Application.

41. Schlich et. al. Critical Parameters for Direct Injection Moulding of Glass Fibre Thermoplastic Blends. S.P.E. Journal, February, 1968, Vol. 24.

42. Filbert, W.C., S.P.E. Journal, January 1969.

43. Yang, H.W.H. et al. Study of the Effect of Regrinding on the Cumulative Damage to the Mechanical Properties of Fiber - Reinforced Nylon 6.6. Journal of Applied Polymer Science, Vol. 23, 3375-3382 (1979).

44. Aveston, J., Cooper, G.A., and Kelly, A., The Properties of Fibre Composites, I.P.C., Science and Technology Press, 1971, p. 15-26.

45. Pennington, D., Ph.D. Thesis, 1979.

46. Kelly, Strong Solids 2nd Edition, Clarendon Press, 1973.

47. Broutmann and Krock. Modern Composite Materials - Addison and Wesley Publishing Co., 1967.

48. Cox, H.L., Br. J. Applied Physics, 3 (1952), 72..

49. Dow, N.F. G.E.C. Missile and Space Division Report No. R635D61.

50. Rosen, B. Walter, Fiber Composite Materials Chapter 3, A.S.M. Publication.

51. Fujiwara (McGarry)., Mod. Plastics, <u>45</u> 11 (1968) 143.

52. Outwater, J. Ogden., Jr. (1956). Modern Plastics, March p. 56.

53. Kelly, A., and Tyson, W.R., J. Mech. Phys. Solids, 13 No.6, 329.

54. Piggot, M.R., Acta Metallurgica, Vol. 14, 1966, p. 1429.

55. Lees, J.K., Polym. Eng and Sci., Vol. 8, No. 3 (1968), p. 195.

56. Neilson and Chen, J., Materials, <u>3</u>, 352, June 1969.

57. Bader, M.G., and Curtis, P.T., Strength and Failure Modes in Short Fibre Reinforced Thermoplastics. TMS-AIME Fall Meeting, Chicago, October 1977.

58. Kelly, A., and Davies, G., Metallurgical Reviews, 10, No. 37, 1965.

59. Krenchel, H., Fibre Reinforcement, Akademisk Forlag, Copenhagen, 1964.

60. Karpov, V., and Kaufmann, M., Brit. Plastics, <u>38</u>, 498, (1965).

61. Kaliske, G., and Seifert, H., Plaste. U. Kaut, 20, (1973).

62. Darlington, M.W., et. al. J. Mat. Sci., 10, 906, (1975).

63. Goettler, L.A., Mod. Plast. (U.S.) 47, 140, (1970).

64. Darlington, M.W., et al. J. Mat. Sci., 11, 877, (1976).

65. Thomas, R., and Meyer, D.E., R.P.G., 4th Conf. Feb. 1976, Paper 9.

66. Metcalfe, P.J., and Hull, D., R.P.G. 4th Conf. Feb. 1976, Paper 8.

67. Johnson, A.E., Pilkington confidential report FT/79/16.

68. Bader, M.G., and Bowyer, Composites, <u>4</u>, p. 150, (1973).

69. Williams, et. al. S.P.I. 23rd Conf., 1968, Section 2C.

70. Ramsteiner, F., and Theysohn, R., Composites, April 1979. p. 111-119.

71. Burns, R., et. al. S.P.I. 29th Conf. 1974, Section 20A.

72. Endter, F., and Gebauer, H., Optik, 13, 1956, p. 97-101.

73. Sawyer, L.C., S.P.I., 33rd Conf. 1968, Section 20C.

74. MOP/AMO3, Modular Image Analysis System - Reichert Jung, U.K. (Agents, American Optical).

75. B.S. 2782: 1970 Methods 501A and 501B.

76. A.S.T.M. D 1895-67.

77. Nelson, W.E. Nylon plastics technology, P.R.I. Monograph 1976.

78. Barker, R.S., Transactions of the Society of Glass Technology, 1958, Vol. XLII pp. 101-108.

79. Wolf, D., and White, D.H., "Experimental Study of the Residence Time Distribution in Plasticating Extruders". Am., Inst. Chemical Engineering Journal, 22, 122-131 (1976).

80. Private correspondence D.P. Pimblett and M. Lyon, Pilkington Brothers Limited.

81. British Plastics, "Injection Moulding of Glass Reinforced Nylon". May 1969 pp. 89-92.

82. Rank Precision Industries Limited, Meterology Division, Leicester.

83. Zimmermann, H., Faserforch Textilech, 17, 228 (1966).

84. Korshak, V.V., et al. Acta. Physics U.S.S.R. 21 723 (1946).

85. Merz, E.H., and Colwell, R.E. "A High Shear Rate Capillary Rheometer for Polymer Melts". A.S.T.M. Bulletin, September 1958.

86. Bagley, E.B.," End Corrections in the Capillary Flow of Polyethylene" J. Appl. Phys., 28, 624, (1957).

87. Rabinowitsch, B.Z., Physik, Chem. A145, 1 (1929).

88. Ives, G.C., et al. Handbook of Plastics Test Methods. Plastics Institute Publication, 1971.

89.   Cameron, N.M. "An Investigation into the effects of
       Environmental Treatments on the Strength of E-glass Fibres",
       Univ. of Illinois, T and AM Report No 274, Contract No.
       NOw 64-0178-d, January, 1965.

90.   Thomas, W.F., Glass Technology, Vol. 12 No 3, June 1971,
       p. 60-64.

91.   Lindsay, E.M. and Hood, J.C., "Final Report on Glass
       Reinforcements for Filament Wound Composites". Owens
       Corning Fibreglas Corp., TR-63-8-104, Contract No. AF 33
       (657)-9623, 1963.

92.   Thomas, W.F., Glass Technology, Vol. 13, No. 5, October,
       1972. p. 141-144.

93.   Tadmor, Z., and Gogos, G.C., "Principles of polymer
       processing", S.P.E. Monograph 1979.

94.   Johanson, J.R., "Feeding" Chem. Eng., 75-82, 1969.

95.   I.C.I. Technical Service Note N104.

96.   Curtis, P.T., Bader, M.G., Bailey, J.E., J. Mat. Sci.
       13 (1978) 317 - 390.

97.   Cox, A.P.D., and Fenner, R.T., "Experimental comparisons
       of extruder screw performance", Plastics and Rubber
       Processing, Sept. 1978.

98.   Marshall, D.I., and Klein, I., Polym. Eng. Sci., 1966,
       6, 191.

99.   Klein, I., and Marshall, D.I., Polym. Eng. Sci., 1966,
       6, 198.

100.   Hinrichs, D.R., and Lilleleht, L.U., Polym. Eng. Sci.,
       1970, 10, 268.

101.   Vermeulen, J.R., Scargo, P.G., and Beek, W.G.,
       Chem. Eng. Sci. 1971, 26, 1457.

102. Shapiro, J., Halmos, A.L., and Pearson, J.R.A., Polymer, 1976, 17, 905.

103. Shapiro, J., Halmos, A.L., and Pearson, J.R.A., Polymer, 1976, 17, 912.

104. Martin, B., Int. J. Non Linear Mech. 1967, 2, 285.

105. Whybrew, K., "The effects of flow on the strength of polyester dough moulding compounds" Ph.D. Thesis 1972.

106. Bright, P.F., et. al. "A study of the effect of injection speed on fibre orientation in simple mouldings of short glass-fibre filled polypropylene", J. Mat. Sci., 13, (1978), 2497-2506.

107. Cogswell, F.N., I.C. I. Plastics Division, Private correspondence.

108. Englehardt, J.T., Krautz, F.G., Philipps, T.E., Preston, J.A., Wood, R.P., "The influence of reinforcements on strength and performance of fibreglass reinforced thermo-plastics". S.P.I. 22nd Annual Meeting.

109. Bessell, T.J., Hull, D., Shortall, J.B., "The effect of polymerisation conditions and crystallinity on the mechanical properties and fracture of spherulitic nylon 6". J. Mat. Sci. 10 (1975) 1127-1136.

110. Curtis, P.T., Ph.D. Thesis 1976, "The strength of fibre filled thermoplastics."

111. Jackson, J.R., "Acoustic emission in glass fibre reinforced plastic composites" Pilkington confidential report no. FT/79/7.

112. Bessell, T., and Shortall, J.B., "The crystallisation and interfacial bond strength of nylon 6 at carbon and glass fibre surfaces". J. Mat. Sci. 10 (1975), 2035-2043.

113. Kamerbeek, B., Kroes, G.H., and Grolle, W., "Thermal degradation of some polyamides" S.C.I. Monograph No.13, (1961).

114. Bowyer, W.H., and Bader, M.G., Reinforcement of thermoplastics using carbon fibres Faraday Spec. Disc. 1972.

115. McNally, D., Freed, W.T., Shaner, J.R., and Sell, J.W., "A method to evaluate the effect of compounding technology on the stress transfer interface in short fiber reinforced thermoplastics". Polym. Eng. and Sci. April, 1978, Vol. 18, No. 5.

116. Bowyer, W.H., Bader, M.G., "On the reinforcement of thermoplastics by imperfectly aligned discontinuous fibres", J. Mat. Sc i. 7 (1972) 1315-1321.

117. Therberge, J.E., and Hull, N.T., Mod. Plast. 46 p. 114, (1969).

118. Kaliske, G., and Seifert, H., "Ways in which fibre decomposition can be influenced in the spraying of glass fibre reinforced thermoplasts". Plaste and Kautschuk Vol. 22 9/1975.

119. "Reinforced Thermoplastics - a moulders view" Anon.

120. Fenner, R.T., and Nunn, E.R., "Reciprocating screw plastication", unpublished.

121. Berry, J.P., and Stanford, J.L., "Time - temperature - moisture effects on the mechanical properties of glass reinforced nylon 6.6" Reinforced thermoplastics II, 9-10, Nov. 1977.

122. Parrat, J.N., Rubber Plast. Age, 41, p. 263 (1960).

123. Coleman, B.D., J. Mech. Phys. Sol. 7 p. 60 (1958).

124. Tyson, W.R., and Davies, G.J., Brit. J. App. Phys. 16 p. 199 (1965).

125. Mullin, J., Berry, J.M., and Gatti, A.J., Comp. Mat. <u>2</u>
     p. 82 (1968).

126. Holister, G.S., and Thomas, C., Fibre Reinforced Materials,
     Elsevier Publishing Co. Ltd. 1966.

127. Stade, K.H., "New achievements in compounding Glass fiber -
     Reinforced Thermoplastics" Reinforced Thermoplastics
     Symposium, Plastics Inst. April, 1975.

128. Lovegrove, J.G.A., "The Importance of the feeding Zone"
     P.R.I. International Conference, Polymer extrusion 27/28,
     June 1979.

129. Yagi, S., and Kunii, D., A.I. Ch. E.J., 3, 373 (1957).

130. Lyon, M., Pilkington confidential report FT/80/13.

APPENDIX 1 - DETERMINATION OF INTERLAMINAR SHEAR STRENGTH - PUNCH SHEAR TEST

1. ## Object

   To determine the interlaminar shear strength of thermoplastic materials.

2. ## Test Apparatus

   2.1 Instron Universal Testing Instrument:-

   Tension/Compression load cell:- 2511 - 318

   2.2 Punch Shear Jig:-

PLUNGER
6·35mm φ × 25mm

INSERT
19·03mm φ × 12mm

SAMPLE

JIG BODY
32mm φ × 20mm
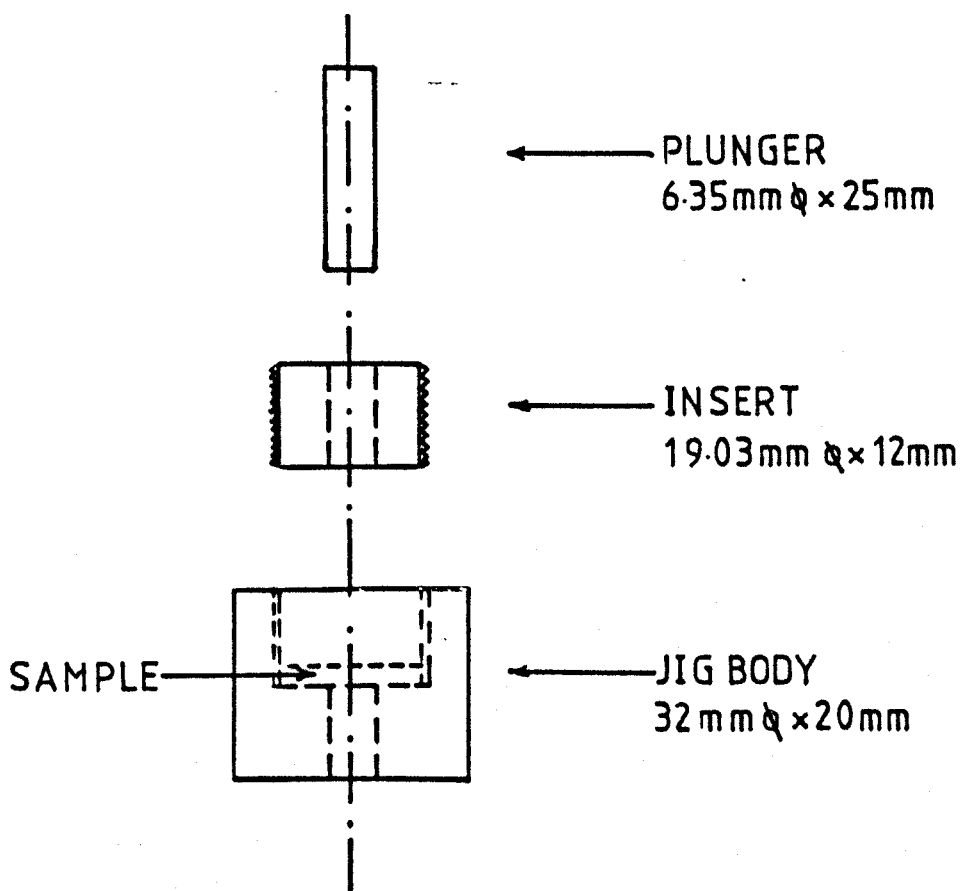
3. ## Form of Test Specimen

   Specimens should be cut from the injection moulded article so as to fit comfortably in the test jig. For tensile bars, samples 12 mm x 12 mm, cut from the parallel portion, are convenient.

4. ## Number of Specimens

   At least five specimens should be prepared, taken from different samples moulded in the same series.

5. Speed of Test

Instron crosshead speed = 2.0 cm/min.

6. Procedure

6.1 The sample should be conditioned prior to testing by vacuum drying for 16 hours at 90°C or boiling for 72 hours in water.

6.2 The test is carried out with the Instron in the compression mode.

6.3 The cross-head travel should be set such that the maximum plunger movement is just sufficient to penetrate the sample.

6.4 The specimen thickness is accurately determined. The sample is placed in the jig and the jig assembled such that the plunger just contacts the surface of the specimen.

6.5 The maximum load achieved during testing is recorded from the Instron chart.

6.6 Repeat steps 6.4 to 6.5 for the remaining specimens.

The interfacial shear strength is given by:-

$$T = \frac{F}{T.\pi D} \times 10^{-6} \; MPa.$$

where F = force in Newtons

and D = plunger diameter = 6.35×10^{-3} metres

T = sample thickness in metres .

APPENDIX 2 - MEASUREMENT OF APPARENT BULK DENSITY

1. **Object**

    To determine the apparent bulk density (A.B.D.) of short

fibre - polymer 'tumble' blends.

2. **Apparatus**

    2.1 Jolting Volumeter:- Model JELST2, manufactured by

J. Englesmann, A.G. Ludvigschafen a Rh. Germany. Operates at

250 falls/min. from a height of 3.0 $\pm$ 0.2 mm.

    2.2 Graduated glass measuring cylinder, 250 cm^3 capacity

graduated to 2 cm^3. External diameter should be about 25 mm

and its mass 220 $\pm$ 40 grams.

    2.3 Metallic or plastic piston of diameter slightly smaller

than the internal diameter of the cylinder and weighing 5.0 $\pm$

0.5 grams.

3. **Sample Weight**

    150 grams of chopped strands and 350 grams of Polymer

pellets are tumble blended for 3 minutes $\pm$ 5 seconds to produce

a 30% by weight blend. These weights can be adjusted to

produce other concentrations of fibres to polymer. 60 grams of

the mixture is taken for testing.

4. **Number of Specimens**

    At least five samples of the blended material are taken.

5. **Time of Test**

    1 minute, equivalent to 250 falls.

6. **Procedure**

    6.1 Place the measuring cylinder on a balance and carefully

weigh 60 grams of sample into the cylinder.

    6.2 Gently place the cylinder into the holding fixture of

the Jolting Volumeter and tighten the holding fixture. Place the

piston in the cylinder.

6.3 Zero the counter by turning the right hand handle on the revolution counter in a clockwise direction.

6 4 Bring the left hand handle of the counter down to position A.

6.5 Set the counter to 250 falls.

6.6 Return the left hand handle of the counter to position B and switch on the counter.

6.7 After 250 falls have been completed, record the level to the nearest 1 cm^3..

6.8 Discard this sample and repeat steps 6.1 to 6.8 for the remaining four samples.

The apparent bulk density is given by:-

$$A.B.D. = \frac{W}{V} \times 10^3 \; Kg. \; m^{-3}$$

where W = sample weight in grams

V = final volume in cm^3

APPENDIX 3 - FIBRE LENGTH DISTRIBUTION BY THE WET SIEVING TECHNIQUE

1. Object

To determine the fibre length distribution of extracted fibre samples.

2. Apparatus

2.1 38 mm diameter sieves comprising apertures:- 4.0 mm, 2.80, 1.40, 0.710, 0.310, 0.150, 0.075, 0.045 mm.

2.2 250 cm^3 measuring cylinder.

2.3 Vitrosil or nickle dish.

2.4 Filter papers.

2.5 Buchner flask.

2.6 P.V.C. tape.

2.7 Microscope slides, 76 x 51 mm.

2.8 Polaroid camera mounted on a transmission microscope having a magnification range of 4 to 100X.

2.9 Ultrasonic bath.

2.10 Xerox copying machine.

2.11 Zeiss particle size analyser or MOP/AMO3 modular pen system.

3. Specimen Extraction

3.1 Cut a sample 1 cm. either side of the fracture surface of a tensile bar. For extrudates take approximately 3 grams of sample.

3.2 Accurately weigh the sample dish and then reweigh with the sample.

3.3 Place the sample in a muffle furnace at $610^{\circ} \pm 10^{\circ}$C and leave for 30 minutes.

3.4 Remove the container and sample and allow to cool to room temperature before reweighing.

3.5 Calculate the glass content.

Note: At least two samples should be taken for this stage.

4. Sieving Procedure

4.1 Assemble the sieve stack using the required combination of sieves, arranged in descending mesh sizes.

4.2 Seal the edges of the sieves by binding with P.V.C. tape.

4.3 Place the stack into the fines receiver and again seal with P.V.C. tape.

4.4 Flush through with water and then close the base tap and allow the stack to fill until the water level is approximately 3.0 cms above the top sieve.

4.5 Accurately weigh 0.2 ± 0.02 grams of fibres into a 250 cm^3 measuring cylinder containing 50 cm^3 of water, taking care not to damage the fibres. Wash any fibres off the sides of the cylinder with 20 cm^3 of water.

4.6 Set the water flow rate through the sieve stack at approximately 100 cm^3/min. by means of the base tap, and place a suitable container below the stack to collect the fines.

4.7 Decant the dispersed fibres into the sieve stack at such a rate as to maintain a constant water level above the top sieve. Add additional water to the measuring cylinder in 50 cm^3 aliquots and decant into the stack until no dispersed fibres remain.

4.8 Add a further 100 cm^3 of water to the measuring cylinder and place the cylinder in an ultrasonic bath for approximately 30 seconds to disperse any integral fibre bundles remaining in the cylinder. Decant this material into the sieve stack as before. The total sieving process should take approximately ten minutes.

4.9 When all the fibres have been added allow the water level to fall until the stack is empty.

4.10 Collect the fines which have passed through the sieve by filtering onto a weighed filter paper, using a Buchner flask.

4.11 Dismantle the sieve stack and place the sieves and filter paper in an air oven, maintained at $90 \pm 5^{\circ}C$, for 15 minutes, or until constant weight is achieved.

4.12 Remove the sieves and filter paper from the oven and allow to cool to room temperature.

4.13 Weigh each sieve and filter paper and then disperse the individual fractions in isopropanol and cast onto microscope slides.

4.14 Reweigh the sieves and determine the total sample weight recovered. If this weight is less than 95% of the original sample then the analysis must be repeated.

4.15 Photograph the fibres at a suitable magnification such that no fibre exceeds 27.7 mm or is below 1 mm in length.

4.16 Photocopy the resultant photographs using the Xerox copier and retain the original photographs.

4.17 Draw a perimeter on each photocopy such that no fibres crossing the boundaries of the original photograph are cut by the perimeter.

4.18 Determine the fibre length distributions for each fraction using the Z.P.S.A. or MOP/MO3 counting systems. Fibres crossing the perimeter on the top and left hand sides are included in the fibre count, whereas those entering at the bottom and right hand side are omitted.

4.19 Using the estabished computer programme determine the original fibre length distribution.

APPENDIX 4 SIEVE COMBINATION PROGRAMME

```
        ∇HIST[□]∇
     ∇ FR←HIST;WS;X;ANS;S;MG;A;CF;KWA;KNA;E;F;NA;WA;BANS
[1]    'INITGRAPH/CONTGRAPH/RETURN'
[2]    □←'□:'
[3]    ⍎E←□
[4]    'ALLOC/RETURN'
[5]    □←'□:'
[6]    ⍎E←□
[7]    'ENTER EXPT NO'
[8]    E←□
[9]    'HAVE COMMON BOUNDARIES CHANGED ?'
[10]   →((BANS←□)[1]='N')/F
[11]   'LOG OR LIN ?'
[12]   →(SCALE←((SCALE←□)[2]='I'))/B
[13]   '2000,3000,6000 OR 10000 MNS ?'
[14]   ANS←□
[15]   →(~∨/(2000,3000,6000,10000)=ANS)/7
[16]   ⍎(ANS=2000)/'K←79↑LK'
[17]   ⍎(ANS=3000)/'K←86↑LK'
[18]   ⍎(ANS=6000)/'K←98↑LK'
[19]   ⍎(ANS=10000)/'K←LK'
[20]   KL←⁻1↓K←K÷1000
[21]   KU←1↓K
[22]   Y←(L←10×⁻1↓(10⍟K)+0.5×(10⍟K)[2]-(10⍟K)[1])×1000
[23]   →L1
[24]   B:'ENTER LOWEST BOUNDARY'
[25]   M←□
[26]   'ENTER INTERVAL WIDTH'
[27]   I←□
[28]   'ENTER NUMBER OF INTERVALS'
[29]   K←M+I×0,⍳N←□
[30]   KL←⁻1↓K
[31]   KU←1↓K
[32]   Y←1000×L←⁻1↓K+0.5×K[2]-K[1]
[33]   L1:FR←NF←(⍴KL)⍴0
[34]   F:'HAS FIBRE WEIGHT CHANGED ?'
[35]   →((ANS←□)[1]='N')/Z
[36]   'ENTER WEIGHT OF FIBRE PER UNIT LENGTH'
[37]   WF←□
[38]   FR←NF←(⍴KL)⍴0
[39]   →W
[40]   Z:→(BANS[1]='Y')/W
[41]   'FREQUENCIES SET TO ZERO ?'
[42]   ANS←□
[43]   FR←(ANS[1]='N')×TF
[44]   ⍎(ANS[1]='Y')/'NF←(⍴KL)⍴0'
[45]   W:WRITE1 132
[46]   Q1:'ENTER SET OF FREQUENCIES'
[47]   →((⍴A←□)≠48)/Q1
[48]   Q2:'ENTER WEIGHT ON SIEVE'
[49]   →((WS←□)≥1)/Q2
[50]   Q3:'ENTER MAGNIFICATION FACTOR'
[51]   →((MG←□)<5)/Q3
[52]   WRITE2 132
[53]   CALC1
[54]   TF←FR
[55]   'ARE THERE ANY MORE SIEVES ?'
[56]   →((ANS←□)[1]='Y')/Q1
[57]   WRITEEND 132
[58]   FORMAT
[59]   CLTS E
[60]   E HISTP(3,⍴K)⍴K,F,0,CF,0
[61]   '    MID PT   PERCENT   CUM PERC'
     ∇

     ∇FROM[□]∇
     ∇ R←A FROM S;CL;CU;R1
[1]    CL←⁻1↓S
[2]    CU←1↓S
[3]    R←(KU∘.-CL)⌊(-KL)∘.+CU
[4]    R←R×R>0
[5]    R1←(⍴R)⍴CU-CL
[6]    R←R÷R1
[7]    R←(R>1)+R×R≤1
[8]    R←+/R×(⍴R)⍴A
     ∇
```

- 257 -

```
      ∇CLTS[□]∇
      ∇ CLTS TITLE;DD;LC;VF;B;R;X;FR1;FR2;ANS
[1]   FR1←⍕,FR[;⍳10] ACAT 1⍴' '
[2]   FR2←⍕,FR[;10+⍳10] ACAT 1⍴' '
[3]   ' '
[4]  L1:'ENTER DATA: SF SM TAU D VF K'
[5]   →L1×⍳(6≠⍴DD←□)
[6]   ' '
[7]   'CRITICAL LENGTH :',1↓LC←DD[4]×DD[1]÷2×DD[3]
[8]   VF←DD[5]×FR2÷100
[9]   B←LC≤FR1
[10]  R←+/DD[1]×(B/VF)×(1-LC÷2×B/FR1)
[11]  R←R++/((~B)/VF)×DD[3]×((~B)/FR1)÷DD[4]
[12]  R←(DD[6]×R)+(1-DD[5])×DD[2]
[13]  RANS←R
[14]  ' '
[15]  'TENSILE STRENGTH OF COMPOSITE :',2↑R
[16]  ' '
[17]  'SNAP AGAIN ?'
[18]  →((ANS←□)[1]='Y')/L1
[19]  ' '
      ∇

      ∇CALC1[□]∇
      ∇ CALC1
[1]   X←¯1↓S+0.5×S[2]-(S←C÷MG)[1]
[2]   WA←WS×A×X÷+/A×X
[3]   NA←A×WS÷(WF×+/A×X)
[4]   FR←FR+WA FROM S
[5]   NF←NF+NA FROM S
      ∇




      ∇FORMAT[□]∇
      ∇ FORMAT
[1]   KWA← 10 4 ⍕(+/NF×L×L)÷+/NF×L
[2]   KNA← 10 4 ⍕(+/NF×L)÷+/NF
[3]   CF←100-+\FR←100×FR÷+/FR
[4]   F←FR
[5]   FR←((3×⍴KL),10)⍴((⌈(3×⍴KL)÷13),130)⍴(10 2 ⍕Y),(10 4 ⍕FR,CF),500⍴
      ' '
[6]   FR←FR[⍳⍴KL;],FR[(⍴KL)+⍳⍴KL;],FR[(2×⍴KL)+⍳⍴KL;]
[7]   ' '
[8]   'EXPT NO   ',E
[9]   ' '
[10]  (SCALE=1)/('LINEAR SCALE')
[11]  (SCALE=0)/('LOG SCALE')
[12]  ' '
[13]  'NUMBER AVERAGE = ',KNA
[14]  'WEIGHT AVERAGE = ',KWA
[15]  ' '
      ∇
```

APPENDIX 5 - EVALUATION OF FIBRE DISPERSION

1. Object

To assess the fibre dispersion achieved in injection moulded thermoplastic articles.

2. Test Apparatus

2.1 Quantimet 720 Image Analysing Computer.

2.2 Andrex x-ray unit.

2.3 Industrex C, X-ray film.

3. Form of Test Specimen

Injection moulded discs 50 mm. dia. x 3 mm thick.

4. Number of Specimens

Two discs are required for each measurement.

5. Procedure

5.1 Preparation of X-ray radiographs

5.1.1 Place the discs so as to be one metre from the X-ray source.

5.1.2 Expose for 8 minutes using settings of 2 milli amperes and 12 KV.

5.1.3 Develop the film and allow to dry.

5.2 Quantimet Evaluation

5.2.1 Switch on the instrument.

5.2.2 Place the X-ray radiograph on the epidiascope and set the switch to transmitted light.

5.2.3 Focus the lens to produce the sharpest image on the display screen.

5.2.4 Set the instrument to measure Area.

5.2.5 Adjust the frame size to encompass the largest area of the sample.

- 259 -

5.2.6 The area of undispersed fibres is determined using the detector in the white on black mode.

5.2.7 Express the result as a percentage of the frame area.